

## INFLUENCE OF DUCTILITY IN THE DESIGN OF (HIGH STRENGTH) STEEL BRIDGES



### **Student**

Mircea Dobrescu

Student number: 4260996

TU Delft - Faculty of Civil Engineering and Geosciences

Master of Science Civil Engineering - Structural Engineering Track

Specialisation Steel and Timber Construction

Iv-Infra bv, Amsterdam

### **Graduation committee:**

Prof. Ir. F.S.K. Bijlaard

Ir. R. Abspoel

Dr. Ir. M.A.N. Hendriks

Ir. W.P.J. Langedijk

Ir. L.J.M. Houben

Steel Structures, Delft University of Technology

Steel Structures, Delft University of Technology

Structural Mechanics, Delft University of Technology

Iv-Infra bv

Road & Railway Engineering, Delft University of Technology

October 2014



## ABSTRACT

In connections of steel structures stress concentrations occur due to the rapid geometric changes in the cross section. If the material has sufficient ductility then, due to plastic deformations, forces are redistributed so there will be equilibrium in the internal forces. In design codes this is accounted for by imposing certain requirements with respect to the tensile/yield strength ratio and minimal strain at fracture. This problem is of particular importance when high strength steels are used as questions are raised related to their ductility capacity. Over the past decades, high strength steel has gained significant ground in the steel structures market. A steel grade such as S355, which was considered to be a high strength steel 20 years ago, is now one of the predominant grades used for steel construction. In practice the occurrence of stress concentrations raises questions on how to deal with them and how to ensure a certain amount of ductility to avoid brittle fracture. In most cases an inelastic finite element analysis in shell elements and based on the nonlinear behaviour of the material is required in order to calculate the strains at the notch-tips and prove redistribution of stresses takes place. However this is a time consuming and costly procedure. This paper addresses such issues and, based on Neuber's formula for nonlinear material behaviour, a new method is developed to calculate the strains at the locations of the stress concentrations. This new approach, entitled Stefanescu Method (SM), is based only on the results of the linear finite element analysis to estimate the value of the strains. The procedure is first developed in theory and applied to a simple case of a plate with a hole in tension because in this case the stress concentration factors are already known. The results of the SM are checked with those of an inelastic finite element analysis. Based on the simple case of a plate with a hole in tension, the SM approach gives good estimates of the strains up to a limit load value of approximately 90% of the smallest force that would cause yielding in any nominal section of the plate. The applicability of this method is extended to a bridge connection from a real life project (the A1/A6 Diemen-Almere Havendreef steel railway arch bridge developed by Iv-Infra). The method is first studied on a simplified geometry of the gusset plate from the bridge connection. As the method again yields good results it is extended to the more complex geometry of the bridge connection. Comparing the results of the SM with those of an IFEA, the method gives good estimates of the strains. Based on the models used it can be concluded that the SM method can be applied to estimate strains at the location of the stress concentrations under the conditions that the loads are known and these are below 90% of the smallest force that would cause yielding in any section of the elements subject to the stress concentrations. Also, this paper addresses the issue of the ultimate to yield strength ratio and to which extent this influences the ductility capacity of the material with respect to stress concentrations. For this purpose three different ratios were studied and their influence on the strains at the notch-tips is compared. With respect to stress concentrations and the local demand for ductility to redistribute stresses, the presence of strain hardening significantly increases the ductility capacity. The lack of strain hardening leads to low deformation capacities of the plates studied. The  $f_u/f_y$  parameter together with a minimum elongation at fracture can lead to very high ductility capacities of the elements.

Keywords: High Strength Steel, Ductility, Yield-Tensile Ratio, Linear to Nonlinear Analysis Correlation, Bridges, Stefanescu Method.



*To my parents for their love and support*



## ACKNOWLEDGEMENTS

I am very grateful to my graduation committee members, Prof. Ir. F.S.K. Bijlaard, Ir. R. Abspoel and Dr. Ir. M.A.N. Hendriks for all the time they have devoted to reviewing my thesis and for their contribution and guidance on a regular basis.

I would also like to express my deepest gratitude to Ir. W.P.J. Langedijk for his constant support and guidance through the completion of this work. His knowledge and experience have been invaluable through the duration and have contributed to making this project successful.

Special thanks to my colleagues in Iv-Infra M. Koop, P. van Lierop, C. Hattink, B. Jadi and N. Broekhoff for their direct help, support and engineering guidance. Their advice and engineering knowledge were of valuable help in the successful completion of this work.

I would also want to thank all of my colleagues in the Iv-Infra office in Amsterdam for creating a friendly and pleasant working environment beyond all my expectations. I am very grateful to each and every one of you for the great experiences I went through in the past few months. My deepest gratitude to the company Iv-Infra for offering me the opportunity to work in their office. The experience and knowledge I have gained in the past few months have been of great value in the development of my professional career.

I would also like to thank Mr. Bogdan Stefanescu, for encouraging and guiding me to leave my country. Without his advice I would have probably never come to study in the Netherlands. This is the reason the method developed in this paper has been named after him.

Last but not least, special thanks to my family and friends for the moral and financial support through these years. The present accomplishments would be impossible without them and I am extremely grateful for their influence that led me to become the person I am today.

Amsterdam, 19.09.2014

Mircea Dobrescu



## TABLE OF CONTENTS

ABSTRACT .....	iii
ACKNOWLEDGEMENTS .....	vii
Table of Figures .....	xiii
List of Tables.....	xxi
List of Symbols and Abbreviations .....	xxiii
1 Introduction .....	1
1.1 Problem Statement.....	1
1.2 Objectives of the Research .....	2
1.3 Report Overview.....	3
2 Steel Grades.....	5
2.1 Introduction .....	5
2.2 Definition of Steel .....	5
2.3 Classification of Steel Grades.....	6
2.3.1 Classification by chemical composition.....	6
2.3.2 Classification of main quality classes .....	7
2.4 Quality Standards for Structural Steels .....	7
2.4.1 Delivery conditions .....	7
2.4.2 Chemical composition.....	9
2.5 Mechanical Properties .....	11
2.5.1 Tensile properties .....	11
2.5.2 Ductility properties.....	14
2.5.3 Notch toughness properties .....	15
2.5.4 Through thickness properties .....	17
2.5.5 Design values of material coefficients .....	17
2.6 Technological Properties .....	18
2.6.1 Weldability .....	18
2.6.2 Formability .....	20
2.7 High Strength Steel Grades .....	20
2.8 Bridge Applications in High Strength Steel .....	21
2.8.1 In Europe .....	21
2.8.2 In the USA.....	25
2.8.3 In Japan .....	25
2.8.4 In South Korea .....	27
3 Literature Review .....	29
3.1 Issues Related to Ductility .....	29

3.1.1	Influence of the yield-tensile ratio .....	29
3.1.2	Conclusions from previous scientific works .....	49
3.2	Structural Failures.....	50
3.3	Current Design Code Requirements With Regard to Ductility .....	52
3.3.1	Eurocode.....	52
3.3.2	Rijkswaterstaat limitations in the Netherlands.....	52
3.3.3	American Institute of Steel Construction .....	52
3.3.4	Other (older) design codes .....	52
3.4	Structural Modelling.....	53
3.5	Stress Concentrations .....	56
3.5.1	Static stress and stress concentration factors.....	56
3.5.2	Neuber's formula for nonlinear material behaviour.....	57
3.5.3	Equivalent strain energy density method .....	59
4	Linear to Nonlinear Analysis Correlation .....	60
4.1	Application of the SM Method on a Plate with a Hole .....	61
4.1.1	Plate A (r=375mm) WoSH.....	64
4.1.2	Plate B (r=250mm) WoSH.....	69
4.1.3	Plate C (r=187.5mm) WoSH.....	71
4.1.4	Plate D (r=150mm) WoSH.....	73
4.1.5	Plate E (r=75mm) WoSH .....	75
4.1.6	Plate A (r=375mm) WSH.....	77
4.1.7	Plate B (r=250mm) WSH.....	80
4.1.8	Plate C (r=187.5mm) WSH.....	83
4.1.9	Plate D (r=150mm) WSH.....	85
4.1.10	Plate E (r=75mm) WSH .....	88
4.1.11	Conclusions on SM applied to a plate with a hole .....	90
5	Application of the SM and the Influence of the Tensile-Yield Ratio .....	93
5.1	Description of Connection.....	93
5.2	Finite Element Modelling.....	99
5.2.1	Mesh .....	101
5.3	Application of the SM Correlation Method to the Gusset Plate.....	102
5.3.1	Gusset plate with $f_u/f_y=1.00$ .....	105
5.3.2	Gusset plate with $f_u/f_y=1.05$ .....	110
5.3.3	Gusset plate with $f_u/f_y=1.10$ .....	113
5.3.4	Conclusions on the simplified gusset plate .....	116
5.4	Application of the SM Correlation Method to the Bridge Joint .....	119
5.4.1	Linear static structural analysis .....	119

5.4.2	Estimation of strains using the SM approach.....	127
5.4.3	IFEA .....	131
5.4.4	Conclusions on the SM application to the bridge connection.....	132
6	Recommendations With Respect to the SM Approach.....	133
7	Concluding Remarks .....	134
7.1	Future Research .....	135
	Bibliography.....	136
A.	APPENDIX A .....	141
Plate A	.....	141
Plate B	.....	143
Plate C	.....	145
Plate D	.....	147
Plate E	.....	149
B.	APPENDIX B .....	152
Material Properties	.....	152
Geometry	.....	152
Boundary Conditions	.....	163
Loadings	.....	164
Mesh	.....	168
Simplified Gusset Plate	.....	185
Nonlinear Analysis – Bridge Joint	.....	195



## TABLE OF FIGURES

Figure 1.1 – Stress Concentrations Encountered in Practice .....	2
Figure 2.1 – Iron-carbon phase diagram [2].....	5
Figure 2.2 – Microstructures of various delivery conditions [5].....	8
Figure 2.3 – Influence of increasing tempering temperatures on the tensile properties (left) and on the Charpy V transition temperature (right) –S890QL, 60mm [5].....	8
Figure 2.4 – Attainable yield strength in dependence on the carbon equivalent CE [5].....	9
Figure 2.5 – Initial portions of stress-strain curve for mild steel [13] .....	13
Figure 2.6 – Initial portions of stress-strain curve for high strength steel [13].....	14
Figure 2.7 – Stress-strain curves for some structural steel grades [14].....	14
Figure 2.8 – Fracture toughness behaviour of steel [15].....	15
Figure 2.9 – Comparison of the Charpy-V-temperature transition curve for a conventional normalized steel S355J2+N and a TM rolled steel S355ML [16].....	15
Figure 2.10 – Charpy V-temperature transition curves for S460ML and S690QL with S355J2 for comparison [17].....	16
Figure 2.11 – Example of variation of weldability with composition: limiting conditions requiring a minimum pre-heat of 100°C for different values of carbon equivalent for MAG welding [2] .....	18
Figure 2.12 – Calculated hardness in the coarse grained HAZ as a function of weld cooling time (t/5) for some structural steels in the as welded condition text [5] .....	19
Figure 2.13 – Comparison of preheating temperatures according to [19] between normalized steel S460N and higher strength steel S460M [16].....	19
Figure 2.14 – The Nesenbachtalbrücke [21] .....	21
Figure 2.15 – Cross section of the Nesenbachtalbrücke [21].....	21
Figure 2.16 – Truss element for Fast Bridge 48 developed by Karlskronavarvet AB, Sweden [21] .....	22
Figure 2.17 – The Prince Clause bridge.....	22
Figure 2.18 – The bridge over the Hollandsch Diep.....	23
Figure 2.19 - The Ennéus Heerma bridge .....	23
Figure 2.20 – Bridge of Remoulins and repartition of steel grades in the main girders [23]...	23
Figure 2.21 – Erasmus bridge in Rotterdam, The Netherlands.....	24
Figure 2.22 – Ilverich bridge, Dusseldorf, Germany .....	24
Figure 2.23 – High performance steel bridges in the USA [25] .....	25
Figure 2.24 – Characteristic of Japanese SBHS steels [26] .....	25
Figure 2.25 – Nagata bridge, Japan [Nippon Steel & Sumitomo Metal].....	26
Figure 2.26 – Tokyo Gate bridge, Japan [27] .....	26
Figure 2.27 – Adoption of high tensile-strength steel for the Akashi Kaikyo Bridge [27].....	27
Figure 2.28 – Straight web-type sheet piles used in the cell shell [27].....	27
Figure 2.29 – Anti-collision structures in the Incheon bridge, South Korea [27].....	28
Figure 3.1 – General Flow Chart of Tasks [28] .....	29
Figure 3.2 – Dimensions and instrumentation of surface-cracked tensile specimen [28].....	30
Figure 3.3` - Notch Nomenclature and Dimensions [28].....	31
Figure 3.4 – Wide plate dimensions and instrumentation [28] .....	32
Figure 3.5 – Locations of strain gauges in welded surface cracked tensile tests [28].....	32
Figure 3.6 – Stress-Strain Curves Reflecting Conventional and New Processes [29].....	34
Figure 3.7 – Effect of Yield-Tensile Ratio on Local Yielding. (a) Stress-strain curves. (b) Tension strap with bolt hole. (c) Strain at maximum load for steel A. (d) Strain at maximum load for steel B [29].....	37

Figure 3.8 – Dimensionless load-deflection plots for tension strap with yield-tensile ratio of 0.75, 0.95 and 1.00 [29] .....	38
Figure 3.9 – Effect of yield-tensile ratio on moment-rotation behaviour of cantilever beam. (a) Stress-strain curves. (b) Cantilever beam with end load. (c) Moment-curvature plots for sections 1 and 2 for steel A. (d) Moment-curvature plots for sections 1, 2 and 3 for steel B [29] .....	39
Figure 3.10 – Illustration of effect of yield-tensile ratio on moment-rotation behaviour of cantilever beam [29] .....	39
Figure 3.11 – Charpy V-notch Number transition curve [30] .....	41
Figure 3.12 – Geometry of wide-plate tension specimen [31] .....	42
Figure 3.13 – Identification system for specimens [31] .....	43
Figure 3.14 – Typical specimen finite element model [31] .....	44
Figure 3.15 – Maximum gage-length elongation for all steel grades [31] .....	44
Figure 3.16 – Large-scale girder test specimen geometry [31] .....	45
Figure 3.17 – Comparison of predicted and measured moment-rotation curves [31] .....	46
Figure 3.18 – Relationship between ductility parameter and moment capacity [32] .....	47
Figure 3.19 – Geometry of specimens POS1 and POS 2 (mm) [32] .....	48
Figure 3.20 – The parts having the major buckles – close to the inner support of the main span, and in the centre part of the first span [33] .....	50
Figure 3.21 – Bowing at gusset plate U10 before the collapse [35] .....	51
Figure 3.22 – Location of failed A354 grade BD anchor rods [36] .....	51
Figure 3.23 – Modelling of material behaviour [39] .....	53
Figure 3.24 – Classification of joints by stiffness [40] .....	55
Figure 3.25 – Circular hole in a plate loaded in tension [41] .....	56
Figure 3.26 – Tangential stress distribution for $\theta = 0^\circ$ and $90^\circ$ [41] .....	57
Figure 3.27 – Graphical interpretation of Neuber’s formula .....	58
Figure 3.28 – Graphical interpretation of the equivalent strain energy density method .....	59
Figure 4.1 – Graphical interpretation of the SM method .....	61
Figure 4.2 – Geometrical layout of a plate with hole .....	61
Figure 4.3 – Stress-strain curve WoSH .....	63
Figure 4.4 – Stress-strain curve WSH .....	63
Figure 4.5 – The Von-Mises yield surfaces in principal stress coordinate [49] .....	64
Figure 4.6 – Plate A (r=375mm) WoSH: Displacement field [mm] .....	64
Figure 4.7 – Plate A (r=375mm) WoSH: Load-Displacement diagram .....	65
Figure 4.8 – Plate A (r=375mm) WoSH: Equivalent strain (non-linear) at $q_y = 7020N/mm$ .....	65
Figure 4.9 – Plate A (r=375mm) WoSH: Load-Equivalent Strain diagram .....	66
Figure 4.10 - Plate A (r=375mm) WoSH: Equivalent strain (linear) at $q_y = 7020N/mm$ .....	67
Figure 4.11 - Plate A (r=375mm) WoSH: Load-Equivalent Strain diagram up to $q_y$ .....	67
Figure 4.12 – Stress and strain at different location from linear and non-linear analysis .....	68
Figure 4.13 – Plate B (r=250mm) WoSH: Load-Displacement diagram .....	69
Figure 4.14 – Plate B (r=250mm) WoSH: Load-Equivalent Strain diagram .....	70
Figure 4.15 – Plate C (r=187.5mm) WoSH: Load-Displacement diagram .....	71
Figure 4.16 – Plate C (r=187.5mm) WoSH: Load-Equivalent Strain diagram .....	72
Figure 4.17 - Plate D (r=150mm) WoSH: Load-Displacement diagram .....	73
Figure 4.18 - Plate D (r=150mm) WoSH: Load-Equivalent Strain diagram .....	74
Figure 4.19 - Plate E (r=75mm) WoSH: Load-Displacement diagram .....	75
Figure 4.20 - Plate E (r=75mm) WoSH: Load-Equivalent Strain diagram .....	76
Figure 4.21 - Plate A (r=375mm) WSH: Displacement field [mm] .....	77
Figure 4.22 – Plate A (r=375mm) WSH: Load-Displacement diagram .....	77

Figure 4.23 – Plate A (r=375mm) WSH: Equivalent strain (non-linear) at $qy = 7100N/mm$	78
Figure 4.24 – Plate A (r=375mm) WSH: Load-Equivalent Strain diagram	78
Figure 4.25 - Plate A (r=375mm) WSH: Equivalent strain (linear) at $qy = 7100N/mm$	79
Figure 4.26 – Plate A (r=375mm) WSH: Load-Equivalent Strain diagram up to $qy$	79
Figure 4.27 - Plate B (r=250mm) WSH: Load-Displacement diagram	80
Figure 4.28 - Plate B (r=250mm) WSH: Load-Equivalent Strain diagram	81
Figure 4.29 - Plate B (r=250mm) WSH: Load-Equivalent Strain diagram up to $qy$	82
Figure 4.30 - Plate C (r=187.5mm) WSH: Load-Displacement diagram	83
Figure 4.31 - Plate C (r=187.5mm) WSH: Load-Equivalent Strain diagram	84
Figure 4.32 - Plate C (r=187.5mm) WSH: Load-Equivalent Strain diagram up to $qy$	84
Figure 4.33 - Plate D (r=150mm) WSH: Load-Displacement diagram	85
Figure 4.34 - Plate D (r=150mm) WSH: Load-Equivalent Strain diagram	86
Figure 4.35 - Plate D (r=150mm) WSH: Load-Equivalent Strain diagram up to $qy$	87
Figure 4.36 - Plate E (r=75mm) WSH: Load-Displacement diagram	88
Figure 4.37 - Plate E (r=75mm) WSH: Load-Equivalent Strain diagram	89
Figure 4.38 - Plate E (r=75mm) WSH: Load-Equivalent Strain diagram up to $qy$	89
Figure 5.1 – Steel Structure Isometry [Iv-Infra]	93
Figure 5.2 – Side View K050 [Iv-Infra]	94
Figure 5.3 – Section C-C [Iv-Infra]	94
Figure 5.4 – Joint Isometry [Iv-Infra]	94
Figure 5.5 – Joint Top View [Iv-Infra]	95
Figure 5.6 – Joint Side View [Iv-Infra]	95
Figure 5.7 – Sections A-A, B-B and C-C [Iv-Infra]	95
Figure 5.8 – Sections F-F and H-H [Iv-Infra]	96
Figure 5.9 – Original tension in upper flange of global model [Iv-Infra]	97
Figure 5.10 – Single plate model, elastic analysis [Iv-Infra]	97
Figure 5.11 – Single plate model, plastic analysis, material properties input [Iv-Infra]	98
Figure 5.12 – Single plate model, plastic analysis [Iv-Infra]	98
Figure 5.13 – Geometry of the joint with notations	99
Figure 5.14 – Global and local coordinate axis directions	99
Figure 5.15 – Boundary conditions	100
Figure 5.16 – Loads acting on the bridge connection	100
Figure 5.17 – SHELL281 geometry [ANSYS 14.5 Help]	101
Figure 5.18 – Mesh used in the bridge connection modelling	101
Figure 5.19 – Gusset plate model used in the finite element analysis	102
Figure 5.20 – Stress-strain curves used based on test results from [50]	103
Figure 5.21 – Measured displacement and equivalent strain locations	103
Figure 5.22 – Gusset plate with $f_u/f_y=1.00$ : Load-displacement diagram	105
Figure 5.23 - Gusset plate with $f_u/f_y=1.00$ : location of the stress concentrations	105
Figure 5.24 - Gusset plate with $f_u/f_y=1.00$ : Load-Equivalent strain diagram at pos. A	106
Figure 5.25 - Gusset plate with $f_u/f_y=1.00$ : Load-Equivalent strain diagram at pos. B	108
Figure 5.26 - Gusset plate with $f_u/f_y=1.00$ : Differences in equivalent strains from SM and IFEA versus load	109
Figure 5.27 – Gusset plate with $f_u/f_y=1.05$ : Load-displacement diagram	110
Figure 5.28 - Gusset plate with $f_u/f_y=1.05$ : Load-Equivalent strain diagram at pos. A	111
Figure 5.29 - Gusset plate with $f_u/f_y=1.05$ : Load-Equivalent strain diagram at pos. B	111
Figure 5.30 - Gusset plate with $f_u/f_y=1.05$ : Differences in equivalent strains from SM and IFEA versus load	112
Figure 5.31 – Gusset plate with $f_u/f_y=1.10$ : Load-displacement diagram	113

Figure 5.32 - Gusset plate with $f_u/f_y=1.10$ : Load-Equivalent strain diagram at pos. A .....	114
Figure 5.33 - Gusset plate with $f_u/f_y=1.10$ : Load-Equivalent strain diagram at pos. B.....	114
Figure 5.34 - Gusset plate with $f_u/f_y=1.10$ : Differences in equivalent strains from SM and IFEA versus load .....	115
Figure 5.35 – Load-Displacement diagram for the three ultimate-yield ratios.....	116
Figure 5.36 – Load-Equivalent strain diagram for the three ultimate-yield ratios.....	117
Figure 5.37 – The equivalent (Von-Mises) stress in the joint.....	120
Figure 5.38 – Maximum principal stress in the top flange.....	121
Figure 5.39 – Equivalent stress in the top flange .....	121
Figure 5.40 – Equivalent strain in the top flange .....	121
Figure 5.41 – Minimum principal stress in the gusset plate at diagonal D .....	122
Figure 5.42 – Maximum principal stress in the gusset plate at diagonal D .....	122
Figure 5.43 – Equivalent stress in the gusset plate at diagonal D.....	122
Figure 5.44 – Equivalent strain in the gusset plate at diagonal D.....	123
Figure 5.45 – Minimum principal stress in the gusset plate at diagonal C .....	123
Figure 5.46 – Maximum principal stress in the gusset plate at diagonal C.....	123
Figure 5.47 – Equivalent stress in the gusset plate at diagonal C .....	124
Figure 5.48 – Equivalent strain in the gusset plate at diagonal C .....	124
Figure 5.49 – Equivalent stresses at the stress concentration locations in the top flange at diagonal D: $\sigma_{el}$ .....	125
Figure 5.50 – Equivalent strains at the stress concentration locations in the top flange at diagonal D: $\varepsilon_{el}$ .....	125
Figure 5.51 – Equivalent stresses at the stress concentration locations in the gusset plate at diagonal D: $\sigma_{el}$ .....	126
Figure 5.52 - Equivalent strains at the stress concentration locations in the gusset plate at diagonal D: $\varepsilon_{el}$ .....	126
Figure 5.53 – Stresses in the girder cross-section .....	127
Figure 5.54 – Averaged stress in the nominal section.....	128
Figure 5.55 – Loads and boundary conditions of the gusset plate .....	128
Figure 5.56 – Expected shear plane and equivalent loads on the gusset plate.....	129
Figure 5.57 – Elastic-plastic strains in the top flange calculated with the SM .....	130
Figure 5.58 - Elastic-plastic strains in the gusset plate calculated with the SM .....	130
Figure 5.59 - Elastic-plastic strains in the top flange calculated with the IFEA.....	131
Figure 5.60 - Elastic-plastic strains in the gusset plate calculated with the IFEA .....	131
Figure A.1 – SHELL281 element .....	141
Figure A.2 – Plate A: Mesh geometry, load and boundary conditions of the finite element model.....	141
Figure A.3 – Plate A (WoSH): Equivalent strain at $qu = 7060N/mm$ (non-linear analysis) .....	141
Figure A.4 – Plate A (WoSH): Equivalent strain at $qu = 7060N/mm$ (linear analysis).....	142
Figure A.5 – Plate A (WoSH): Equivalent stress at $qu = 7060N/mm$ (linear analysis).....	142
Figure A.6 – Plate A (WoSH): Equivalent strain at $0.9qy = 6390N/mm$ (non-linear analysis).....	142
Figure A.7 – Plate A (WoSH): Equivalent strain at $0.9qy = 6390N/mm$ (linear analysis) .....	142
Figure A.8 – Plate A (WoSH): Equivalent stress at $0.9qy = 6390N/mm$ (linear analysis) .....	142
Figure A.9 – Plate A (WSH): Equivalent strain at $qu = 10200N/mm$ (non-linear analysis) .....	143
Figure A.10 – Plate A (WSH): Equivalent strain at $qu = 10200N/mm$ (linear analysis)...	143
Figure A.11 – Plate A (WSH): Equivalent stress at $qu = 10200N/mm$ (linear analysis)...	143

Figure A.12 – Plate B: Mesh geometry, load and boundary conditions of the finite element model.....	143
Figure A.13 – Plate B (WoSH): Equivalent strain at $qu = 9425N/mm$ (non-linear analysis) .....	143
Figure A.14 – Plate B (WoSH): Equivalent strain at $qu = 9425N/mm$ (linear analysis) ...	144
Figure A.15 – Plate B (WoSH): Equivalent stress at $qu = 9425N/mm$ (linear analysis) ...	144
Figure A.16 - Plate B (WoSH): Equivalent strain at $0.9qy = 8520N/mm$ (non-linear analysis).....	144
Figure A.17 – Plate B (WoSH): Equivalent strain at $0.9qy = 8520N/mm$ (linear analysis) .....	144
Figure A.18 – Plate B (WoSH): Equivalent stress at $0.9qy = 8520N/mm$ (linear analysis) .....	144
Figure A.19 – Plate B (WSH): Equivalent strain at $qu = 13600N/mm$ (non-linear analysis) .....	145
Figure A.20 – Plate B (WSH): Equivalent strain at $qu = 13600N/mm$ (linear analysis)...	145
Figure A.21 – Plate B (WSH): Equivalent stress at $qu = 13600N/mm$ (linear analysis)...	145
Figure A.22 – Plate C: Mesh geometry, load and boundary conditions of the finite element model.....	145
Figure A.23 – Plate C (WoSH): Equivalent strain at $qu = 10610N/mm$ (non-linear analysis) .....	145
Figure A.24 – Plate C (WoSH): Equivalent strain at $qu = 10610N/mm$ (linear analysis). 146	
Figure A.25 – Plate C (WoSH): Equivalent stress at $qu = 10610N/mm$ (linear analysis). 146	
Figure A.26 - Plate C (WoSH): Equivalent strain at $0.9qy = 9585N/mm$ (non-linear analysis).....	146
Figure A.27 – Plate C (WoSH): Equivalent strain at $0.9qy = 9585N/mm$ (linear analysis) .....	146
Figure A.28 – Plate C (WoSH): Equivalent stress at $0.9qy = 9585N/mm$ (linear analysis) .....	146
Figure A.29 – Plate C (WSH): Equivalent strain at $qu = 15300N/mm$ (non-linear analysis) .....	147
Figure A.30 – Plate C (WSH): Equivalent strain at $qu = 15300N/mm$ (linear analysis)...	147
Figure A.31 – Plate C (WSH): Equivalent stress at $qu = 15300N/mm$ (linear analysis)...	147
Figure A.32 – Plate D: Mesh geometry, load and boundary conditions of the finite element model.....	147
Figure A.33 – Plate D (WoSH): Equivalent strain at $qu = 11340N/mm$ (non-linear analysis) .....	147
Figure A.34 – Plate D (WoSH): Equivalent strain at $qu = 11340N/mm$ (linear analysis). 148	
Figure A.35 – Plate D (WoSH): Equivalent stress at $qu = 11340N/mm$ (linear analysis). 148	
Figure A.36 - Plate D (WoSH): Equivalent strain at $0.9qy = 10224N/mm$ (non-linear analysis).....	148
Figure A.37 – Plate D (WoSH): Equivalent strain at $0.9qy = 10224N/mm$ (linear analysis) .....	148
Figure A.38 – Plate D (WoSH): Equivalent stress at $0.9qy = 10224N/mm$ (linear analysis) .....	148
Figure A.39 – Plate D (WSH): Equivalent strain at $qu = 16320N/mm$ (non-linear analysis) .....	149
Figure A.40 – Plate D (WSH): Equivalent strain at $qu = 16320N/mm$ (linear analysis)...	149
Figure A.41 – Plate D (WSH): Equivalent stress at $qu = 16320N/mm$ (linear analysis)...	149
Figure A.42 – Plate E: Mesh geometry, load and boundary conditions of the finite element model.....	149

Figure A.43 – Plate E (WoSH): Equivalent strain at $qu = 12780N/mm$ (non-linear analysis)	149
Figure A.44 – Plate E (WoSH): Equivalent strain at $qu = 12780N/mm$ (linear analysis)	150
Figure A.45 – Plate E (WoSH): Equivalent stress at $qu = 12780N/mm$ (linear analysis)	150
Figure A.46 - Plate E (WoSH): Equivalent strain at $0.9qy = 11502N/mm$ (non-linear analysis)	150
Figure A.47 – Plate E (WoSH): Equivalent strain at $0.9qy = 11502N/mm$ (linear analysis)	150
Figure A.48 – Plate E (WoSH): Equivalent stress at $0.9qy = 11502N/mm$ (linear analysis)	150
Figure A.49 – Plate E (WSH): Equivalent strain at $qu = 18360N/mm$ (non-linear analysis)	151
Figure A.50 – Plate E (WSH): Equivalent strain at $qu = 18360N/mm$ (linear analysis)	151
Figure A.51 – Plate E (WSH): Equivalent stress at $qu = 18360N/mm$ (linear analysis)	151
Figure B.1 – Girder Sketch	153
Figure B.2 – Section and diaphragm planes with diaphragm sketch	153
Figure B.3 – Stiffness plate sketch	154
Figure B.4 – Diagonal sketch	155
Figure B.5 – Sliceweb plane	155
Figure B.6 – Girder extrusion	156
Figure B.7 – Diaphragm geometry	156
Figure B.8 – Geometry of upper flange	157
Figure B.9 – Geometry of the longitudinal stiffener	158
Figure B.10 – Geometry of the diagonal stiffeners	158
Figure B.11 – Geometry of the diagonals	159
Figure B.12 – Extra solids and surface bodies	160
Figure B.13 – Joint geometry	161
Figure B.14 – Clearance around diagonal	161
Figure B.15 – Thickness and material assignment in “Mechanical”	162
Figure B.16 – Thickness flanges and inner web	162
Figure B.17 – Thickness diagonals, gusset plates and stiffeners	163
Figure B.18 – Thickness of the outer web	163
Figure B.19 – Boundary conditions at the joint ends	163
Figure B.20 – Bending moment at A	164
Figure B.21 – Bending moment at B	165
Figure B.22 – Axial force in Diagonal C	165
Figure B.23 – Axial force in Diagonal D	166
Figure B.24 – Bending moment in Diagonal C	166
Figure B.25 – Bending moment in Diagonal D	167
Figure B.26 – Axial force at A	167
Figure B.27 – Mesh details	182
Figure B.28 – Ideal and skewed triangles and quadrilaterals [ANSYS 14.5 Help]	183
Figure B.29 – Mesh metrics	183
Figure B.30 – Generated mesh	184
Figure B.31 – Displacement field for $f_u/f_y=1.00$ (IFEA) at load levels a,b,c,d and e	186
Figure B.32 – Displacement field (EFEA) at load levels a,b,c,d and e	187
Figure B.33 – Equivalent strain field for $f_u/f_y=1.05$ (IFEA) at load levels a,b,c,d and e	188
Figure B.34 – Displacement field for $f_u/f_y=1.05$ (IFEA) at load levels a,b,c,d and e	189
Figure B.35 – Equivalent strain field for $f_u/f_y=1.10$ (IFEA) at load levels a,b,c,d and e	190
Figure B.36 – Displacement field for $f_u/f_y=1.10$ (IFEA) at load levels a,b,c,d and e	191

Figure B.37 – Equivalent strain field at $0.9f_y$ (IFEA) for $f_u/f_y=1.00$ .....	192
Figure B.38 – Equivalent strain field at $0.9f_y$ (EFEA) .....	192
Figure B.39 – Equivalent stress field at $0.9f_y$ (EFEA) .....	193
Figure B.40 – Equivalent strain field at $0.9f_y$ (IFEA) for $f_u/f_y=1.05$ .....	193
Figure B.41– Equivalent strain field at $0.9f_y$ (IFEA) for $f_u/f_y=1.10$ .....	194
Figure B.42 – IFEA of bridge connection: settings .....	195
Figure B.43 - Elastic-plastic strains over the top flange (IFEA).....	196
Figure B.44 – Equivalent total strains in the diagonal-gusset plate part.....	197
Figure B.45 - Elastic-plastic strains over the joint (IFEA) .....	197
Figure B.46 - Elastic-plastic strains in the joint (IFEA) .....	198



## LIST OF TABLES

Table 1 – Boundary between non alloy and alloy steels (ladle analysis) [1] .....	6
Table 2 – Chemical composition of the ladle analysis for flat and long products of steel grades and qualities with values for the impact strength [3] .....	9
Table 3 – Chemical composition of the ladle analysis for normalized steel [7] .....	10
Table 4 – Chemical composition of the ladle analysis for the thermo mechanical rolled steel [8] .....	10
Table 5 – Chemical composition of the ladle analysis of steels with improved atmospheric corrosion resistance [9] .....	11
Table 6 – Chemical composition of the ladle analysis for quenched and tempered steels [4].	11
Table 7 – Nominal values of yield strength $f_y$ and ultimate tensile strength $f_u$ for hot rolled structural steel [10].....	12
Table 8 - Nominal values of yield strength $f_y$ and ultimate tensile strength $f_u$ for structural hollow sections [10] .....	12
Table 9 – Nominal values of yield strength $f_y$ and ultimate tensile strength $f_u$ for hot rolled structural steel [11].....	13
Table 10 – Nominal values of yield strength $f_y$ and ultimate tensile strength $f_u$ for hot rolled flat products [11] .....	13
Table 11 – Maximum permissible values of element thickness in mm [12].....	16
Table 12 – Maximum permissible values of element thickness $t$ in mm [11] .....	17
Table 13 – Choice of quality class according to [18].....	17
Table 14 – HSS grade types [20] .....	20
Table 15 - Basic Details of Steel Grades Included in Test Programme as per Requirements of Relevant Specifications [28] .....	30
Table 16 - Processing Conditions and Properties of Plates as Quoted on Mill Certificates [28] .....	30
Table 17 – Failure Modes and Fracture Appearance of Surface-Cracked Tensile Tests on Parent Materials [28].....	31
Table 18 – Chemistry for conventional and high performance steels [30] .....	40
Table 19 – Mechanical properties for high performance steel plates [30].....	40
Table 20 – Comparison of individual and average tensile test results [31] .....	42
Table 21 – Summary of HPS70W wide-plate tensile test results [31].....	43
Table 22 – Parameters of $f_y/f_u$ distribution and safe $f_y/f_u$ ratios for various levels of reliability [31] .....	47
Table 23 – Assumptions for FE-methods [39] .....	54
Table 24 – Type of joint model [40] .....	54
Table 25 – Plate with hole geometries .....	62
Table 26 – Plate A (r=375mm) WoSH: Equivalent strain at 0.9qu .....	68
Table 27 – Plate B (r=250mm) WoSH: Equivalent strain at 0.9qu .....	70
Table 28 – Plate C (r=187.5mm) WoSH: Equivalent strain at 0.9qu .....	72
Table 29 – Plate D (r=150mm) WoSH: Equivalent strain at 0.9qu .....	74
Table 30 – Plate E (r=75mm) WoSH: Equivalent strain at 0.9qu .....	76
Table 31 – Plate A (r=375mm) WSH: Equivalent strain at 0.9qy .....	80
Table 32 – Plate B (r=250mm) WSH: Equivalent strain at 0.9qy .....	82
Table 33 – Plate C (r=187.5mm) WSH: Equivalent strain at 0.9qy .....	85
Table 34 – Plate D (r=150mm) WSH: Equivalent strain at 0.9qy .....	87
Table 35 – Plate E (r=75mm) WSH: Equivalent strain at 0.9qy.....	90
Table 36 – $f_u/f_y$ ratio on strain development at 0.9qy .....	90

Table 37 – IFEA: Equivalent strains at a load level of 0.9qy for the cases WoSH and WSH	92
Table 38 – SM: Equivalent strains at a load level of 0.9qy for the cases WoSH and WSH....	92
Table 39 – Material properties for different $f_u/f_y$ ratios.....	103
Table 40 – Displacement values at a load of 58000kN for the three $f_u/f_y$ ratios.....	116
Table 41 – Equivalent strains at the notch-tip at 58000kN axial force in the diagonal .....	117
Table 42 – Peak stresses in the top flange at diagonal D .....	127
Table 43 – Peak stresses in the gusset plate at diagonal D .....	127
Table 44 – Girder: acting forces, bending moments and cross-sectional characteristics.....	127
Table 45 – Notch-tip elastic-plastic strain calculated using the SM approach for the top flange .....	129
Table 46 - Notch-tip elastic-plastic strain calculated using the SM approach for the gusset plate .....	130
Table 47 – Difference between the IFEA and SM strains in the top flange .....	132
Table 48 – Difference between the IFEA and SM strains in the gusset plate.....	132
Table 49 – Material properties bridge connection .....	152
Table 50 – Equivalent strain and displacement values for different load levels.....	185

## LIST OF SYMBOLS AND ABBREVIATIONS

$A_g$	Gross cross section area;
$A_{net}$	Net cross sectional area;
$D_m$	Correlation factor;
$K_t$	Theoretical elastic stress concentration factor;
$K_\varepsilon$	Effective strain concentration factor;
$K_\sigma$	Effective stress concentration factor;
$f_u$	Ultimate strength;
$f_y$	Yield strength;
$q_l$	Load corresponding to occurrence of localized yield (plate with a hole);
$q_u$	Ultimate load corresponding to failure (for the plate in tension with a hole);
$q_y$	Yield load corresponding to yielding of the net section (plate with a hole)
$\gamma_{M0}$	Partial safety factor of 1.00;
$\gamma_{M2}$	Partial safety factor of 1.25;
$\delta_u$	Displacement at ultimate load (plate with a hole);
$\varepsilon_{NL}$	Notch-tip elastic-plastic strain;
$\varepsilon_e$	Equivalent strain;
$\varepsilon_{el}$	Notch-tip elastic equivalent strain (obtained from a linear elastic analysis);
$\varepsilon_{ij}^{el}$	Notch-tip strain components obtained from linear elastic calculations;
$\varepsilon_{ij}^{ep}$	Plastic components of the notch-tip strain tensor;
$\varepsilon_{max}$	Notch-tip real elastic-plastic strain (Neuber's formula);
$\varepsilon_{nom}$	Nominal strain;
$\varepsilon_u$	Ultimate strain;
$\varepsilon_y$	Yield strain;
$\sigma_1$	Maximum principal stress (maximum normal stress);
$\sigma_2$	Medium principal stress (maximum shear stress);
$\sigma_3$	Minimum principal stress (minimum normal stress);
$\sigma_{NL}$	Notch-tip elastic-plastic stress;
$\sigma_e$	Equivalent stress (Von-Mises);
$\sigma_{el}$	Notch-tip elastic equivalent stress (obtained from a linear elastic analysis);
$\sigma_{ij}^{el}$	Notch-tip stress tensor components obtained from linear elastic calculations;
$\sigma_{ij}^{ep}$	Plastic components of the notch-tip stress tensor;
$\sigma_{max}$	Notch-tip real elastic-plastic stress (Neuber's formula);
$\sigma_{nom}$	Nominal stress;
<b>AASHTO</b>	American Association of State Highway and Transportation Officials;
<b>AISC</b>	American Institute of Steel Construction;
<b>AR</b>	As-rolled;
<b>D</b>	Width of plate with hole;
<b>E</b>	Modulus of elasticity (for steel 210GPa);
<b>EFEA</b>	Elastic finite element analysis
<b>ESED</b>	Equivalent strain energy density rule;
<b>FEM</b>	Finite Element Method;
<b>G</b>	Shear modulus;
<b>HAZ</b>	Heat affected zone;
<b>HSS</b>	High strength steel (460-700MPa minimum yield strength);

<i>IFEA</i>	Inelastic finite element analysis (nonlinear finite element analysis based on the materials nonlinear behaviour);
<i>N</i>	Normalized;
<i>NR</i>	Normalized-Rolled;
<i>Q</i>	Quenched;
<i>QT</i>	Quenched and tempered;
<i>SLS</i>	Serviceability Limit State;
<i>SM</i>	Stefanescu method
<i>TM</i>	Thermo-mechanically rolled;
<i>ULS</i>	Ultimate Limit State;
<i>VHSS</i>	Very high strength steel (with minimum yield strength above 700MPa);
<i>WSH</i>	With strain hardening;
<i>WoSH</i>	Without strain hardening;
<i>r</i>	Radius (of the hole);
<i>v</i>	Poisson's ratio;

# 1 INTRODUCTION

## 1.1 Problem Statement

In details (connections) of steel structures stress concentrations occur due to rapid geometric changes in the cross section. If the material has sufficient ductility then, due to plastic deformations, forces are redistributed so there will be equilibrium in the internal forces. This behaviour can occur if the material has sufficient deformation capacity which is translated as: tensile strength higher than the yield strength and minimal strain at fracture (material properties usually dictated by design codes). In the case of hand calculations (possible based on a model with beam elements) the force distribution in a detail is based on plastic deformation. This is an acceptable method when the material has sufficient ductility.

In case of modelling a detail with shell elements stress concentrations will arise in the results. Often it is not clear how to deal with these stress concentrations for an ultimate limit state (ULS) check, especially in relation to the approach of a hand calculation or based on a linear elastic analysis. A possible method is to calculate the strain with a physical nonlinear calculation, based on the nonlinear behaviour of the material.

This problem is of particular importance when high strength steels (HSS) are used as questions are raised related to their ductility capacity. Over the past decades, HSS has gained significant ground in the steel structures market. A steel grade such as S355, which was considered to be a HSS 20 years ago, is now one of the predominant grades used for steel construction. Great potential for the use of HSS can be found in elements where strength is the governing criterion. The advantages are generally the reduced self-weight and cross-sectional dimensions. Also, due to the higher yield strength, reduced plate thickness can result in saving on welding costs, transportation and erection. The reduced self-weight can also result in reduced foundation costs. Using hybrid bridge designs the full potential of such steels can be put to use.

Products are available today in grades S420 and S460 as thermo-mechanically rolled (TM) and plates of quenched and tempered (QT)-steel with grades up to S1100 (although not yet standardized above S960). Extremely high strength is usually associated with an increase in alloying elements which results in a higher risk of brittle fracture. The lack of long term experience and design rules (EN 1993-1-12 only recently covered steel grades only up to S700) results in limited applications in Europe compared to the United States and Japan where the market has shown a significant increase of this kind of bridges. These results in the fact that the higher yield strength is not made use of, resulting in a less economical design than its full potential.

The Eurocode has requirement criteria for the ductility of steel products. These are translated into limiting values of the ratio  $f_u/f_y$ , a minimum elongation at failure and minimum ultimate strain  $\varepsilon_u$  with respect to  $\varepsilon_y$  ratio. These criteria depend on the steel grade. However, the ratio limit between the tensile strength and the yield strength differ per country. In The Netherlands, Rijkswaterstaat and ProRail dictates stricter criteria for bridges, while for example in Scandinavian countries these criteria are less strict. Such requirements are mostly based on lack of long term experience with HSS rather than scientific background.

The problems encountered in practice are related to the occurrence of stress concentrations (Figure 1.1) and how to deal with them. A certain amount of ductility must be

ensured by the structure in order to avoid brittle fracture and have a warning mechanics in case of failure. This would result in the occurrence of plastic deformations and redistribution of stresses.

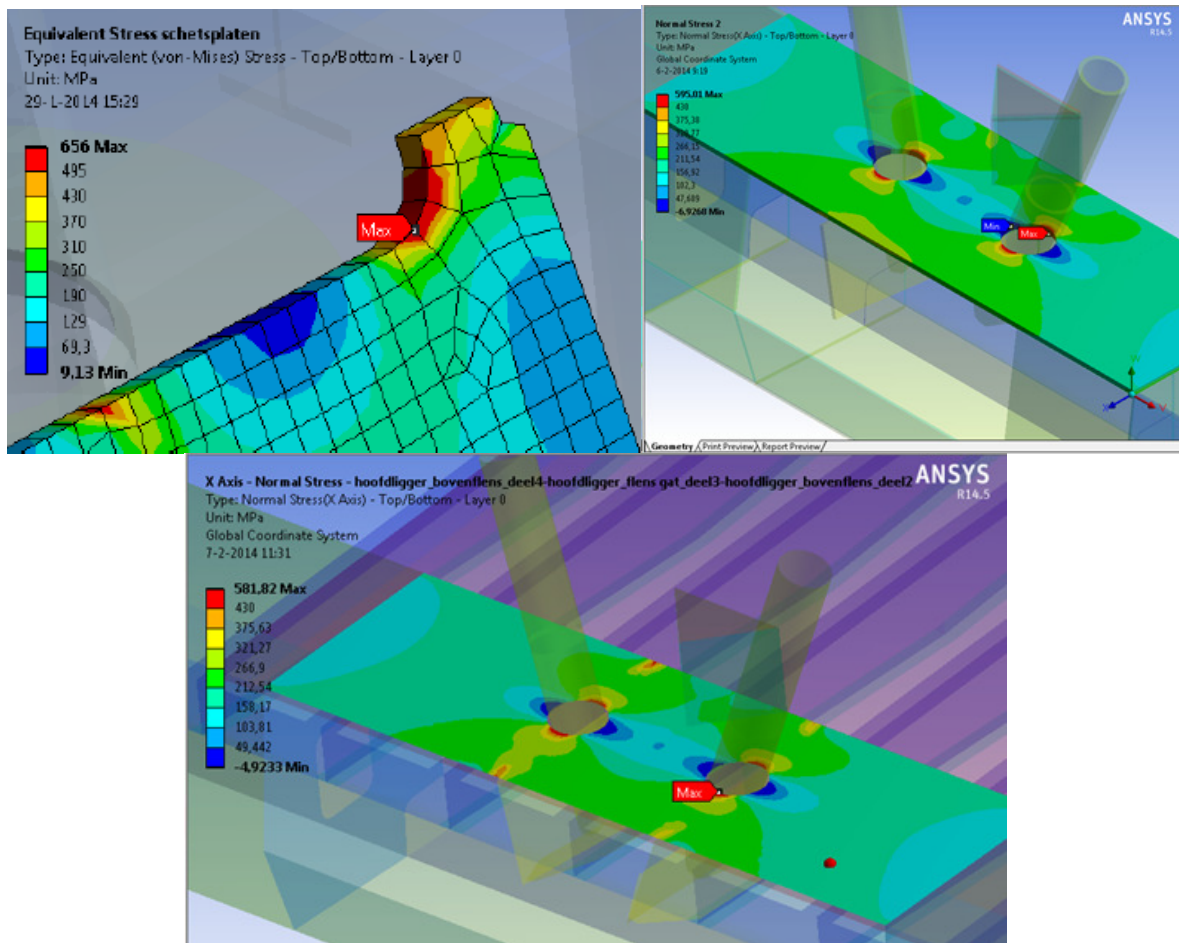


Figure 1.1 – Stress Concentrations Encountered in Practice

The issue addressed in this work is how to deal with this? What would be a simple approach to estimating the strains and stresses occurring at a stress concentration factor? How are the stress concentrations in the connections influenced by the overall ductility requirements of the structure?

## 1.2 Objectives of the Research

The main problem that will be addressed by the research is related to the occurrence of stress concentrations in bridge connections. It's not always clear how to deal with stress concentrations when modelling a steel structure in shell elements. The relation between the actual strain and the criteria for ductility is not known.

When dealing with high stress concentrations, it is common practice to run nonlinear analysis, based on the material nonlinear behaviour, to have an estimate of the real stress and strain occurring at the specific (stress concentration) location. This is quite a demanding process with respect to computer performance requirements and time. The goal of this project is to determine a relation that can be used to estimate the real stress and strain occurring at stress concentrations, based only on a linear finite element analysis. This can be used to give

insight with respect to ductility and strength capacity requirements, and also how to deal with stress concentrations in shell models in order to achieve an (economic) optimal design.

The objectives are achieved through completion of the following tasks:

- Literature research on the topic in order to gain insight in which are the decisive factors influencing ductility. Previous works on the topic of ductility in HSS, examples of successful bridge applications and available steel grades are studied. Also an overview of a possible approach for calculating stress concentrations in the nonlinear range in simple elements and Eurocode restrictions with regard to software modelling of HSS is given;
- Development of the Stefanescu Method (SM) approach that can be used to estimate the real plane stress and strain occurring at stress concentrations, based only on a linear finite element analysis. Finite element models of a plate with a hole in mild steel and built-up in shell elements will be developed. Here the influence of the stress-strain curve and geometry of the element on the proposed theory will be checked. The validity of the approach will be verified by comparing the results with those of a nonlinear finite element calculation based on the nonlinear behaviour of the material.
- Based on the results from the simple example of a plate with a hole, an attempt to extend the newly proposed approach to more complicated geometries where the development of strains is not known will be made. This is done by applying the newly proposed approach on a connection from a real-life bridge project;
- On the same bridge connection the influence of the  $f_u/f_y$  ratio on the strain developments at the stress concentrations is studied. In this step the bridge connection is modelled in HSS, S690 with ratios of 1.00, 1.05 and 1.10;
- Based on the results obtained recommendations are given on how to apply the SM method to estimate strains at notch-tips using only the results of the linear finite element analysis. Also recommendations on which parameters are more important to define ductility with respect to stress concentrations.

### 1.3 Report Overview

The thesis contains a total of seven chapters. The first chapter states the problem to be dealt with and presents the objectives of the research. The work then continues with the second chapter where available steel grades are presented. Types of available steels, their chemical composition, properties and also some successful applications that make use of HSSs are illustrated. In the third chapter, the conducted literature research and obtained information is detailed. Issues with regard to the application of HSS, current design requirements from codes and some examples of bridge failures are presented here. Also a discussion about calculating stress concentrations in simple elements and the Eurocode limitations with respect to modelling of structures in HSS is carried out. This has the purpose to present the background behind the ideas that will be later used in chapter four. There a new approach to estimating the nonlinear stresses and strains occurring at stress concentration locations is developed. This is at first applied to a simple example of a plate with a hole in mild steel. Several models are created in order to study the influence of the shape of the stress-strain curve and geometry on the results. Based on the output obtained in chapter 4, the application of the new proposed theory on more complicated examples is researched in

chapter 5. There a bridge connection from a real-life project is analysed. Firstly a simplified model of the gusset plate is built and the SM applicability to this case is studied. Based on the results the method is afterwards extended to the bridge joint. There the strain values from the inelastic finite element analysis based on the material nonlinear behaviour are compared with those from the newly proposed approach and the applicability of the SM method is checked. Also the bridge joint is modelled in HSS (S690) with three different  $f_u/f_y$  ratios in order to have a better understanding of the influence of this parameter with respect to the ability of the material to yield locally and redistribute stresses. In chapter 6 recommendations on the application of the new theorem are given based on the numerical results obtained in the previous sections. These have the purpose to give some guidelines on how the SM approach can be applied and its limitations. Finally chapter 7 gives the conclusions of the present paper and proposes future research topics.

## 2 STEEL GRADES

### 2.1 Introduction

The advantages of high strength, good machinability and high economic efficiency make steel one of the most important construction materials nowadays. Depending on its chemical composition and production conditions, steel properties can be adapted to the requirements of the specific application. The most important requirements of steel are related to:

- Strength: deformation and fatigue resistance;
- Toughness: ductility and resistance to brittle fracture;
- Weldability: resistance to cold cracking and good toughness in the HAZ;
- Corrosion resistance: minimum rust formation and resistance to hydrogen induced cracking;
- Homogeneity

In order to improve production and the use of steel products, quality standards and specifications have been developed which list steel grades and qualities and their chemical composition, mechanical and technological properties. In this chapter an overview is given of the classification of European steels and details of the main grades used for structural steelwork. Also high strength steels grades from different countries are compared and examples of successful applications are listed.

### 2.2 Definition of Steel

European standard EN 10020 defines steel as: “Material which contains by mass more iron than any other single element, having carbon content generally less than 2% and containing other elements. A limited number of chromium steels may contain more than 2% of carbon, but 2% is the usual dividing line between steel and cast iron” [1]

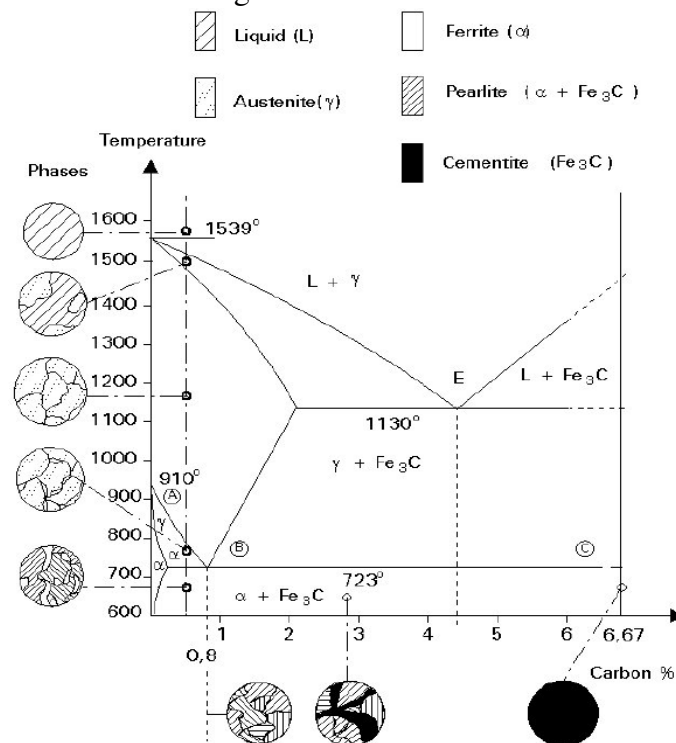


Figure 2.1 – Iron-carbon phase diagram [2]

Figure 2.1 presents the iron-carbon phase diagram. Depending on the carbon content, three types of ferrous alloys can be distinguished:

- Iron: less than 0.008% carbon content
- Steels: between 0.008 and 2.14% carbon content;
- Cast iron: between 2.14 to 6.7% carbon content;

### 2.3 Classification of Steel Grades

The European standard [1] classifies steel grades into:

- non alloy, stainless and other alloy steels by chemical composition;
- main quality classes defined by main property or application characteristics for non-alloy, stainless and other alloy steels.

#### 2.3.1 Classification by chemical composition

Classification is based on the ladle analysis specified in the product standard or specification and is determined by the minimum value specified for each element. The ladle analysis is a chemical analysis of a sample taken from the molten material.

Classes are defined as [1]:

- Non alloy steels: steel grades in which none of the limit values in Table 1 are reached;
- Stainless steels: steels with at least 10.5% of chromium and maximum 1.2% carbon content;
- Other alloy steels: steel grades that are not stainless steels and in which at least one of the limit values from Table 1 is reached.

Table 1 – Boundary between non alloy and alloy steels (ladle analysis) [1]

Specified element		Limit value % by mass
Al	Aluminium	0,30
B	Boron	0,0008
Bi	Bismuth	0,10
Co	Cobalt	0,30
Cr	Chromium	0,30
Cu	Copper	0,40
La	Lanthanides (each)	0,10
Mn	Manganese	1,65 <sup>a)</sup>
Mo	Molybdenum	0,08
Nb	Niobium	0,06
Ni	Nickel	0,30
Pb	Lead	0,40
Se	Selenium	0,10
Si	Silicon	0,60
Te	Tellurium	0,10
Ti	Titanium	0,05
V	Vanadium	0,10
W	Tungsten	0,30
Zr	Zirconium	0,05
Others (except carbon, phosphorus, sulphur, nitrogen) (each)		0,10
a) Where manganese is specified only as a maximum the limit value is 1,80 % and the 70 % rule (see 3.1.2) does not apply.		

### 2.3.2 *Classification of main quality classes*

Steel grades can be classified into the following quality classes [1]:

- Non alloy steels:
  - Non alloy quality steels: in general they have specified property requirements such as toughness, grain size control and formability;
  - Non alloy special steels: have a higher degree of cleanness than quality steels (especially with respect to non-metallic inclusions) and have improved properties related to yield strength or hardenability associated with suitability for cold forming, welding or toughness.
- Stainless steels: steels with at least 10.5% of chromium and maximum 1.2% of carbon. They are further subdivided depending on the nickel content (nickel content of 2.5%) or main property (corrosion, heat or creep resisting);
- Other alloy steels:
  - Alloy quality steels: steel grades with requirements for toughness, grain size control or formability.
  - Alloy special steels: steel grades characterized by precise control of chemical composition and particular conditions of manufacture and process control to ensure improved properties.

## 2.4 **Quality Standards for Structural Steels**

In this section the form of a quality standard is described and the main points are analysed.

### 2.4.1 *Delivery conditions*

The following delivery conditions are available for European steels:

- Normalized: the steel is heated slightly above its upper critical temperature and held for sufficient time to allow new, smaller grains to form and high energy grain shapes to blend, also known as grain refinement;
- Normalized rolled: rolling process in which the final deformation is carried out in a certain temperature range leading to a material condition equivalent to that obtained after normalizing so that the specified values of the mechanical properties are retained even after normalizing [3];
- As-rolled: delivery condition without any special rolling and/or heat treatment condition [3];
- Thermo mechanical rolled: rolling process in which the final deformation is carried out in a certain temperature range leading to a material condition with certain properties which cannot be achieved or repeated by heat treatment alone [3];
- Quenched: operation which consists of cooling a ferrous product more rapidly than in still air [4];
- Tempered: heat treatment applied to a ferrous product generally after quench hardening or other heat treatment to bring the properties to the required level [4].

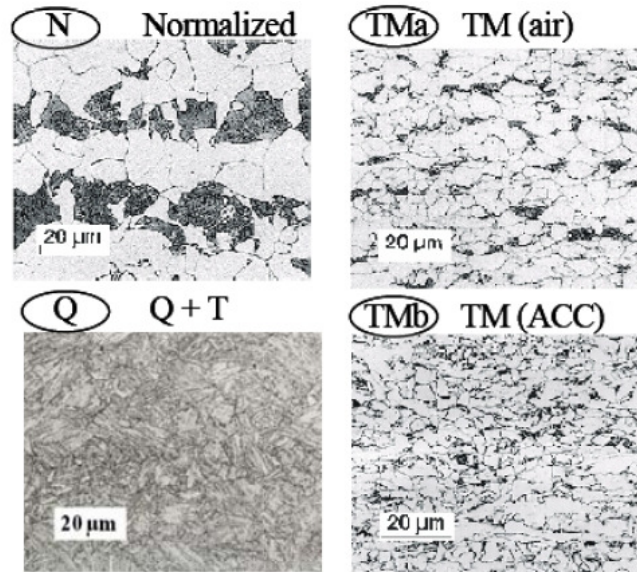


Figure 2.2 – Microstructures of various delivery conditions [5]

Where: ACC – Accelerated cooling

Depending on the different delivery conditions the steel properties can be greatly influenced due to the changes in the microstructure. In the N condition steels with moderate strength and toughness requirements up to S460N can be produced. In the QT condition the plate is reheated and then cooled in water (Q). This results in a structure with a high strength but low toughness and with an additional tempering process a satisfactory combination of tensile and toughness properties can be produced. The effect of tempering on the mechanical properties is shown in Figure 2.3. In this delivery condition steels with yield strengths of up to 1100MPa can be produced [5].

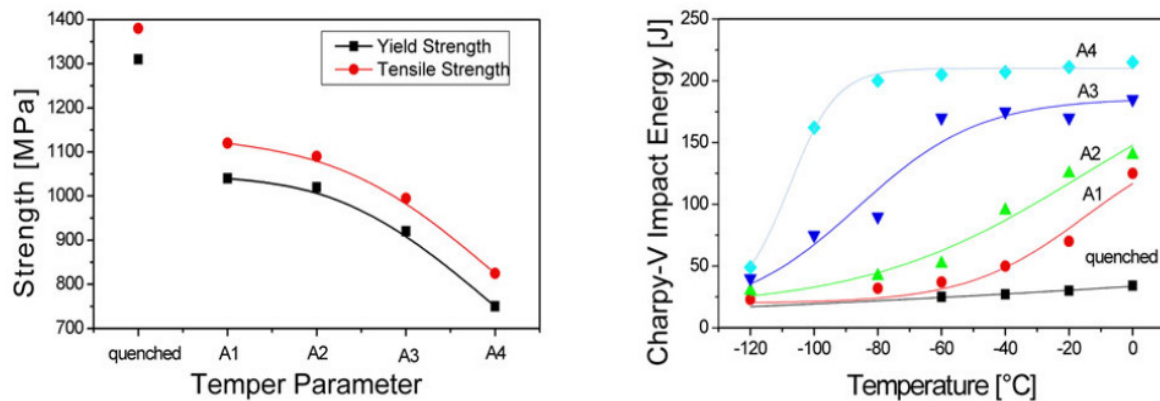


Figure 2.3 – Influence of increasing tempering temperatures on the tensile properties (left) and on the Charpy V transition temperature (right) –S890QL, 60mm [5]

The TM method results in a fine grained microstructure which leads to an increased tensile and toughness property of the steel. This is realised through a skilled combination of rolling steps at particular temperatures and close temperature control. Due to the improved microstructure reduced carbon content is allowed which has the advantage of an improved weldability. Plates with minimum yield strength of 500MPa and thicknesses up to 100mm can be supplied. Even higher yield strength of up to 690MPa is available but only with limited thickness [6]

### 2.4.2 Chemical composition

The strength of steel is dictated by its microstructure which depends on the chemical composition, the thermal history and deformation process undertaken in the production process. In order to improve the strength property, there are two options: grain refinement (depends on the delivery condition) or by increasing the carbon content. The advantage of the previous is that the material has a gain in strength along with good toughness and excellent weldability, while the later results in a more brittle material. Figure 2.4 plots the attainable yield strength function of the carbon equivalent and delivery condition. Besides Carbon other alloying elements may be present in the steel. For hot rolled products of structural steels the chemical composition determined by ladle analysis shall comply in all cases with the specified values of Table 2 to Table 6 [3].

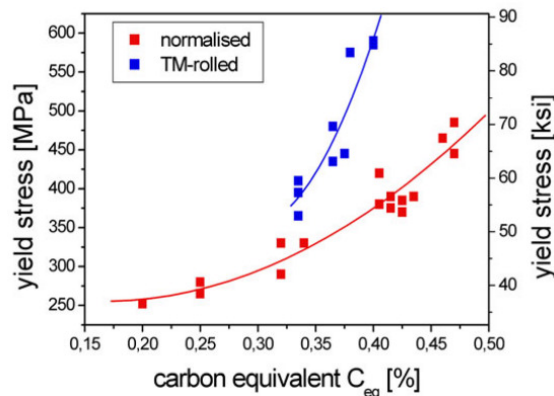


Figure 2.4 – Attainable yield strength in dependence on the carbon equivalent CE [5]

Table 2 – Chemical composition of the ladle analysis for flat and long products of steel grades and qualities with values for the impact strength [3]

Designation		Method of deoxidation b	C in % max. for nominal product thickness in mm			Si % max.	Mn % max.	P % max.	S % max.	N % max.	Cu % max.	Other % max.
According EN 10027-1 and CR 10260	According EN 10027-2		≤ 16	> 16 ≤ 40	> 40 <sup>c</sup>							
S235JR	1.0038	FN	0,17	0,17	0,20	-	1,40	0,035	0,035	0,012	0,55	-
S235J0	1.0114	FN	0,17	0,17	0,17	-	1,40	0,030	0,030	0,012	0,55	-
S235J2	1.0117	FF	0,17	0,17	0,17	-	1,40	0,025	0,025	-	0,55	-
S275JR	1.0044	FN	0,21	0,21	0,22	-	1,50	0,035	0,035	0,012	0,55	-
S275J0	1.0143	FN	0,18	0,18	0,18 <sup>i</sup>	-	1,50	0,030	0,030	0,012	0,55	-
S275J2	1.0145	FF	0,18	0,18	0,18 <sup>i</sup>	-	1,50	0,025	0,025	-	0,55	-
S355JR	1.0045	FN	0,24	0,24	0,24	0,55	1,60	0,035	0,035	0,012	0,55	-
S355J0	1.0553	FN	0,20 <sup>j</sup>	0,20 <sup>k</sup>	0,22	0,55	1,60	0,030	0,030	0,012	0,55	-
S355J2	1.0577	FF	0,20 <sup>j</sup>	0,20 <sup>k</sup>	0,22	0,55	1,60	0,025	0,025	-	0,55	-
S355K2	1.0596	FF	0,20 <sup>j</sup>	0,20 <sup>k</sup>	0,22	0,55	1,60	0,025	0,025	-	0,55	-
S450J <sup>l</sup>	1.0590	FF	0,20	0,20 <sup>k</sup>	0,22	0,55	1,70	0,030	0,030	0,025	0,55	<sup>m</sup>

<sup>a</sup> See 7.2.  
<sup>b</sup> FN = rimming steels not permitted; FF = fully killed steel (see 6.2.2).  
<sup>c</sup> For sections with nominal thickness > 100 mm the C content by agreement.  
 See option 26.  
<sup>d</sup> For long products the P and S content can be 0,005 % higher.  
<sup>e</sup> For long products the max. S content can be increased for improved machinability by 0,015 % by agreement if the steel is treated to modify the sulphide morphology and the chemical composition shows min. 0,0020 % Ca.  
 See option 27.  
<sup>f</sup> The max. value for nitrogen does not apply if the chemical composition shows a minimum total Al content of 0,020 % or alternatively min. 0,015 % acid soluble Al or if sufficient other N binding elements are present. In this case the N binding elements shall be mentioned in the inspection document.  
<sup>g</sup> Cu content above 0,40 % may cause hot shortness during hot forming.  
<sup>h</sup> If other elements are added, they shall be mentioned on the inspection document.  
<sup>i</sup> For nominal thickness > 150 mm: C = 0,20 % max..  
<sup>j</sup> For grades suitable for cold roll forming (see 7.4.2.2.3): C = 0,22 % max..  
<sup>k</sup> For nominal thickness > 30 mm: C = 0,22 % max..  
<sup>l</sup> Applicable for long products only.  
<sup>m</sup> The steel may show a Nb content of max. 0,05 %, a V content of max. 0,13 % and a Ti content of max. 0,05 %.

Table 3 – Chemical composition of the ladle analysis for normalized steel [7]

Designation		C % max.	Si % max.	Mn %	P % max. <sup>a</sup>	S % max. <sup>a, b</sup>	Nb % max.	V % max.	Al <sup>total</sup> % min. <sup>c</sup>	Ti % max.	Cr % max.	Ni % max.	Mo % max.	Cu % max. <sup>d</sup>	N % max.
According EN 10027-1 and CR 10260	According EN 10027-2														
S275N	1.0490	0,18	0,40	0,50 - 1,50	0,030	0,025	0,05	0,05	0,02	0,05	0,30	0,30	0,10	0,55	0,015
S275NL	1.0491	0,16			0,025	0,020									
S355N	1.0545	0,20	0,50	0,90 - 1,65	0,030	0,025	0,05	0,12	0,02	0,05	0,30	0,50	0,10	0,55	0,015
S355NL	1.0546	0,18			0,025	0,020									
S420N	1.8902	0,20	0,60	1,00 - 1,70	0,030	0,025	0,05	0,20	0,02	0,05	0,30	0,80	0,10	0,55	0,025
S420NL	1.8912				0,025	0,020									
S460N <sup>e</sup>	1.8901 <sup>e</sup>	0,20	0,60	1,00 - 1,70	0,030	0,025	0,05	0,20	0,02	0,05	0,30	0,80	0,10	0,55	0,025
S460NL <sup>e</sup>	1.8903 <sup>e</sup>				0,025	0,020									

<sup>a</sup> For long products the P and S content can be 0,005 % higher.  
<sup>b</sup> For railway applications a maximum S content of 0,010 % may be agreed at the time of enquiry and order.  
 See option 32.  
<sup>c</sup> If sufficient other N-binding elements are present the minimum total Al content does not apply.  
<sup>d</sup> Cu content above 0,40 % may cause hot shortness during hot forming.  
<sup>e</sup> V + Nb + Ti ≤ 0,22 % and Mo + Cr ≤ 0,30 %.

Table 4 – Chemical composition of the ladle analysis for the thermo mechanical rolled steel [8]

Designation		C % max.	Si % max.	Mn % max.	P % max. <sup>a</sup>	S % max. <sup>a, b</sup>	Nb % max.	V % max.	Al <sup>total</sup> % min. <sup>c</sup>	Ti % max.	Cr % max.	Ni % max.	Mo % max.	Cu % max. <sup>d</sup>	N % max.
According EN 10027-1 and CR 10260	According EN 10027-2														
S275M	1.8818	0,13 <sup>e</sup>	0,50	1,50	0,030	0,025	0,05	0,08	0,02	0,05	0,30	0,30	0,10	0,55	0,015
S275ML	1.8819				0,025	0,020									
S355M	1.8823	0,14 <sup>e</sup>	0,50	1,60	0,030	0,025	0,05	0,10	0,02	0,05	0,30	0,50	0,10	0,55	0,015
S355ML	1.8834				0,025	0,020									
S420M	1.8825	0,16 <sup>f</sup>	0,50	1,70	0,030	0,025	0,05	0,12	0,02	0,05	0,30	0,80	0,20	0,55	0,025
S420ML	1.8836				0,025	0,020									
S460M	1.8827	0,16 <sup>f</sup>	0,60	1,70	0,030	0,025	0,05	0,12	0,02	0,05	0,30	0,80	0,20	0,55	0,025
S460ML	1.8838				0,025	0,020									

<sup>a</sup> For long products the P and S content can be 0,005 % higher.  
<sup>b</sup> For railway applications a maximum S content of 0,010 % may be agreed at the time of enquiry and order.  
 See option 32.  
<sup>c</sup> If sufficient other N-binding elements are present the minimum total Al content does not apply.  
<sup>d</sup> Cu content above 0,40 % may cause hot shortness during hot forming.  
<sup>e</sup> For long products a maximum C content of 0,15 % for grade S275 and a maximum C content of 0,16 % for grade S355 applies.  
<sup>f</sup> For long products of the grades S420 and S460 a maximum C content of 0,18 % applies.

Table 5 – Chemical composition of the ladle analysis of steels with improved atmospheric corrosion resistance [9]

Designation		Method of deoxidation a	C % max.	Si % max.	Mn %	P % b	S % max. b	N % max.	Addition of nitrogen binding elements c	Cr %	Cu %	Others
According EN 10027-1 and CR 10260	According EN 10027-2											
S235J0W	1.8958	FN	0,13	0,40	0,20 - 0,60	max. 0,035	0,035	0,009 <sup>d e</sup>	-	0,40 - 0,80	0,25 - 0,55	*
S235J2W	1.8961	FF							yes			
S355J0WP	1.8945	FN	0,12	0,75	max. 1,0	0,06 - 0,15	0,035	0,009 <sup>g</sup>	-	0,30 - 1,25	0,25 - 0,55	e
S355J2WP	1.8946	FF							yes			
S355J0W	1.8959	FN	0,16	0,50	0,50 - 1,50	max. 0,035 max. 0,030	0,035 0,030	0,009 <sup>d e</sup>	-	0,40 - 0,80	0,25 - 0,55	* f
S355J2W	1.8965	FF							yes			
S355K2W	1.8967	FF							yes			

\* FN = rimming steels not permitted; FF = fully killed steel (see 6.2.2).  
 b For long products the P and S content can be 0,005 % higher.  
 c The steels shall contain at least one of the following elements: Al total  $\geq 0,020$  %, Nb: 0,015 - 0,060 %, V: 0,02 - 0,12 %, Ti: 0,02 - 0,10 %. If these elements are used in combination, at least one of them shall be present with the minimum content indicated.  
 d It is permissible to exceed the specified values provided that for each increase of 0,001 % N the P max. content will be reduced by 0,005 %; the N content of the ladle analysis, however, shall not be more than 0,012 %.  
 e The steels may show a Ni content of max. 0,65 %.  
 f The steels may contain max. 0,30 % Mo and max. 0,15 % Zr.  
 g The max. value for nitrogen does not apply if the chemical composition shows a minimum total Al content of 0,020 % or if sufficient other N binding elements are present. The N binding elements shall be mentioned in the inspection document.

Table 6 – Chemical composition of the ladle analysis for quenched and tempered steels [4]

Grade	Quality	C % max.	Si % max.	Mn % max.	P % max.	S % max.	N % max.	B % max.	Cr % max.	Cu % max.	Mo % max.	Nb % max. b	Ni % max.	Ti % max. b	V % max. b	Zr % max. b
All grades	(no symbol) L L1	0,20	0,80	1,70	0,025 0,020 0,020	0,015 0,010 0,010	0,015	0,005 0	1,50	0,50	0,70	0,06	2,0	0,05	0,12	0,15

a Depending on the thickness of the product and the manufacturing conditions, the manufacturer may add to the steel one or several alloying elements up to the maximum values given in order to obtain the specified properties (see 7.2.2).  
 b There shall be at least 0,015 % of a grain-refining element present. Aluminium is also one of these elements. The minimum content of 0,015 % applies to soluble aluminium, this value is regarded as attained if the total aluminium content is at least 0,018 %; in case of dispute the soluble aluminium content shall be determined.

## 2.5 Mechanical Properties

Quality standards generally specify tensile (minimum yield strength, tensile strength and elongation) and notch toughness properties. [10] and [11] describe the material requirements with respect to mild steels and high strength steels while [12] gives values of notch toughness. The material properties described should be adopted as characteristic values in the design calculations.

### 2.5.1 Tensile properties

The nominal values of the yield strength and ultimate strength can be obtained either from the product standard or by using the simplification given by the tables below.

The grain refinement during rolling is smaller for thicker plates which results in lower yield strength and tensile strength with increasing thickness. This is translated into a dependency of the required values function of the material thickness.

Table 7 – Nominal values of yield strength  $f_y$  and ultimate tensile strength  $f_u$  for hot rolled structural steel [10]

Standard and steel grade	Nominal thickness of the element t [mm]			
	t ≤ 40 mm		40 mm < t ≤ 80 mm	
	$f_y$ [N/mm <sup>2</sup> ]	$f_u$ [N/mm <sup>2</sup> ]	$f_y$ [N/mm <sup>2</sup> ]	$f_u$ [N/mm <sup>2</sup> ]
<b>EN 10025-2</b>				
S 235	235	360	215	360
S 275	275	430	255	410
S 355	355	510	335	470
S 450	440	550	410	550
<b>EN 10025-3</b>				
S 275 N/NL	275	390	255	370
S 355 N/NL	355	490	335	470
S 420 N/NL	420	520	390	520
S 460 N/NL	460	540	430	540
<b>EN 10025-4</b>				
S 275 M/ML	275	370	255	360
S 355 M/ML	355	470	335	450
S 420 M/ML	420	520	390	500
S 460 M/ML	460	540	430	530
<b>EN 10025-5</b>				
S 235 W	235	360	215	340
S 355 W	355	510	335	490
<b>EN 10025-6</b>				
S 460 Q/QL/QL1	460	570	440	550

Table 8 - Nominal values of yield strength  $f_y$  and ultimate tensile strength  $f_u$  for structural hollow sections [10]

Standard and steel grade	Nominal thickness of the element t [mm]			
	t ≤ 40 mm		40 mm < t ≤ 80 mm	
	$f_y$ [N/mm <sup>2</sup> ]	$f_u$ [N/mm <sup>2</sup> ]	$f_y$ [N/mm <sup>2</sup> ]	$f_u$ [N/mm <sup>2</sup> ]
<b>EN 10210-1</b>				
S 235 H	235	360	215	340
S 275 H	275	430	255	410
S 355 H	355	510	335	490
S 275 NH/NLH	275	390	255	370
S 355 NH/NLH	355	490	335	470
S 420 NH/NLH	420	540	390	520
S 460 NH/NLH	460	560	430	550
<b>EN 10219-1</b>				
S 235 H	235	360		
S 275 H	275	430		
S 355 H	355	510		
S 275 NH/NLH	275	370		
S 355 NH/NLH	355	470		
S 460 NH/NLH	460	550		
S 275 MH/MLH	275	360		
S 355 MH/MLH	355	470		
S 420 MH/MLH	420	500		
S 460 MH/MLH	460	530		

Where:

EN 10210-1 Hot finished structural hollow sections of non-alloy and fine grain steels

EN 10219-1 Cold formed welded structural hollow sections of non-alloy and fine grain steels

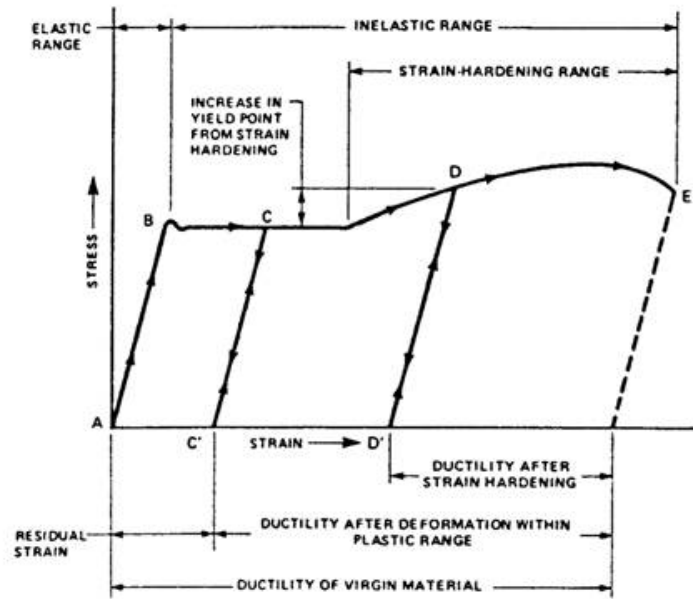


Figure 2.5 – Initial portions of stress-strain curve for mild steel [13]

Figure 2.5 illustrates the stress-strain curve of mild steel. A clear yielding strength (point B), yielding plateau and strain hardening can be noticed. This ensures the material has high deformation capacity.

In the case of high strength steels the nominal strength values are given in Table 9 and Table 10 from [11].

Table 9 – Nominal values of yield strength  $f_y$  and ultimate tensile strength  $f_u$  for hot rolled structural steel [11]

EN10025-6 Steel grade and qualities	Nominal thickness of the element $t$ mm					
	$t \leq 50$ mm		$50 \text{ mm} < t \leq 100$ mm		$100 \text{ mm} < t \leq 150$ mm	
	$f_y$ [N/mm <sup>2</sup> ]	$f_u$ [N/mm <sup>2</sup> ]	$f_y$ [N/mm <sup>2</sup> ]	$f_u$ [N/mm <sup>2</sup> ]	$f_y$ [N/mm <sup>2</sup> ]	$f_u$ [N/mm <sup>2</sup> ]
S 500Q/QL/QL1	500	590	480	590	440	540
S 550Q/QL/QL1	550	640	530	640	490	590
S 620Q/QL/QL1	620	700	580	700	560	650
S 690Q/QL/QL1	690	770	650	760	630	710

Table 10 – Nominal values of yield strength  $f_y$  and ultimate tensile strength  $f_u$  for hot rolled flat products [11]

EN 10149-2a)	$1,5 \text{ mm} \leq t \leq 8 \text{ mm}$		$8 \text{ mm} < t \leq 16 \text{ mm}$	
	$f_y$ [N/mm <sup>2</sup> ]	$f_u$ [N/mm <sup>2</sup> ]	$f_y$ [N/mm <sup>2</sup> ]	$f_u$ [N/mm <sup>2</sup> ]
S 500MC	500	550	500	550
S 550MC	550	600	550	600
S 600MC	600	650	600	650
S 650MC	650	700	630	700
S 700MC	700	750	680	750

a) Verification of the impact energy in accordance with EN 10149-1 Clause 11, Option 5 should be specified.

Where:

EN 10149-2 Specifications for hot-rolled flat products made of high yield strength steels for cold forming. Delivery conditions for thermo mechanically rolled steels.

The stress-strain curve for mild and high strength steels differ significantly. In the case of high strength steel the yield strength is defined as the 0.2 percent offset (permanent elongation). This is used due to the lack of a clearly defined yield plateau.

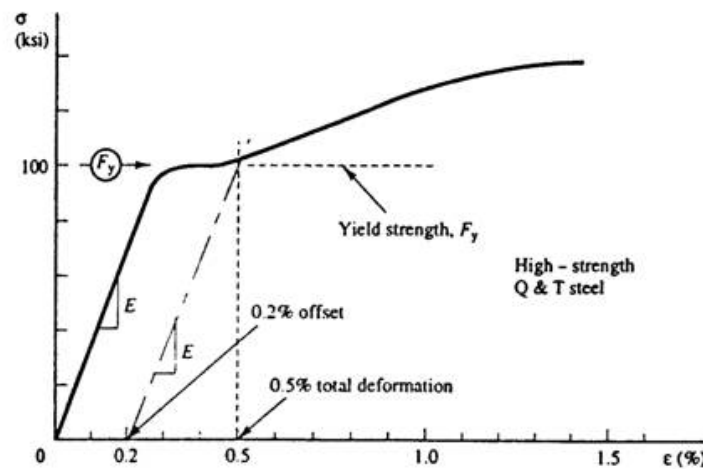


Figure 2.6 – Initial portions of stress-strain curve for high strength steel [13]

### 2.5.2 Ductility properties

In [10], Section 3.2.2 specifies the following ductility requirement limits for mild steels (up to and including steel grade S460):

- the ratio  $f_u/f_y$  of the specified minimum ultimate tensile strength  $f_u$  to the specified minimum yield strength  $f_y$  should be greater or equal to 1.10:  $f_u/f_y \geq 1.10$  ( $f_y/f_u \leq 0.91$ );
- the elongation at failure should not be less than 15%;
- the ultimate strain  $\epsilon_u \geq 15\epsilon_y$ .

In [11], Section 3.2.2(1) specifies the ductility requirements for high strength (steel grades higher than S460 and up to grade S700):

- $f_u/f_y \geq 1.05$  ( $f_y/f_u \leq 0.95$ );
- elongation at failure not less than 10%;
- $\epsilon_u \geq 15f_y/E$

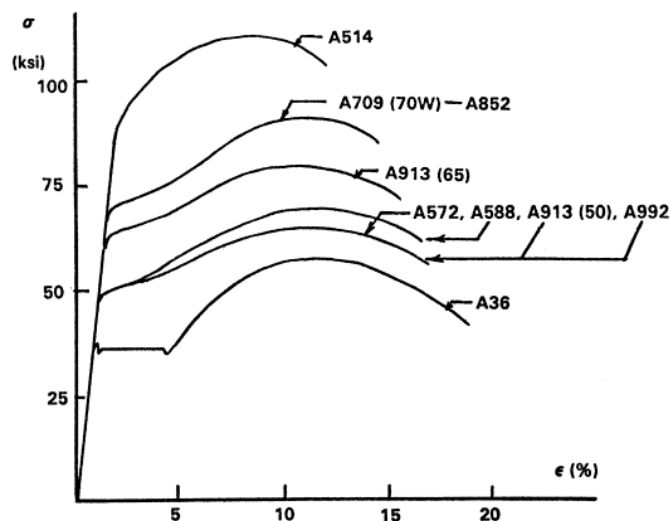


Figure 2.7 – Stress-strain curves for some structural steel grades [14]

With increasing strength of steel the ductility behaviour is lower. Figure 2.7 plots the stress-strain diagram for different steel grades (American steel grades with yield strengths ranging from 250MPa to 700MPa). As the strength of the grade increases there is a lack of a clear yielding plateau and the elongation at failure becomes lower.

### 2.5.3 Notch toughness properties

Notch toughness is influenced by the temperature and the type of loading. Figure 2.8 illustrates the fracture toughness-temperature response of steel under both static and dynamic loading. The results are obtained using Charpy V-Notch tests.

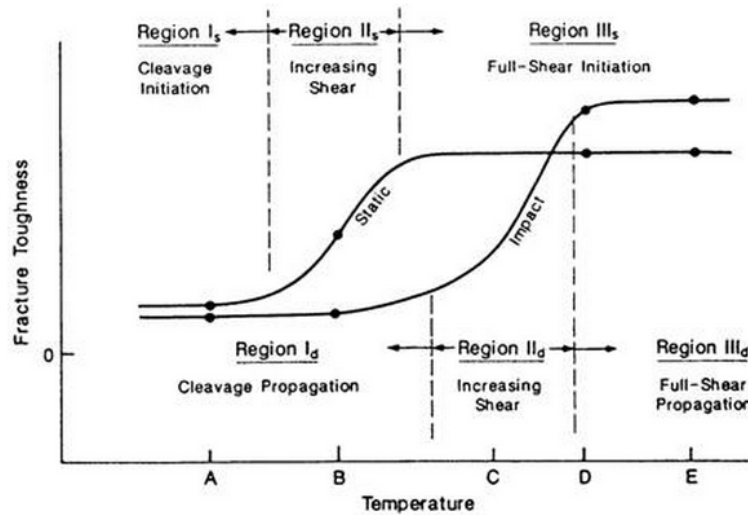


Figure 2.8 – Fracture toughness behaviour of steel [15]

An increase in the temperature results in a change from brittle to ductile fracture. At low temperatures the toughness is approximately the same for both static and dynamic loads while at higher temperatures it is higher for impact loading.

The delivery condition also has an impact on the toughness of the material. Figure 2.9 illustrates the difference between a normalized and a thermo-mechanically rolled steel of the same grade. The transition temperature between brittle and tough fracture behaviour (defined by the temperature where Charpy-V impact energy of 27J is attained) is reduced significantly in the TM rolling compared to the N steel [16].

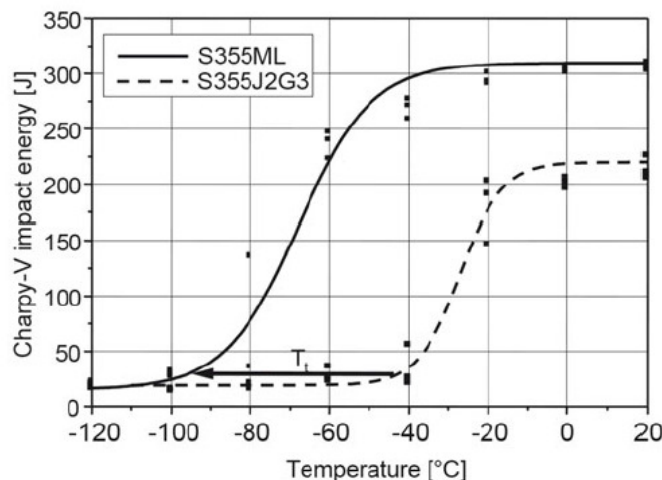


Figure 2.9 – Comparison of the Charpy-V-temperature transition curve for a conventional normalized steel S355J2+N and a TM rolled steel S355ML [16]

The material must have sufficient fracture toughness to avoid brittle fracture of tension elements at the lowest service temperature that can occur during the designed lifetime of the structure. Table 11 specifies maximum values of element thickness depending on the steel grade and the minimum Charpy-V energy values. If the steel grades are taken from this table and they comply with the conditions given in [12] then no further testing is required.

Table 11 – Maximum permissible values of element thickness in mm [12]

Steel grade	Sub-grade	Charpy energy CVN at T [°C]	J <sub>min</sub>	Reference temperature T <sub>Ed</sub> [°C]																				
				σ <sub>Ed</sub> = 0,75 f <sub>y</sub> (t)							σ <sub>Ed</sub> = 0,50 f <sub>y</sub> (t)							σ <sub>Ed</sub> = 0,25 f <sub>y</sub> (t)						
				10	0	-10	-20	-30	-40	-50	10	0	-10	-20	-30	-40	-50	10	0	-10	-20	-30	-40	-50
S235	JR	20	27	60	50	40	35	30	25	20	90	75	65	55	45	40	35	135	115	100	85	75	65	60
	J0	0	27	90	75	60	50	40	35	30	125	105	90	75	65	55	45	175	155	135	115	100	85	75
	J2	-20	27	125	105	90	75	60	50	40	170	145	125	105	90	75	65	200	200	175	155	135	115	100
S275	JR	20	27	55	45	35	30	25	20	15	80	70	55	50	40	35	30	125	110	95	80	70	60	55
	J0	0	27	75	65	55	45	35	30	25	115	95	80	70	55	50	40	165	145	125	110	95	80	70
	J2	-20	27	110	95	75	65	55	45	35	155	130	115	95	80	70	55	200	190	165	145	125	110	95
	M,N	-20	40	135	110	95	75	65	55	45	180	155	130	115	95	80	70	200	200	190	165	145	125	110
	ML,NL	-50	27	185	160	135	110	95	75	65	200	200	180	155	130	115	95	230	200	200	190	165	145	130
S355	JR	20	27	40	35	25	20	15	10	65	55	45	40	30	25	20	110	95	80	70	60	55	45	
	J0	0	27	60	50	40	35	25	20	15	95	80	65	55	45	40	30	150	130	110	95	80	70	60
	J2	-20	27	90	75	60	50	40	35	25	135	110	95	80	65	55	45	200	175	150	130	110	95	80
	K2,M,N	-20	40	110	90	75	60	50	40	35	155	135	110	95	80	65	55	200	200	175	150	130	110	95
	ML,NL	-50	27	155	130	110	90	75	60	50	200	180	155	135	110	95	80	210	200	200	200	175	150	130
S420	M,N	-20	40	95	80	65	55	45	35	30	140	120	100	85	70	60	50	200	185	160	140	120	100	85
	ML,NL	-50	27	135	115	95	80	65	55	45	190	165	140	120	100	85	70	200	200	200	185	160	140	120
S460	Q	-20	30	70	60	50	40	30	25	20	110	95	75	65	55	45	35	175	155	130	115	95	80	70
	M,N	-20	40	90	70	60	50	40	30	25	130	110	95	75	65	55	45	200	175	155	130	115	95	80
	QL	-40	30	105	90	70	60	50	40	30	155	130	110	95	75	65	55	200	200	175	155	130	115	95
	ML,NL	-50	27	125	105	90	70	60	50	40	180	155	130	110	95	75	65	200	200	200	175	155	130	115
	QL1	-60	30	150	125	105	90	70	60	50	200	180	155	130	110	95	75	215	200	200	200	175	155	130
S690	Q	0	40	40	30	25	20	15	10	10	65	55	45	35	30	20	20	120	100	85	75	60	50	45
	Q	-20	30	50	40	30	25	20	15	10	80	65	55	45	35	30	20	140	120	100	85	75	60	50
	QL	-20	40	60	50	40	30	25	20	15	95	80	65	55	45	35	30	165	140	120	100	85	75	60
	QL	-40	30	75	60	50	40	30	25	20	115	95	80	65	55	45	35	190	165	140	120	100	85	75
	QL1	-40	40	90	75	60	50	40	30	25	135	115	95	80	65	55	45	200	190	165	140	120	100	85
QL1	-60	30	110	90	75	60	50	40	30	160	135	115	95	80	65	55	200	200	190	165	140	120	100	

Table 12 specifies maximum element thickness depending on the steel grade and the minimum Charpy-V energy values. Grades taken from this table and satisfying the conditions given in [12] for the lowest temperature do not require any further testing against brittle fracture as they are assumed to have sufficient toughness [10].

Figure 2.10 illustrates the transition curves for the Charpy-V energy against the test temperature for S460ML, S690QL and S355J2. High strength steels show significantly higher values at the testing temperature than given in the standards [17].

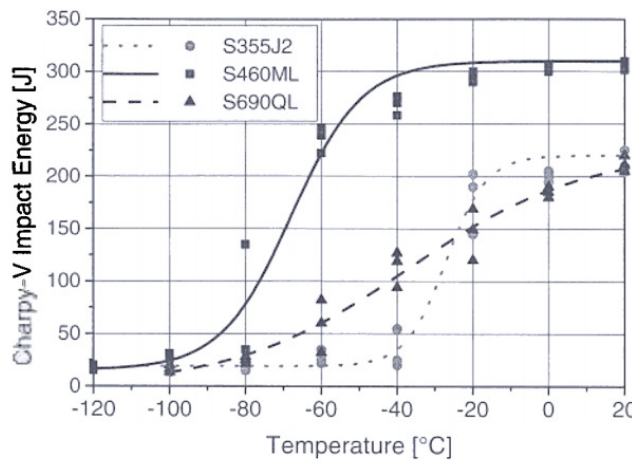


Figure 2.10 – Charpy V-temperature transition curves for S460ML and S690QL with S355J2 for comparison [17]

Table 12 – Maximum permissible values of element thickness  $t$  in mm [11]

Steel grade	Subgrade	Charpy energy CVN	Reference temperature $T_{Ed}$ [°C]																																									
			10						0						-10						-20						-30						-40						-50					
			at $T$ [°C]		$J_{min}$		$\sigma_{Ed} = 0,75 f_y(t)$						$\sigma_{Ed} = 0,50 f_y(t)$						$\sigma_{Ed} = 0,25 f_y(t)$																									
<b>EN 10025-6</b>																																												
S500	Q	0	40	55	45	35	30	20	15	15	85	70	60	50	40	35	25	145	125	105	90	80	65	55																				
	Q	-20	30	65	55	45	35	30	20	15	105	85	70	60	50	40	35	170	145	125	105	90	80	65																				
	QL	-20	40	80	65	55	45	35	30	20	125	105	85	70	60	50	40	195	170	145	125	105	90	80																				
	QL	-40	30	100	80	65	55	45	35	30	145	125	105	85	70	60	50	200	195	170	145	125	105	90																				
	QL1	-40	40	120	100	80	65	55	45	35	170	145	125	105	85	70	60	200	200	195	170	145	125	105																				
	QL1	-60	30	140	120	100	80	65	55	45	200	170	145	125	105	85	70	205	200	200	195	170	145	125																				
S550	Q	0	40	50	40	30	25	20	15	10	80	65	55	45	35	30	25	140	120	100	85	75	60	50																				
	Q	-20	30	60	50	40	30	25	20	15	95	80	65	55	45	35	30	160	140	120	100	85	75	60																				
	QL	-20	40	75	60	50	40	30	25	20	115	95	80	65	55	45	35	185	160	140	120	100	85	75																				
	QL	-40	30	90	75	60	50	40	30	25	135	115	95	80	65	55	45	200	185	160	140	120	100	85																				
	QL1	-40	40	110	90	75	60	50	40	30	160	135	115	95	80	65	55	200	200	185	160	140	120	100																				
	QL1	-60	30	130	110	90	75	60	50	40	185	160	135	115	95	80	65	200	200	200	185	160	140	120																				
S620	Q	0	40	45	35	25	20	15	10	10	70	60	50	40	30	25	20	130	110	95	80	65	55	45																				
	Q	-20	30	55	45	35	25	20	15	15	85	70	60	50	40	30	25	150	130	110	95	80	65	55																				
	QL	-20	40	65	55	45	35	25	20	15	105	85	70	60	50	40	30	175	150	130	110	95	80	65																				
	QL	-40	30	80	65	55	45	35	25	20	125	105	85	70	60	50	40	200	175	150	130	110	95	80																				
	QL1	-40	40	100	80	65	55	45	35	25	145	125	105	85	70	60	50	200	200	175	150	130	110	95																				
	QL1	-60	30	120	100	80	65	55	45	35	170	145	125	105	85	70	60	200	200	200	175	150	130	110																				
S690	Q	0	40	40	30	25	20	15	10	10	65	55	45	35	30	20	20	120	100	85	75	60	50	45																				
	Q	-20	30	50	40	30	25	20	15	10	80	65	55	45	35	30	20	140	120	100	85	75	60	50																				
	QL	-20	40	60	50	40	30	25	20	15	95	80	65	55	45	35	30	165	140	120	100	85	75	60																				
	QL	-40	30	75	60	50	40	30	25	20	115	95	80	65	55	45	35	190	165	140	120	100	85	75																				
	QL1	-40	40	90	75	60	50	40	30	25	135	115	95	80	65	55	45	200	190	165	140	120	100	85																				
	QL1	-60	30	110	90	75	60	50	40	30	160	135	115	95	80	65	55	200	200	190	165	140	120	100																				
<b>EN 10149-2</b>																																												
S500	MC	-20	40	80	65	55	45	35	30	20	125	105	85	70	60	50	40	195	170	145	125	105	90	80																				
S550	MC	-20	40	75	60	50	40	30	25	20	115	95	80	65	55	45	35	185	160	140	120	100	85	75																				
S600	MC	-20	40	70	55	45	35	30	20	15	105	90	75	60	50	40	35	180	155	130	110	95	80	70																				
S650	MC	-20	40	65	50	40	30	25	20	15	100	85	70	55	45	35	30	170	145	125	105	90	75	65																				
S700	MC	-20	40	60	45	35	30	25	20	15	95	80	65	50	45	35	30	165	140	120	100	85	70	60																				

2.5.4 Through thickness properties

In the case when steel with improved through-thickness properties is required the choice of quality class should be made according to [12]. Depending on the chosen quality class, the through thickness properties should be specified from [18] or post fabrication inspection should be used to identify the occurrence of lamellar tearing.

Table 13 – Choice of quality class according to [18]

Target value of $Z_{Ed}$ according to EN 1993-1-10	Required value of $Z_{Rd}$ expressed in terms of design $Z$ -values according to EN 10164
$Z_{Ed} \leq 10$	—
$10 < Z_{Ed} \leq 20$	Z 15
$20 < Z_{Ed} \leq 30$	Z 25
$Z_{Ed} > 30$	Z 35

2.5.5 Design values of material coefficients

The material coefficients to be adopted in calculations for the structural steels should be taken as follows [10]:

- modulus of elasticity  $E=210000\text{N/mm}^2$ ;
- shear modulus  $G=E/(2+2\nu)=81000\text{N/mm}^2$ ;
- Poisson’s ratio in elastic range  $\nu=0.3$ ;
- coefficient of linear thermal expansion  $\alpha=12 \times 10^{-6}$  perK (for  $T \leq 100^\circ\text{C}$ ).

## 2.6 Technological Properties

Technological properties include weldability and formability.

### 2.6.1 Weldability

Weldability of a material refers to its ability to be welded and is judged on the basis of tendency to cold cracking and toughness of the heat affected zone. This is influenced by the chemical composition and metallographic structure of the steel. An increase in alloying elements will lead to a decrease in weldability while an improvement in grain refinement will have the opposite effect. The most common measure for weldability is the carbon equivalent. It is used to assess the combined effect of carbon and the other chemical elements on the cracking susceptibility. Weldability improves with lower values of the carbon equivalent. Figure 2.11 illustrates the effect of the carbon equivalent on the range of conditions which can be welded with a particular preheat (100°C) and a particular welding process (MAG with conventional wire electrodes) [2].

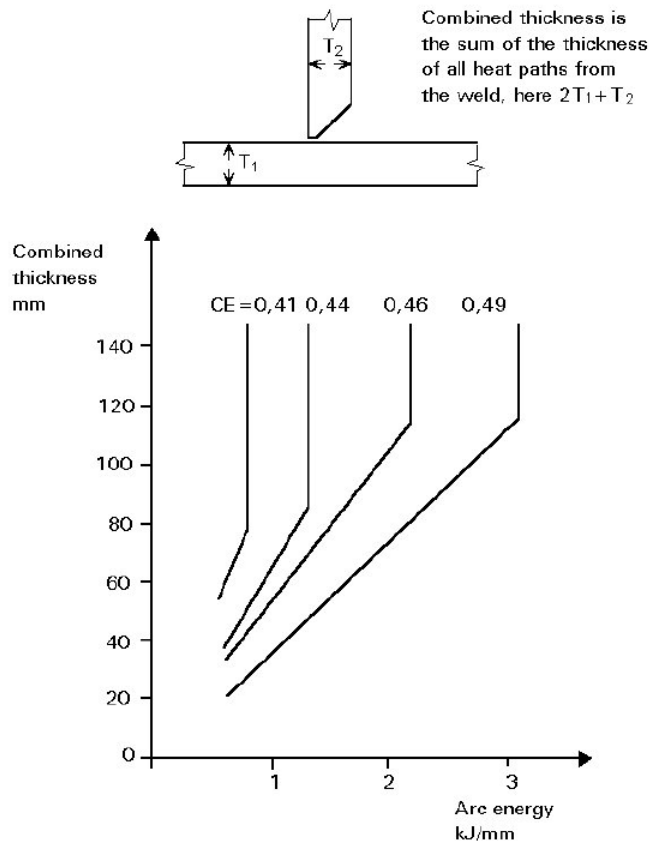


Figure 2.11 – Example of variation of weldability with composition: limiting conditions requiring a minimum pre-heat of 100°C for different values of carbon equivalent for MAG welding [2]

The temperature-time cycles during welding have a significant effect on the mechanical properties of a welded joint. The cooling time from 800°C to 500°C ( $t_{8/5}$ ) characterises the cooling conditions of an individual weld pass for the weld metal and the corresponding HAZ. An increase in the heat input and interpass temperature will slow down the cooling rate and result in longer cooling time and thus lower hardness in the HAZ [5].

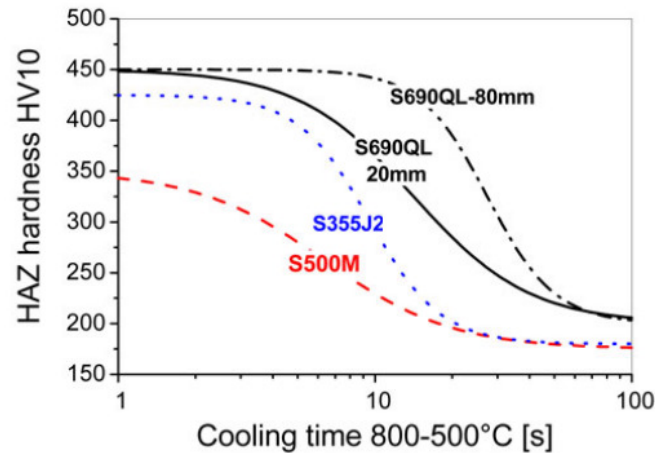


Figure 2.12 – Calculated hardness in the coarse grained HAZ as a function of weld cooling time ( $t_{8/5}$ ) for some structural steels in the as welded condition text [5]

In order to avoid cold cracking the following points should be considered [17]:

- The joint surfaces should be clean and dry;
- Preheating the parent material when recommended;
- Ensure a good fit and well planned sequence of weld runs in order to minimise the shrinkage stress;
- Use of a filler material with low hydrogen content.

The heat input determines the properties of the weld. A low heat input increases the hardness and the risk for cold cracking while a high heat input decreases the toughness. Examples of recommendations are: for S420M, S460M up to 5.3 kJ/mm; for S690Q up to 3.5 kJ/mm, depending in both cases on the combined plate thickness. For thinner combined thicknesses, below 60 to 80mm, the heat input must be reduced [17].

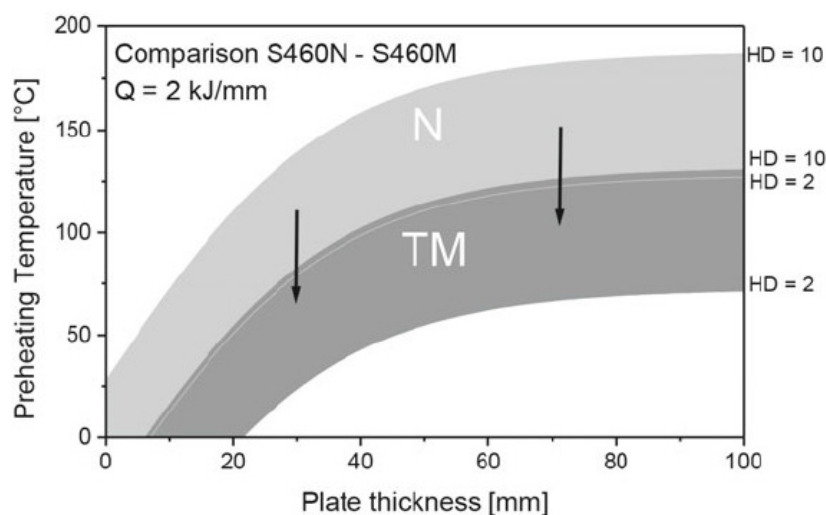


Figure 2.13 – Comparison of preheating temperatures according to [19] between normalized steel S460N and higher strength steel S460M [16]

General recommendations for welding steels are given in [19]. Most steel producers provide detailed information on welding.

### 2.6.2 Formability

Formability represent the ability of a given metal work piece to undergo plastic deformation without being damaged. Structural steels are suitable for hot and cold forming. [8] Restricts TM steels from undertaking hot forming. QT steels can be hot formed and [4] permits the process up to around 580°C (stress relief annealing temperature) [17].

Cold forming leads to reduction in the ductility. It includes flangeability, roll forming and drawing of bars. Cold formability is evaluated by bend tests for which samples can be taken in the longitudinal or transverse direction. The specified inside bending radius increases with increasing material thickness and tensile strength [2].

### 2.7 High Strength Steel Grades

Different countries from around the world have developed different steel grades depending on their specific needs. Of particular interest are the high strength steels that emerged in Europe, North America, Japan and South Korea. Table 14 gives a general picture of the material properties of each of the grades and chemical composition that has an impact on weldability (cold cracking and preheating temperature) [20].

Table 14 – HSS grade types [20]

	HSB800 (L/W)	BHS700W	HPS100W(690W)	S690Q
Process	TMCP	Direct QT	QT	QT
Max. Thick.	80 mm	100 mm	64 mm	100 mm
Min. Yp	690 MPa	700 MPa	690 MPa	690 MPa
Min. Ts	800 MPa	780 MPa	760 MPa	770 MPa
Toughness	47J @ -20°C 47J @ -40°C (L)	100J @ -40°C (Base) 47J @ -15°C (HAZ)	48J @ -34°C (FCM) 34J @ -34°C (Non-FCM)	40J @ -20°C (QL) 40J @ -40°C (QL1)
Ceq	≤ 0.55 ≤ 0.60 (W)	≤ 0.84	≤ 0.76	≤ 0.57
Pcm	≤ 0.25 ≤ 0.27 (W)	≤ 0.30 (t<50) ≤ 0.32 (t<100)	≤ 0.33	≤ 0.30
Spec.	KS D 3868	JIS G 3140	ASTM A709	EN10025 Part6

HSB800 and HPS100W represents South Korea’s and the United States of America’s developed high performance steels for bridges, BHS700W is Japan’s high-yield-point steel plates for bridges and S690Q is the high strength steel developed in the European Union. As illustrated in the table above, the minimum yield and tensile strength is approximately the same for all the steel grades. A significant difference is between the improved toughness of the Japanese, and the reduced carbon content and composition parameter of the Korean and European grades which lead to improved weldability.

## 2.8 Bridge Applications in High Strength Steel

### 2.8.1 In Europe

- Nesenbachtalbrücke, Germany

Built between 1998 and 2000, the Nesenbachtalbrücke is a 572 m long composite bridge with span lengths of 35.1 to 89.5m. Due to the slenderness requirements and high peak stresses in particular areas, the higher strength of S690QL1 was used for the design [21].



Figure 2.14 – The Nesenbachtalbrücke [21]

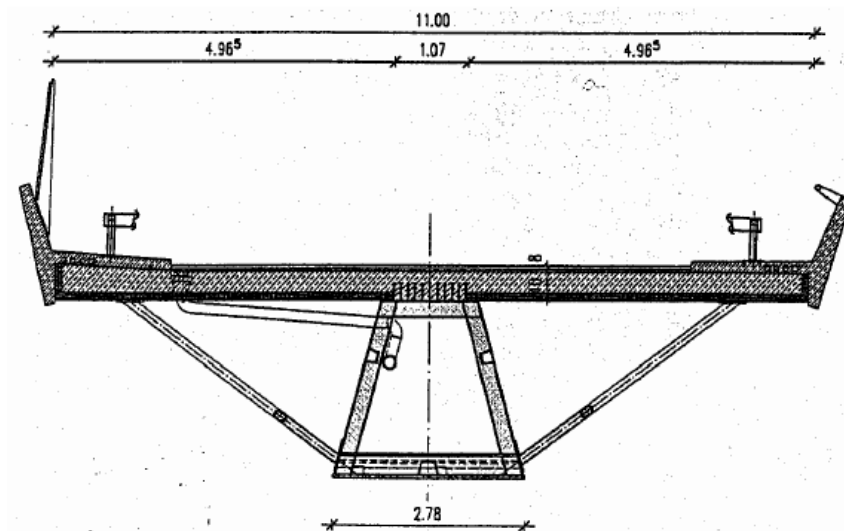


Figure 2.15 – Cross section of the Nesenbachtalbrücke [21]

- Fast bridge 48, Sweden

Developed by a shipyard company for the Swedish army, it is designed to resist a 65t tank for 1000 crossings. The clear span can reach up to 46m and the bridge should be transported by standard army lorries and be erected in 75 minutes by six men. The bridge was designed as a truss bridge using steel grade S1100 and has a working stress of 700MPa. Due to this high loading, deflection under full working load is as high as 0.65m (span/70), but because of its particular application there are no restrictions with respect to this [21].

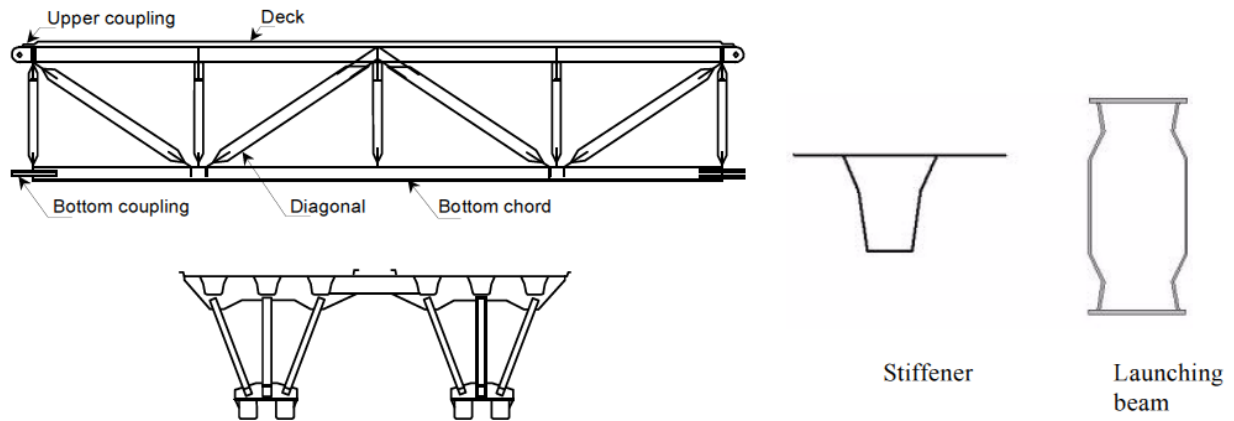


Figure 2.16 – Truss element for Fast Bridge 48 developed by Karlskronavarvet AB, Sweden [21]

- The Prince Clause bridge, The Netherlands

Opened in June 2003, this cable-stayed bridge has a total length of 300m (out of which 150m cable stayed main span) and 37m width, with a pylon height of 91.7m. High strength S460 weldable fine-grained structural steel in thicknesses of 20-100mm was used for the pylon elements. The bridge is used by the regional tramway rail, road traffic, cyclists and pedestrians to cross the Amsterdam Rhine canal [22].



Figure 2.17 – The Prince Clause bridge

- The bridge over the Hollandsch Diep, The Netherlands

This bridge was designed to carry the new high-speed railway connecting Brussels to Amsterdam. It spans over the Hollandsch Diep, having a length of 1400m divided into 12x105m spans and 2x70m spans. The steel structure consists of hammer-head-shaped elements above the piers, with connecting box-girder sections. Around 9700t of grade S355J2G3 and S460N plate in thicknesses of 210mm and up to 100mm were used for the fabrication of the bridge [22].



Figure 2.18 – The bridge over the Hollandsch Diep

- The Ennëus Heerma Bridge

With a 230m length and 28m width, this bowstring bridge carries a total of four motor-traffic carriageways, two tram lines, two cycle tracks and a pedestrian walkway. It has two main spans of 75m consisting of a 20m high centre-arch with two inclined side arches, connected to form inverse arches for the 30m central span. Around 1700t of heavy plate was used in the construction. Out of this, around 600t consisted of high-strength TM fine-grained structural steel with specified minimum yield strength of 460MPa in thicknesses of up to 100mm [22].



Figure 2.19 - The Ennëus Heerma bridge

- Remoulins bridge, France

Double-girder bridge, constructed from a combination of the TM-steels S355ML and S460ML. The later was applied in the high stressed areas near the piles in order to reduce the maximum thickness from 120mm (if only S355ML was used) to 80mm. This resulted in significant weight reduction and easier fabrication and erection [23].

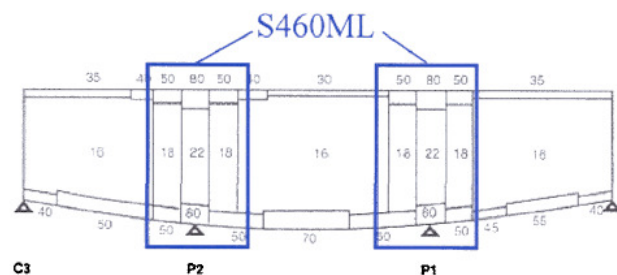


Figure 2.20 – Bridge of Remoulins and repartition of steel grades in the main girders [23]

- Erasmus bridge, The Netherlands

The bridge has a total length of 499m, with a 410m cable-stayed span and 89m flap bridge span. 4200t of S355M (with a thickness up to 100mm), 2000t of S460L (thickness up to 80mm) and some S460QL (thickness up to 125mm) were used for the construction [23].



Figure 2.21 – Erasmus bridge in Rotterdam, The Netherlands

- Ilverich bridge, Germany

The bridge crosses the river Rhine near Dusseldorf and due to its location near the airport the height had to be maintained as low as possible. This cable-stayed bridge, with a main span of 275m, was designed with V shaped pylons having the legs connected by a cross beam at the top. In order to resist the high arising stresses, the pylon heads were designed in S460ML with thickness up to 100mm [23].



Figure 2.22 – Ilverich bridge, Dusseldorf, Germany

### 2.8.2 In the USA

The first high performance HPS70W steel bridge was built in 1997 in Dodge County, Nebraska. The Snyder bridge is a 46m long single-span plate-girder bridge designed in HPS70W. Later, in 1998, the second bridge in high performance steel opened in Jackson County, Tennessee. It has a two 72m long HPS70W continuous plate-girder spans. Due to the redesign to optimize HPS70W, the superstructure weight was reduced about 25% at a cost saving of 10%. Since then more than 250 bridges with high performance steel components have been opened to traffic and more than 150 are in design or under construction [24].

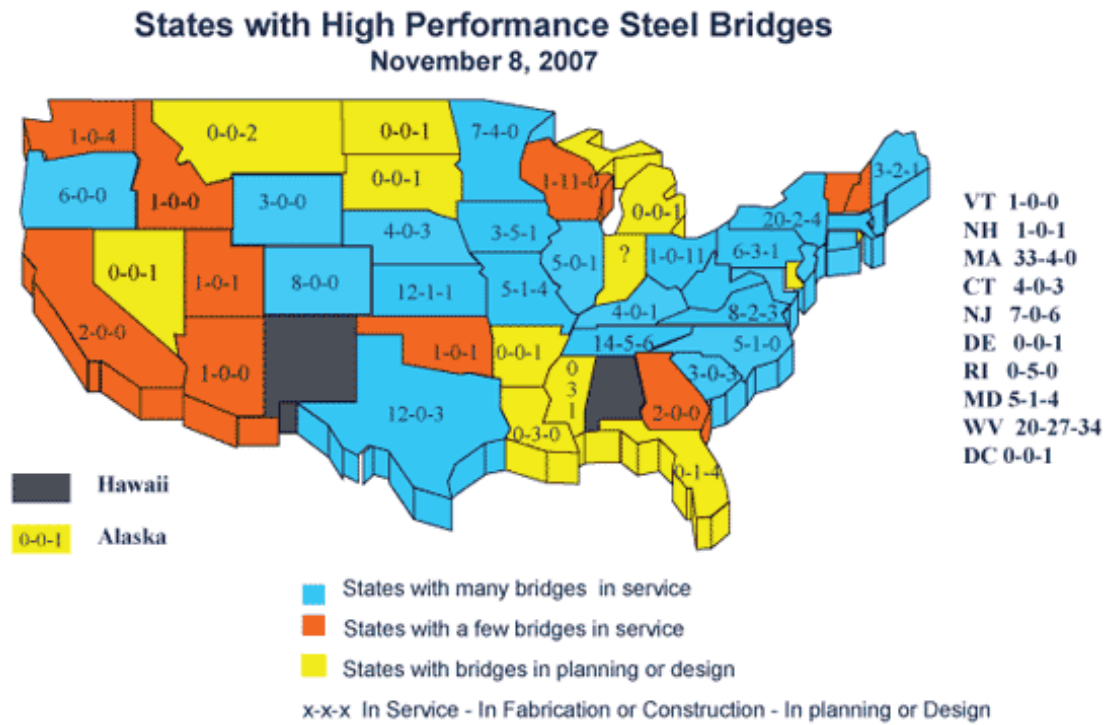


Figure 2.23 – High performance steel bridges in the USA [25]

### 2.8.3 In Japan

High-yield-point steel plates for bridges (SBHS) were developed in a joint project carried out by industry and academia in Japan with the purpose of reducing the construction costs of steel bridges [26].

Steel	Yield strength (N/mm <sup>2</sup> )	Tensile strength (N/mm <sup>2</sup> )	Preheating	Charpy test		
				Test temperature (°C)	Absorption energy (J)	Test direction
SBHS500(W)	500 or more	570 - 720	Not required	-5	100-104.99	Perpendicular to direction of rolling
SBHS700(W)	700 or higher	780 - 930	50°C	-40	100-104.99	

Figure 2.24 – Characteristic of Japanese SBHS steels [26]

- Nagata bridge

This was the first structure to use SBHS after the steel was covered by the Japanese Industrial Standards. The bridge is continuous over four spans and has an entire length of

250m. SBHS500 steel with a maximum plate thickness of 67mm and yield strength of  $500\text{N/mm}^2$  was used for the construction. The design strength is 10-20% higher than conventional steel which allowed for economical design and weight savings [27]



Figure 2.25 – Nagata bridge, Japan [Nippon Steel & Sumitomo Metal]

- Tokyo Gate bridge

It is the World's largest-scale fully welded continuous truss bridge with a marine area of  $1618\text{m}^2$ , a centre span of 440m and an entire length of 2933m. BHS500 was used for the project, having excellent weldability, cold formability, and high strength and toughness compared to conventional rolled steel for welded structures. The design resulted in a 3% reduction of the steel weight and 12% in total costs [27].



Figure 2.26 – Tokyo Gate bridge, Japan [27]

- Akashi Kaikyo bridge

The bridge links the city of Kobe on the mainland of Honshu to Iwaya on Awaji Island. It is a three span, two-hinge stiffened truss suspension bridge, having 3911m in length and the world's longest centre span of 1991m. Around 4200 tons of HT690 and HT780 steel was used for the stiffening girders (steel that can decrease preheating temperatures). For the cables high-strength wires with a tensile strength of  $180\text{kgf/mm}^2$  (approx.  $1765\text{N/mm}^2$ ) were used [27].

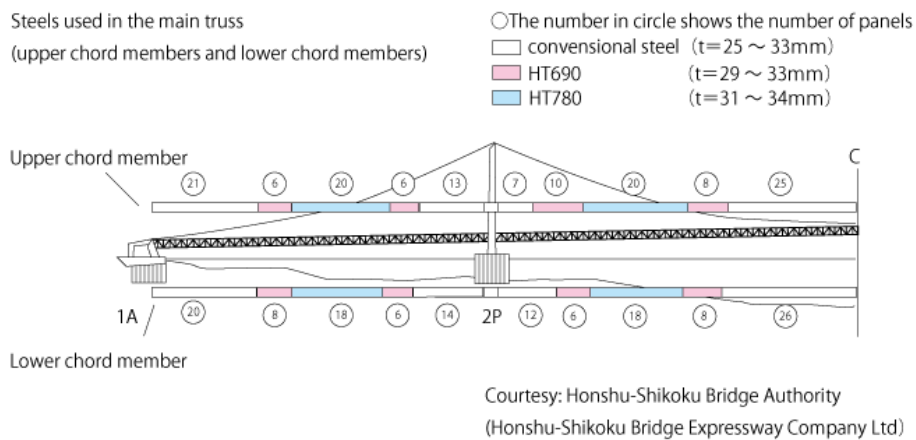


Figure 2.27 – Adoption of high tensile-strength steel for the Akashi Kaikyo Bridge [27]

#### 2.8.4 In South Korea

- Incheon bridge

The structure is a second connecting bridge to Incheon International Airport, linking the airport to the Songdo Free Trade Zone in Incheon City. It has an overall length of 21.38km and it was finalised in October 2009. The bridge used straight web steel sheet-piles as cylindrical (cell) anti-collision structures in order to prevent vessels from accidentally colliding with the bridge piers. The cylinders were driven into the seabed and filled with earth and sand. The straight web-type sheet-piles have lengths of up to 38m and maximum tensile strength of 5880 kN/m (the highest in the world) [27].

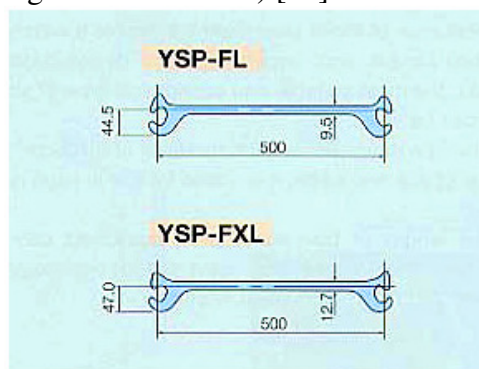


Figure 2.28 – Straight web-type sheet piles used in the cell shell [27]

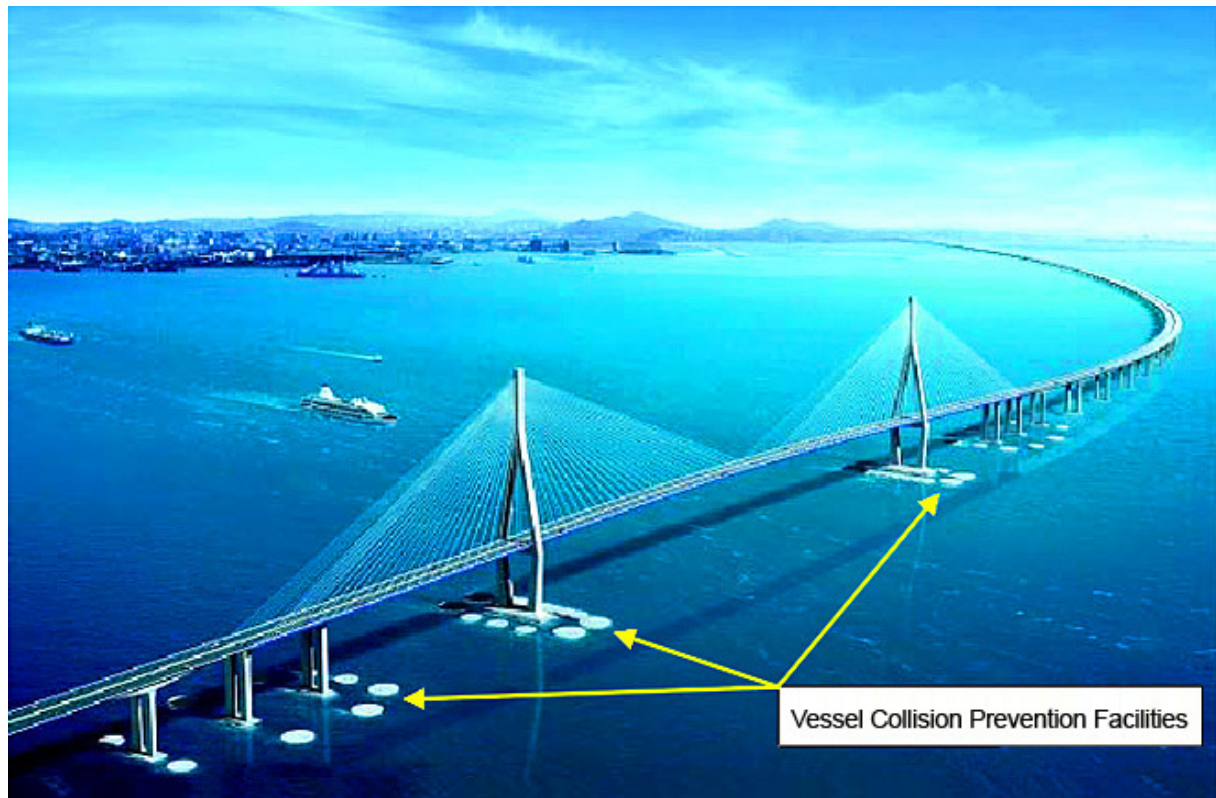


Figure 2.29 – Anti-collision structures in the Incheon bridge, South Korea [27]

### 3 LITERATURE REVIEW

The purpose of the literature review is to collect information from previous studies, experimental work and projects utilizing HSS for application in bridges around the world. The relevant information sought for is related to ductility. Points of interest that are addressed in this section are related to the yield-tensile ratio and its influence in design, past failures and their cause, current design code requirements with respect to material ductility and stress concentrations.

#### 3.1 Issues Related to Ductility

The biggest question that HSS poses is regarding ductility, which together with the lack of long term experience and design rules, results in limited applications. In practice this problem occurs in details of steel structures where stress concentrations occur due to the irregularities in the cross section. If the material has sufficient ductility, minimum yield-tensile ratio and minimal extend, forces are redistributed due to plastic deformations. In the case of HSSs questions arise with respect to redistribution of internal forces and how to deal with this for a ULS check.

##### 3.1.1 Influence of the yield-tensile ratio

**Bannister (1999)** conducted an experimental programme to study the yield stress/tensile stress ratio's relevance for structural integrity assessments. The aim of the work is to gain insight into:

- The dependence of basic mechanical and fracture properties on  $f_y/f_u$  ratio;
- The relationship between the tensile parameters ( $f_y/f_u$ , strain hardening exponent, yield point elongation);
- The behaviour of wide-plate type tests from a  $f_y/f_u$  perspective;

A summary of the structure of the programme carried out is presented in Figure 3.1. The authors used twelve plate materials with yield strength ranging from 303 MPa to 991 MPa and  $f_y/f_u$  ratios from 0.65 to 0.95. These covered six grades, five process routes (N, NR, TM, QT and Q) and four thicknesses. The processing details of each of the plates and their mechanical properties values as quoted on the test certificate are shown in Table 16.

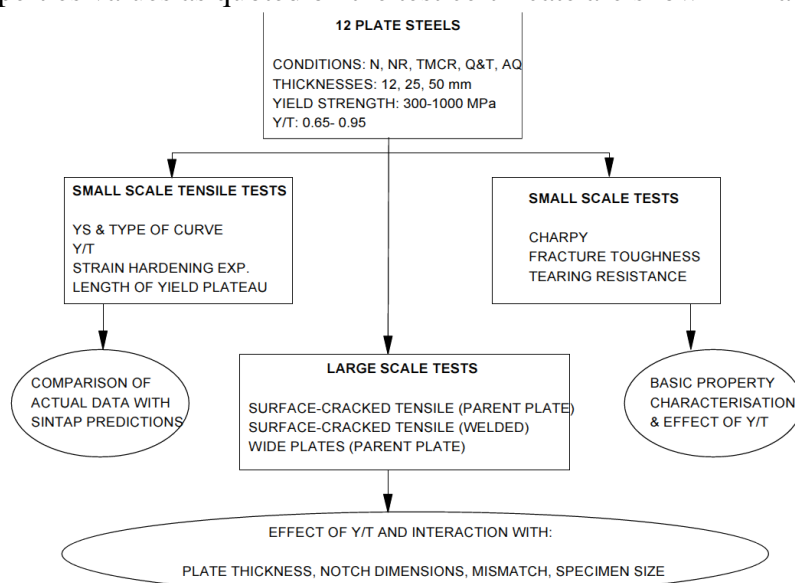


Figure 3.1 – General Flow Chart of Tasks [28]

Table 15 - Basic Details of Steel Grades Included in Test Programme as per Requirements of Relevant Specifications [28]

Grade	Thickness Tested (mm)	Steel Type	Minimum Specified Tensile Properties (MPa) for Lowest Thickness Range		Condition	Typical Charpy Requirement	Typical Specification
			YS	UTS			
S275J0	25	Low strength structural	275	430	Normalised	27 J @ 0°C	BS EN 10025
S355J2	25	Medium strength structural	355	490	Normalised Rolled	27 J @ -20°C	BS EN 10025
355 EMZ	25, 50	Offshore	355	450	TMCR	50 J @ -40°C	EN 10113 & 10225
450 EMZ	12.5, 25, 50	Offshore	450	560	Quenched & Tempered	50 J @ -40°C	EN 10113, 10225 & 10137
S690Q	12, 25, 40	High strength structural	690	770	Quenched & Tempered	27 J @ -60°C	EN 10137
ABRAZO 400 (Abrev. ABR400)	12.5, 25	Wear plate	None specified but YS usually ~1000 MPa		Quenched	None	None

Table 16 - Processing Conditions and Properties of Plates as Quoted on Mill Certificates [28]

Grade	Thickness (mm)	CEV (%) (IIW)	Process Conditions	Yield Stress (MPa)	UTS (MPa)	Y/T Ratio	Elong. (%)	Charpy Properties
S275J0	25.0	0.320	Normalised.	310	470	0.660	33	181 J @ 0°C
S355J2	25.0	0.391	Normalised Rolled.	380	555	0.685	33	139 J @ -20°C
355 EMZ	25.0	0.365	1200°C Re-heat, Reduction Ratio >1:4, End Hold Temperature ≤ 830°C.	431	523	0.824	31	209 J @ -40°C
355 EMZ	50.0	0.360	1200°C Re-heat, Reduction Ratio >1:4, End Hold Temperature ≤ 830°C.	366	498	0.735	30	241 J @ -40°C
450 EMZ	12.5	0.356	Quenched at 930°C (after 35 min hold) Tempered at 625°C for 40 min.	494	577	0.856	28	225 J @ -40°C
450 EMZ	25.0	0.369	Quenched at 930°C (after 50 min hold) Tempered at 670°C for 1 h 35 min.	478	566	0.845	30	298 J @ -40°C
450 EMZ	50.0	0.380	Quenched at 930°C (after 1 h 45 min hold) Tempered at 650°C for 3 h 25 min.	490	571	0.858	30	274 J @ -40°C
S690Q	12.0	0.390	Quenched at 930°C (after 30 min hold) Tempered at 580°C for 34 min.	802	862	0.930	26	114 J @ -45°C
S690Q	25.0	0.390	Quenched at 930°C (after 50 min hold) Tempered at 580°C for 1 hour.	789	834	0.946	29	117 J @ -45°C
S690Q	40.0	0.490	Not available.	735	814	0.903	26	111 J @ -45°C
ABR400	12.5	0.380	Quenched at 930°C (after 38 min hold).	993 <sup>(1)</sup>	1279 <sup>(1)</sup>	0.776 <sup>(1)</sup>	16 <sup>(1)</sup>	60 J @ RT <sup>(1)</sup>
ABR400	25.0	0.495	Quenched at 930°C (after 54 min hold).	1060 <sup>(1)</sup>	1401 <sup>(1)</sup>	0.757 <sup>(1)</sup>	10 <sup>(1)</sup>	52 J @ RT <sup>(1)</sup>

<sup>(1)</sup>Laboratory values, property not quoted on test certificate.

Contribution to BE05-1426 Task 2 Sub-Task 2.3 19/2/99

The tensile properties of the twelve steels are measured at room temperature using three different small scale specimen types: flat plate tensile specimen sampling the full plate cross-section, round tensile specimens with parallel sides for which the strain was measured using length extension and wasted tensile specimens with reduced cross-sectional area with the strain measured using diametrical contraction. Charpy impact properties and fracture toughness values were also quantified by tests.

Large scale tensile tests were carried out on surface-cracked specimens on all of the 12 mm and 25 mm plates, on specimens of 100 mm width having a gauge length for strain measurement of 340mm and semi-elliptical surface notches with three different geometries and a nominal notch width of 0.15mm. The notch geometry and nomenclature are presented in Figure 3.2. The tests were carried out at room temperature and the measured data included the overall extension on both the notched and un-notched face and local strains.

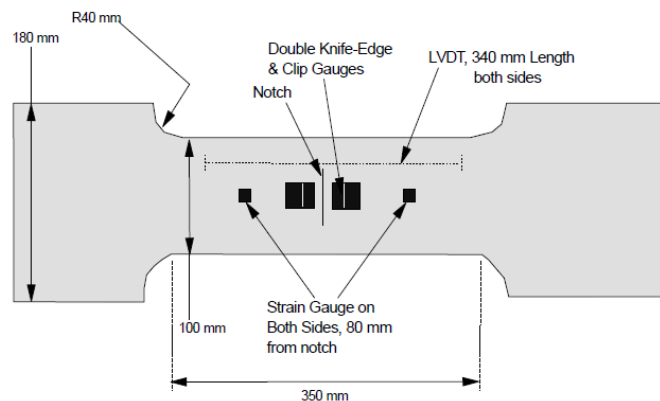


Figure 3.2 – Dimensions and instrumentation of surface-cracked tensile specimen [28]

## Influence of Ductility in the Design of (High Strength) Steel Bridges

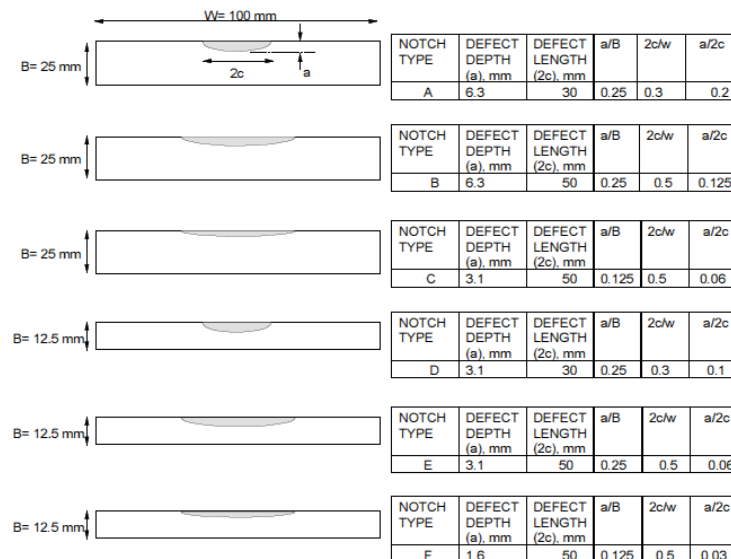


Figure 3.3` - Notch Nomenclature and Dimensions [28]

The behaviour of the various combinations of grade, plate thickness and notch dimensions have been assessed in terms of: gross stress vs average linear voltage displacement transducers strain, crack tip opening displacement vs gross stress and crack tip opening displacement vs average linear voltage displacement transducers strain.

For all the plates below grade 450 failures were all fully ductile while for the higher strength plates (S690Q and ABRAZO 400) the failure mechanism was influenced by both plate thickness and notch geometry. The failure mode and fracture appearance for each set of surface cracked tensile tests is summarised in Table 17:

Table 17 – Failure Modes and Fracture Appearance of Surface-Cracked Tensile Tests on Parent Materials [28]

Grade	Thickness (mm)	Mode	Fracture Appearance
S275J0	25.0	GSY	Ductile failure at maximum load; 5-10 mm ductile tearing.
S355J2	25.0	GSY	Ductile failure at maximum load; 1-3 mm ductile tearing.
355 EMZ	25.0	GSY	Ductile failure at maximum load; stretch zone, 0.5 mm ductile tearing, splits on fracture surface.
450 EMZ	12.5	GSY	Ductile failure at maximum load; 1-5 mm ductile tearing.
450 EMZ	25.0	GSY	Ductile failure at maximum load; 2-3 mm ductile tearing.
S690Q	12.0	GSY	Ductile failure at maximum load; tearing followed by fracture or collapse of remaining ligament depending on notch depth.
S690Q	25.0	GSY	Ductile failure at maximum load; 0.8-1.5 mm ductile tearing.
ABR400	12.5	GSY	Ductile failure at a maximum load; tearing to back face then ductile shear fracture to edges of specimen.
ABR400	25.0	GSY for notches A&C NSY for notch B	Unstable brittle fracture, 0.2-0.8 mm ductile tearing.

GSY = Gross Section Yielding.  
NSY = Net Section Yielding.

In the case of wide plate tests, all but the 25 mm thick S355J2 plate were tested. The specimen was designed with a width of 450 mm, a parallel gauge length for strain measurement of 400 mm and semi-elliptical surface crack having a length of 0.3 times the plate width and depth of 0.2 times plate thickness. The tests were instrumented similar to the surface-cracked-tensile tests and carried out at a temperature of -20°C.

Five of the plates failed during the test, the remainder reached maximum load but did not fail within the displacement limits of the testing machine. Except the ABRAZO 400 plates which failed at strains of 0.784% (12.5 mm thickness) and 0.64% (25 mm thickness), all the

others exceeded 1%. All the plates achieved a gross stress greater than the yield stress, with ratios varying from 1.05 to 1.35.

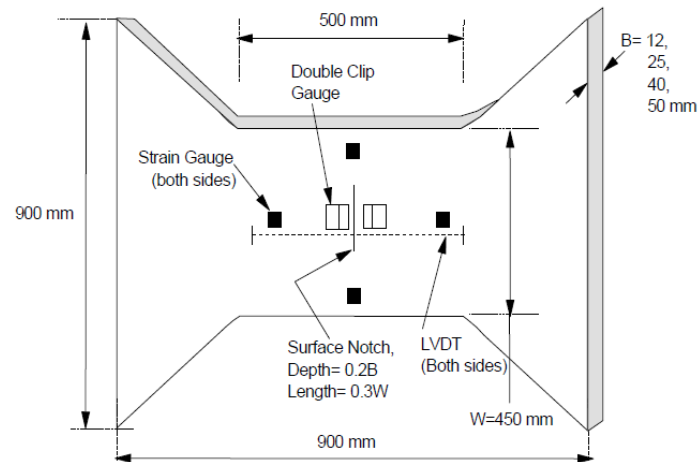


Figure 3.4 – Wide plate dimensions and instrumentation [28]

A series of tests on welded plates from three different grades (355EMZ, 450EMZ, S690Q) was also carried out in addition to the tests on parent metals. The scope was to assess the interaction of the  $f_y/f_u$  ratio with issues such as mismatch, toughness of the Heat Affected Zone and residual stress. Surface cracked tensile tests were carried out on the welded 25mm plates with the location of the strain gauges presented in the figure below:

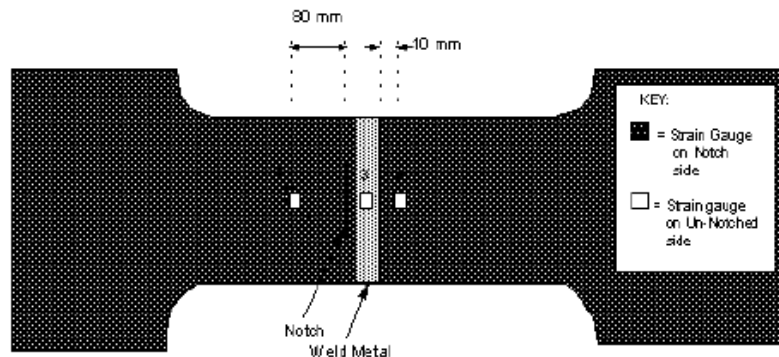


Figure 3.5 – Locations of strain gauges in welded surface cracked tensile tests [28]

The author concludes that in the case of small scale tensile properties, there is no systematic effect of the specimen type on the measured value of the yield stress. The different  $f_y/f_u$  ratio values from the results are a consequence of the difference in the measured ultimate strain. A decrease in thickness will result in an increased  $f_y/f_u$  ratio for the same given composition. The strain hardening exponents (defined as the slope of the log-log plot of true stress vs true plastic strain), were determined for each steel. The proposed expression for determining a conservative estimate of strain hardening exponent from  $f_y/f_u$  is:

$$N=0.3(1- f_y/f_u))$$

In the case of surface cracked tensile tests, the  $f_y/f_u$  ratio has an influence in the load bearing capacity of the element when the stresses are higher than the yielding point. Other

factors influencing this capacity are the plate thickness, degree of strain hardening and resistance to ductile tearing. The notch depth and length have a lower effect on the failure stress than the  $f_y/f_u$  ratio. Grade S275J0, having the lowest  $f_y/f_u$  ratio (0.649) and a high resistance to ductile tearing, yields a high maximum net stress/yield stress. As the  $f_y/f_u$  ratio increases there is a gradual decrease in maximum stress and for the highest ratio of 0.949 with a 12mm thick plate the maximum net stress is only slightly higher than the yield stress.

Wide plate tests were carried out with only one notch geometry, the defect area being negligible with respect to the plate cross-sectional area. All the plates managed to achieve stress levels higher than the yield stress, with ABRAZO 400 being the only plate with low  $f_y/f_u$  ratio failing during the test. Compared to the surface cracked tensile tests, there is no tendency in decreasing maximum stress/yield stress as  $f_y/f_u$  increases. This leads to the conclusion that edge effects influence the result of the smaller tests. In order to resist the enhanced crack opening, a high  $f_y/f_u$  ratio material will need an increased level of toughness for the case of thin plates.

In welded joints the stress-strain properties of the parent metal, weld metal and HAZ have a significant effect on the relationship between crack opening and applied strain. It is concluded that the level of mismatch between parent metal, weld metal and HAZ has a higher importance compared to the  $f_y/f_u$  ratio and strain hardening. [28]

The author finally concludes that:

- The  $f_y/f_u$  ratio increases with decreasing thickness for a given grade within the thickness range for which the alloying system is the same;
- The  $f_y/f_u$  ratio increases with yield strength in accordance with a power-law relationship;
- The relationship of decreasing strain hardening exponents with increasing  $f_y/f_u$  has been further confirmed
- In the case of surface-cracked tensile tests, the maximum achieved ratio of net section stress/yield stress decreased slightly with increasing  $f_y/f_u$  ratio although all of the values were above 1
- For low  $f_y/f_u$  steels, the applied strain in large scale tests tends to be concentrated in plate deformation since the zone ahead of the crack tip readily undergoes work hardening and has a high resistance to ductile tearing; the opposite is true for steels with high  $f_y/f_u$  ratios and the effect is increased in the case of thin plates;
- Steels with high  $f_y/f_u$  and therefore low strain hardening exponent values, give a high crack opening for a given applied strain;
- The  $f_y/f_u$  ratio and its effect on crack opening, is more significant for thin plates
- Steels showing  $f_y/f_u$  ratios less than 0.85 and a yield plateau in the tensile tests tend to show a plateau in crack opening in larger scale tests
- Qualitatively, high  $f_y/f_u$  ratio steels give greater crack driving force in thin plates than in thicker ones whereas the reverse is true for low  $f_y/f_u$  ratios.
- In case of welded joints, the level of weld metal and HAZ mismatch and the toughness of the various regions of the HAZ are more significant than the  $f_y/f_u$  ratio of the parent plate and weld metal
- The current results suggest that  $f_y/f_u$  is only an issue when in excess of 0.9 ( $f_u/f_y \leq 1.11$ ), and then only in the case of thin plates.

**R.L. BROCKENBROUGH & ASSOCIATES INC (1995)** studied the effect of the yield-tensile ratio on the structural behaviour. Developments of newer production methods resulted in production of steels with increased strength and lower yield-tensile ratios. In Japan steels with a maximum ratio of 0.80 ( $f_u/f_y \geq 1.25$ ) for yield strengths from 345MPa (50ksi) to 448MPa (65ksi) and 0.85 ( $f_u/f_y \geq 1.17$ ) for a 690MPa (100ksi) yield strength were developed for seismic applications. Figure 3.6 illustrates the effect of the new production processes on the shape of the stress-strain curve:

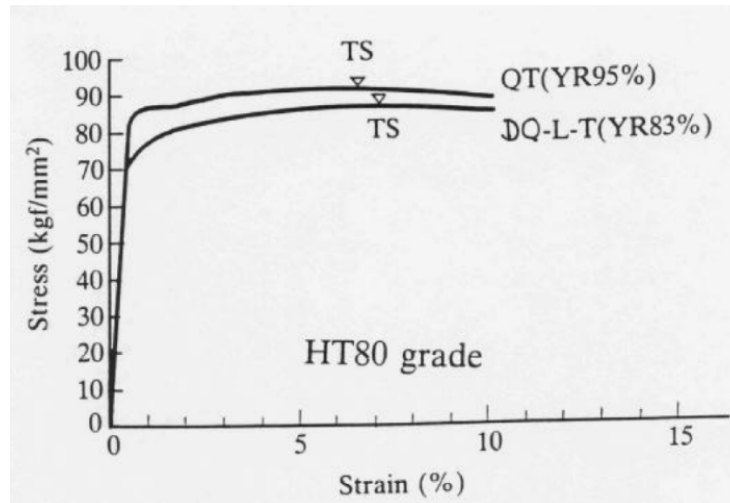


Figure 3.6 – Stress-Strain Curves Reflecting Conventional and New Processes [29]

The lower curve represents Nippon Steel's HT80 grade which has a minimum yield strength of 690MPa (100ksi), a tensile strength between 786MPa (114ksi) and 930MPa (135ksi) and a maximum yield-tensile ratio of 0.85. The two steels in the graph have the same composition; the only difference is the production method. The Nippon steel is made by the DQ-L-T (direct quenched, lamellarized and tempered) process while the other grade is made by QT. Both curves are terminated at 10 percent strain but have about the same total elongation (24 and 23%). The yield-tensile ratios in this case were 0.83 and 0.95. The lower curve is for Nippon Steel.

The study made in [29] gives an insight on how the behaviour of members and connections might be affected by the yield-tensile ratio and is partly based on previous literature work which addresses issues as:

Research in Japan:

- The effect of the yield-tensile ratio on the structural performance of steel tension members, flexural members, and beam columns;
- The inelastic rotation capacity of I-section members subjected to bending or bending and axial compression;
- Review of studies made on the inelastic behaviour of high strength steels with low yield-tensile ratios;
- Sumitomo Steel's development of SM50B steel for large buildings and Kawasaki Steel's development of steel plates with high strength and low yield-tensile ratio for building frameworks;
- Considerations in Nippon Steel's development of steel plates with high strength and low yield-tensile ratio for building structures;
- Market trends and the underlying technology for steel plates used in the construction of buildings, bridges and transmission towers in Japan;

Research at U.S. Steel:

- Local plastic buckling of flanges in A514 steel members;
- Plastic bending behaviour of A514 steel beams;

Research at Lehigh University:

- Compression tests on cellular sections;
- Fatigue tests of HSLA-80 steel I-section and box-section beams with weld details characteristic of double-hull ship construction;
- Problems with present high-strength steels and potential applications for new high-performance steels;

Other structural research:

- Tests on large rack structures fabricated from steel with a high yield-tensile ratio performed in England;
- Design recommendations under the auspices of the Research Council on Structural Connections, based on ultimate load tests performed on large bolted tension splices with steel ranging from carbon to A514 steel;
- The role of welding in the structural distress observed after the Northridge earthquake;

Considering just the yield-tensile ratio when comparing different steels is somewhat of an over-simplification because of the influence the shape of the stress-strain curve has for different steels. The implications of the yield-tensile ratio in member behaviour are [29]:

- Bending members: in the case the member is proportioned so that local and lateral instability is prevented, the maximum rotation is reached when the flange reaches its tensile strength or, if the member is braced to prevent torsional-flexural buckling, the rotation will be limited by local buckling of the flange and web. In the case of a beam with a moment gradient and  $f_y < f_u$ , the plastic region can extend over some length of the beam as the bending moment increases above the plastic moment by virtue of strain hardening. In the case of  $f_y/f_u = 1.0$ , there is no extension of the plastic zone as the tension flange will rapidly reach the ultimate strain and rupture as the plastic moment is reached. The inelastic rotation capacity of a beam with a moment gradient tends to zero as the  $f_y/f_u$  ratio approaches 1. The deformation capacity is also affected by the uniform elongation of the steel. This tends to increase with decreasing yield-tensile ratio;
- Columns and beam columns: short compression members compressed into the inelastic range can have their capacity enhanced with decreasing width-to-thickness ratios of flange and web elements and decreasing yield-tensile ratios of the steel. In the case that ultimate load is controlled by inelastic local buckling, beams and columns with lower yield-tensile ratios have larger deformation capacity. For beam-columns with the combined effects of bending and axial compression, the maximum strength and the rotation capacity decreases with increasing yield-tensile ratios
- Tension members: if there is no reduced section, the entire length of the member will stretch when the yield strength is reached and the deformation will tend to be large (the total deformation only depending on the strain at which the tensile strength is reached). In the case of a reduced section, the behaviour will depend on the ratio of the net section area to the gross section area and the yield-tensile ratio.

- Fatigue: from the previous research carried on this topic, there is no reason to suspect that the yield-tensile ratio is a factor in the fatigue of fabricated members or that it would have any negative effect in low cycle fatigue.;
- Toughness: adequate notch toughness and fracture ductility must be provided both in the parent metal and in the weld material. This is provided by the steel manufacturer depending on the environmental conditions, loading characteristics and the fabrication details. [29]

The report concludes that the stress-strain curve characteristics (length of the yield plateau, the slope of the stress-strain curve in the inelastic range, local elongation and uniform elongation) are also important properties that can influence the structural behaviour. If required levels of deformation capacity are pre-established, the maximum yield-tensile ratio that would provide that capacity can be determined by analytical and experimental studies. Present relationships can also be used to reasonably predict the strength of columns with a  $f_y/f_u$  ratio up to about 0.95 ( $f_u/f_y \geq 1.05$ ). Also, when the ultimate load is controlled by inelastic local buckling, elements with low yield-tensile ratios will withstand larger deformations and the ratio will not have significant influence in the fatigue strength.

The authors address application considerations of the yield-tensile ratio. The following questions are answered:

- Ability to yield locally and redistribute stresses under static loads: in bolted joints (and in welded joints where similar situations occur) the material around the most highly stressed bolt must yield in order to allow redistribution of stresses. The most important factor is the local ductility and the elongation capacity increases with decreasing yield-tensile ratio;
- Ability to yield locally and redistribute stresses under dynamic loads: in the case of dynamic loading, fabrication imperfections can lead to crack propagation. The most important factor is the fracture toughness or V-notch impact toughness of the steel, which is a consequence of the steel chemistry and processing. The requirements depend on the environmental conditions, loading characteristics and fabrication details;
- Effect of the lower strain hardening on behaviour in compression, specifically local-buckling and column buckling: the strength of columns with yield-tensile ratios up to about 0.95 ( $f_u/f_y \geq 1.05$ ) can be reasonably predicted with the present relationships that are used for other steels. When inelastic local buckling is determinant in the ultimate load, lower yield-tensile ratios will lead to higher deformation capacity. In order to achieve an efficient design, compression members are generally designed to buckle in the inelastic range;
- Effect of the lower strain hardening on the moment-rotation behaviour: the rotation capacity tends to decrease with increasing yield-tensile ratio and it can affect the final failure mode;
- Consequences of using structural members with a significantly higher strength than anticipated: if the beams are likely to have a higher yield strength than specified, the columns must be oversized to account for this, in order to ensure yielding in the beams before the columns;
- Consequences of designing with a stress-strain curve with very limited strain hardening: traditional analytical methods and numerical methods can be applied with the new steels as no particular problems regarding the shape of the curve were reported;

In order to show trends in behaviour that are influenced by the yield-tensile ratio, simple illustrative models are developed by the authors [29]:

- Local yielding and stress redistribution:

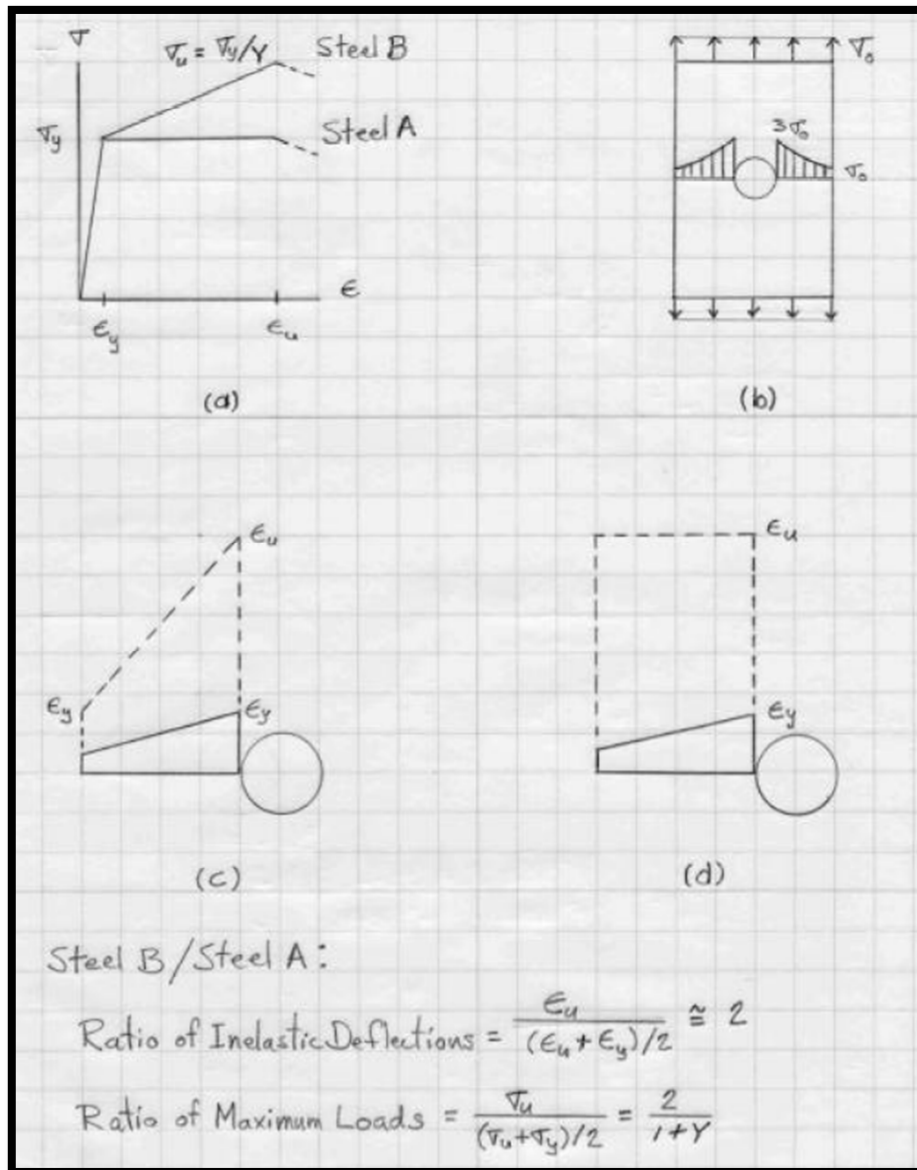


Figure 3.7 – Effect of Yield-Tensile Ratio on Local Yielding. (a) Stress-strain curves. (b) Tension strap with bolt hole. (c) Strain at maximum load for steel A. (d) Strain at maximum load for steel B [29]

The expressions at the bottom of Figure 3.7 point out that the inelastic deformation of strap with steel B would be approximately twice that of the strap of steel A, and the maximum load ratio would approach  $2/(1+f_y/f_u)$ .

The influence of the yield-tensile ratio on a tension member is illustrated in Figure 3.8. A significant increase in the elongation and slight increase in the maximum load can be observed for a lower yield-tensile ratio.

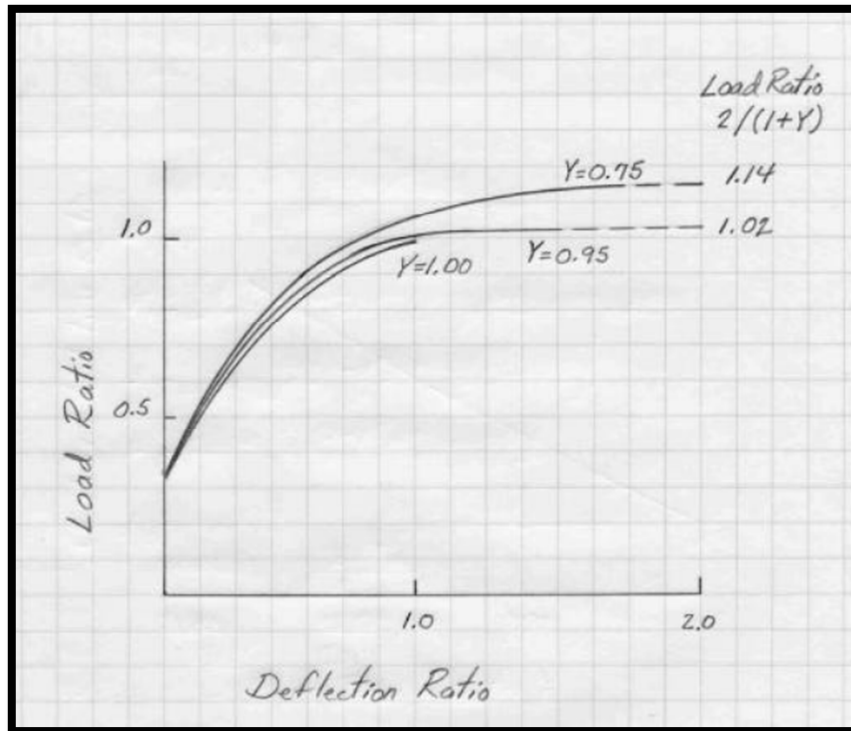


Figure 3.8 – Dimensionless load-deflection plots for tension strap with yield-tensile ratio of 0.75, 0.95 and 1.00 [29]

- Moment-rotation behaviour: the end rotation for steel beams of grades A and B is given by the relationships for  $\Theta_A$  and  $\Theta_B$  at the bottom of Figure 3.9.

In Figure 3.10, the effect of yield-tensile ratio on moment-rotation behaviour of the cantilever beam is illustrated. The solid line plot represents an upper limit as it is not reasonable to expect the whole section to strain harden and to reach the ultimate stress. The dashed line represents reaching a maximum stress of  $(f_u+f_y)/2$ . The dimensionless maximum stress is  $(1/f_u)(f_u+f_y)/2=(f_y/f_u +1)/2$  instead of  $f_y/f_u$ .

From Figure 3.9 it can be observed that for a cantilever beam a lower yield-tensile ratio tends to increase the end rotation significantly. Comparing a yield-tensile ratio of 0.85 to 0.95, it results that the end rotation at maximum load would increase by about 40%.

The relationships are based on the assumption that the member is proportioned and braced so that premature failure by local or lateral instability does not occur.

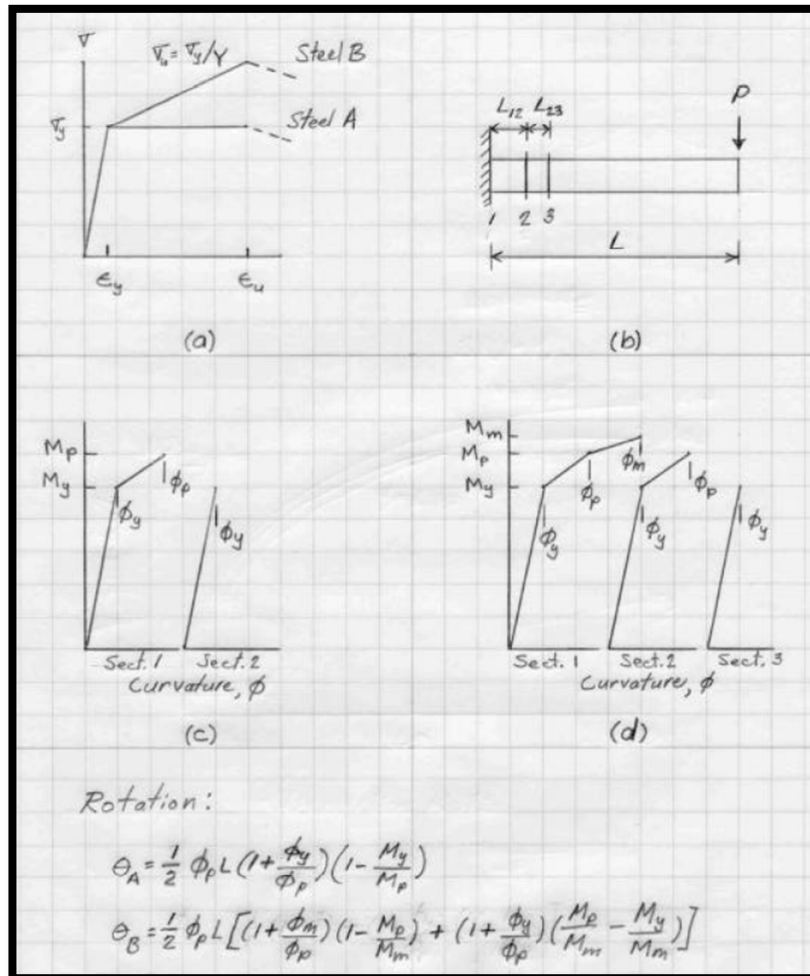


Figure 3.9 – Effect of yield-tensile ratio on moment-rotation behaviour of cantilever beam. (a) Stress-strain curves. (b) Cantilever beam with end load. (c) Moment-curvature plots for sections 1 and 2 for steel A. (d) Moment-curvature plots for sections 1, 2 and 3 for steel B [29]

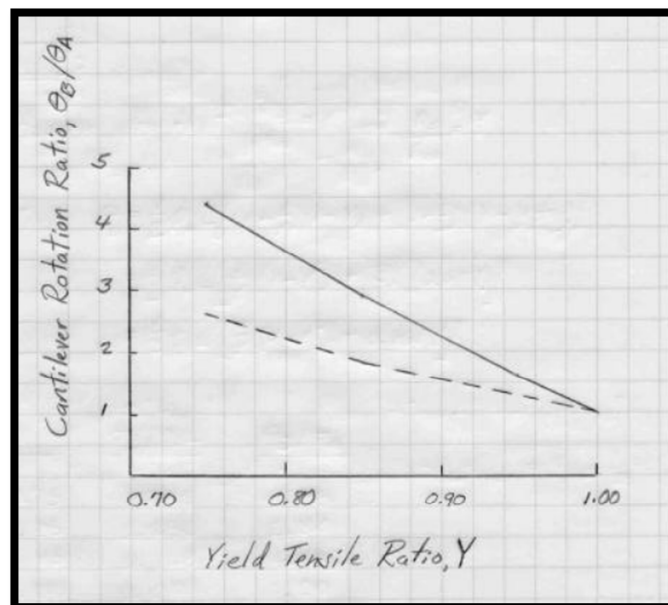


Figure 3.10 – Illustration of effect of yield-tensile ratio on moment-rotation behaviour of cantilever beam [29]

- Local buckling behaviour: the inelastic deformations that the member is able to sustain increases as the yield-tensile ratio decreases.

**Collin & Johansson (2006)** give insight on the recent EN 1993-1-12 code development on HSS. The authors draw some conclusions regarding local and global buckling based on previous works. Studies showed that HSS performs better than ordinary steel or at least the same. This is due to the fact that in HSS imperfections have a smaller influence because of the higher yield strength and residual stresses are a smaller fraction of the yield strength. The normal design rules can be used as a conservative approach, although the authors suggest that a gradual increase of the buckling curves by modifying the imperfection parameter would be recommended. Based on previous conducted testing on local buckling, most results pointed to the fact that HSS has a better performance compared to mild steels or about the same relative resistance.

**Dexter et al. (2002)** conduct experimental and analytical research to determine the strength and ductility performance of tension members and the tension flange of flexural members fabricated with HPS70W steel.

AASHTO included American Society for Testing and Materials (ASTM) A709 Grade HPS70W as a replacement of AASHTO M270 Grade 70W. The new grade has excellent fracture toughness compared to the old grade. The difference in chemical and mechanical property requirements, fatigue and fracture properties, and weldability are presented in Table 18 and Table 19.

Table 18 – Chemistry for conventional and high performance steels [30]

		C	Mn	P	S	Si	Cu	Ni	Cr	Mo	V	Al	N
Old 70W *	Min.	-	0.8	-	-	0.25	0.2	-	0.4	-	0.02	-	
	Max.	0.19	1.35	0.035	0.04	0.65	0.4	0.5	0.7	-	0.1	-	
HPS 70W & HPS 50W	Min.	-	1.1	-	-	0.3	0.25	0.25	0.45	0.02	0.04	0.01	
	Max.	0.11	1.35	0.02	0.006	0.5	0.4	0.4	0.7	0.08	0.08	0.04	0.015

HPS70W can be delivered by quenching and tempering or thermo-mechanical controlled processing. The difference is that in the QT delivery condition lengths are limited to 15m (50ft) in the United States.

Table 19 – Mechanical properties for high performance steel plates [30]

	HPS 50W Up to 4" As-Rolled	HPS 70W Up 4" (Q&T). 2" (TMCP)
Yield Strength, F <sub>y</sub> , ksi (MPa) min.	50 (345)	70 (485)
Ultimate Tensile Strength, F <sub>u</sub> ksi (MPa)	70 (485)	85-110 (585-760)
CVN, minimum*Longitudinal orientation	25 ft.-lbs. (41 J)@ 10°F (-12°C)	30 ft.-lbs. (48 J)@ -10°F (-23°C)

HPS70W remains fully ductile at lower temperatures compared with conventional Grade 50W which shows a more brittle behaviour at the same temperatures. Thus the fracture toughness of high performance steels is higher than the conventional bridge steels. This is highlighted in Figure 3.11

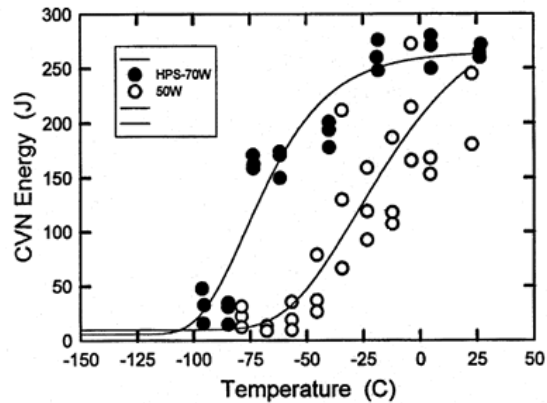


Figure 3.11 – Charpy V-notch Number transition curve [30]

Reduced carbon content means that HPS70W has excellent weldability resulting in reduced fabrication costs. Also, in order to eliminate hydrogen-induced cracking, minimum preheat and interpass temperature for welding are specified.

The authors address the relationship of strain hardening to tensile ductility. As the tensile ductility is limited by the strain at which necking begins, a theoretical connection between the strain at which necking begins (point of ultimate strength in a tension test) and the strain hardening of the steel can be stated (for the case when the inelastic region of a stress-strain curve is represented by a power law):

$$\sigma_{\text{True}} = K \varepsilon_{\text{Natural}}^n$$

Where K is the strength coefficient and n is the strain-hardening exponent.

In case of steel grade A514, with a  $f_y/f_u$  ratio higher than 0.9 the strain hardening exponent can be as low as 0.08 which indicates that necking could start at about 8% strain, while ordinary Grade 50 steel with  $f_y/f_u$  ratios less than 0.8 have a strain hardening exponent of 0.2 indicating that necking will not start until 20% strain. However it is quite an oversimplification to idealize the stress-strain curve as a power law or to characterize the tensile behaviour with a single parameter ( $f_y/f_u$ ).

The authors conducted tensile experiments on 200mm (8-inch) wide and 19mm (0.75-inch) thick plates with various net-section configurations. Plates without holes, with single holes of varying size, with hole groups and with splice connections were tested. The experiments were conducted to characterize the effect of the net section on the tensile ductility of HPS70W and compare it to the ductility of similar specimens made with HSP100W and A709 Grade 50 steel. Also one flexural test was conducted on a girder featuring a tension flange identical in cross section to the tension specimens and without any holes. The behaviour of the tension flange to the tension members and a characterization of the ductility demand for the tension flange was obtained.

The authors quantify the tensile properties of the materials. The steel plates used to fabricate the wide-plate tensile specimens were obtained from two different heats of HPS70W (represented by L and H). They state that there is no consistent trend in the differences between the mill test reports, the coupon tests and the wide-plate tests. Thus the results of the wide plate tests are applicable to other tension members and flange plates with different widths. The tensile properties of the grades are listed in Table 20.

Table 20 – Comparison of individual and average tensile test results [31]

Material	$F_y$	$F_y$	$F_y$	$F_u$	$F_u$	$F_u$	Y/T	Y/T	Y/T
	8" WIDE (ksi)	COUPON (ksi)	MILL (ksi)	8" WIDE (ksi)	COUPON (ksi)	MILL (ksi)	8" WIDE	COUPON	MILL
HPS70W-L	79.95	81.50	77.80	89.81	95.00	89.80	0.89	0.86	0.87
		79.50	79.60		94.70	90.00		0.84	0.88
		80.50	78.70		94.85	89.90		0.85	0.88
HPS70W-H	76.00	75.90	79.90	86.89	92.30	94.00	0.87	0.82	0.85
		75.50	94.40		88.80	104.4		0.85	0.90
		75.70	87.15		90.55	99.20		0.84	0.88
A709 Gr 50	60.75	56.00	59.00	80.99	82.40	80.00	0.75	0.68	0.74
		52.10	58.00		81.30	79.00		0.64	0.73
		54.05	58.50		81.85	79.50		0.66	0.74
HPS100W	115.95	104.93	-	121.33	109.44	-	0.96	0.96	-
		103.23	-		112.34	-		0.92	-
		104.08	-		110.89	-		0.94	-

The wide-plate tests were first conducted in order to establish the fundamental behaviour of HPS70W tension members. The basic specimen design is presented in Figure 3.12. By adjusting the diameter of the hole a variety of  $A_n/A_g$  ratios could be tested.

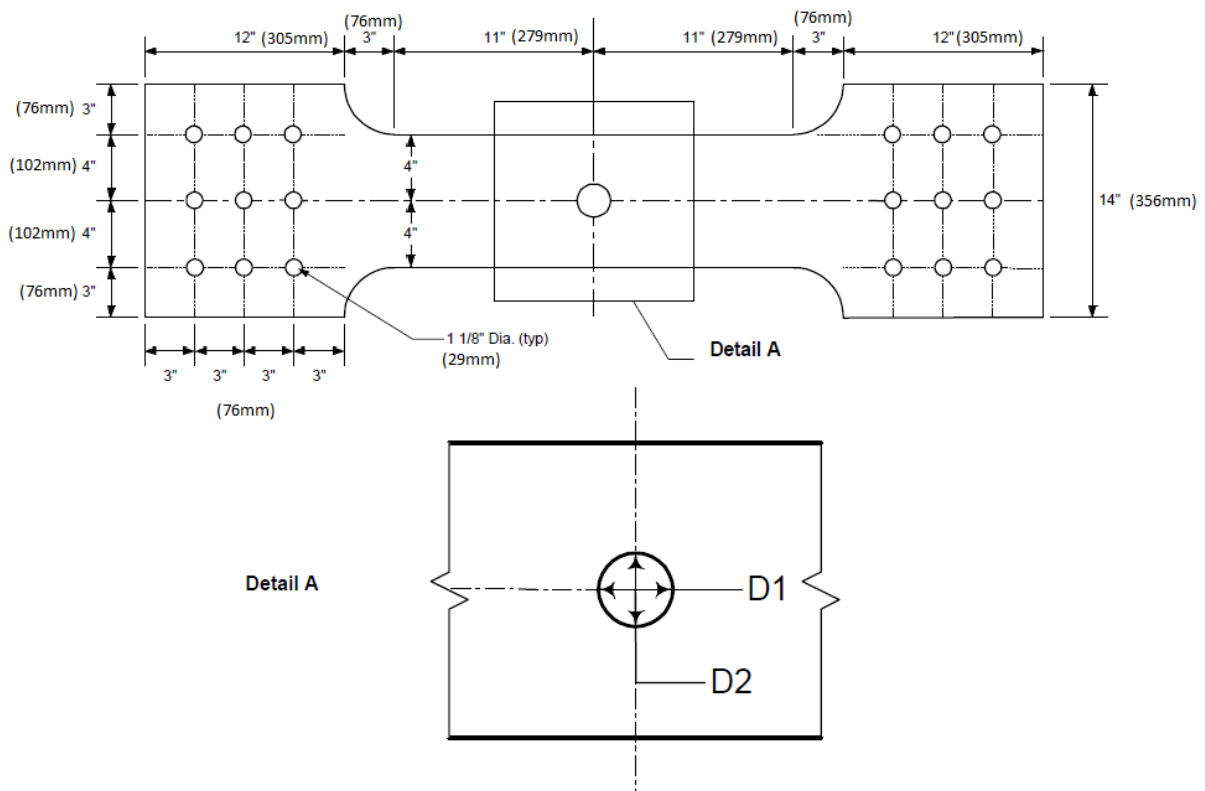


Figure 3.12 – Geometry of wide-plate tension specimen [31]

Additionally specimens with 12 holes, specimens with a splice joint and an unspliced specimen with the exact same net section properties as the spliced one were tested.

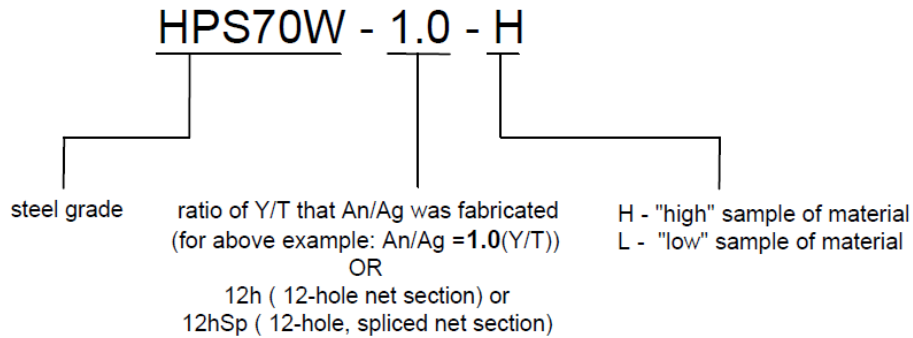


Figure 3.13 – Identification system for specimens [31]

Strains were measured on the gross section using high-elongation strain gages. The results of the wide-plate tensile tests are listed in Table 21 [31].

Table 21 – Summary of HPS70W wide-plate tensile test results [31]

Specimen	Peak Load (kips)	$F_{An}$ (ksi)	$\frac{F_{An}}{F_u}$	$F_{Ag}$ (ksi)	$\frac{F_{Ag}}{F_y}$	Total Elongation $\epsilon_{total}$ (%)	Net Plastic Elongation $\epsilon_{plastic}$ (%)	$\frac{\epsilon_{plastic}}{\epsilon_y}$
HPS70W-0.0-H	538	86.8	1.00	86.8	1.14	14.59	14.35	59.5
HPS70W-0.0-L	557	89.8	1.00	89.8	1.12	13.34	13.10	54.3
HPS70W-0.9-H	446	91.0	1.05	71.7	0.94	2.38	2.14	8.8
HPS70W-0.9-L	463	93.5	1.04	75.3	0.94	2.72	2.48	10.2
HPS70W-1.0-H	517	94.6	1.09	82.5	1.09	2.72	2.48	10.2
HPS70W-1.0-L	523	92.8	1.03	82.9	1.04	2.94	2.70	11.2
HPS70W-1.1-H	549	92.8	1.07	89.4	1.18	9.19	8.95	37.1
HPS70W-12h-H	423	89.9	1.04	66.8	0.88	6.54	5.10	3.5*
HPS70W-12h-L	431	95.0	1.06	69.7	0.87	6.12	4.68	3.2*
HPS70W-12hSp-H	430	94.1	1.08	68.9	0.91	3.68	3.20	6.6**
HPS70W-12hSp-L	452	97.8	1.09	72.2	0.90	3.60	3.12	6.4**

\*tensile ductility divided by 6 for comparison to results with single hole

\*\*tensile ductility divided by 2 for comparison to results with single hole

Finite element software was used in modelling of the specimens. Two-dimensional plane-stress elements with reduced integration representing a thin-shell element with eight nodes and four integration points were used. A typical specimen finite element model is illustrated in Figure 3.14.

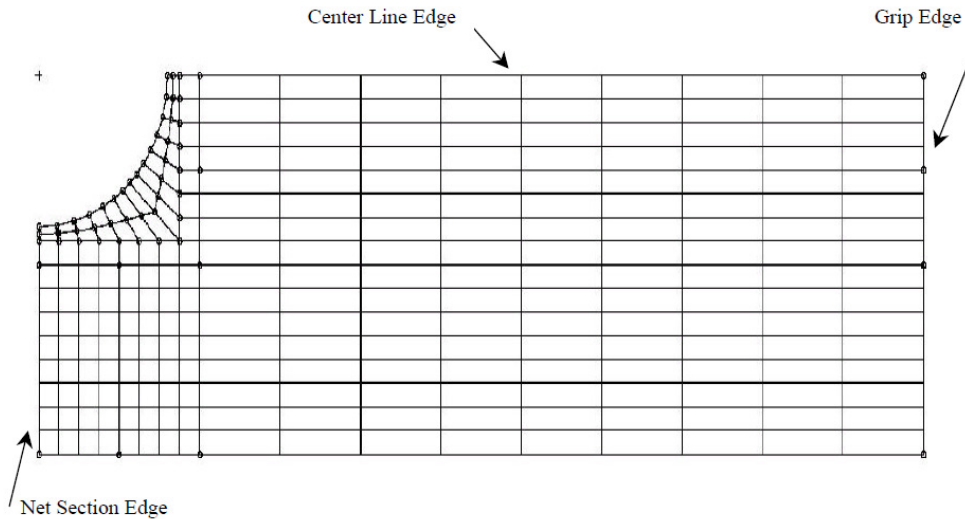


Figure 3.14 – Typical specimen finite element model [31]

The difference between the finite element results and experimental net-section and gross-section strength results was quite small. The finite element models slightly over-predicted the measured ultimate capacities of the specimens.

Ductility of the tensile members was measured function of the  $A_n/A_g$  ratio to the  $f_y/f_u$  ratio  $[(A_n/A_g)/(f_y/f_u)]$ , which can also be thought of as the ratio of the nominal fracture limit state  $A_n f_u$  to the nominal gross-section yielding limit state  $A_g f_y$ . The maximum gage length elongation with respect to the  $(A_n/A_g)/(f_y/f_u)$  ratio is illustrated in Figure 3.15.

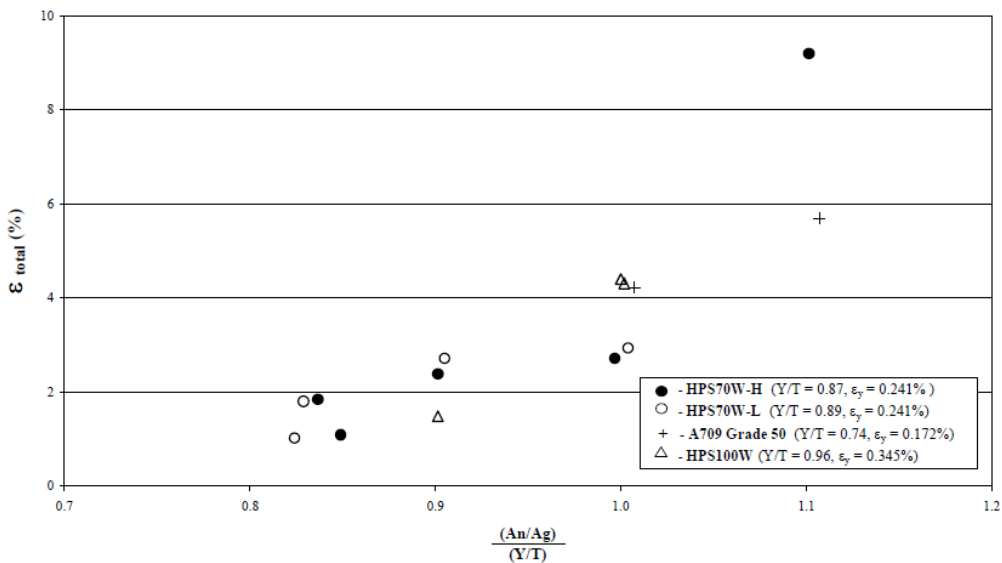


Figure 3.15 – Maximum gage-length elongation for all steel grades [31]

Where: Y –  $f_y$   
 T –  $f_u$

The data obtained from wide-plate tensile tests point out that the net section behaviour can be described entirely by the  $(A_n/A_g)/(f_y/f_u)$  ratio. If the ratio is greater or equal than 1, this leads to gross section yielding and adequate ductility.

One girder with HPS70W web and tension flange was fabricated and tested to failure. This was done in order to investigate the potential for tension flange rupture in a girder and to relate tension panel ductility to girder ductility.

The geometry of the test specimen is illustrated in Figure 3.16. The design was constrained by the capacity of the testing machine. The tension flange in HPS70W had the same cross section as the wide-plate tension test specimens. The compression flange was chosen such as to shift the plastic neutral axis in the top flange and thus eliminate the possibility of flange local buckling. The web was designed such as to avoid shear buckling and without stiffeners. Bearing stiffeners were placed at midspan and at the supports.

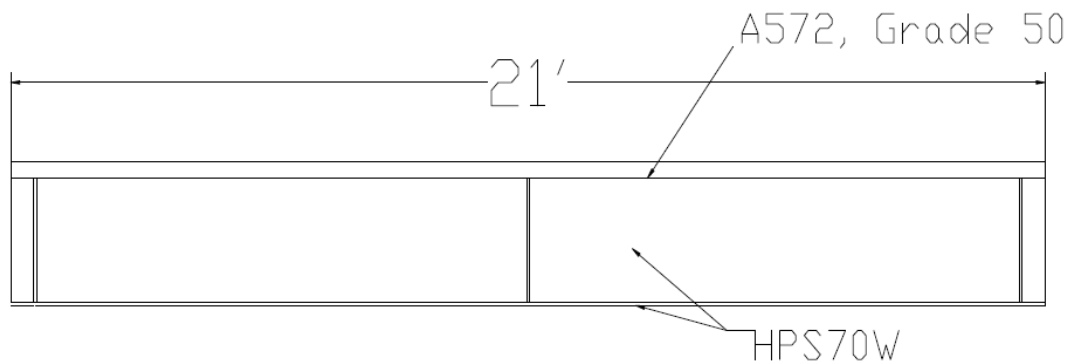


Figure 3.16 – Large-scale girder test specimen geometry [31]

The girder was supported on roller supports with a span of 6m (20 feet) and a three-point bending test was carried out.

The girder reached the plastic moment capacity and continued to increase in load capacity until lateral torsional buckling took place at a moment of around 110% of the plastic moment capacity. At this point the tension flange reached a 6.5% strain and 11% rotation. This demonstrates that HPS70W exhibits adequate tensile ductility in flexure and no premature necking occurs for this case.

The moment vs. rotation behaviour of hybrid unsymmetrical cross sections was predicted using finite element software with a simple cross-section analysis model. The stress-strain data from the HPS70W coupon test and elasticity modulus of 200000MPa (29000ksi) were used in the modelling.

A comparison between the predicted moment vs rotation and measured moment vs rotation (from the three-point bending test of HPS70W girder) curve is illustrated in Figure 3.17. The results obtained from the analysis also appear to be reasonably consistent with the measured strain in the tension flange.

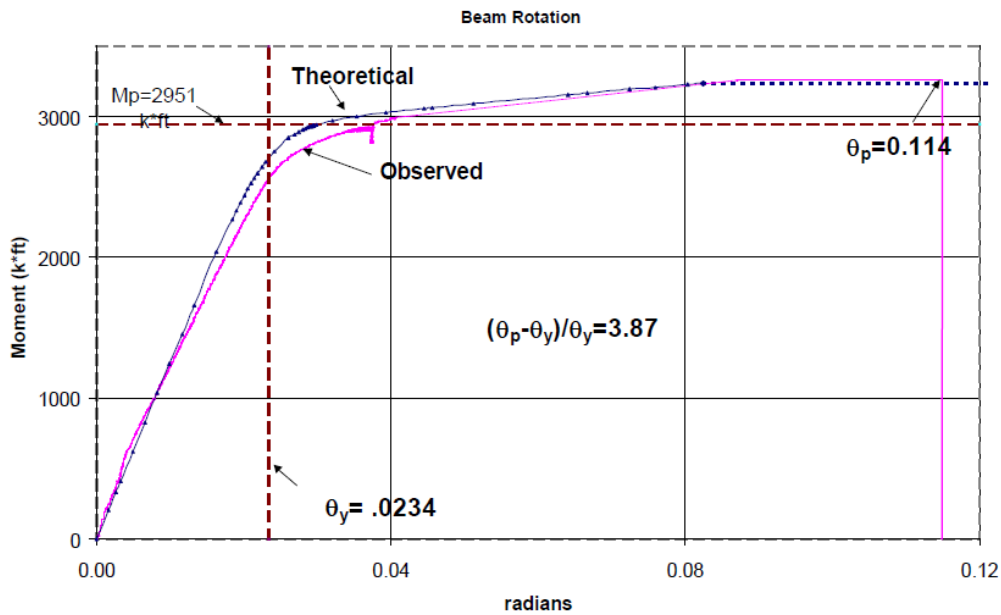


Figure 3.17 – Comparison of predicted and measured moment-rotation curves [31]

From the analysis of the cross sections it is shown that between 6 to 10 times the yield strain in the tension flange is required to be able to develop the plastic moment capacity of a girder. In the test performed in [31] the strain was around 10 times the yield strain when the plastic moment was developed. Any specimen with  $A_n/A_g$  equal or greater than  $f_y/f_u$  would have sufficient ductility to develop the plastic moment [31].

The statistical variation of  $f_y/f_u$  is also studied in order to determine adequate margins of safety to use in design equations when only the ratio of the minimum specified values of yield strength and tensile strength ( $F_y/F_u$ ) are known rather than the actual  $f_y/f_u$ .

In Load and Resistance Factor Design specifications, the allowable  $A_n/A_g$  is defined in terms of the minimum specified yield and tensile strengths. AISC (American Institute of Steel Construction) specifications, equation B10-1, states that no reduction in the moment capacity of a flexural member needs to be made for holes in the tension flange if:

$$0.75F_u A_n > 0.9F_y A_g$$

This can be re-written as:

$$A_n/A_g > (0.9/0.75)(F_y/F_u) = \gamma(F_y/F_u)$$

Where:  $\gamma=1.2$

The authors make use of the AISC reliability equation (modified for the presented problem):

$$\gamma R_n f_y/f_u = R_m f_y/f_u \times e^{0.55\beta V_r}$$

Where:

$\gamma$  - factor

$\gamma R_n f_y/f_u = \gamma(F_y/F_u)$

$R_m f_y/f_u$  – mean value of  $f_y/f_u$

$\beta$  – reliability index

$V_r$  – coefficient of variation of the  $f_y/f_u$  distribution

Table 22 – Parameters of  $f_y/f_u$  distribution and safe  $f_y/f_u$  ratios for various levels of reliability [31]

Steel	$F_y/F_u$	mean Y/T	COV	$\beta=2.0$		$\beta=2.6$		$\beta=3.5$	
				safe Y/T	$\gamma$	safe Y/T	$\gamma$	safe Y/T	$\gamma$
A36 t>0.75"	0.62	0.61	0.080	0.67	1.07	0.68	1.10	0.71	1.15
A572 50 t>0.5"	0.77	0.72	0.052	0.76	0.99	0.77	1.00	0.80	1.03
A588 50 t<2"	0.77	0.74	0.066	0.80	1.03	0.81	1.06	0.84	1.09
A992 shapes	0.77	0.76	0.04	0.79	1.03	0.81	1.05	0.82	1.07
A514 t<2.5"	0.87	0.94	0.017	0.95	1.10	0.96	1.11	0.97	1.12
HPS70W	0.82	0.84	0.060	0.89	1.08	0.91	1.10	0.93	1.14

The authors conclude that:

- HPS70W performs well in both tensions and flexural tests. HPS70W performed extremely well in both tension and flexural tests. Minimum ductility requirements in both tension and flexural bending were exceeded by the grade;
- Strength and ductility can be predicted on the basis of the  $(A_n/A_g)/(f_y/f_u)$  parameter, which in the case of wide-plate tests adequate ductility was provided at a ratio of 1 for all the grades’;
- Shell finite elements can predict with reasonable accuracy the behaviour of tension members up to the point of failure;
- It may be better to characterize tensile ductility just in terms of elongation;
- Simple cross-sectional moment-curvature analysis can be used to predict with reasonable accuracy the behaviour of flexural members;;
- The present AISC and AASHTO provisions for tension members and for holes in flexural members would be conservative when applied to HPS70W.

**Mans et al (2001)** conducted research with the purpose of removing the limitations of AASHTO on the use of HPS-485W (referred to hereinafter as HPS70W) steel in composite beams within the positive bending-regions. In steel bridges concrete slab on steel (composite girders) are widely used. In order to ensure ductile behaviour in composite members sufficient yielding of the steel prior to concrete crushing is required. Some concerns are raised regarding the capability of high-strength steel to achieve sufficient deformation without rupture prior to concrete failure.

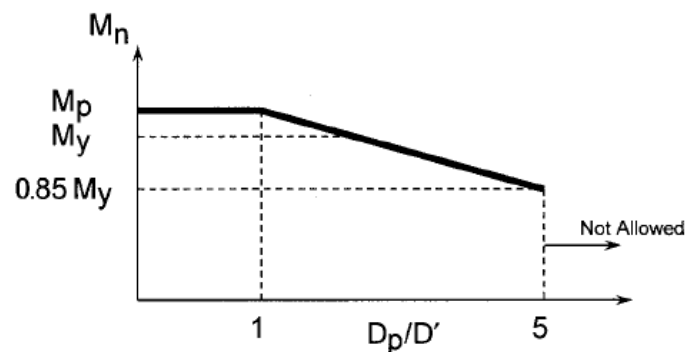


Figure 3.18 – Relationship between ductility parameter and moment capacity [32]

Where:

$D_p$  – depth of the neutral axis at theoretical plastic moment

$D'$  – modified ductility factor ( $0.7D_t/7.5$  for 345MPa section and  $0.9D_t/7.5$  for 250MPa sections)

The authors, in order to evaluate the steels' ability to achieve the required large levels of inelastic deformation, conducted experimental positive bending testing on girders constructed from HPS70W. The specimens used were designed to have a  $D_p/D' < 1$  and  $D_p/D' = 2$ . The geometry of the specimens is illustrated in Figure 3.19.

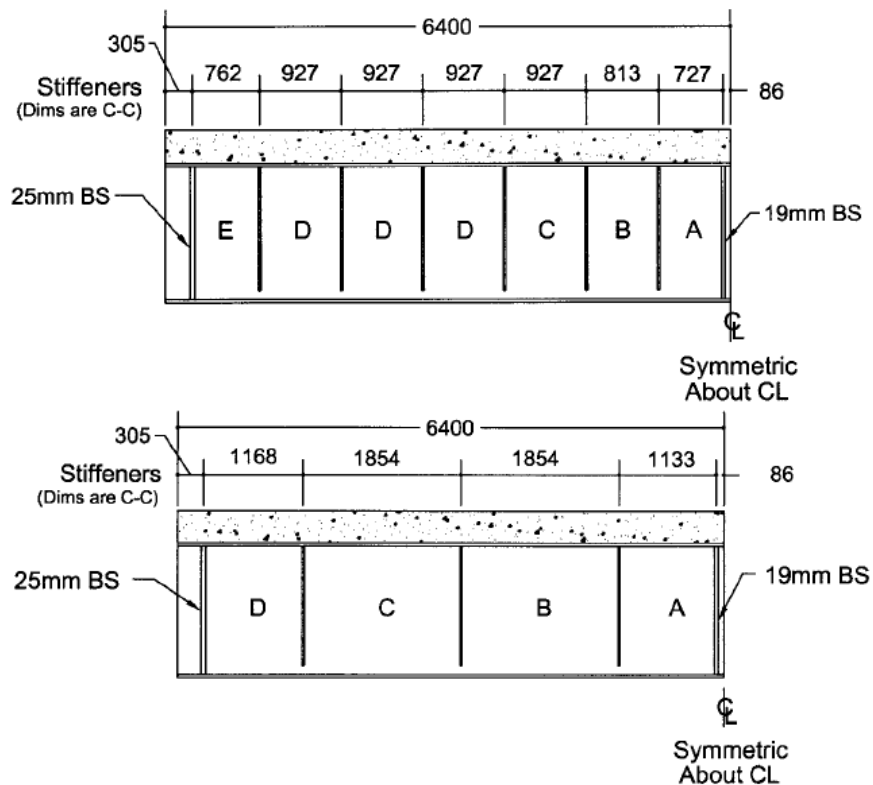


Figure 3.19 – Geometry of specimens POS1 and POS 2 (mm) [32]

Where:

CL – Centre Line

BS – Bearing Stiffener

The composite girders were tested as simply supported beams with a single point load applied at midspan and the behaviours was monitored using strain gauges glued to the flanges, web and reinforced concrete deck.

In both cases the obtained results were positive. The first specimen (POS1) resulted in a maximum load greater by 7% than the theoretical predicted value. The second specimen had a moment capacity slightly higher than the theoretical plastic moment and the tension flange achieved strains 9.5 times the yield strain with no problems.

The authors concluded that the design of HPS70W composite girders using existing provisions results in sections with higher capacity than the predicted values.

### 3.1.2 Conclusions from previous scientific works

Based on the studied material it can be concluded that considering just the yield-tensile ratio for comparison of different steels is somewhat of an over-simplification. Other factors such as the length of the yield plateau, the slope of the stress-strain curve in the inelastic range, local elongation and uniform elongation are also important properties that can influence the structural behaviour [29].

If the required levels of deformation capacity are pre-established then the maximum yield-tensile ratio that would fulfil the requirements could be determined based on analytical and experimental studies. Based on the experiments conducted in [28], the authors suggest that  $f_y/f_u$  is only an issue when in excess of 0.9 ( $f_u/f_y \leq 1.11$ ), and then only in the case of thin plates. The obtained value is of quite significant importance as the Eurocode criteria with regard to ductility require a minimum  $f_u/f_y \geq 1.10$  for mild steels and  $f_u/f_y \geq 1.05$  for HSS.

Other important points that were covered in the studied papers are:

- Fatigue: from the previous research carried out on this topic there is no reason to suspect that the yield-tensile ratio is a factor in the fatigue of fabricated members [29];
- Toughness: adequate notch toughness and fracture ductility must be provided both in the parent metal and in the weld material. This is provided by the steel manufacturer depending on the environmental conditions, loading characteristics and the fabrication details [29];
- The  $f_y/f_u$  ratio increases with decreasing thickness for a given grade within the thickness range for which the alloying system is the same [28];
- The  $f_y/f_u$  ratio increases with yield strength in accordance with a power-law relationship [28];
- The relationship of decreasing strain hardening exponents with increasing  $f_y/f_u$  has been further confirmed [28];
- In case of welded joints, the level of weld metal and HAZ mismatch and the toughness of the various regions of the HAZ are more significant than the  $f_y/f_u$  ratio of the parent plate and weld metal [28];
- HSS performs better than ordinary steel or at least the same with regard to local and global buckling [21].

In the case of structures subject to dynamic loadings (e.g. seismic loading) large deformation capacities are required in order to ensure energy dissipating mechanisms and prevention of collapse. When such loadings are not determinant, ductility requirements are related to the occurrence of stress concentrations and the ability of connections to yield locally and redistribute loads. These factors are related to local ductility and elongation capacity which increase with a decreasing yield-tensile ratio. Based on the literature review it is clear that a lower  $f_y/f_u$  ratio will result in improved ductility (more material will yield before failure). However in none of the studied works a clear statement of what would be a recommended  $f_y/f_u$  ratio in order to ensure redistribution of stresses was provided. Thus in order to have an estimate of ductility in this work, both the  $f_y/f_u$  ratio and strain are taken into account.

The scope of this work is to provide a scientific approach and look into depth at the phenomena of stress concentrations, and based on a correlation between a nonlinear and linear calculations determine criteria for ductility and strength capacity.

### 3.2 Structural Failures

In this section some examples of structural failures from the past are described. This has the purpose of providing some insight into the causes that lead previous structures to not fulfil their intended function.

- The Fourth Danube Bridge in Vienna (Austria, 6 November 1969): a continuous twin-box girder bridge in three spans, having haunches over the inner supports, with a total length of 412 meters and a main span of 210 meters. The free cantilever erection method was chosen and, as the two cantilever ends met in the middle, the final section had to be adjusted because of temperature deformations during the day (sunny and warm). The final closing section was shortened by 15 mm at the top and, as the temperature dropped during the evening, this introduced a constraint in the structure, resulting in tensile forces in the top flange and, as a result, compression stresses in the lower flange. This led to buckling in the mid-span regions of the lower flange [33];

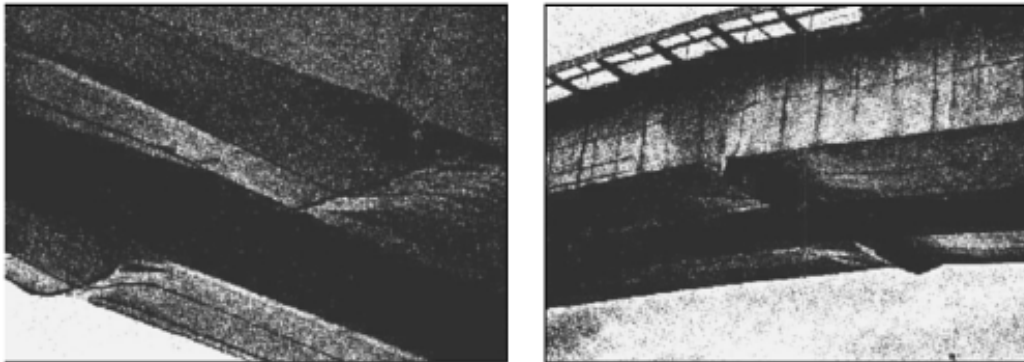


Figure 3.20 – The parts having the major buckles – close to the inner support of the main span, and in the centre part of the first span [33]

- Milford Haven Bridge (United Kingdom, 2 June 1970): single continuous box girder bridge of welded steel, with spans of 77m, 77m, 77m, 149m, 213m, 149m and 77m. The cantilever erection method was chosen and the failure was initiated by buckling of the support diaphragm at the root of the cantilever being erected. The span to collapse was the second 77m, leading to global collapse [33];
- Rhine Bridge in Koblenz (West Germany, 10 November 1971): single steel box bridge, 16.4m wide at the top and 11m wide at the bottom, with the box being erected by cantilevering. Failure occurred due to buckling of the bottom flange splice at the pier [33];
- Sgt Aubrey Cosens VC Memorial Bridge (Canada, 14 January 2003): arch bridge where deck failure occurred due to fractures in two of the hanger rods which connected the deck to the overhead arch. The fatigue induced fracture of the hanger rods was induced by defects introduced in the hanger threads during construction and steel that did not remain ductile in very cold temperatures [34];
- I-35W Bridge (U.S.A., 1 August 2007): three-span continuous deck-truss structure flanked by steel-girder and concrete-slab approaches, with a 140m main span and two 80m side spans. The bridge was designed in 1964, opened to traffic in 1967 with 6 through-traffic lanes and two auxiliary lanes. In 1977 and 1998 two rehabilitations

took place which increased the average concrete deck thickness from 16.5cm to 21.5cm and the width to 8 lanes. The collapse of the structure took place after the bridges gusset plates, due to under sizing, suffered plastic deformations which lead to bowing and eventual buckling. The steel used to build the bridge had a yield strength of 348MPa (50.5ksi) and allowed a 10% plastic strain at an ultimate strength of 593MPa (86ksi), which was about 70% higher than  $f_y$ . This held the bridge until the accumulated damages caused by the environment factors, the additional weight and increased traffic induced material fatigue led to the collapse [35];

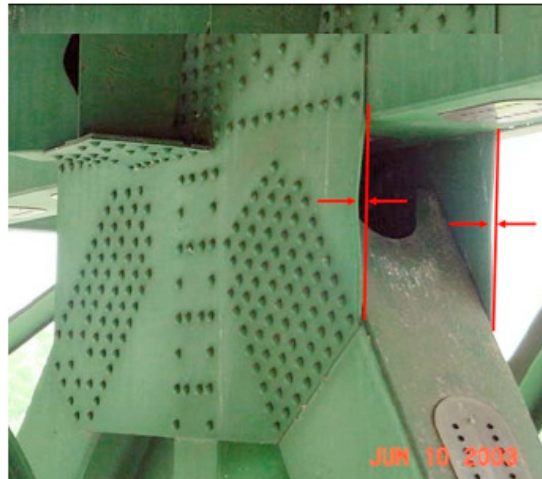


Figure 3.21 – Bowing at gusset plate U10 before the collapse [35]

- New East Span of the San Francisco-Oakland Bay Bridge (U.S.A., 1 March 2013): self-anchored suspension bridge was built to replace an unsafe cantilever portion of the Bay Bridge. On the 1<sup>st</sup> of March 2013, following load transfer of the weight of the roadway deck from the temporary falsework onto the main cable, the anchor rods were tensioned. Between March 8 and March 14, 32 out of the 96 rods were discovered to have fractured. Failure of the elements was caused by hydrogen embrittlement and it was attributed to higher than normal susceptibility of the steel to hydrogen embrittlement [36].

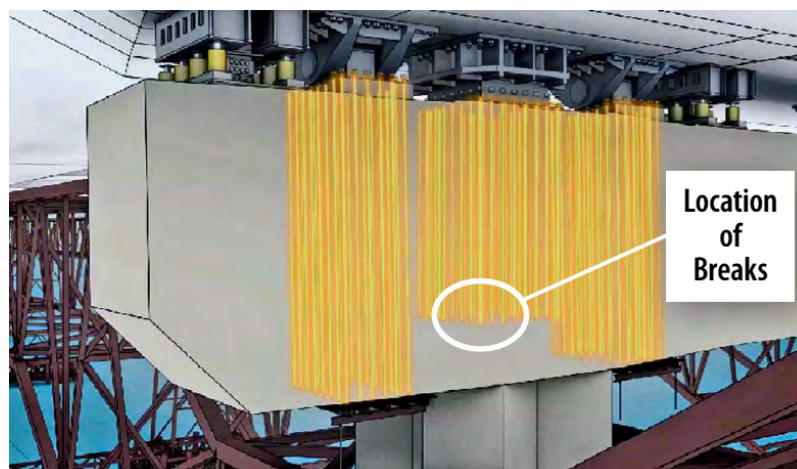


Figure 3.22 – Location of failed A354 grade BD anchor rods [36]

Based on the examples described above it can be stated that the ductility or yield-tensile ratio was in none of the cases a decisive factor leading to structural failure.

### 3.3 Current Design Code Requirements With Regard to Ductility

One of the most important material properties with regard to steel is ductility. Design codes have different requirements with regards to this property. The most common rule of expressing this is by limiting the yield-tensile ratio to a maximum value (or tensile-yield ratio to a minimum value) in order to ensure the material has a reserve of strength beyond yield.

#### 3.3.1 Eurocode

The Eurocode has two separate material specifications depending on whether it is mild steel (up to and including grade S460) or high strength steel (steel grades up to S700). EN 1993-1-1, Section 3.2.2 specifies the following ductility requirement limits for mild steels:

- the ratio  $f_u/f_y$  of the specified minimum ultimate tensile strength  $f_u$  to the specified minimum yield strength  $f_y$  should be greater or equal to 1.10:  $f_u/f_y \geq 1.10$  ( $f_y/f_u \leq 0.91$ );
- the elongation at failure should not be less than 15%;
- the ultimate strain  $\epsilon_u \geq 15 \epsilon_y$ .

EN 1993-1-12 specifies the ductility requirements for high strength steels up to grade S700:

- $f_u/f_y \geq 1.05$  ( $f_y/f_u \leq 0.95$ );
- elongation at failure not less than 10%;
- $\epsilon_u \geq 15 f_y/E$

For each country a recommendation is given in the National Annex. In the Dutch National Annex the  $f_u/f_y$  requirement for HSS is the same as for mild steels ( $f_u/f_y \geq 1.10$ ). These values are based on test results. However in the UK National Annex to EN 1993-1-12 for example, the  $f_u/f_y$  ratio is kept at 1.05 and the minimum elongation at failure of 10% is increased to 15% in order to provide greater ductility [37].

#### 3.3.2 Rijkswaterstaat limitations in the Netherlands

The Rijkswaterstaat has stricter ductility requirements compared to the Eurocode. A minimum tensile-yield ratio of 1.20 ( $f_u/f_y \geq 1.20$ ) is required as material property. The basis behind this increased performance requirement is:

- Maintenance and repair are carried out by a third party without the intervention of Dienst Infrastructuur and welding of S460 requires specific measures which often depend on the type of S460 grade
- Reparation of damaged S460M is risky with respect to deterioration of strength.

#### 3.3.3 American Institute of Steel Construction

The AISC Specification for Steel Buildings manual limits in hollow section connections the  $f_u/f_y \leq 0.8$  (Tables K1.1 to K3.2) for steels with  $f_y$  lower than 360MPa (52ksi). Also A992 has a specified maximum yield-tensile strength ratio of 0.85 ( $f_u/f_y \geq 1.17$ ).

The AISC Specification for Steel Buildings manual lists in Appendix 1 “Design by Inelastic Analysis” provisions for the inelastic analysis and design of structural steel systems. Regarding the material properties and yield criteria for the analysis requirements, the code states that modelling of strain hardening that result in strengths greater than the plastic strength of the cross section is not permitted.

#### 3.3.4 Other (older) design codes

The older Norwegian code required a ratio of  $f_y/f_u \leq 0.83$  ( $f_u/f_y \geq 1.20$ ) for all steels. The British Standards BS 5950 also limited the  $f_y/f_u$  to a value of 0.84 ( $f_u/f_y \geq 1.19$ ).

Detailed information on steel grades and their related material properties can be found in [38].

### 3.4 Structural Modelling

As the current work is mainly focused on stress concentrations which arise in connections due to irregularities in the cross section, a background survey on modelling as prescribed by design codes is carried out. The limitations of the Eurocode with respect to software modelling of HSS structures are presented in this section. In order to gain a better insight into the occurrence of stress concentrations, a possible method is to calculate the strain with a physical nonlinear calculation, based on the nonlinear behaviour of the material. Annex C of EN 1993-1-5 gives insight on modelling of material properties. Function of the accuracy and the allowable strain required for the analysis different material behaviours may be used: elastic-plastic without strain hardening, elastic-plastic with a nominal plateau slope, elastic-plastic with linear strain hardening and true stress-strain curve.

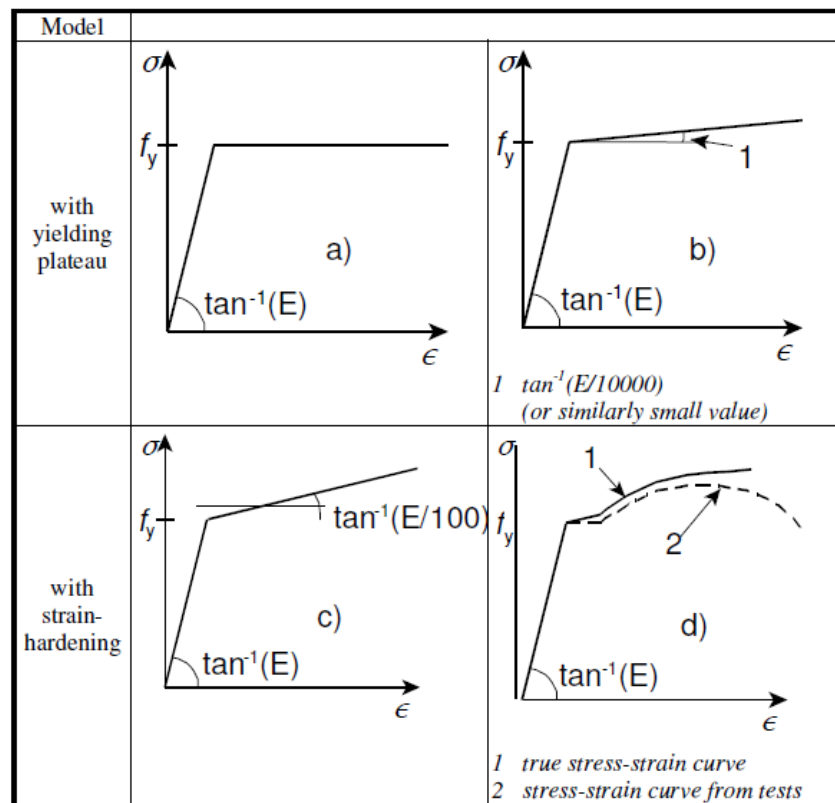


Figure 3.23 – Modelling of material behaviour [39]

EN 1993-1-1 and EN 1993-1-5 give general guidelines for structural modelling for analysis of the structure. The codes present basic assumptions regarding the analysis and calculation model to be used. Annex C of EN 1993-1-5 gives guidance on the use of finite element methods for the limit state and fatigue verifications of plated structures. Depending on the problem to be analysed and the assumptions made, a choice for the finite element method to be used is made. Annex C also underlines important points that must be taken into consideration when using FEM, such as: modelling of the structural component and its boundary conditions, choice of software and documentation, use of imperfections, modelling of material properties, loads, limit state criteria, and the partial factor to be applied.

Table 23 – Assumptions for FE-methods [39]

No	Material behaviour	Geometric behaviour	Imperfections, see section C.5	Example of use
1	linear	linear	no	elastic shear lag effect, elastic resistance
2	non linear	linear	no	plastic resistance in ULS
3	linear	non linear	no	critical plate buckling load
4	linear	non linear	yes	elastic plate buckling resistance
5	non linear	non linear	yes	elastic-plastic resistance in ULS

EN 1993-1-1, Section 5.4 states methods of analysis considering the material non-linearity. The internal forces and moments can be determined by elastic global analysis (which may be used in all cases) and plastic global analysis (which may be used only if the structure has sufficient rotation capacity). EN 1993-1-12 which provides additional rules for steel grades up to S700 restricts the use of plastic global analysis in structures built up of high strength steel grades.

EN 1993-1-8 provides rules for analysis, classification and modelling of joints (in general joints in frame-structures). According to the standard, if the effects on the distribution of internal forces and moments within a structure due to the joint behaviour are sufficiently small, they can be ignored. In order to establish their effect three simplified joint models are described: simple (joint may be assumed not to transmit bending moments), continuous (the behaviour of the joint may be assumed to have no effect on the analysis) and semi-continuous (the behaviour of the joint needs to be taken into account in the analysis). Depending on the classification of the joint and on the chosen method of analysis, the appropriate type of joint model should be determined from Table 28.

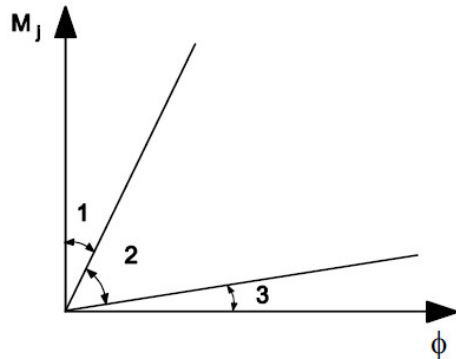
Table 24 – Type of joint model [40]

Method of global analysis	Classification of joint		
	Nominally pinned	Rigid	Semi-rigid
Elastic	Nominally pinned	Rigid	Semi-rigid
Rigid-Plastic	Nominally pinned	Full-strength	Partial-strength
Elastic-Plastic	Nominally pinned	Rigid and full-strength	Semi-rigid and partial-strength Semi-rigid and full-strength Rigid and partial-strength
Type of joint model	Simple	Continuous	Semi-continuous

EN 1993-1-8 also states possible methods of analysis. The global analysis can be: elastic (joints should be classified according to their rotational stiffness), rigid-plastic (joints should be classified according to their strength), elastic-plastic (joints should be classified according to both stiffness and strength), global analysis of lattice girders.

The classification of joints by stiffness is done according to Figure 3.24. In the case of classifying joints by strength, this is done by comparing the design moment resistance of the joint with that of the member it connects. Nominally pinned joints should be capable of transmitting the internal forces without developing significant moments, full-strength joints should have their design resistance no less than that of the connected members and partial-strength joints do not meet the criteria for neither of the full-strength or the nominally pinned joints.

EN 1993-1-12 restricts the applicability of rigid-plastic and elastic-plastic global analysis for steel grades higher than S460 up to S700. Also, joints built of HSS grades are not allowed to be classified as semi-rigid joints.



Zone 1: rigid, if  $S_{j,ini} \geq k_b EI_b / L_b$

where:

$k_b = 8$  for frames where the bracing system reduces the horizontal displacement by at least 80 %

$k_b = 25$  for other frames, provided that in every storey  $K_b/K_c \geq 0,1$  \*)

Zone 2: semi-rigid

All joints in zone 2 should be classified as semi-rigid. Joints in zones 1 or 3 may optionally also be treated as semi-rigid.

Zone 3: nominally pinned, if  $S_{j,ini} \leq 0,5 EI_b / L_b$

\*) For frames where  $K_b/K_c < 0,1$  the joints should be classified as semi-rigid.

Key:

- $K_b$  is the mean value of  $I_b/L_b$  for all the beams at the top of that storey;
- $K_c$  is the mean value of  $I_c/L_c$  for all the columns in that storey;
- $I_b$  is the second moment of area of a beam;
- $I_c$  is the second moment of area of a column;
- $L_b$  is the span of a beam (centre-to-centre of columns);
- $L_c$  is the storey height of a column.

Figure 3.24 – Classification of joints by stiffness [40]

Due to the lack of long term experience with HSS, applications in Europe compared to the United States and Japan are still limited. This leads to higher requirements in design codes (especially with respect to deformation capacity of HSS elements) translated in the Eurocode limitations regarding modelling of steel structures in HSS.

The scope of this work is not to limit itself to the design code requirements but rather study in depth the influence of ductility in design, based on scientific work. An attempt to prove the applicability of HSS beyond current limitations is made based on engineering judgement.

### 3.5 Stress Concentrations

When a large stress gradient occurs in a small, localized area of a structure, the high stress that appears is referred to as a stress concentration. When the smooth flow of stresses through the structure is disrupted by rapid geometry change or material properties, high stress gradients occur.

Changes in material properties can occur both at macroscopic and microscopic levels which include alloy formulation, grain size and orientation, foreign materials, etc. Simple geometric changes are plate or shafts with holes, notches, steps, etc. Plates in tension or bending with holes, notches, steps are simple examples involving direct normal stresses, while shafts in tension, bending, torsion, with holes, notches, steps are examples involving direct and bending normal stresses and torsional shear stresses. Other geometric changes include rough surface finishes, internal and external cracks, and in the case of more complicated geometries, finite element methods should be used [41].

The maximum stress and strain concentrations that occur can greatly exceed the nominal/averaged values obtained from hand calculations. In steel connections stress concentrations occur due to irregularities in the cross section. If the material has sufficient ductility then, due to plastic deformations, forces are redistributed so there will be equilibrium in the internal forces. This behaviour can occur if the material has sufficient deformation capacity: tensile strength higher than the yield strength and minimal extend and strain in case of fracture.

#### 3.5.1 Static stress and stress concentration factors

The following plate loaded in tension with a force per unit area  $\sigma$  and outer dimensions infinite compared to the hole diameter is considered:

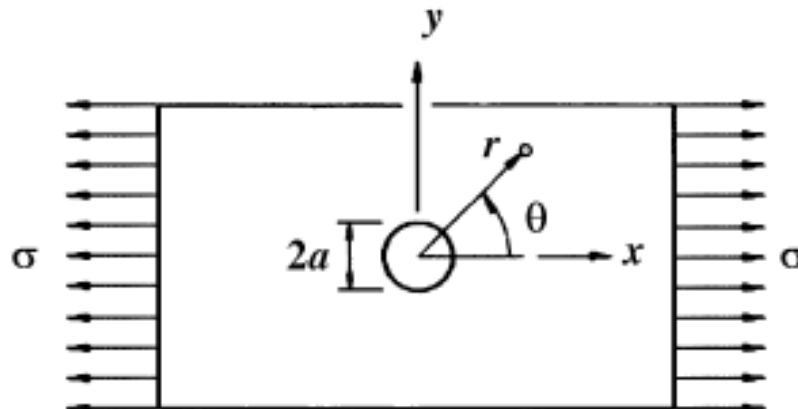


Figure 3.25 – Circular hole in a plate loaded in tension [41]

From linear elasticity it can be shown that the tangential stress throughout the plate is:

$$\sigma_{\theta} = \frac{\sigma}{2} \left[ 1 + \frac{a^2}{r^2} - \left( 1 + 3 \frac{a^4}{r^4} \right) \cos(2\theta) \right] \quad [42]$$

At  $r = a$  and  $\theta = \pm 90^\circ$ , the maximum stress is  $3\sigma$ . Figure 3.26 shows how the tangential stresses vary along the x and y axis of the plate:

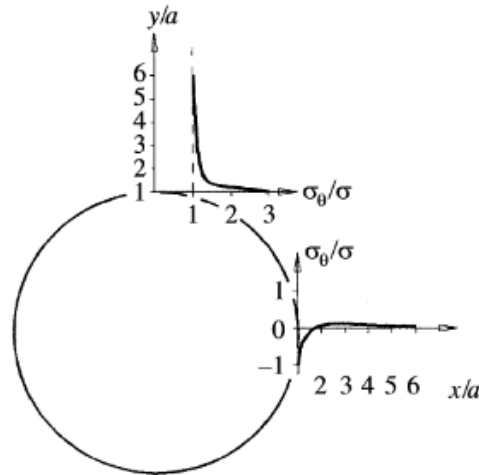


Figure 3.26 – Tangential stress distribution for  $\theta = 0^\circ$  and  $90^\circ$  [41]

In the elastic range, the static stress concentration factor is defined as the ratio of the maximum stress to the nominal stress:

$$K_t = \frac{\sigma_{max}}{\sigma_{nom}}$$

Which in the case of the infinite plate containing a hole and loaded in tension is  $K_t=3$ .

Stress concentration configurations such as holes, grooves, welds and other geometrical discontinuities cannot be avoided in the design of structures. The problem that arises in the design of steel bridges with respect to ductility is related to the stress concentrations occurring at geometry change. Due to discontinuities a large stress gradient occurs in a small, localized area of the structure. If the load on the structure exceeds the value for which the maximum stress at a stress concentration equals the yield stress, the stress distribution changes from elastic to elastic-plastic. Ensuring the structural safety is a basic design requirement and a nonlinear finite element analysis with the nonlinear material behaviour is in general required in order to prove that peak stress concentrations will not lead to structural failure. As this is quite a time consuming process, development of a method that could prove this based only on a linear analysis might be a good alternative to the nonlinear finite element analysis. Thus an estimate of stresses and strains occurring at these locations is required in component design. Several notch stress-strain conversion rules are available. Two of the most commonly used methods are Neuber's formula for nonlinear material behaviour and the equivalent strain energy density method.

### 3.5.2 Neuber's formula for nonlinear material behaviour

Neuber investigated the development of stress and strain concentrations in the case when material behaves nonlinear (deviates from Hooke's law) [43]. In this section the term real stress and real strain ( $\sigma_{max}$  and  $\epsilon_{max}$ ) will be used to define the inelastic stress and strain as opposed to the stress and strain obtained from an elastic calculation. The author established a hypothesis by which the real stress at the location of the concentration can be related, by a simple relation, to the nominal stress as well as elastic stress concentration factor using the elastic stress at the same location. The real strain is greater than the Hookian while the real stress is smaller than the Hookian. Thus the author defines an effective stress concentration factor and an effective strain concentration factor:

$$K_{\sigma} = \frac{\sigma_{max}}{\sigma_{nom}} \quad (1)$$

$$K_{\varepsilon} = \frac{\varepsilon_{max}}{\varepsilon_{nom}} \quad (2)$$

Where  $\sigma_{max}$  and  $\varepsilon_{max}$  represent the real stress and strain, and  $\sigma_{nom}$  and  $\varepsilon_{nom}$  the nominal stress and strain in the net section ( $\sigma_{nom} = A_{net}q$ ). Neuber defines  $K_t$  (stress-concentration factor) as the geometric mean of the effective stress and strain concentration factors:

$$K_t = (K_{\sigma}K_{\varepsilon})^{\frac{1}{2}} \quad (3)$$

This function has the quality that it has the same value for all stress-strain laws and is therefore equal to the Hookian stress concentration factor [43].

Rewriting  $K_t$  in terms of stress and strains, it results that:

$$\sigma_{max}\varepsilon_{max} = K_t^2\sigma_{nom}\varepsilon_{nom} \quad (4)$$

Where  $K_t$  and  $\sigma_{nom}$  are obtained in the same way as when the maximum stress is within the elastic range, and  $\varepsilon_{nom}$ ,  $\sigma_{max}$  and  $\varepsilon_{max}$  are calculated by making use of any stress-strain diagram.

The graphical interpretation of Neuber's formula is illustrated in Figure 3.27.

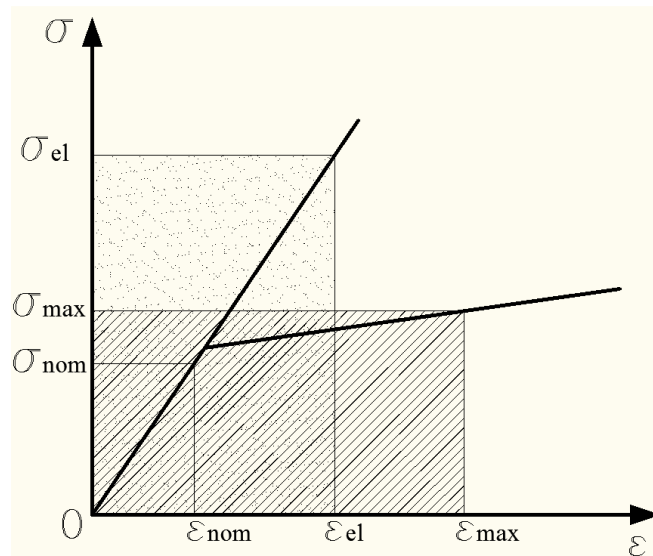


Figure 3.27 – Graphical interpretation of Neuber's formula

Where  $\sigma_{el} = K_t\sigma_{nom}$  and  $\varepsilon_{el} = K_t\varepsilon_{nom}$

Hoffmann and Seeger in [44] and [45] proposed a generalization of Neuber's rule which addresses multiaxial proportional loading sequences. The authors extended Neuber's rule by replacing the uniaxial stress and strain with the equivalent stress and strain.

### 3.5.3 Equivalent strain energy density method

An alternative approximation method to Neuber's formula was proposed by Molski and Glinka in [46]. The authors state that the strain energy at a geometric irregularity will give identical results in both the elastic and elastic-plastic material behaviours. This assumption is based on the supposition that the localized plasticity is surrounded by predominantly elastic material. The relation has the following form:

$$\frac{1}{2} \sigma_{ij}^{el} \varepsilon_{ij}^{el} = \int_0^{\varepsilon_{ij}^{ep}} \sigma_{ij}^{ep} d\varepsilon_{ij}^{ep} \quad (5)$$

Where  $\sigma_{ij}^{el}$  and  $\varepsilon_{ij}^{el}$  represent the stress and strain in the linear elastic range and  $\sigma_{ij}^{ep}$  and  $\varepsilon_{ij}^{ep}$  the stress and strain in the elastic-plastic state. The graphical interpretation of the Molski-Glinka rule is illustrated in Figure 3.28.

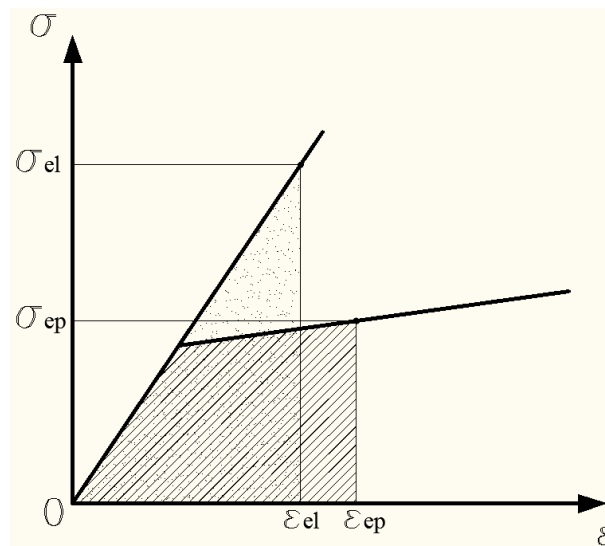


Figure 3.28 – Graphical interpretation of the equivalent strain energy density method

The Equivalent Strain Energy Density method is expected (as it can be noticed from Figure 3.27 and Figure 3.28) to give lower values for the strain in the elastic-plastic region compared to Neuber's rule. In [47] the authors conclude based on finite element analysis that the equivalent strain energy density method gives underestimates of the inelastic strain predictions. Also, the ESED method has two important limitations. Plastic yielding has to be localized (the local plastic region has to be small in comparison to the surrounding elastic region) and the nominal stress level has to be lower than the yielding stress [46]. Considering that in [48] the authors showed that Neuber's rule provides accurate estimations of notch root stress and strain in plane stress situations and in [47] the authors, based on tests, stated that it is the single best model for plane stress situations, Neuber's rule seems to be a better option for estimating stresses and strains at notch-tips. However, the disadvantage of Neuber's rule is that in order to compute the real stress and strain, knowledge of the stress concentration factor and nominal stress value is required. This poses some restrictions when this would be applied to more complicated cases where these values are not known, thus resulting in a limited applicability. In order to have a method for estimating the plane strains and stresses also for these more complicated cases, a new approach is developed in section 4 based on Neuber's formula for nonlinear material behaviour and research carried out in [44], [45], [47] and [48].

#### 4 LINEAR TO NONLINEAR ANALYSIS CORRELATION

In bridge connections, where high stress concentrations occur due to geometric discontinuities, material ductility is required in order to ensure the redistribution of efforts. In such steel joints plated elements are encountered which is translated in the fact that plain stresses and strains occur. Due to these geometric discontinuities yielding of the material will first occur at the stress concentration locations. If the load continues to increase the surrounding material yields until equilibrium is attained. Thus the strain at the location of the stress concentration increases function of the strain hardening law. In order to be able to estimate the real strain (nonlinear) at such a location a nonlinear finite element analysis, based on the material's nonlinear behaviour (stress-strain law), is necessary. This would provide information with regard to the extent to which the material surrounding a geometric irregularity yields and the real stress and strain at the notch-tip. Both information are necessary in order to evaluate the capacity.

When using a linear finite element analysis, the locations of the stress concentrations can easily be pinpointed in the connection. If the load would be further increased (in the case of a linear finite element analysis) the stress and strain would increase linear corresponding to the elasticity modulus, with the highest value corresponding to the stress concentration location. However the results are not based on the real material behaviour and the extent of the yield zone surrounding the notch-tip is not known. Thus at this stage it is possible to estimate only the real stress and strain at the notch-tip based on the linear finite element analysis. In order to do this (based on the conducted literature review) the rectangular areas from the stress-strain diagram (Figure 4.1) are assumed equal in this new approach. The area corresponding to  $\sigma_{el}\varepsilon_{el}$  represents the values of the elastic stress and strain while the area corresponding to  $\sigma_{NL}\varepsilon_{NL}$  represent the values of the estimations of the nonlinear stress and strain. When a linear finite element analysis is available, the stress concentration at a location is known. Dividing this stress with the yielding stress of the material a new correlation factor is defined which is denoted by  $D_m$ :

$$D_m = \frac{\sigma_{el}}{f_y} \quad (6)$$

Where  $\sigma_{el}$  represents the equivalent stress at the stress concentration location or notch-tip (calculated from a linear finite element analysis) and  $f_y$  the yielding strength of the steel grade.

Using this new factor a re-formulation of Neuber's rule can be stated:

$$\sigma_{max}\varepsilon_{max} = \sigma_{NL}\varepsilon_{NL} = D_m^2 f_y \varepsilon_y \quad (7)$$

Where  $\sigma_{NL}$  and  $\varepsilon_{NL}$  represent the stress and strain values in the nonlinear range,  $D_m$  the correlation factor,  $\sigma_{el} = D_m f_y$ ,  $\varepsilon_{el} = D_m \varepsilon_y$  and  $f_y$  and  $\varepsilon_y$  the yield strength and strain. This method will be referred to in the remainder of this paper as the Stefanescu Method, or shortly SM method. The graphical interpretation is illustrated in Figure 4.1.

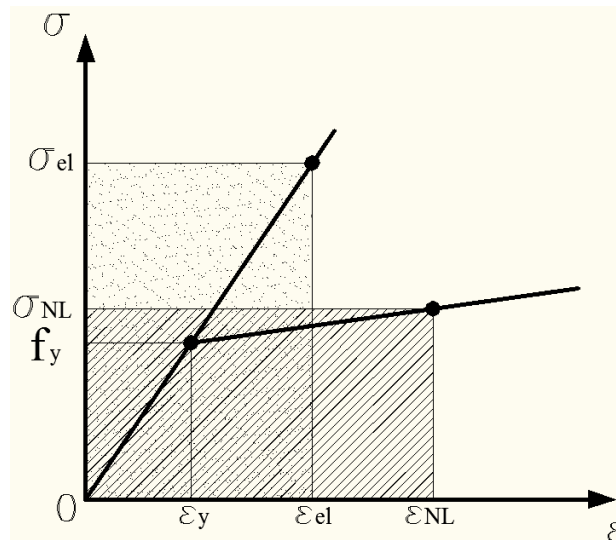


Figure 4.1 – Graphical interpretation of the SM method

The advantage of the newly stated method is that it is no longer dependent on the nominal stress and the Hookian stress concentration factor in order to estimate the nonlinear strains and stresses. It can be applied straight forward based only on a finite element linear elastic analysis. However, using only the SM approach does not give any insight on what would be the relation between the strength capacity and the criteria for ductility. In order to understand how this could be achieved and what the capacity of an element is, a first application of the SM method on a simple case of a plate with a hole loaded in tension is taken as an example.

#### 4.1 Application of the SM Method on a Plate with a Hole

The applicability of the SM method is tested on a plate with a hole. The geometry is presented in Figure 4.2. This element is chosen as prior knowledge on the behaviour, the stress concentrations factors and the nominal stresses are available.

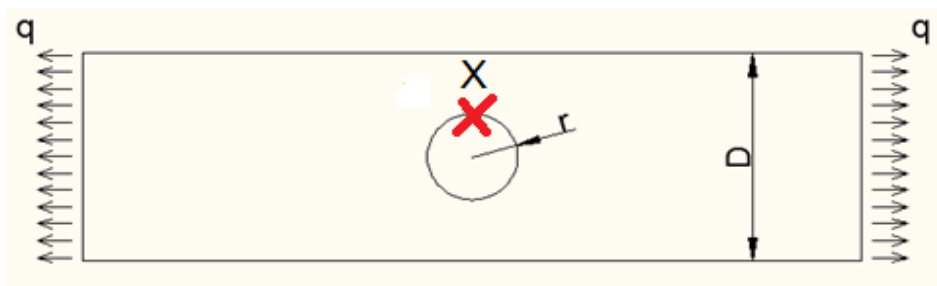


Figure 4.2 – Geometrical layout of a plate with hole

Where:

q – Axial line load;

r – Hole radius;

D – Width of the plate;

X – Location of the stress concentration.

The SM method will be used to estimate the real stress and strain at location X which represents the stress concentration. This is the most loaded point in the plate element and an estimation of the strain at location X can give a general picture of the load state of the plate

with respect to its ultimate capacity. However, in order to understand what is meant by “capacity” of the plate, a failure limit has to be first defined. For practical reasons one of the criteria chosen is that of current design code requirements. The ultimate capacity, as defined in this paper for a plate with a hole, is either of the following two:

- The ultimate resistance of the net cross-section located at the hole:

$$q_u = A_{net}f_u/D \quad (8)$$

- Eurocode 1993-1-5: Plated Structural Elements, in section C.8 – Limit state criteria, has the following requirements: The ultimate limit state criteria - For regions subjected to tensile stresses: attainment of a limiting value of the principal membrane strain  
The Dutch National Annex gives the limit for the principal strain at  $\varepsilon_u=5\%$ .

Thus, in the present paper, attainment of ultimate capacity is defined as reaching ultimate strength in the net cross-section ( $N_u=A_{net}f_u$ ) or attainment of a maximum 5% principal strain in a localised zone of the element.

The plate with a hole loaded by a uniform distributed load  $q$  (Figure 4.2) is modelled in plane stress condition. The stress concentration factor in such a case is given by equation (9):

$$K_t = 3 - 3.13\left(\frac{2r}{D}\right) + 3.66\left(\frac{2r}{D}\right)^2 - 1.53\left(\frac{2r}{D}\right)^3 \quad [41] \quad (9)$$

As the magnitude of the stress concentration factor at the opening (and thus the value of the peak stress and strain) is influenced by the geometry, five different ratios of  $2r/D$  will be studied. The different geometrical configurations and their influence on the stress concentration factor are presented in Table 25. The 5 geometries are denoted with letters from A to E. In all the cases the plate has a thickness of 40mm.

Table 25 – Plate with hole geometries

Plate	r [mm]	D [mm]	(2r)/D	$K_t$	$q_u(A_{net}f_u)$ [N/mm] WoSH	$q_u(A_{net}f_u)$ [N/mm] WSH
A	375	1500	1/2	2.159	7100	10200
B	250	1500	1/3	2.307	9466	13600
C	187.5	1500	1/4	2.422	10650	15300
D	150	1500	1/5	2.508	11360	16320
E	75	1500	1/10	2.722	12780	18360

Besides the influence of the geometry on the SM approach, the shape of the stress-strain diagram is also taken into account. Thus each of the five plates is modelled using two stress-strain diagrams: one without strain hardening (Figure 4.3) and one with strain hardening (Figure 4.4). In both cases steel grade S355 was used with a yield strength of  $f_y=355\text{MPa}$  (which in the case of WoSH is equal to  $f_u$ ) and Young’s modulus  $E=210\text{GPa}$ , and an ultimate strength  $f_u=510\text{MPa}$  ( $f_u/f_y=1.4$ ) and  $E_2 = 1575\text{MPa}$  in the case WSH.

A full description of the finite element models used, the mesh, the boundary conditions and the load layout is presented in APPENDIX A, together with plots of the strains and stresses occurring in the plate at the most important load thresholds.

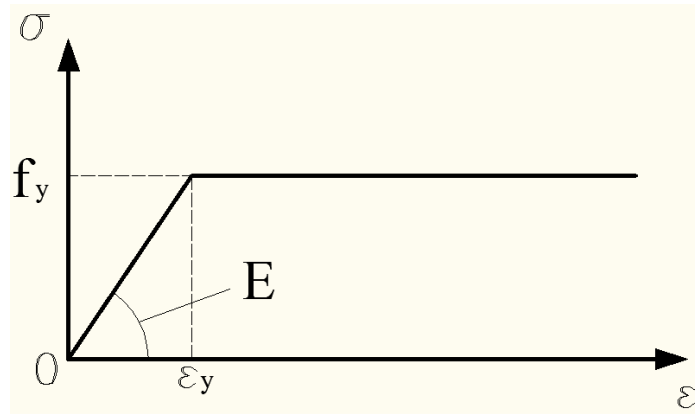


Figure 4.3 – Stress-strain curve WoSH

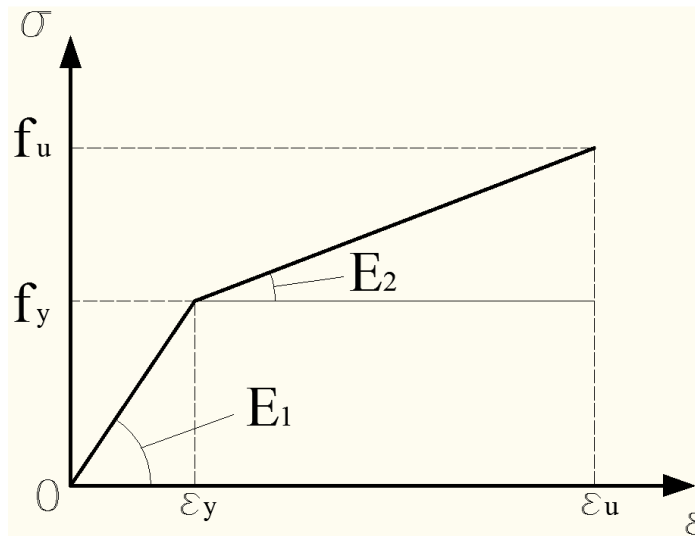


Figure 4.4 – Stress-strain curve WSH

For the analysis the yield criterion chosen is the Von Mises. This means that at any certain point in the material the stresses are different in different directions. There are three principal directions and three principal stresses: the maximum principal stress ( $\sigma_1$ ), minimum principal stress ( $\sigma_3$ ) and medium principal stress ( $\sigma_2$ ). Given the stress state, from the geometry of the Mohr's circle the values and corresponding directions of the principal stresses can be calculated. These represent the points of maximum normal stress, minimum normal stress and maximum shear stress, and are reported by Ansys.

The Von-Mises stress is also of significant interest as it offers a prediction of the yielding. The material yields when the equivalent stress (equations ( 10 ) or ( 11 )) reaches the yield strength. This is expressed for a two-dimensional plane stress state in terms of principal stresses as:

$$\sigma_e = \sqrt{\sigma_1^2 - \sigma_1\sigma_2 + \sigma_2^2} \quad (10)$$

Or in terms of general stress components as:

$$\sigma_e = \sqrt{\sigma_{xx}^2 - \sigma_{xx}\sigma_{yy} + \sigma_{yy}^2 + 3\tau_{xy}^2} \quad (11)$$

The equivalent strain is defined by:

$$\epsilon_e = \frac{1}{1 + \nu} \sqrt{\epsilon_1^2 - \epsilon_1\epsilon_2 + \epsilon_2^2} \quad (12)$$

In order to have a better insight in the Von-Mises yield surface, this is illustrated in Figure 4.5 in the principal stress coordinates.

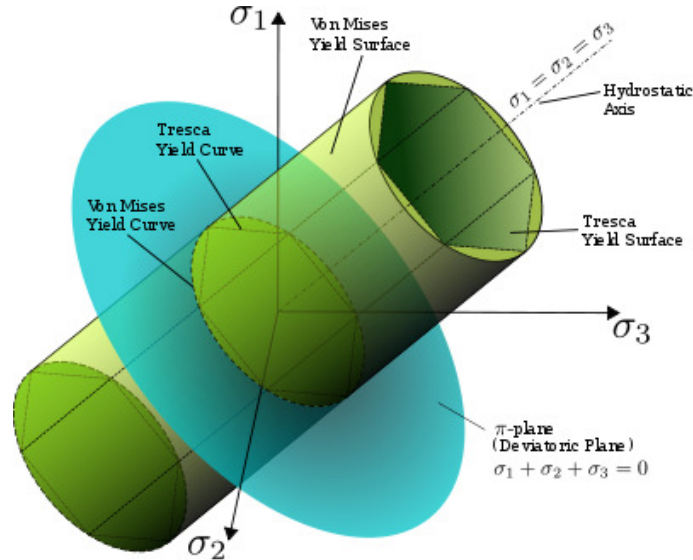


Figure 4.5 – The Von-Mises yield surfaces in principal stress coordinate [49]

The variation of the elastic-plastic strain, predicted with the SM approach and an inelastic finite element analysis, with respect to the load is analysed. The information is interpreted based on the chosen failure limits. Also the estimation of the strains based on the ESED method, Neuber’s rule and a linear calculation are plotted.

#### 4.1.1 Plate A ( $r=375mm$ ) WoSH

Plate A has a width of 1500mm and a radius of the hole of 375mm, with a corresponding stress concentration factor  $K_t = 2.159$ . Based on equation ( 8 ) the load at which failure occurs is  $q_u = 7100N/mm$ . However, due to convergence issues in the non-linear finite element analysis, the maximum attainable load in the model is  $q_u = 7060N/mm$ . The load for which localized yielding occurs (at the location of the stress concentration) is  $q_l = 3289N/mm$ . Firstly, in order to understand the behaviour of the plate with respect to the load, the load-displacement diagram based on the non-linear finite element analysis is plotted (Figure 4.7). In Figure 4.6 the displacement field is also illustrated from the non-linear finite element analysis at the ultimate load of  $q_u = 7060N/mm$ .

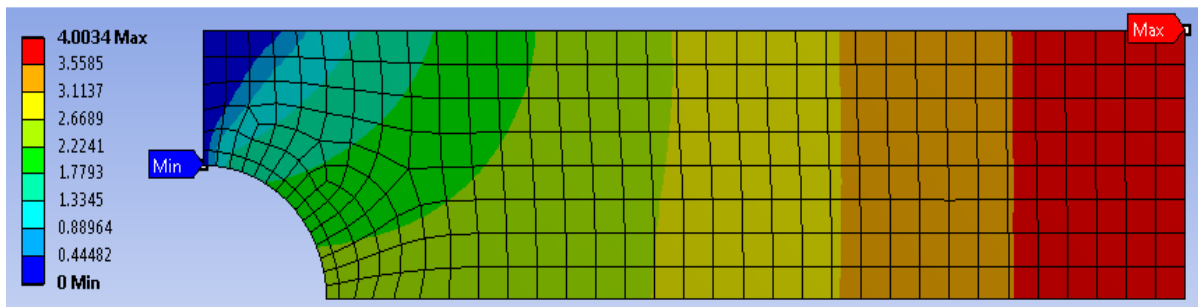


Figure 4.6 – Plate A ( $r=375mm$ ) WoSH: Displacement field [mm]

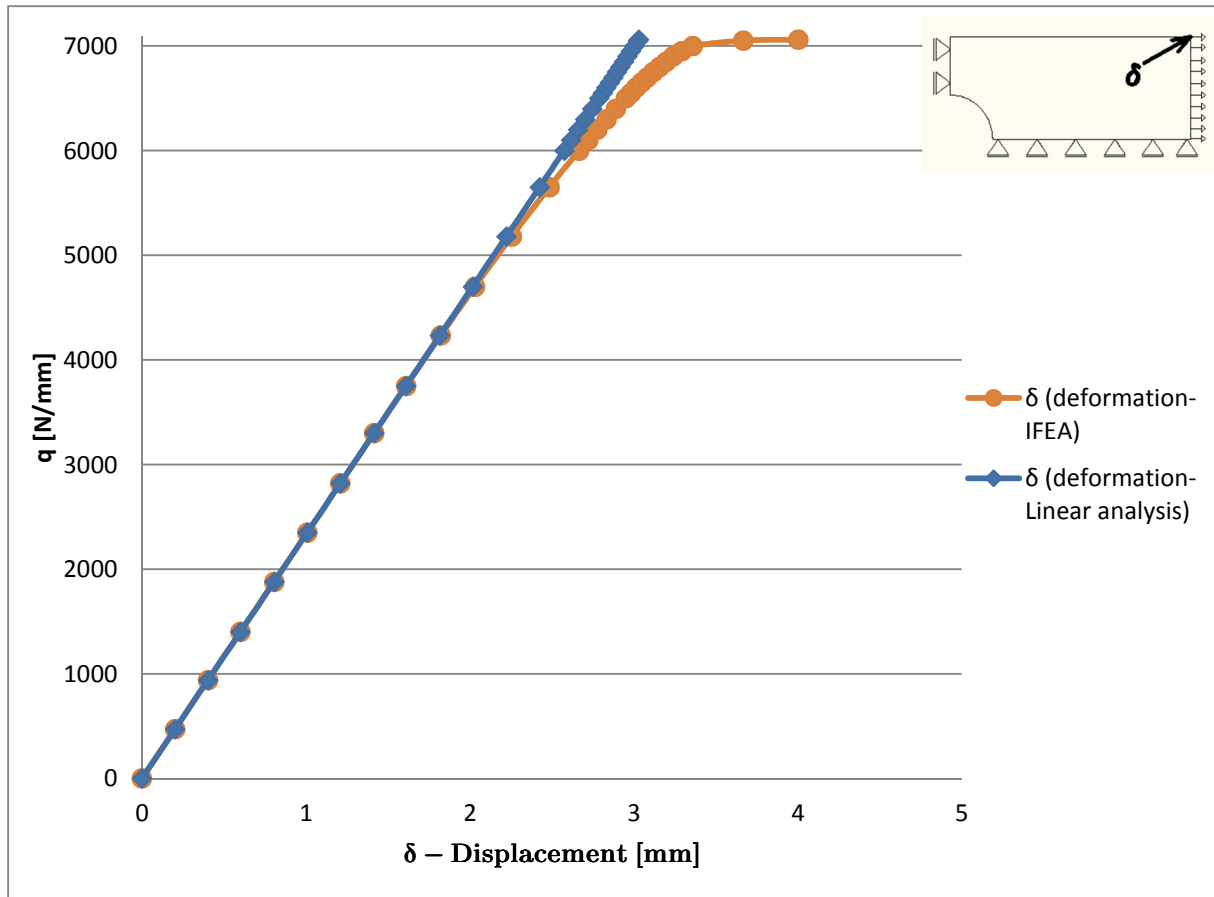


Figure 4.7 – Plate A (r=375mm) WoSH: Load-Displacement diagram

The maximum displacement corresponding to the ultimate load is  $\delta_u = 4\text{mm}$ . From Figure 4.7 it can be noticed that once the load reaches approximately the value of  $7020\text{N/mm}$ , full yielding of the section occurs and the material deforms linear under the same load (as expected from the inputted stress-strain diagram without strain hardening). The equivalent strain of the plate at a load level of  $q_y = 7020\text{N/mm}$  is equal to 1.24% at the notch-tip. This is illustrated from the non-linear finite element analysis (Figure 4.8).

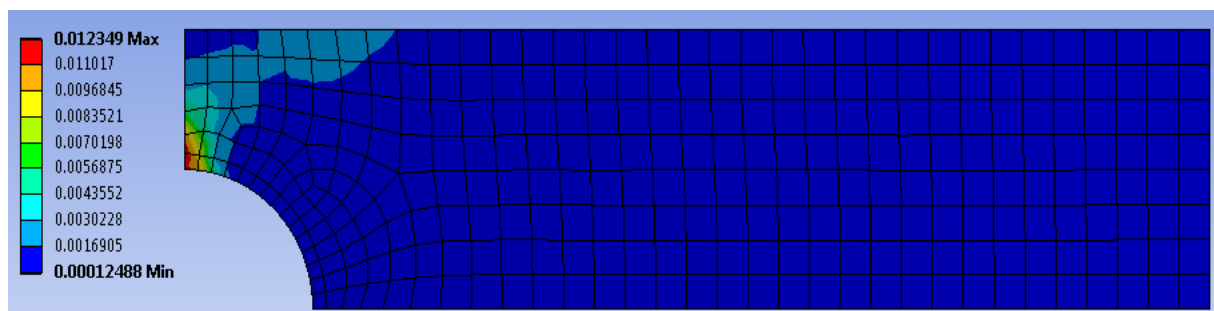


Figure 4.8 – Plate A (r=375mm) WoSH: Equivalent strain (non-linear) at  $q_y = 7020\text{N/mm}$

The dark-blue contour represents the material that has not reached yielding yet, while the rest of the contour is material that has yielded (i.e. the dark-blue contour represents the part of the plate where the strain is lower than  $\epsilon_y = \frac{f_y}{E} = 0.0016905$ ). It can be noticed that the highest strain occurs at the notch-tip. In order to estimate the applicability of the SM method to the plate with hole, the equivalent-strain at the notch-tip versus load is plotted. The results from the SM method are compared to the IFEA results, but also with the ESED

method, Neuber's rule and the linear calculation (Figure 4.9). This comparison is made in order to have insight on the applicability of the other methods in predicting the strains at the notch-tip.

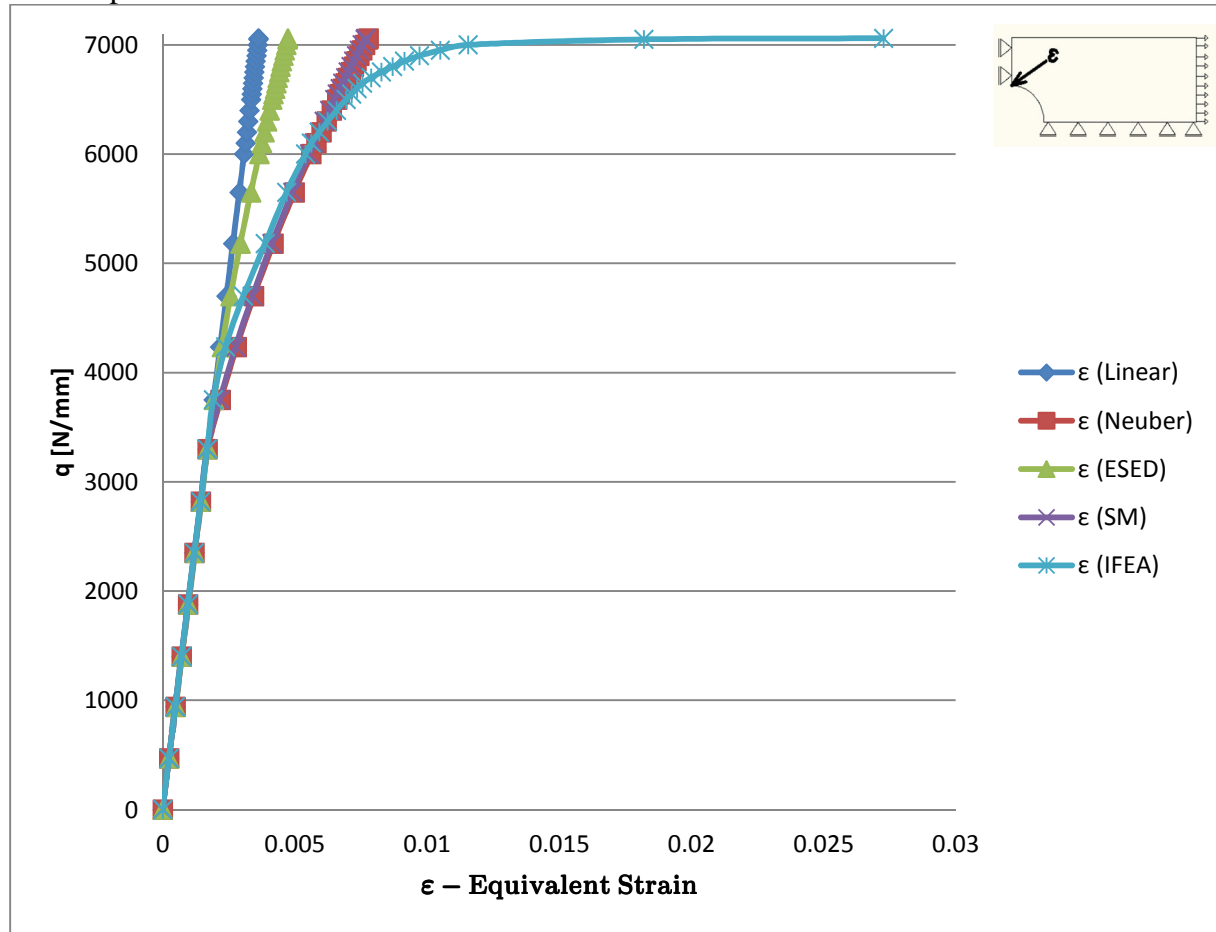


Figure 4.9 – Plate A (r=375mm) WoSH: Load-Equivalent Strain diagram

As it can be noticed from Figure 4.9, Neuber's rule and the SM approach seem more suitable for use in predicting strains than the ESED method as their results are closer to the ones based on the IFEA. At a load of  $q_y = 7020N/mm$  the strain at the notch-tip increases linear at almost constant load. As the SM method and Neuber's rule are based on the same graphical interpretation of the stress-strain diagram (Figure 4.1 and Figure 3.27) their results are comparable. Based on Figure 4.9 it can be stated that the SM method applied to this particular geometry gives good estimates of the strains at a notch-tip up to a certain point. As the load approaches the ultimate capacity of the plate, the equivalent strain estimated using the SM method starts to differ significantly from the results obtained using the non-linear material behaviour in the finite element analysis. If the equivalent strain plot at the same load of  $q_y = 7020N/mm$  from the linear analysis (Figure 4.10) is compared with the non-linear analysis one (Figure 4.8) it can be noticed that once the section goes into yielding, the results from the linear analysis can no longer be used in the SM approach to give estimates of the strain. However, the difference in results between the SM and IFEA seems to occur at a lower value of the load also. Figure 4.11 plots the equivalent strain vs load up to  $q_y$ .

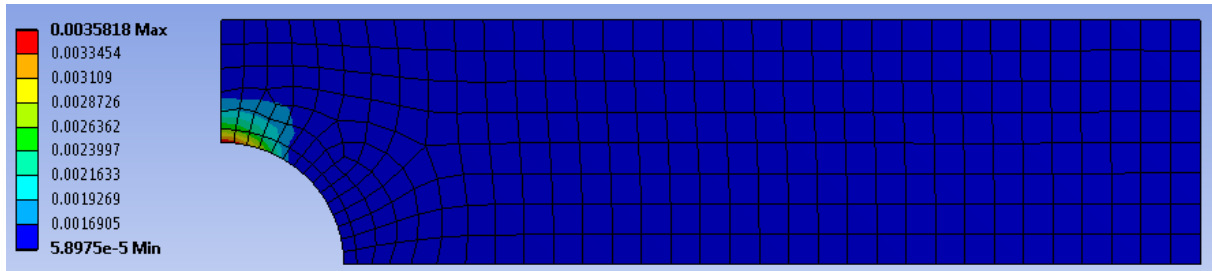


Figure 4.10 - Plate A (r=375mm) WoSH: Equivalent strain (linear) at  $q_y = 7020N/mm$

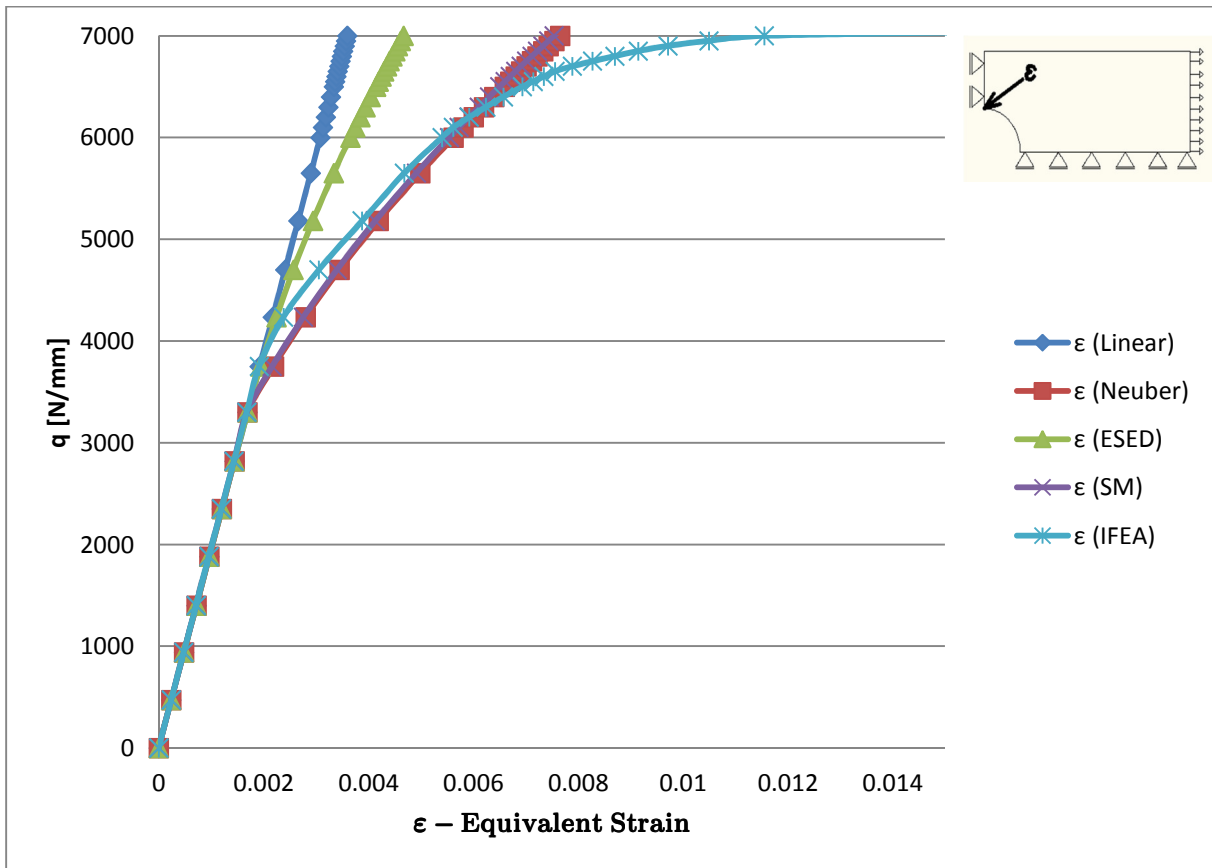


Figure 4.11 - Plate A (r=375mm) WoSH: Load-Equivalent Strain diagram up to  $q_y$

From Figure 4.11 it can be noticed that the SM approach gives good estimates of the strain up to a certain load level where the results are no longer comparable to the IFEA. This can be explained by the fact that as load continues to increase after localized yielding occurs ( $q_l = 3289N/mm$ ) the material surrounding the notch-tip starts to yield. In the case of the non-linear material behaviour, as the surrounding material yields the strain at the notch-tip increases function of the rate of strain hardening. This means that the stress increase is lower while the equivalent strain increases at a higher rate (equal to the strain hardening). However in the linear analysis this does not happen. As the stress in the material surrounding the notch-tip becomes higher than the yield stress the strain continues to increase at the same rate (equal to Young's modulus). The difference is that in the latter case a lower area of material needs to "yield" to have equilibrium which in turn means a poorer approximation of strains at the notch-tip. A graphical interpretation is illustrated in Figure 4.12 for  $q_y = 7020N/mm$ . The equivalent strains in the plate at the  $q_y$  load level are presented for the linear and non-linear analysis results.

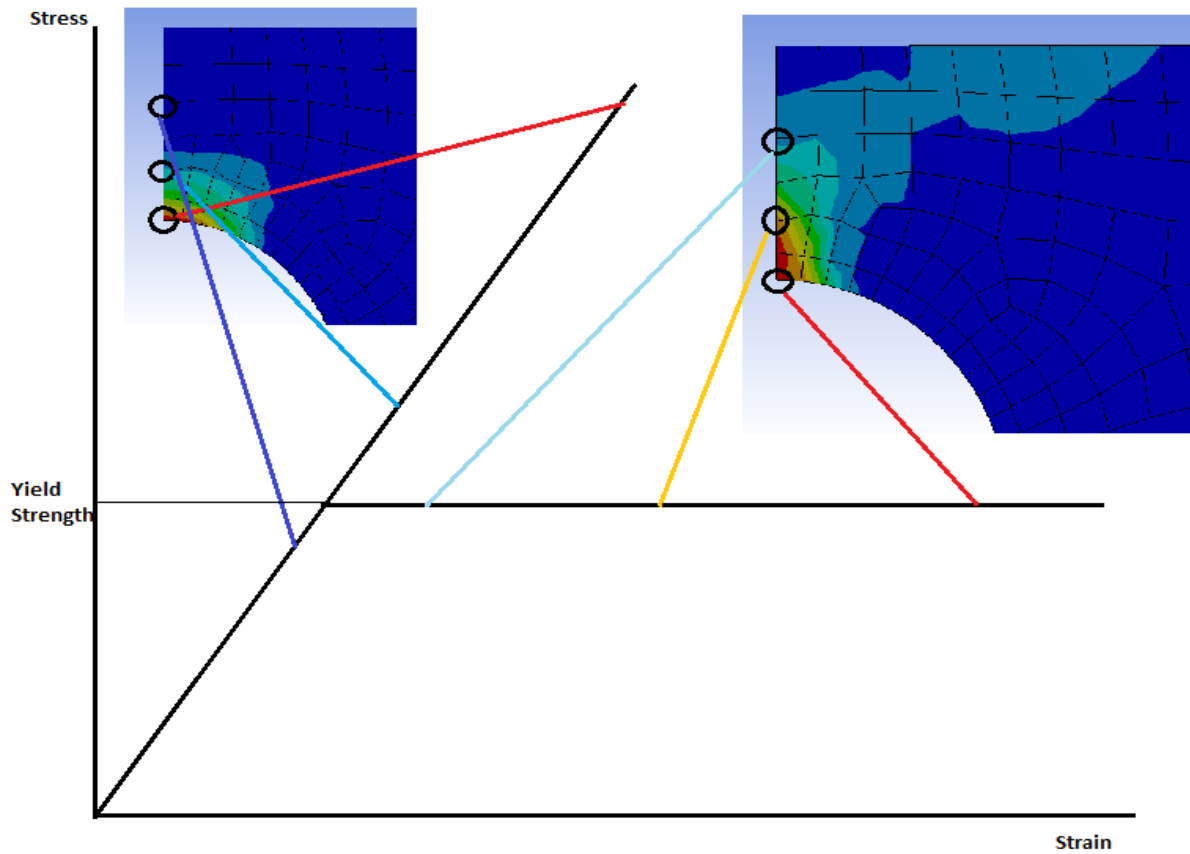


Figure 4.12 – Stress and strain at different location from linear and non-linear analysis

From Figure 4.12 it can be stated that in order to have equilibrium at  $q_y = 7020\text{N/mm}$  in the linear calculation a smaller area needs to “yield”. At the notch-tip this is translated as having very high stresses with corresponding strains function of Young’s modulus. However, in the non-linear analysis the area that yields is much larger. This means that at the notch-tip the stresses are equal to the yield strength while the strains increase significantly in order to have a higher yielded area that can result in equilibrium. The SM seems a good approximation method for the strain up to a certain load level. For this particular case this corresponds to about 90% of the calculated ultimate load ( $q_u = 7100\text{N/mm}$ ). The equivalent strain from the SM and IFEA is compared in Table 26 for this load.

Table 26 – Plate A (r=375mm) WoSH: Equivalent strain at  $0.9q_u$

q [N/mm]	$\epsilon$ (Linear)	$\sigma$ (Linear) [N/mm <sup>2</sup> ]	SM	IFEA	Equivalent strain difference [%]
			$\epsilon$ (NF)	$\epsilon$ (IFEA)	
6390	0.0033	685	0.0063	0.0065	-3.1

Using the SM method, the estimated strain at the notch-tip is lower by approximately 3% from the one calculated using an IFEA at  $0.9q_u$ . This is considered an acceptable difference as the strain is in the range of around 0.65% which is much lower than the usual design code requirements with respect to material properties (section 3.3).

**4.1.2 Plate B ( $r=250mm$ ) WoSH**

Plate B has a width of 1500mm and a radius of the hole of 250mm, with a corresponding stress concentration factor  $K_t = 2.307$ . Based on equation ( 8 ) the load at which failure occurs is  $q_u = 9466N/mm$ . However, due to convergence issues in the non-linear finite element analysis, the maximum load in the model is  $q_u = 9425N/mm$ . The load for which localized yielding occurs (at the location of the stress concentration) is  $q_l = 4104N/mm$ . The behaviour of the plate is similar to plate A, the difference in geometry influencing only the magnitude of the stress concentration. The load-displacement diagram based on the non-linear finite element analysis is plotted (Figure 4.13).

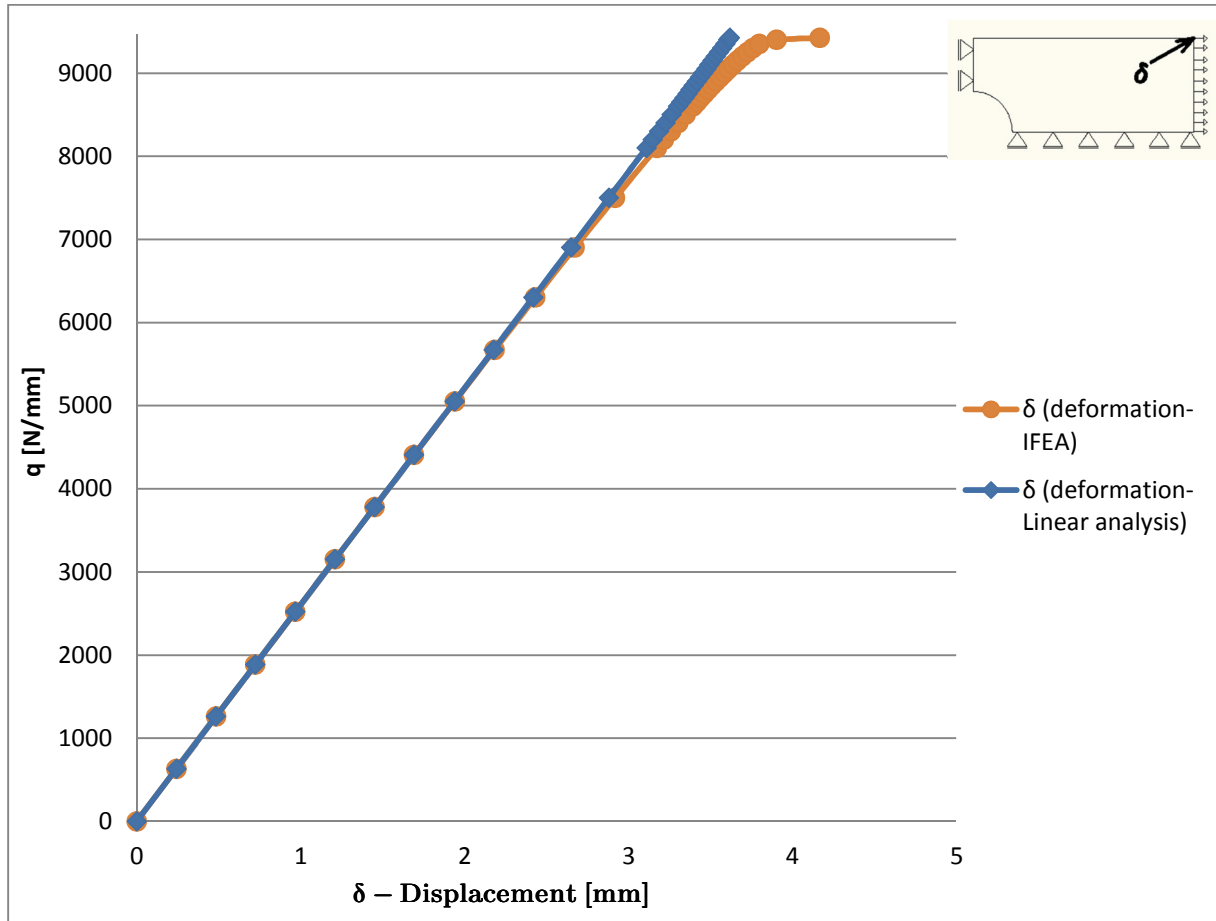


Figure 4.13 – Plate B ( $r=250mm$ ) WoSH: Load-Displacement diagram

The maximum displacement corresponding to the ultimate load is  $\delta_u = 4.2mm$ . This is a bit higher than in the case of plate A due to the fact that the radius of the hole is smaller and thus the influence of the stress concentration becomes more localized.

The equivalent-strain at the notch-tip versus load is plotted for plate B (Figure 4.14).

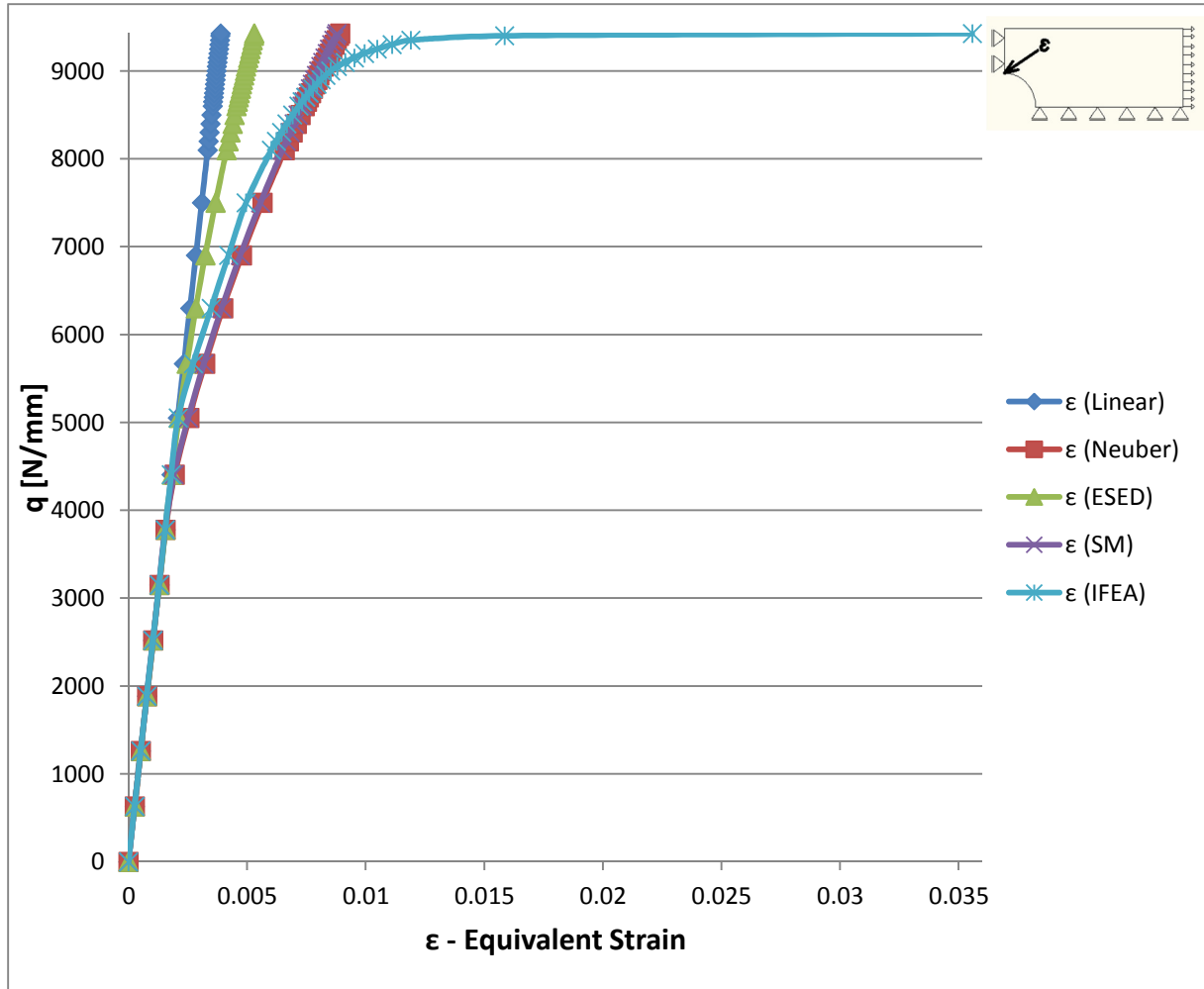


Figure 4.14 – Plate B (r=250mm) WoSH: Load-Equivalent Strain diagram

Once the load reaches approximately the value of 9360N/mm, full yielding of the section occurs with a corresponding notch-tip strain of 1.22% and the strain at the notch-tip continues to increase linear at almost a constant load level.

Based on Figure 4.14 the SM seems a good approximation method for the strain up to about 90% of the calculated ultimate load ( $q_u = 9466N/mm$ ). The equivalent strain from the SM and IFEA is compared in Table 27 for this load.

Table 27 – Plate B (r=250mm) WoSH: Equivalent strain at  $0.9q_u$

q [N/mm]	$\epsilon$ (Linear)	$\sigma$ (Linear) [N/mm <sup>2</sup> ]	SM	IFEA	Equivalent strain difference [%]
			$\epsilon$ (NF)	$\epsilon$ (IFEA)	
8520	0.0035	732	0.0072	0.007	2.8

Using the SM method, the estimated strain at the notch-tip is higher by approximately 3% from the one calculated using an IFEA at  $0.9q_u$ . This is considered an acceptable difference as the strain is in the range of around 0.70% which is much lower than the usual design code requirements with respect to material properties (section 3.3).

**4.1.3 Plate C ( $r=187.5mm$ ) WoSH**

Plate C has a width of 1500mm and a radius of the hole of 187.5mm, with a corresponding stress concentration factor  $K_t = 2.422$ . Based on equation ( 8 ) the load at which failure occurs is  $q_u = 10650N/mm$ . However, due to convergence issues in the non-linear finite element analysis, the maximum load in the model is  $q_u = 10610N/mm$ . The load for which localized yielding occurs (at the location of the stress concentration) is  $q_l = 4398N/mm$ . The behaviour of the plate is similar to the previous examples, the difference in geometry influencing only the magnitude of the stress concentration. The load-displacement diagram based on the non-linear finite element analysis is plotted (Figure 4.15).

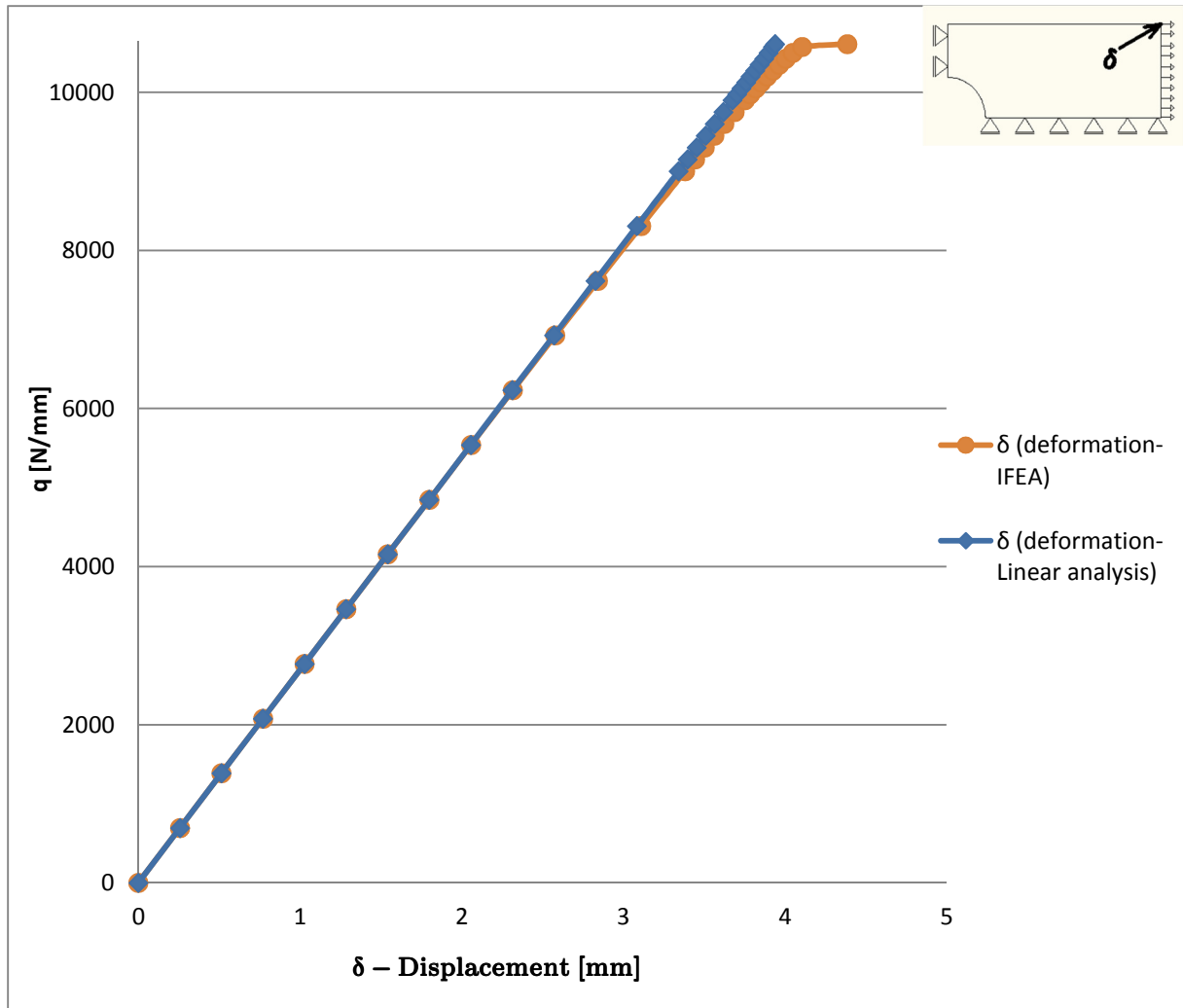


Figure 4.15 – Plate C ( $r=187.5mm$ ) WoSH: Load-Displacement diagram

The maximum displacement corresponding to the ultimate load is  $\delta_u = 4.4mm$ . This is a bit higher than in the case of the previous examples due to the fact that the radius of the hole is smaller and thus the influence of the stress concentration becomes more localized.

The equivalent-strain at the notch-tip versus load is plotted for plate C (Figure 4.16).

Once the load reaches approximately the value of 10575N/mm, full yielding of the section occurs with a corresponding notch-tip strain of 1.39% and the strain at the notch-tip continues to increase linear at almost a constant load level.

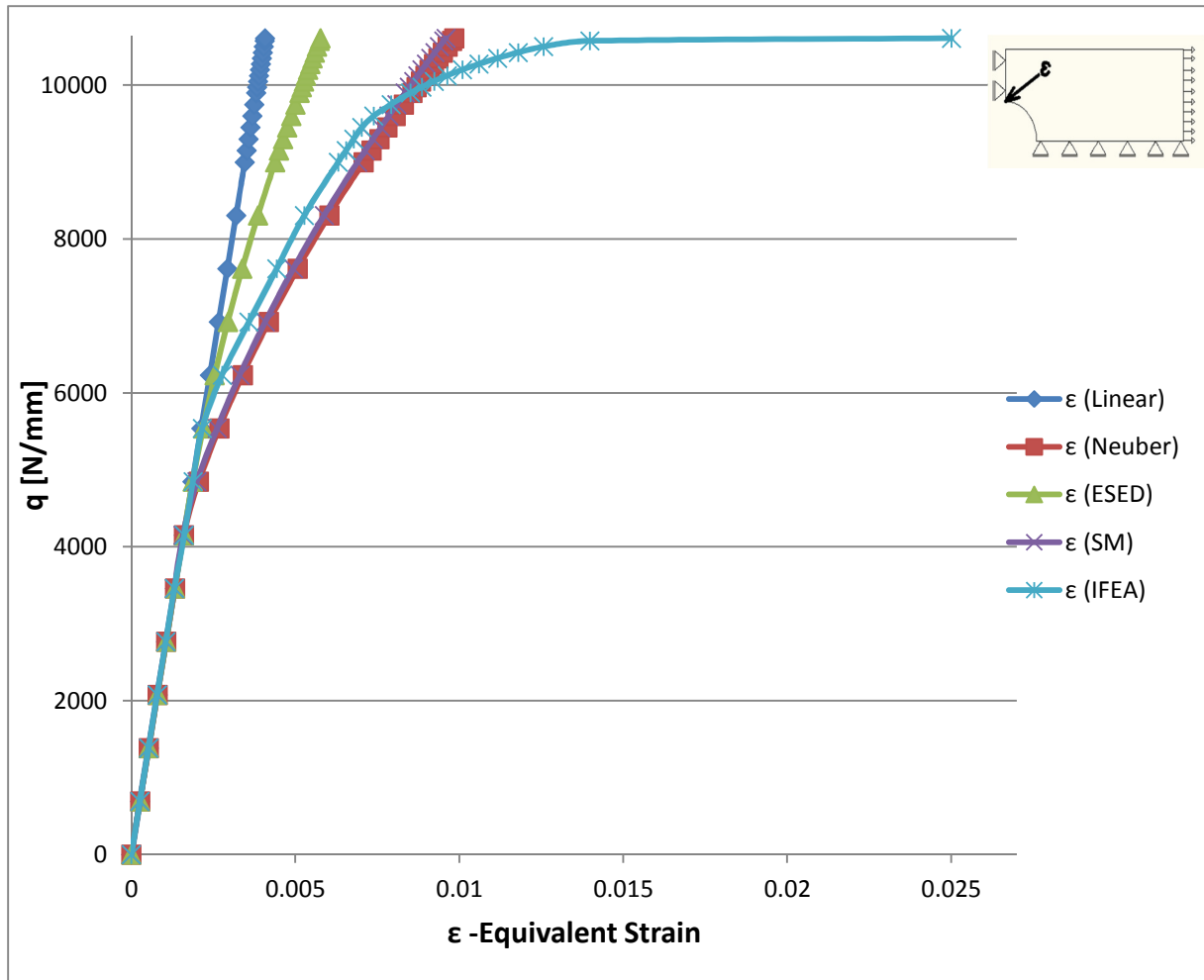


Figure 4.16 – Plate C (r=187.5mm) WoSH: Load-Equivalent Strain diagram

Based on Figure 4.16 the SM seems a good approximation method for the strain up to about 90% of the calculated ultimate load ( $q_u = 10650\text{N/mm}$ ). The equivalent strain from the SM and IFEA is compared in Table 28 for this load.

Table 28 – Plate C (r=187.5mm) WoSH: Equivalent strain at  $0.9q_u$

q [N/mm]	$\epsilon$ (Linear)	$\sigma$ (Linear) [N/mm <sup>2</sup> ]	SM	IFEA	Equivalent strain difference [%]
			$\epsilon$ (NF)	$\epsilon$ (IFEA)	
9585	0.0036	764	0.0078	0.0074	5.4

Using the SM method, the estimated strain at the notch-tip is higher by approximately 5% from the one calculated using an IFEA at  $0.9q_u$ . This is considered an acceptable difference as the strain is in the range of around 0.75% which is much lower than the usual design code requirements with respect to material properties (section 3.3).

**4.1.4 Plate D ( $r=150mm$ ) WoSH**

Plate D has a width of 1500mm and a radius of the hole of 150mm, with a corresponding stress concentration factor  $K_t = 2.508$ . Based on equation ( 8 ) the load at which failure occurs is  $q_u = 11360N/mm$ . However, due to convergence issues in the non-linear finite element analysis, the maximum load in the model is  $q_u = 11340N/mm$ . The load for which localized yielding occurs (at the location of the stress concentration) is  $q_l = 4530N/mm$ . The behaviour of the plate is similar to the previous examples, the difference in geometry influencing only the magnitude of the stress concentration. The load-displacement diagram based on the non-linear finite element analysis is plotted (Figure 4.17).

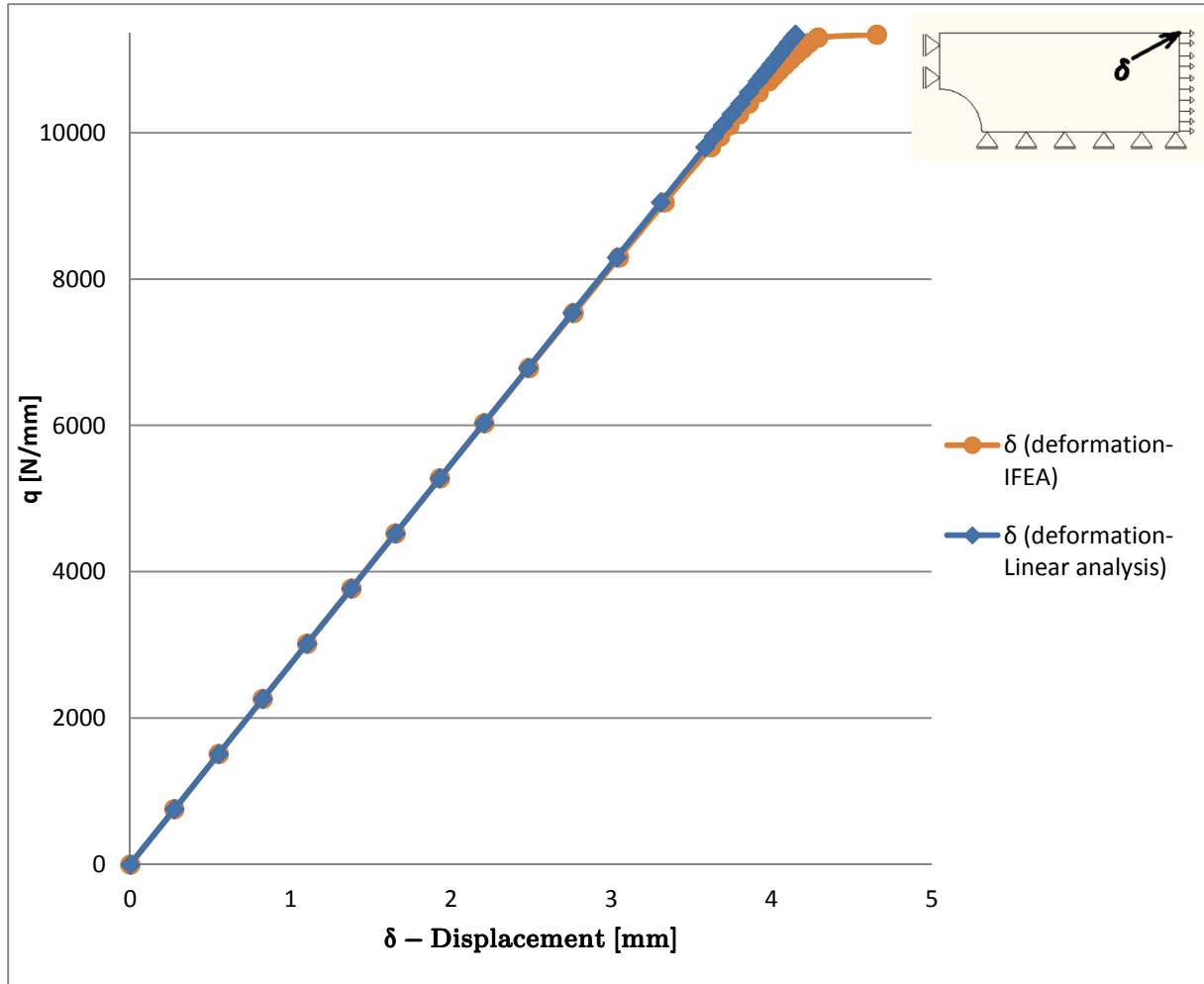


Figure 4.17 - Plate D ( $r=150mm$ ) WoSH: Load-Displacement diagram

The maximum displacement corresponding to the ultimate load is  $\delta_u = 4.7mm$ . This is a bit higher than in the case of the previous examples due to the fact that the radius of the hole is smaller and thus the influence of the stress concentration becomes more localized.

The equivalent-strain at the notch-tip versus load is plotted for plate D (Figure 4.18).

Once the load reaches approximately the value of 11300N/mm, full yielding of the section occurs with a corresponding notch-tip strain of 1.68% and the strain at the notch-tip continues to increase linear at almost a constant load level.

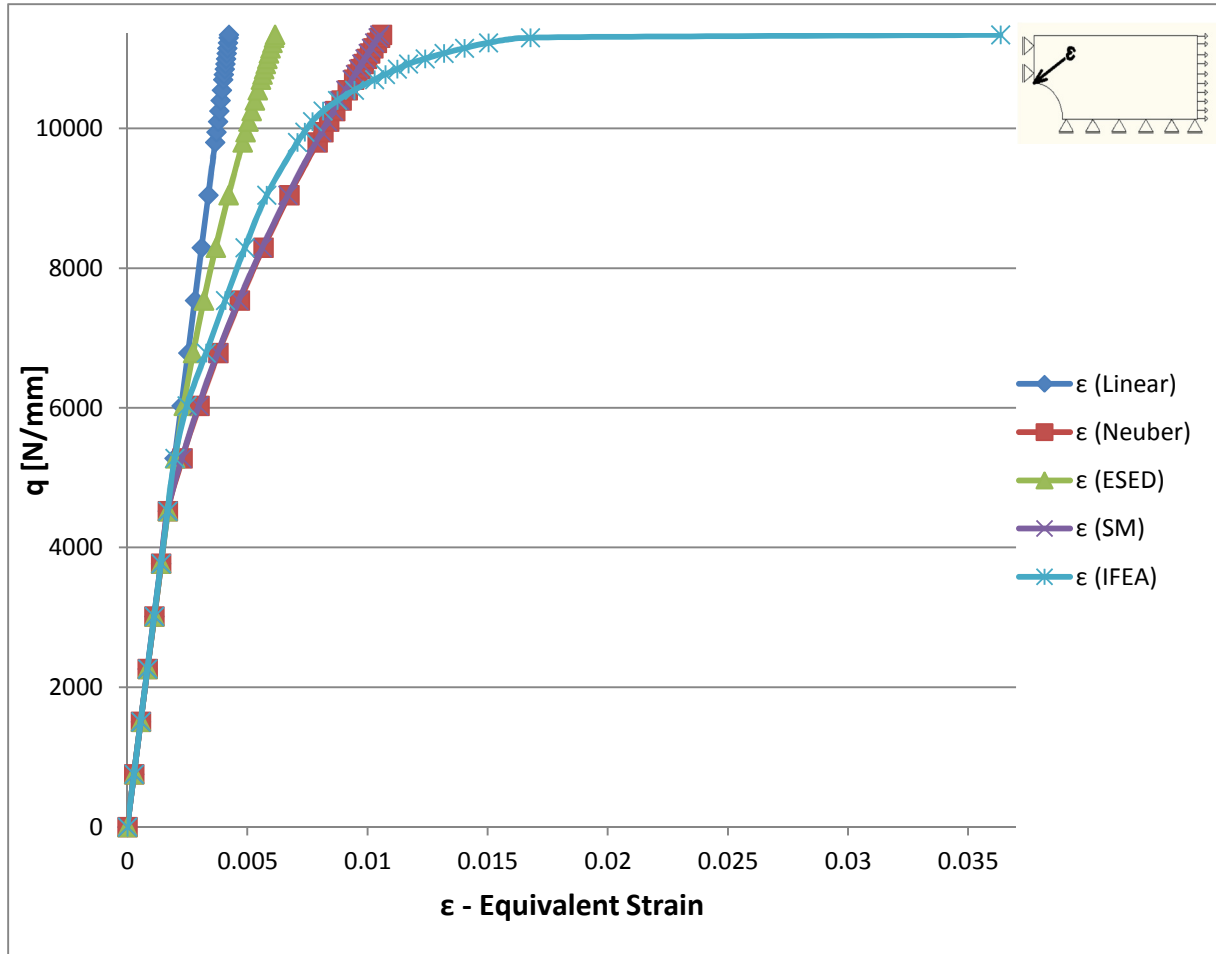


Figure 4.18 - Plate D (r=150mm) WoSH: Load-Equivalent Strain diagram

Based on Figure 4.18 the SM seems a good approximation method for the strain up to about 90% of the calculated ultimate load ( $q_u = 11360 N/mm$ ). The equivalent strain from the SM and IFEA is compared in Table 29 for this load.

Table 29 – Plate D (r=150mm) WoSH: Equivalent strain at  $0.9q_u$

q [N/mm]	$\epsilon$ (Linear)	$\sigma$ (Linear) [N/mm <sup>2</sup> ]	SM	IFEA	Equivalent strain difference [%]
			$\epsilon$ (NF)	$\epsilon$ (IFEA)	
10224	0.0038	800	0.0085	0.0081	4.9

Using the SM method, the estimated strain at the notch-tip is higher by approximately 5% from the one calculated using an IFEA at  $0.9q_u$ . This is considered an acceptable difference as the strain is in the range of around 0.85% which is much lower than the usual design code requirements with respect to material properties (section 3.3).

**4.1.5 Plate E ( $r=75mm$ ) WoSH**

Plate E has a width of 1500mm and a radius of the hole of 75mm, with a corresponding stress concentration factor  $K_t = 2.722$ . Based on equation ( 8 ) the load at which failure occurs is  $q_u = 12780N/mm$ . The load for which localized yielding occurs (at the location of the stress concentration) is  $q_l = 4695N/mm$ . The behaviour of the plate is similar to the previous examples, the difference in geometry influencing only the magnitude of the stress concentration. The load-displacement diagram based on the non-linear finite element analysis is plotted (Figure 4.19).

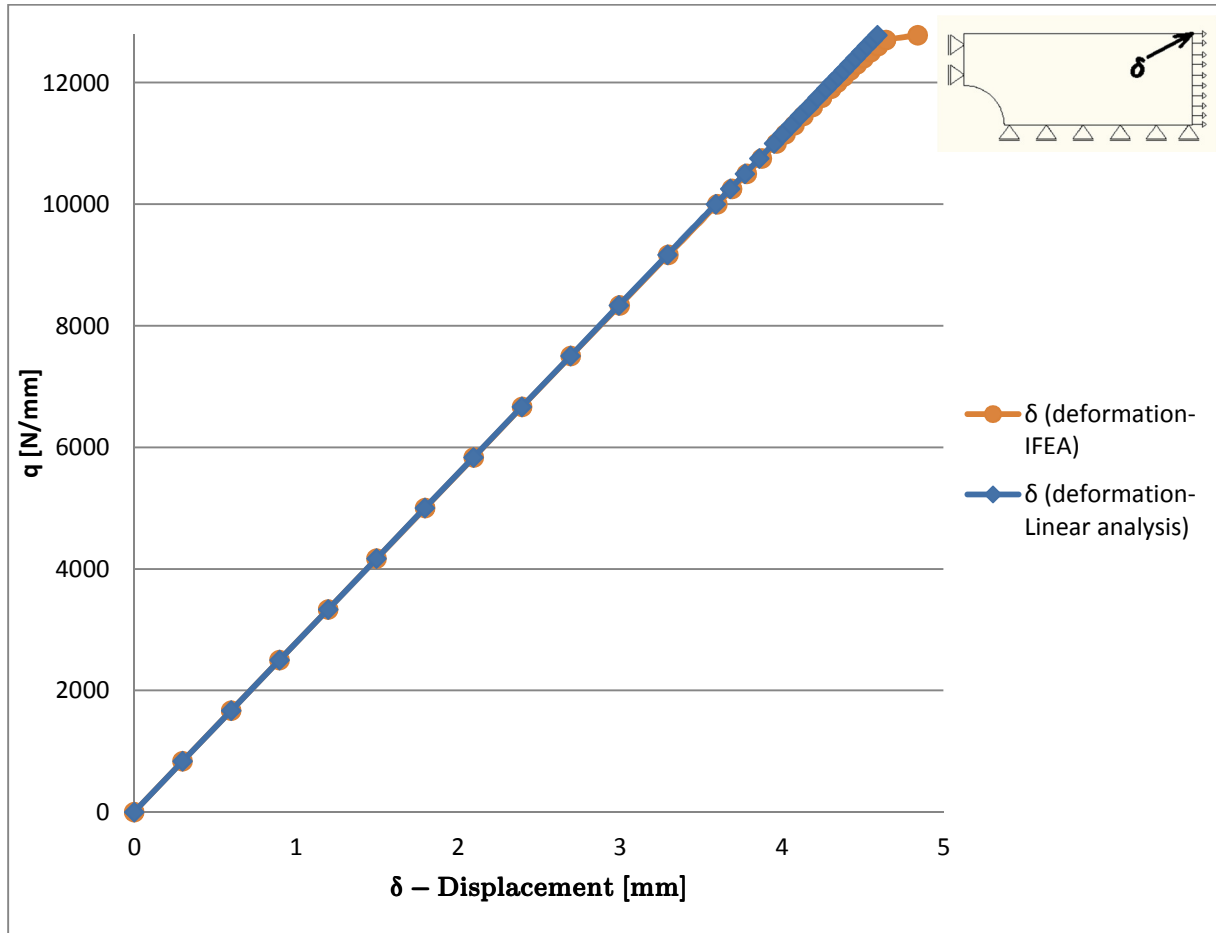


Figure 4.19 - Plate E ( $r=75mm$ ) WoSH: Load-Displacement diagram

The maximum displacement corresponding to the ultimate load is  $\delta_u = 4.8mm$ . This is a bit higher than in the case of the previous examples due to the fact that the radius of the hole is smaller and thus the influence of the stress concentration becomes more localized.

The equivalent-strain at the notch-tip versus load is plotted for plate E (Figure 4.20).

Once the load reaches approximately the value of 12760N/mm, full yielding of the section occurs with a corresponding notch-tip strain of 2.1% and the strain at the notch-tip continues to increase linear at almost a constant load level.

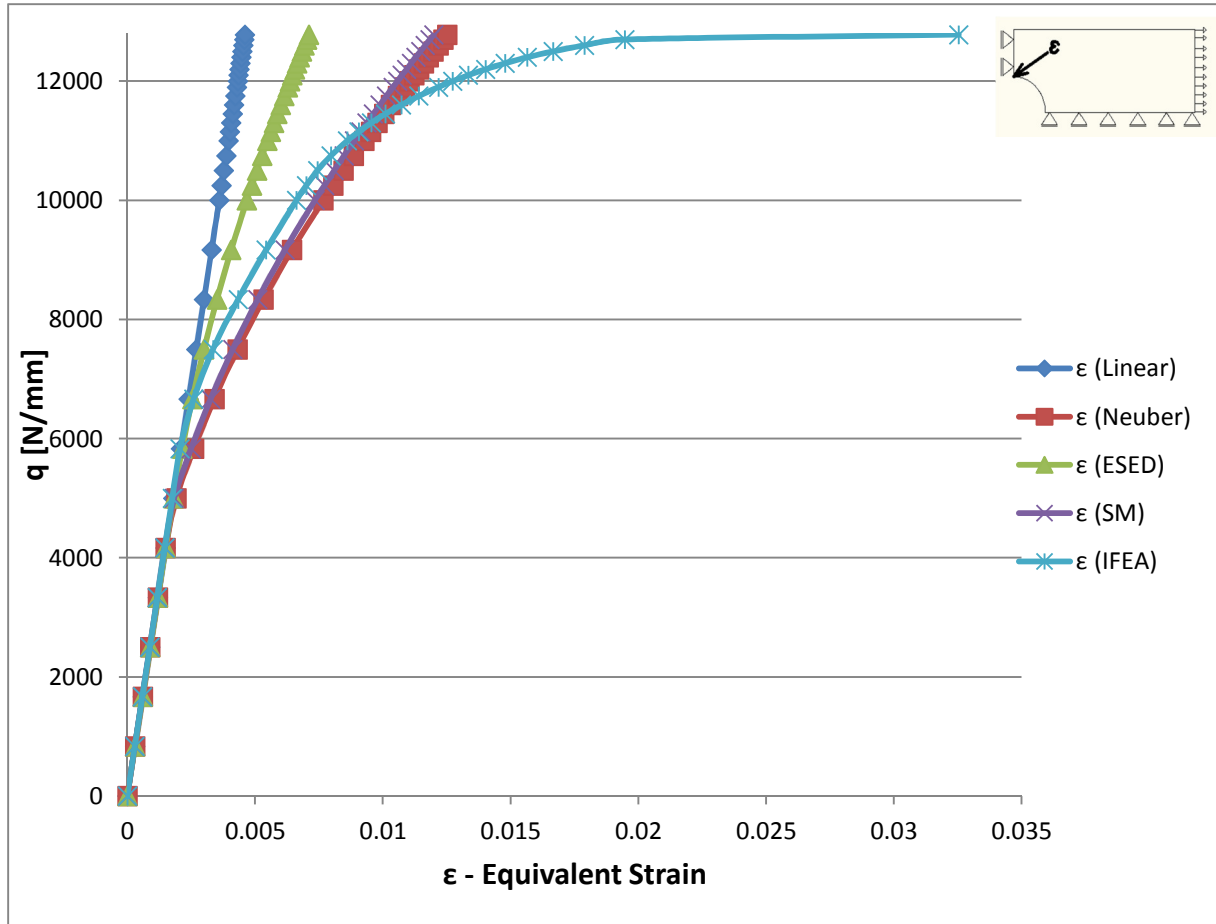


Figure 4.20 - Plate E (r=75mm) WoSH: Load-Equivalent Strain diagram

Based on Figure 4.20 the SM seems a good approximation method for the strain up to about 90% of the calculated ultimate load ( $q_u = 12780\text{N/mm}$ ). The equivalent strain from the SM and IFEA is compared in Table 30 – Plate E (r=75mm) WoSH: Equivalent strain at  $0.9q_u$  Table 30 for this load.

Table 30 – Plate E (r=75mm) WoSH: Equivalent strain at  $0.9q_u$

q [N/mm]	$\epsilon$ (Linear)	$\sigma$ (Linear) [N/mm <sup>2</sup> ]	SM	IFEA	Equivalent strain difference [%]
			$\epsilon$ (NF)	$\epsilon$ (IFEA)	
11502	0.004	849	0.0097	0.0102	-4.9

Using the SM method, the estimated strain at the notch-tip is lower by approximately 5% from the one calculated using an IFEA at  $0.9q_u$ . This is considered an acceptable difference as the strain is in the range of around 1% which is much lower than the usual design code requirements with respect to material properties (section 3.3).

**4.1.6 Plate A ( $r=375mm$ ) WSH**

Plate A has a width of 1500mm and a radius of the hole of 375mm, with a corresponding stress concentration factor  $K_t = 2.159$ . Based on equation ( 8 ) the load at which failure occurs is  $q_u = 10200N/mm$  and at which yielding occurs  $q_y = 7100N/mm$ . The load for which localized yielding occurs (at the location of the stress concentration) is  $q_l = 3289N/mm$ . Firstly, in order to understand the behaviour of the plate with respect to the load, the load-displacement diagram based on the non-linear finite element analysis is plotted (Figure 4.22). In Figure 4.21 the displacement field is also illustrated from the non-linear finite element analysis at the ultimate load of  $q_u = 10200N/mm$ .

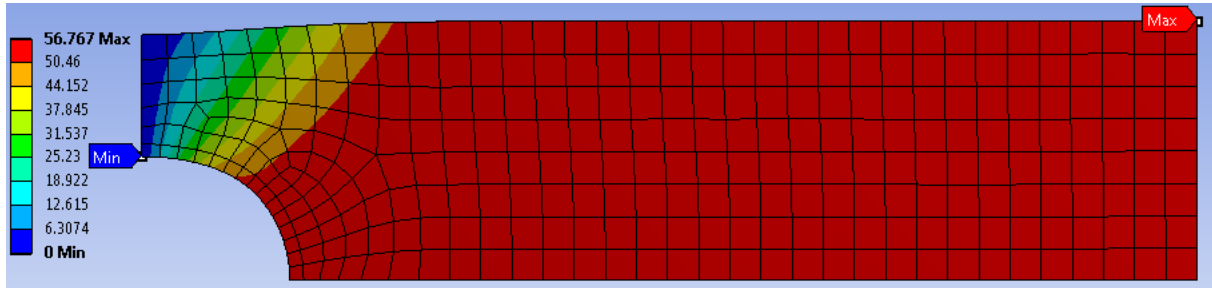


Figure 4.21 - Plate A ( $r=375mm$ ) WSH: Displacement field [mm]

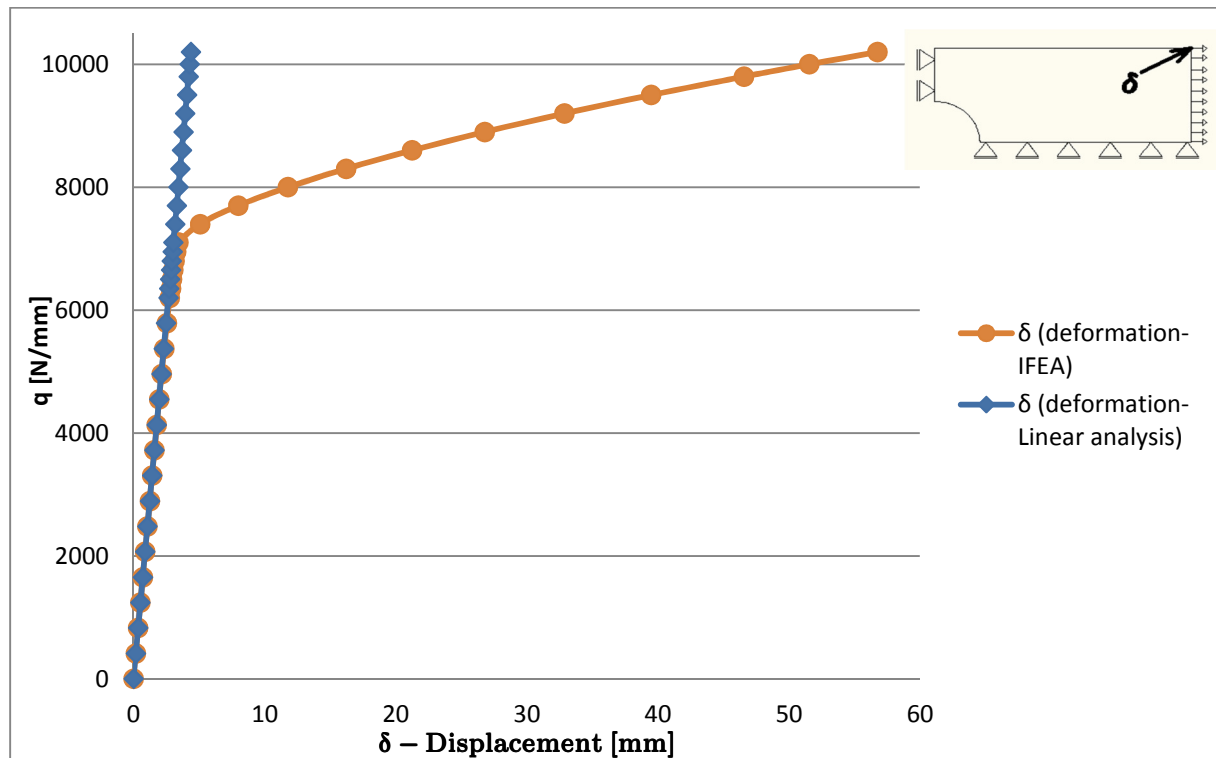


Figure 4.22 – Plate A ( $r=375mm$ ) WSH: Load-Displacement diagram

The maximum displacement corresponding to the ultimate load is  $\delta_u = 56.8mm$ . From Figure 4.22 it is noticed that once the load reaches approximately the value of 7100N/mm, full yielding of the section occurs and the material deforms linear under loading (as expected from the inputted stress-strain diagram with strain hardening). The equivalent strain of the plate at a load level of  $q_y = 7100N/mm$  is equal to 1.13% at the notch-tip. The value of the strain is lower than the equivalent strain at the notch-tip of plate A in the case WoSH (1.24% at a  $q_y = 7020N/mm$ ). This difference is due to the rate of strain hardening

present in the case WSH. The strain state of the plate at  $q_y = 7100N/mm$  is illustrated from the non-linear finite element analysis (Figure 4.23).

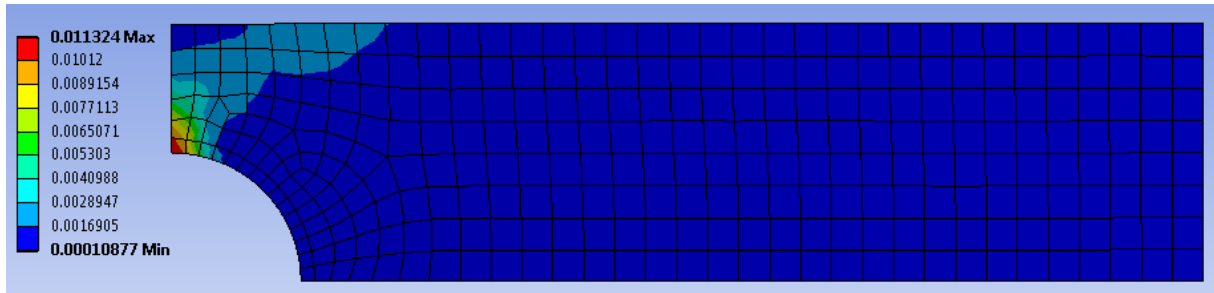


Figure 4.23 – Plate A (r=375mm) WSH: Equivalent strain (non-linear) at  $q_y = 7100N/mm$

The dark-blue contour represents the material that has not reached yielding yet, while the rest of the contour is material that has yielded (i.e. the dark-blue contour represents the part of the plate where the strain is lower than  $\epsilon_y = \frac{f_y}{E} = 0.0016905$ ). It can be noticed that the highest strain occurs at the notch-tip. In order to estimate the applicability of the SM method to the plate with a hole WSH, the equivalent-strain at the notch-tip versus load is plotted. The results from the SM method are compared to the IFEA results, but also with the ESED method, Neuber’s rule and the linear calculation (Figure 4.24).

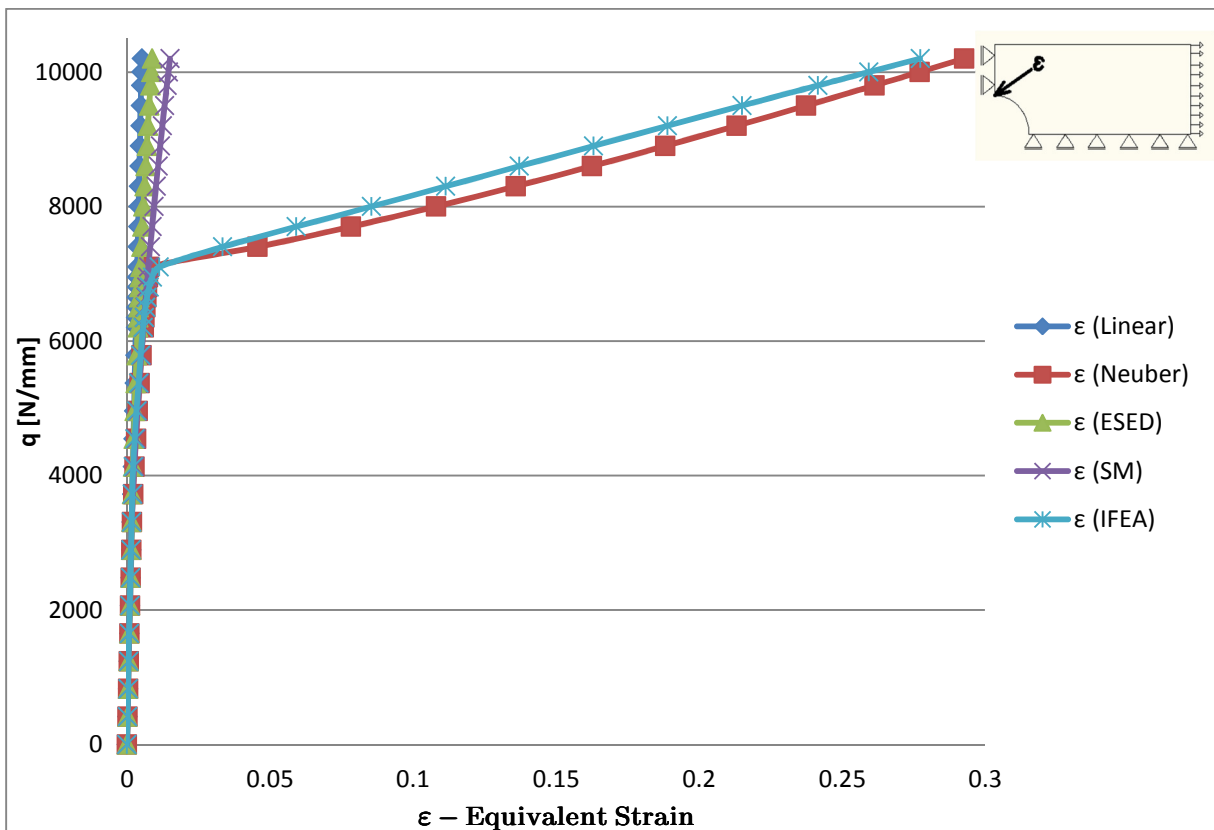


Figure 4.24 – Plate A (r=375mm) WSH: Load-Equivalent Strain diagram

At a load of  $q_y = 7100N/mm$  the strain at the notch-tip increases linear with the load function of the strain hardening. Based on Figure 4.24 it can be stated that the SM method cannot be used to estimate strains at the notch-tip once full yielding of the section occurs. As this method is based on the linear finite element analysis, it is not able to account for full

yielding in a section. On the other hand, Neuber's rule can still be applied beyond the yield load as this method is based on the nominal stress in the section. Thus it takes into account the full yielding of the section and is able to estimate the strains outside of the yield load limit. If the equivalent strain is plotted at the same load of  $q_y = 7100\text{N/mm}$  from the linear analysis (Figure 4.25) and compared with the non-linear analysis one (Figure 4.23) it can be noticed that the results of strain estimates are quite similar to the example WoSH. However, just as in the case WoSH, the difference in results between the SM and IFEA seems to occur at a lower value than  $q_y = 7100\text{N/mm}$ . Figure 4.26 plots the equivalent strain vs load up to  $q_y$ .

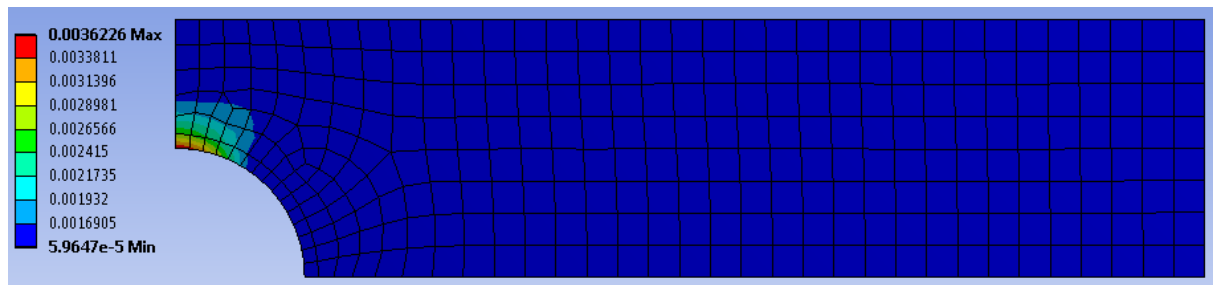


Figure 4.25 - Plate A ( $r=375\text{mm}$ ) WSH: Equivalent strain (linear) at  $q_y = 7100\text{N/mm}$

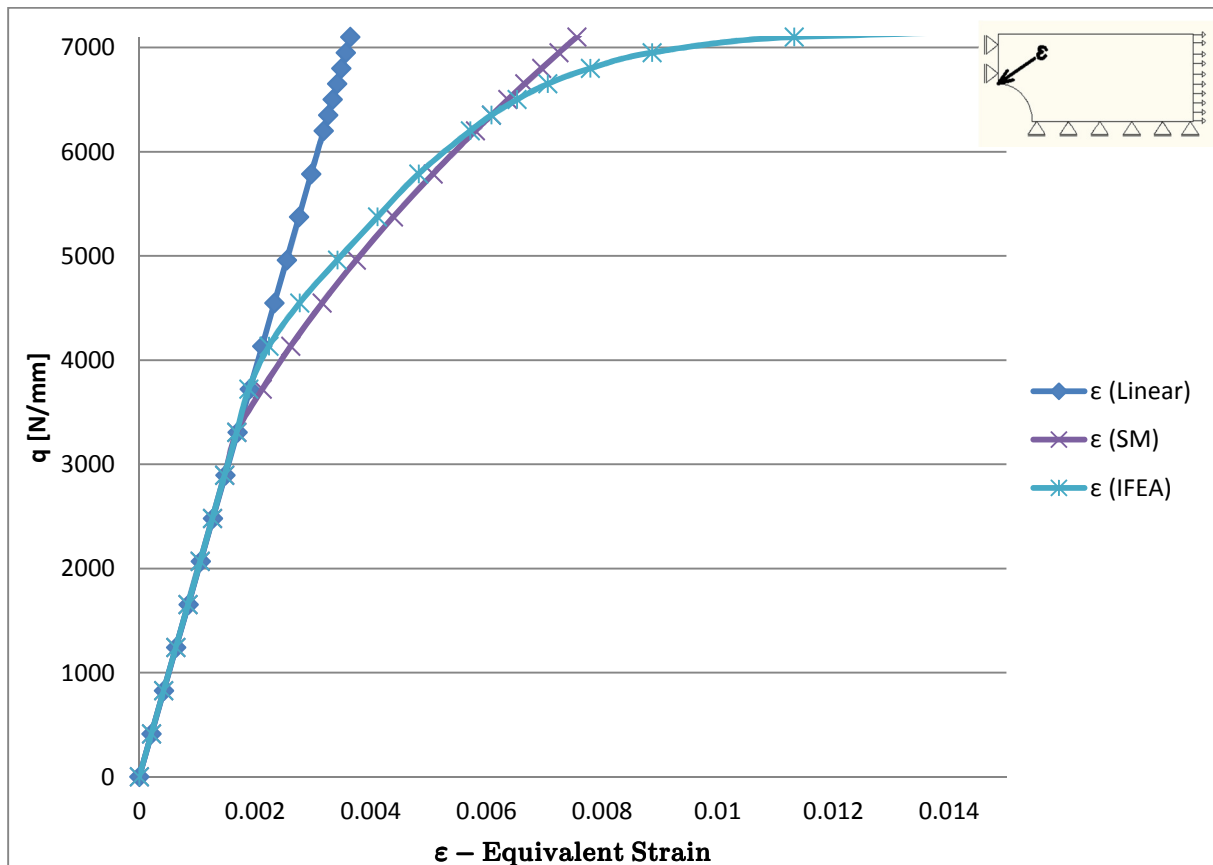


Figure 4.26 – Plate A ( $r=375\text{mm}$ ) WSH: Load-Equivalent Strain diagram up to  $q_y$

Comparing Figure 4.26 – Plate A ( $r=375\text{mm}$ ) WSH: Load-Equivalent Strain diagram up to  $q_y$  Figure 4.26 to Figure 4.9 it can be noticed that the diagrams are quite similar. This is due to the fact that the load only goes up to the value for which full yielding in the net section occurs and thus the strain is not significantly influenced by the rate of strain hardening. From Figure 4.26 it can be noticed that the SM seems a good approximation method for the strain

up to the same load level as in the case WoSH. This corresponds to about 90% of the yield load ( $q_y$  – the lowest value of the load for which yielding is expected in the net cross-section). The equivalent strain from the SM and IFEA is compared in Table 31 for this load.

Table 31 – Plate A ( $r=375\text{mm}$ ) WSH: Equivalent strain at  $0.9q_y$

$q$ [N/mm]	$\epsilon$ (Linear)	$\sigma$ (Linear) [N/mm <sup>2</sup> ]	SM	IFEA	Equivalent strain difference [%]
			$\epsilon$ (NF)	$\epsilon$ (IFEA)	
6390	0.00326	685	0.0063	0.0062	+1.6

Using the SM method, the estimated strain at the notch-tip is higher by approximately 1.6% from the one calculated using an IFEA at  $0.9q_y$ . The difference in strains between the material WoSH and WSH can be explained by the strain hardening rate. In the example illustrated in this section the presence of strain hardening means that the material at the location of the notch-tip has a lower strain increase compared to the example WoSH. The results are acceptable as the strain is in the range of around 0.63% which is much lower than the usual design code requirements with respect to material properties (section 3.3).

**4.1.7 Plate B ( $r=250\text{mm}$ ) WSH**

Plate B has a width of 1500mm and a radius of the hole of 250mm, with a corresponding stress concentration factor  $K_t = 2.307$ . Based on equation ( 8 ) the load at which failure occurs is  $q_u = 13600\text{N/mm}$  and at which yielding occurs  $q_y = 9466\text{N/mm}$ . The load for which localized yielding occurs (at the location of the stress concentration) is  $q_l = 4104\text{N/mm}$ . The behaviour of the plate is similar to the previous example, the difference in geometry influencing only the magnitude of the stress concentration. The load-displacement diagram based on the non-linear finite element analysis is plotted (Figure 4.27).

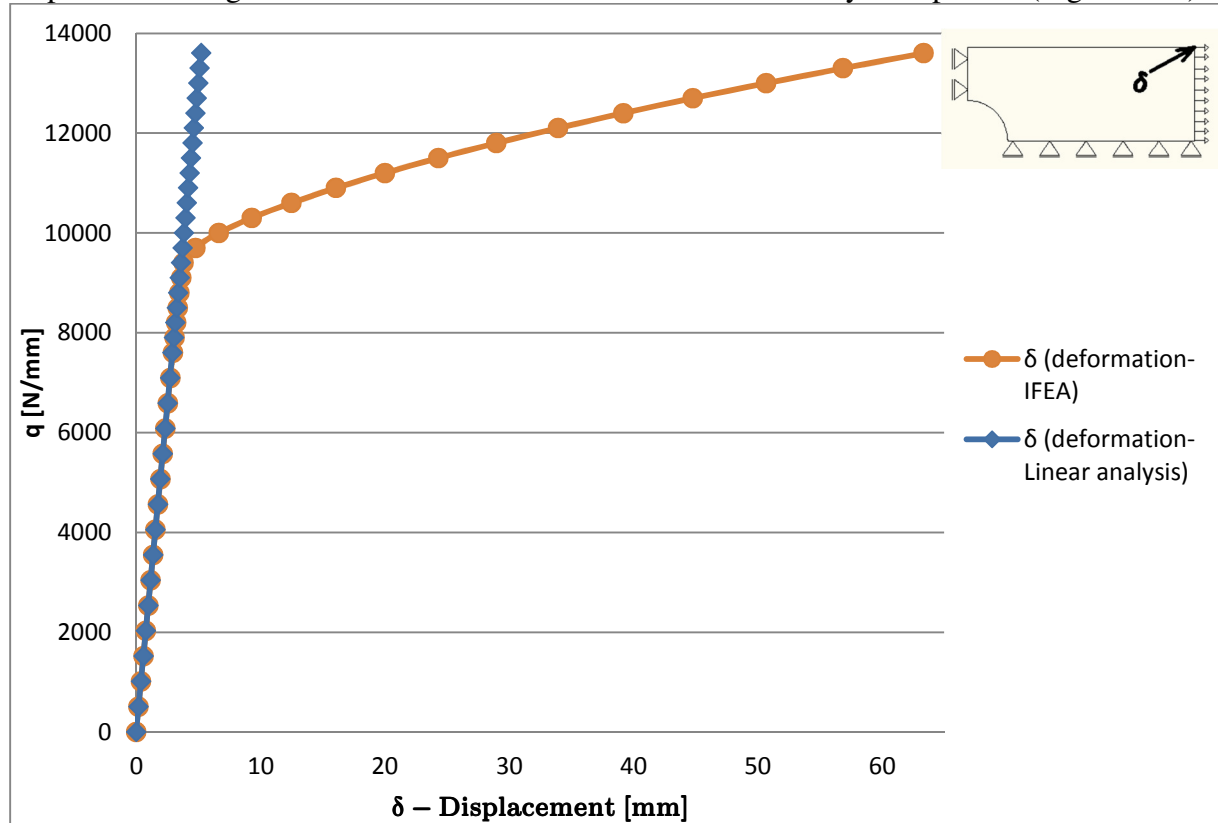


Figure 4.27 - Plate B ( $r=250\text{mm}$ ) WSH: Load-Displacement diagram

The maximum displacement corresponding to the ultimate load is  $\delta_u = 63.3mm$ . In order to estimate the applicability of the SM method to the plate with hole WSH, the equivalent-strain at the notch-tip versus load is plotted. The results from the SM method are compared to the IFEA results, but also with the ESED method, Neuber's rule and the linear calculation (Figure 4.28).

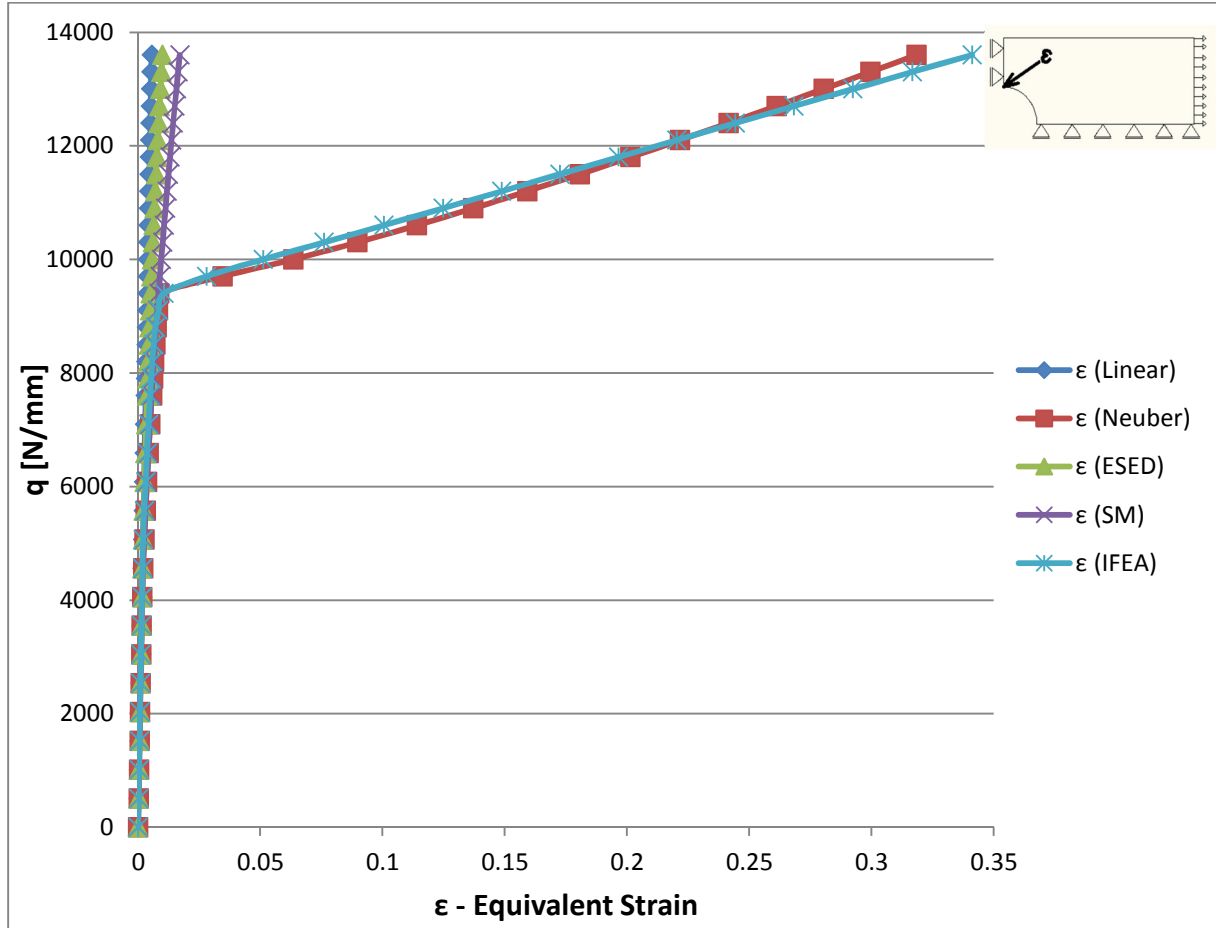


Figure 4.28 - Plate B ( $r=250mm$ ) WSH: Load-Equivalent Strain diagram

Based on Figure 4.28 it can be stated that the SM method cannot be used to estimate strains at the notch-tip once full yielding of the section occurs. As this method is based on the linear finite element analysis, it is not able to account for full yielding in a section. However, just as in the case of plate A WSH, Neuber's rule can still be applied beyond the yield load as this method is based on the nominal stress in the section, thus taking into account the full yielding of the section. Figure 4.29 plots the equivalent strain vs load up to  $q_y$

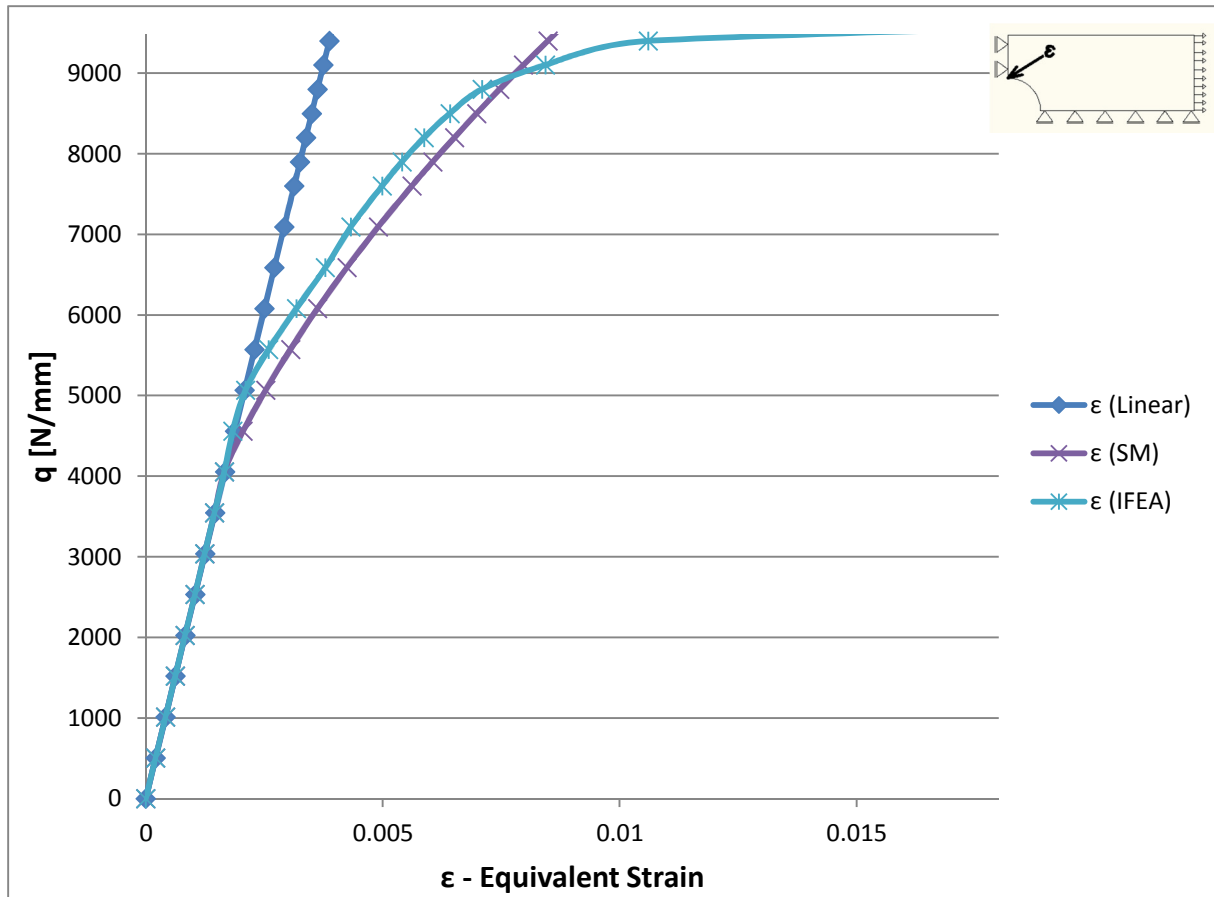


Figure 4.29 - Plate B (r=250mm) WSH: Load-Equivalent Strain diagram up to  $q_y$

It can be noticed that the diagram in the case WSH is quite similar to the one WoSH. This is due to the fact that the load only goes up to the value for which full yielding in the net section occurs and thus the strain is not significantly influenced by the rate of strain hardening. From Figure 4.29 it can be noticed that the SM seems a good approximation method for the strain up to the same load level as in the case WoSH. This corresponds to about 90% of the yield load ( $q_y$  – the lowest value of the load for which yielding is expected in the net cross-section). The equivalent strain from the SM and IFEA is compared in Table 32 for this load.

Table 32 – Plate B (r=250mm) WSH: Equivalent strain at  $0.9q_y$

q [N/mm]	$\epsilon$ (Linear)	$\sigma$ (Linear) [N/mm <sup>2</sup> ]	SM	IFEA	Equivalent strain difference [%]
			$\epsilon$ (NF)	$\epsilon$ (IFEA)	
8520	0.0035	730	0.007	0.0065	+7.7

Using the SM method, the estimated strain at the notch-tip is higher by approximately 7% from the one calculated using an IFEA at  $0.9q_y$ . The difference in strain between the material WoSH and WSH can be explained by the strain hardening rate. In the example illustrated in this section the presence of strain hardening means that the material at the location of the notch-tip has a lower strain increase compared to the example WoSH. The results are acceptable as the strain is in the range of around 0.7% which is much lower than the usual design code requirements with respect to material properties (section 3.3).

**4.1.8 Plate C ( $r=187.5mm$ ) WSH**

Plate C has a width of 1500mm and a radius of the hole of 187.5mm, with a corresponding stress concentration factor  $K_t = 2.422$ . Based on equation ( 8 ) the load at which failure occurs is  $q_u = 15300N/mm$  and at which yielding occurs  $q_y = 10650N/mm$ . The load for which localized yielding occurs (at the location of the stress concentration) is  $q_l = 4398N/mm$ . The behaviour of the plate is similar to the previous examples, the difference in geometry influencing only the magnitude of the stress concentration. The load-displacement diagram based on the non-linear finite element analysis is plotted (Figure 4.30).

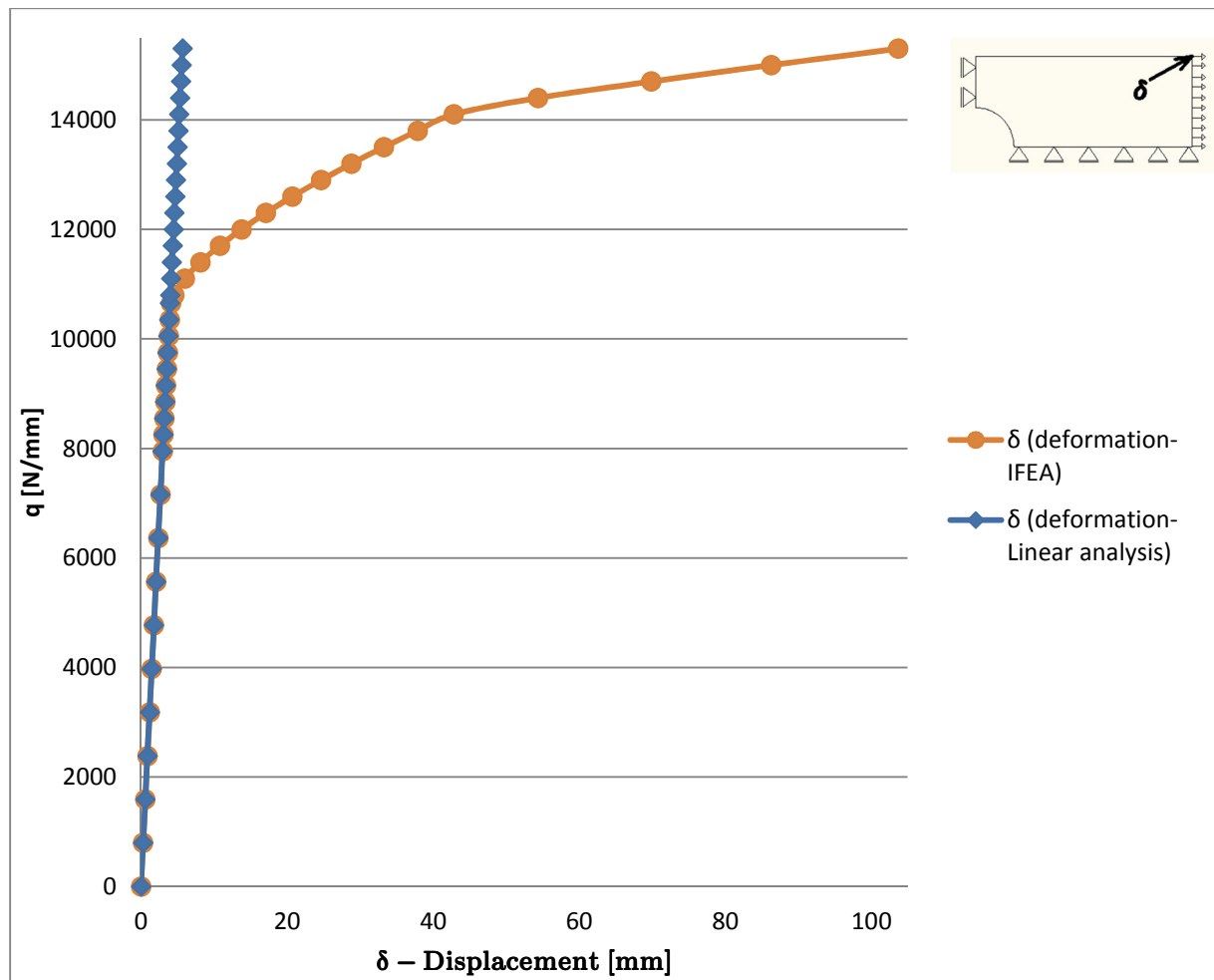


Figure 4.30 - Plate C ( $r=187.5mm$ ) WSH: Load-Displacement diagram

The maximum displacement corresponding to the ultimate load is  $\delta_u = 103.7mm$ . In order to estimate the applicability of the SM method to the plate with hole WSH, the equivalent-strain at the notch-tip versus load is plotted. The results from the SM method are compared to the IFEA results, but also with the ESED method, Neuber's rule and the linear calculation (Figure 4.31).

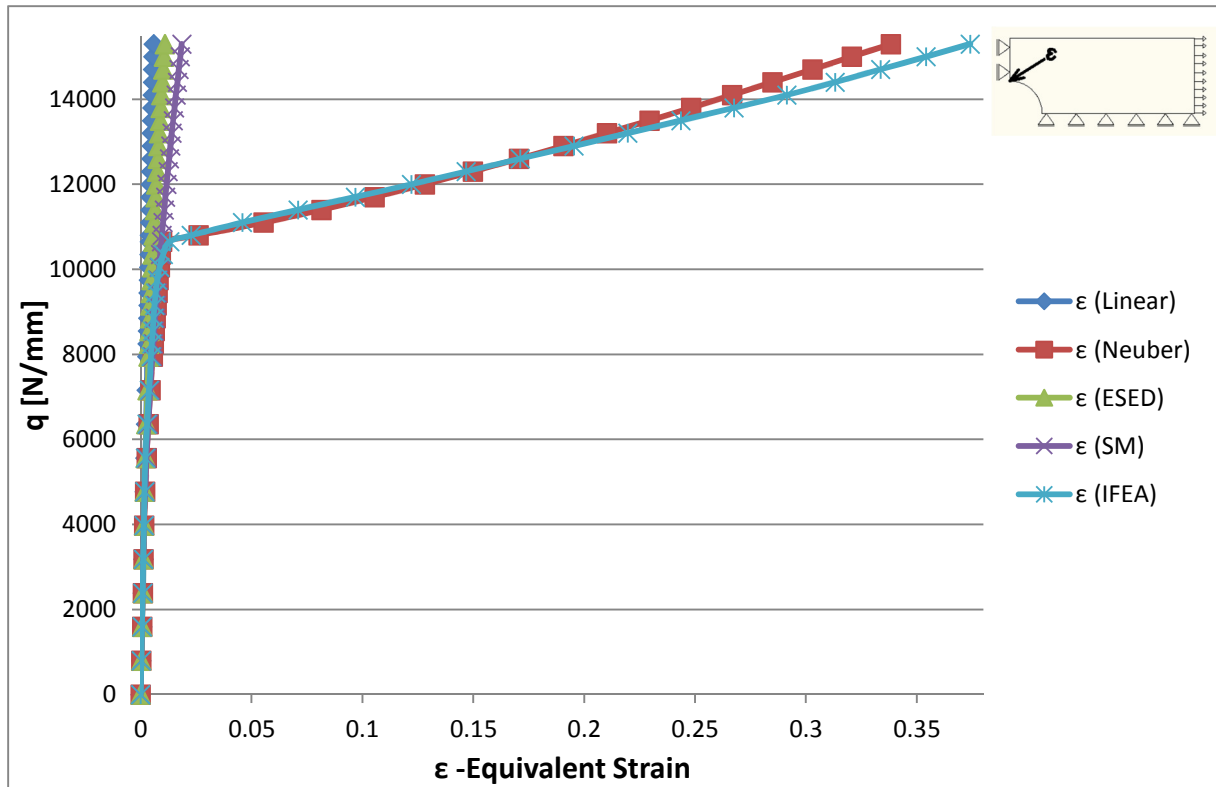


Figure 4.31 - Plate C (r=187.5mm) WSH: Load-Equivalent Strain diagram

Just as in the previous examples WSH, the SM method cannot be used to estimate strains at the notch-tip once full yielding of the section occurs. As this method is based on the linear finite element analysis, it is not able to account for full yielding in a section. Figure 4.32 plots the equivalent strain vs load up to  $q_y$

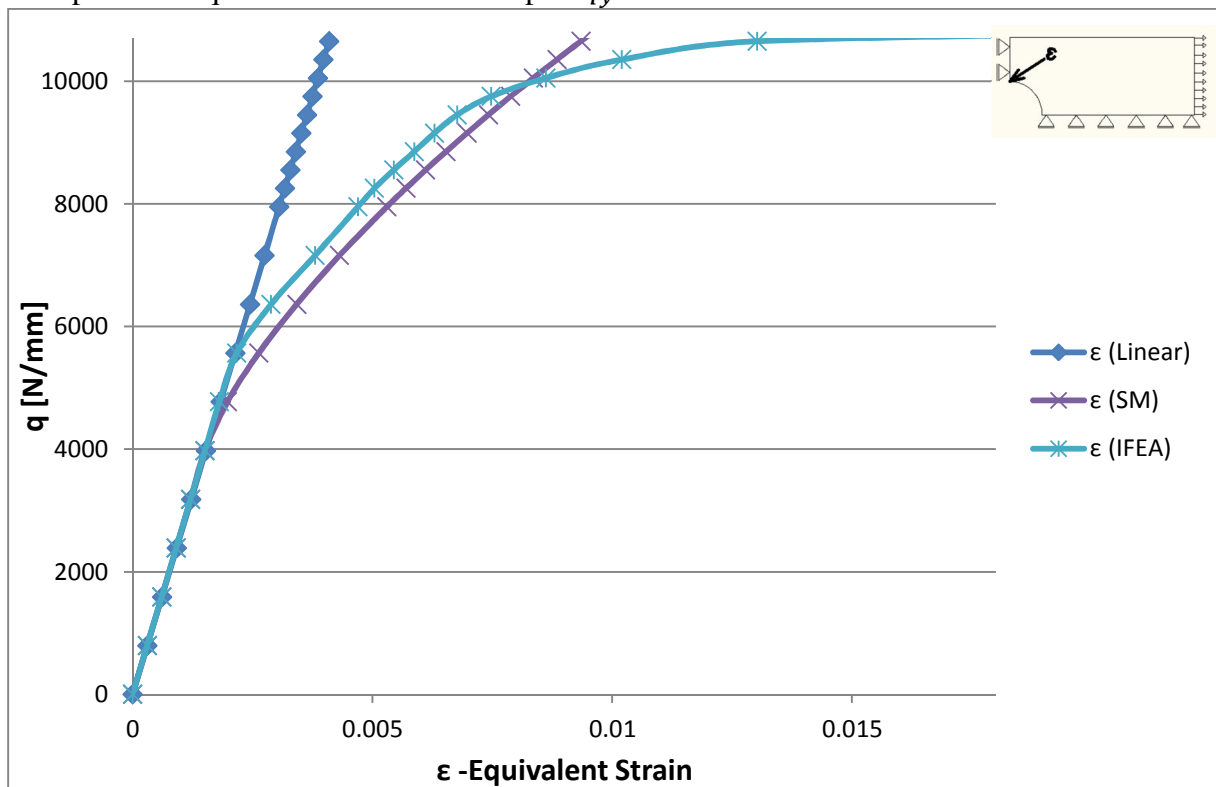


Figure 4.32 - Plate C (r=187.5mm) WSH: Load-Equivalent Strain diagram up to  $q_y$

It can be noticed that the diagram in the case WSH is quite similar to the one WoSH. This is due to the fact that the load only goes up to the value for which full yielding in the net section occurs and thus the strain is not significantly influenced by the rate of strain hardening. From Figure 4.32 it can be noticed that the SM seems a good approximation method for the strain up to the same load level as in the case WoSH. This corresponds to about 90% of the yield load ( $q_y$  – the lowest value of the load for which yielding is expected in the net cross-section). The equivalent strain from the SM and IFEA is compared in Table 33 for this load.

Table 33 – Plate C ( $r=187.5\text{mm}$ ) WSH: Equivalent strain at  $0.9q_y$

q [N/mm]	$\epsilon$ (Linear)	$\sigma$ (Linear) [N/mm <sup>2</sup> ]	SM	IFEA	Equivalent strain difference [%]
			$\epsilon$ (NF)	$\epsilon$ (IFEA)	
9585	0.0036	761	0.0075	0.0069	+8.7

Using the SM method, the estimated strain at the notch-tip is higher by approximately 9% from the one calculated using an IFEA at  $0.9q_y$ . The difference in strain between the material WoSH and WSH can be explained by the strain hardening rate. In the example illustrated in this section the presence of strain hardening means that the material at the location of the notch-tip has a lower strain increase compared to the example WoSH. The results are acceptable as the strain is in the range of around 0.7% which is much lower than the usual design code requirements with respect to material properties (section 3.3).

#### 4.1.9 Plate D ( $r=150\text{mm}$ ) WSH

Plate D has a width of 1500mm and a radius of the hole of 150mm, with a corresponding stress concentration factor  $K_t = 2.508$ . Based on equation ( 8 ) the load at which failure occurs is  $q_u = 16320\text{N/mm}$  and at which yielding occurs  $q_y = 11360\text{N/mm}$ . The load for which localized yielding occurs (at the location of the stress concentration) is  $q_l = 4530\text{N/mm}$ . The behaviour of the plate is similar to the previous examples, the difference in geometry influencing only the magnitude of the stress concentration. The load-displacement diagram based on the non-linear finite element analysis is plotted (Figure 4.33).

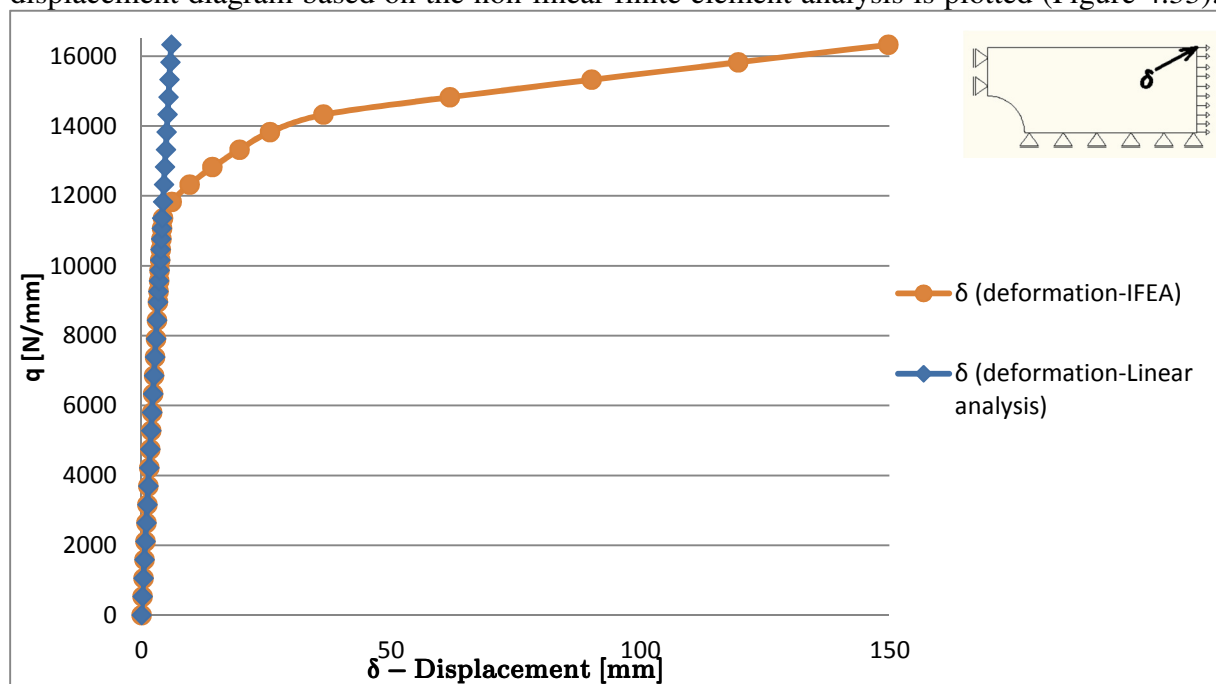


Figure 4.33 - Plate D ( $r=150\text{mm}$ ) WSH: Load-Displacement diagram

The maximum displacement corresponding to the ultimate load is  $\delta_u = 149.8mm$ . In order to estimate the applicability of the SM method to the plate with a hole WSH, the equivalent-strain at the notch-tip versus load is plotted. The results from the SM method are compared to the IFEA results, but also with the ESED method, Neuber's rule and the linear calculation (Figure 4.34).

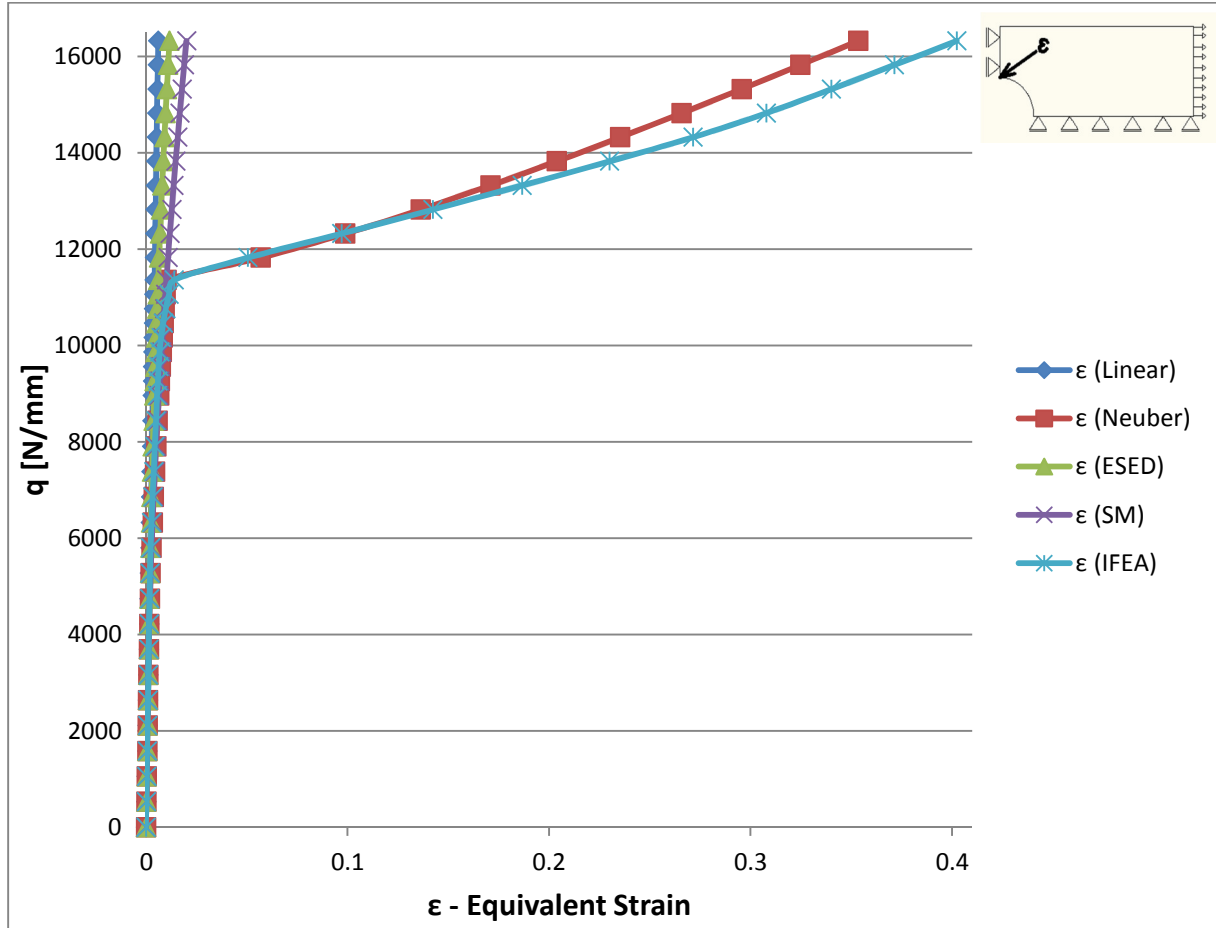


Figure 4.34 - Plate D ( $r=150mm$ ) WSH: Load-Equivalent Strain diagram

Just as in the previous examples WSH, the SM method cannot be used to estimate strains at the notch-tip once full yielding of the section occurs. As this method is based on the linear finite element analysis, it is not able to account for full yielding in a section. Figure 4.35 plots the equivalent strain vs load up to  $q_y$

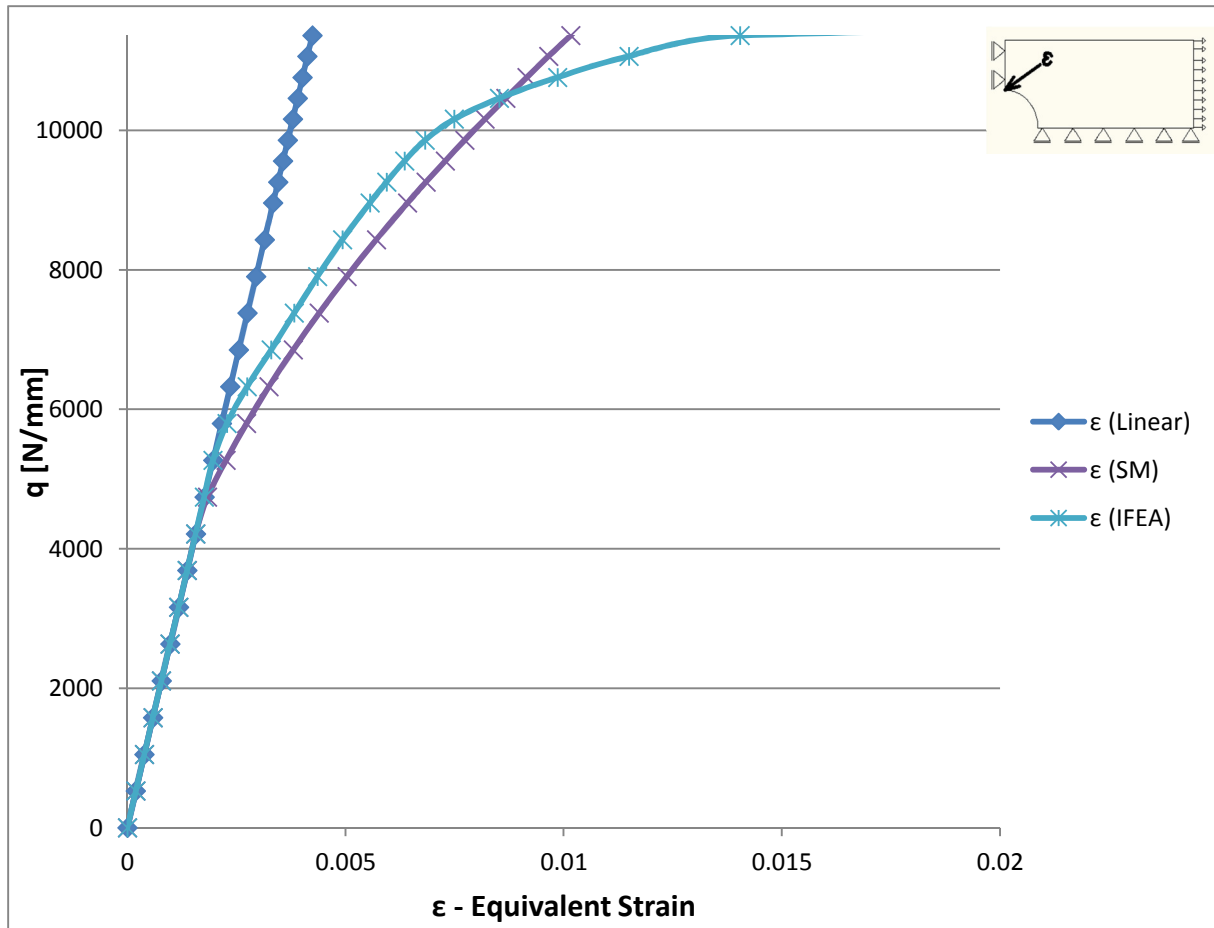


Figure 4.35 - Plate D (r=150mm) WSH: Load-Equivalent Strain diagram up to  $q_y$

It can be noticed that the diagram in the case WSH is quite similar to the one WoSH. This is due to the fact that the load only goes up to the value for which full yielding in the net section occurs and thus the strain is not significantly influenced by the rate of strain hardening. From Figure 4.35 it can be noticed that the SM seems a good approximation method for the strain up to the same load level as in the case WoSH. This corresponds to about 90% of the yield load ( $q_y$  – the lowest value of the load for which yielding is expected in the net cross-section). The equivalent strain from the SM and IFEA is compared in Table 34 for this load.

Table 34 – Plate D (r=150mm) WSH: Equivalent strain at  $0.9q_y$

q [N/mm]	$\epsilon$ (Linear)	$\sigma$ (Linear) [N/mm <sup>2</sup> ]	SM	IFEA	Equivalent strain difference [%]
			$\epsilon$ (NF)	$\epsilon$ (IFEA)	
10224	0.0038	795	0.0082	0.0076	+7.9

Using the SM method, the estimated strain at the notch-tip is higher by approximately 8% from the one calculated using an IFEA at  $0.9q_y$ . The difference in strain between the material WoSH and WSH can be explained by the strain hardening rate. In the example illustrated in this section the presence of strain hardening means that the material at the location of the notch-tip has a lower strain increase compared to the example WoSH. The results are acceptable as the strain is in the range of around 0.8% which is much lower than the usual design code requirements with respect to material properties (section 3.3).

**4.1.10 Plate E ( $r=75mm$ ) WSH**

Plate E has a width of 1500mm and a radius of the hole of 75mm, with a corresponding stress concentration factor  $K_t = 2.722$ . Based on equation ( 8 ) the load at which failure occurs is  $q_u = 18360N/mm$  and at which yielding occurs  $q_y = 12780N/mm$ . The load for which localized yielding occurs (at the location of the stress concentration) is  $q_l = 4695N/mm$ . The behaviour of the plate is similar to the previous examples, the difference in geometry influencing only the magnitude of the stress concentration. The load-displacement diagram based on the non-linear finite element analysis is plotted (Figure 4.36).

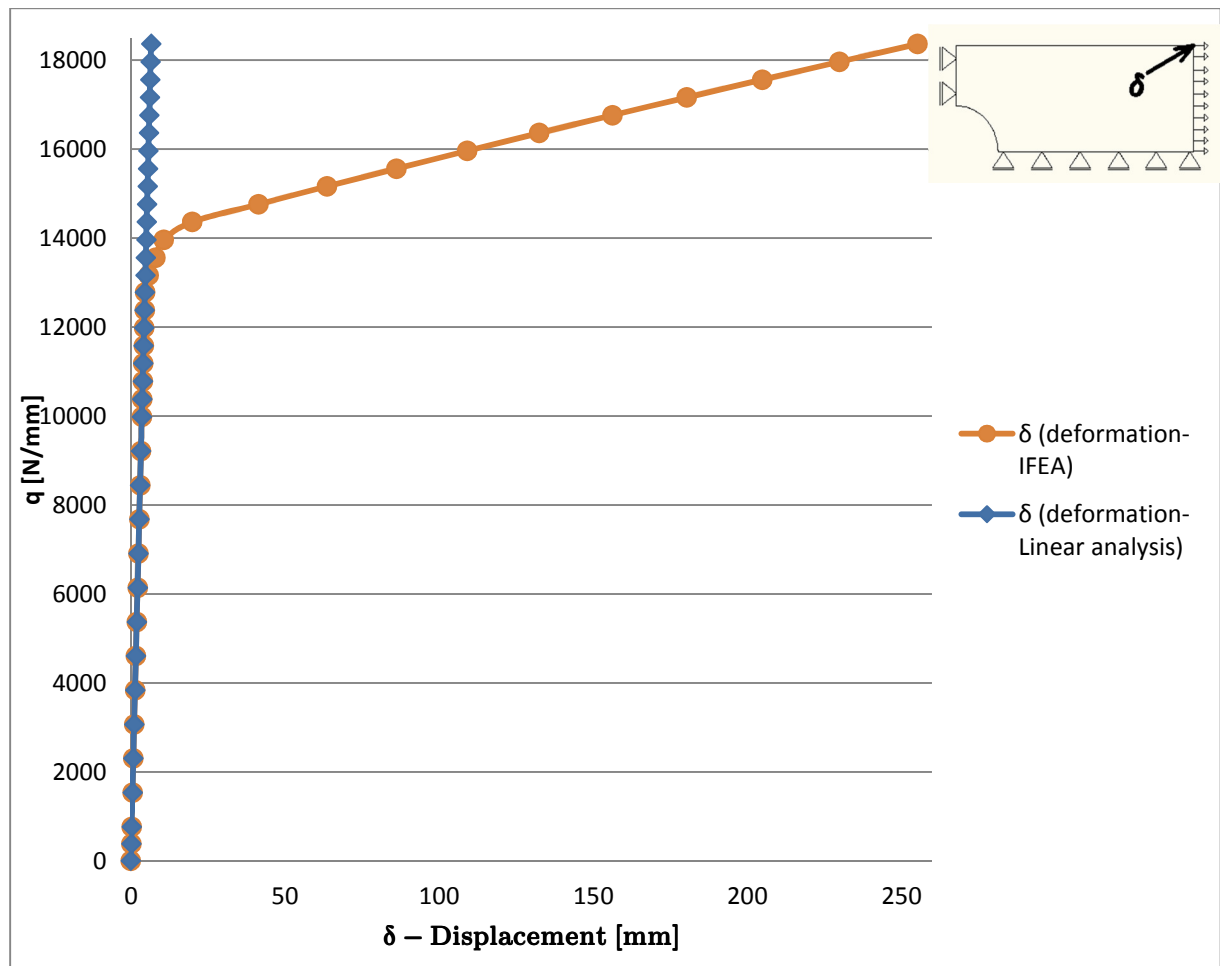


Figure 4.36 - Plate E ( $r=75mm$ ) WSH: Load-Displacement diagram

The maximum displacement corresponding to the ultimate load is  $\delta_u = 225.3mm$ . In order to estimate the applicability of the SM method to the plate with hole WSH, the equivalent-strain at the notch-tip versus load is plotted. The results from the SM method are compared to the IFEA results, but also with the ESED method, Neuber's rule and the linear calculation (Figure 4.37).

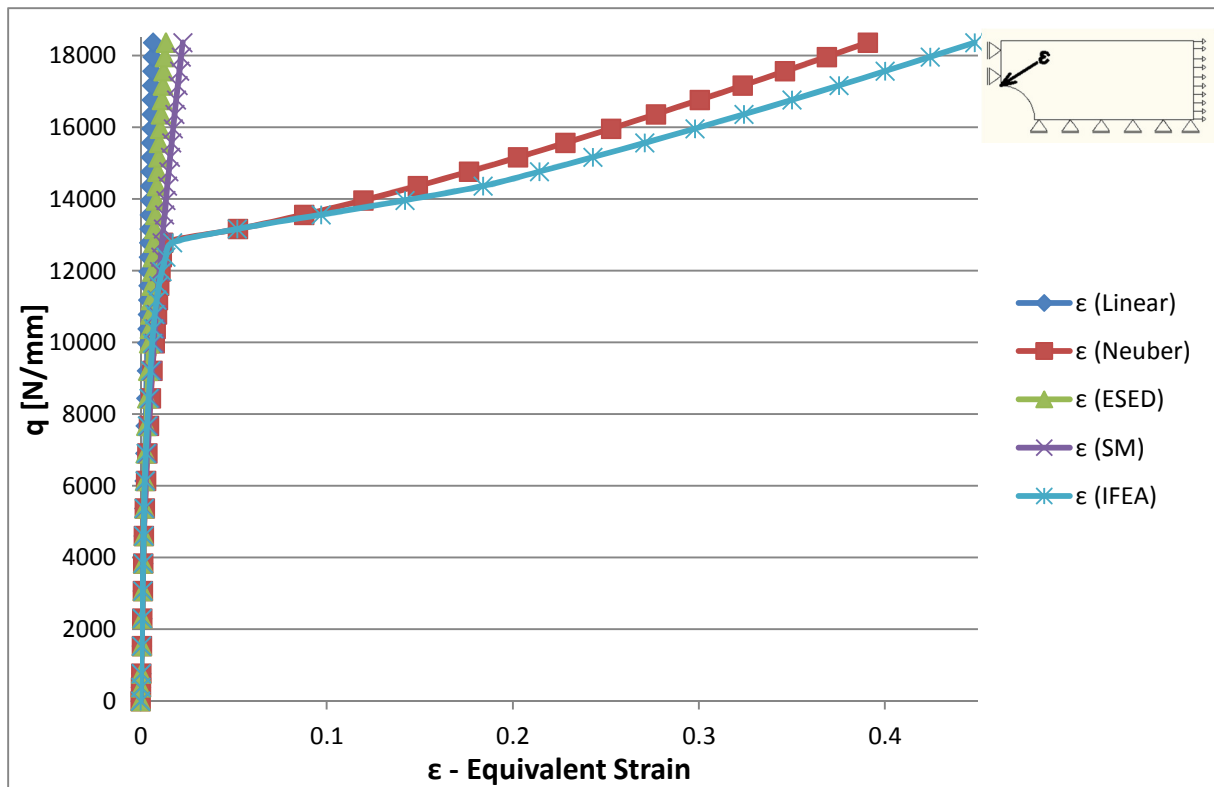


Figure 4.37 - Plate E (r=75mm) WSH: Load-Equivalent Strain diagram

Just as in the previous examples WSH, the SM method cannot be used to estimate strains at the notch-tip once full yielding of the section occurs. As this method is based on the linear finite element analysis, it is not able to account for full yielding in a section. Figure 4.38 plots the equivalent strain vs load up to  $q_y$

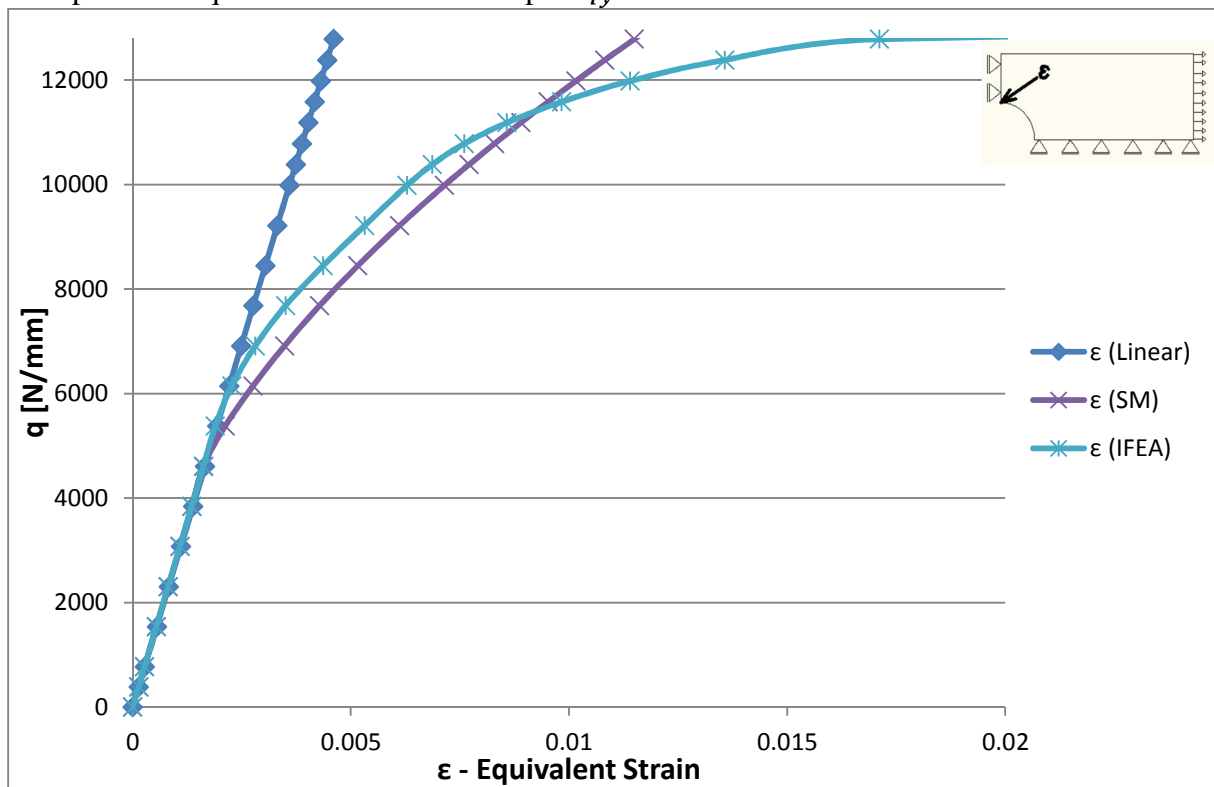


Figure 4.38 - Plate E (r=75mm) WSH: Load-Equivalent Strain diagram up to  $q_y$

It can be noticed that the diagram in the case WSH is quite similar to the one WoSH. This is due to the fact that the load only goes up to the value for which full yielding in the net section occurs and thus the strain is not significantly influenced by the rate of strain hardening. From Figure 4.38 it can be noticed that the SM seems a good approximation method for the strain up to the same load level as in the case WoSH. This corresponds to about 90% of the yield load ( $q_y$  – the lowest value of the load for which yielding is expected in the net cross-section). The equivalent strain from the SM and IFEA is compared in Table 35 for this load.

 Table 35 – Plate E ( $r=75\text{mm}$ ) WSH: Equivalent strain at  $0.9q_y$ 

$q$ [N/mm]	$\varepsilon$ (Linear)	$\sigma$ (Linear) [N/mm <sup>2</sup> ]	SM	IFEA	Equivalent strain difference [%]
			$\varepsilon$ (NF)	$\varepsilon$ (IFEA)	
11502	0.0041	852	0.0095	0.0097	-2.1

Using the SM method, the estimated strain at the notch-tip is lower by approximately 2% from the one calculated using an IFEA at  $0.9q_y$ . The difference in strain between the material WoSH and WSH can be explained by the strain hardening rate. In the example illustrated in this section the presence of strain hardening means that the material at the location of the notch-tip has a lower strain increase compared to the example WoSH. The results are acceptable as the strain is in the range of around 1% which is much lower than the usual design code requirements with respect to material properties (section 3.3).

#### 4.1.11 Conclusions on SM applied to a plate with a hole

The SM method was applied to five different geometries of a plate with a hole for two different stress-strain diagrams( with and without strain hardening:  $f_u/f_y=1$  and  $f_u/f_y=1.4$ ). Based on the results the SM seems to be a good method for predicting strains at the notch-tip up to a certain load level. The following conclusions can be drawn from the results:

- The load for which localized yielding first occurs  $q_l$  and the lowest load for which yielding occurs in a section  $q_y$  are independent of the  $f_u/f_y$  ratio;
- The  $f_u/f_y$  ratio influence on the development of strains up to the yield load limit is quite small (Table 36). Based on the present results a minimum value of strain at fracture seems to be a better way of ensuring ductility with respect to stress concentrations;

 Table 36 –  $f_u/f_y$  ratio on strain development at  $0.9q_y$ 

	$q$ [N/mm]	$\varepsilon_{NL}$ [WoSH]	$\varepsilon_{NL}$ [WSH]	Strain difference [%]
Plate A	6390	0.0065	0.0062	4.84
Plate B	8520	0.007	0.0065	7.69
Plate C	9585	0.0074	0.0069	7.25
Plate D	10224	0.0081	0.0076	6.58
Plate E	11502	0.0102	0.0097	5.15

- The SM method can be used to predict strains at the notch-tip (at the location of stress concentrations) up to a certain load level. Based on the models developed in this section, this limit is equal to 90% of the load which is expected to cause yielding in the net section (in the case of the plate with a hole this is the net section). This can be explained by the fact that, as the SM is based on the results of a linear analysis, it

cannot take into account the high differences that occur once the section yields. The linear analysis simply results in a linear increase of the strains with the loads while the real strain increase depends on the rate of strain hardening (which is much lower than the elasticity modulus). In the IFEA as the load increases, the area surrounding the notch-tip starts to yield in order to attain equilibrium. The main difference between the results from the IFEA and the linear analysis is the fact that in the first case the strain increases at a much higher rate with a lower increase in stresses (which results in a large area that needs to yield in order to have equilibrium with the applied load) while in the latter case the strains and stresses increase at the same rate as in the elastic range (equal to Young's modulus). This means that once yielding is attained in the section the SM method cannot be applied any more as the linear analysis simply does not take account of this;

- The 90% yield load limit might be a conservative approach in some case. However, due to the fact that the finite element results are quite sensitive to the chosen mesh, it is an acceptable value as it is on the safe side and ensures and easier, straight-forward application of the SM;
- In order to apply the SM method, firstly the lowest value of the load for which full yielding of the section can occur must be established. Based on this, the acting load should be compared to  $0.9q_y$ . If the load is below this value then the SM method can be used to estimate the strains at the location of the stress concentrations based on the linear analysis results. Otherwise a non-linear analysis should be performed.
- In all cases studied in this section, full yielding of the net section occurred previous to the attainment of the 5% strain limit. In the case WoSH failure of the plate occurred previous to the attainment of the 5% strain limit. In the case WSH this limit was reached and exceeded in all five cases. This results in the fact that the presence of strain hardening significantly enhances the strength capacity of the plate (i.e. the plate is able to carry higher loads without the occurrence of fracture).

The questions usually raised in practice with respect to stress concentrations are related to the ability of the material to yield locally and redistribute stresses. Thus the problem is related to local yielding and redistribution of stresses, which means that the acting loads are below the ones which are expected to cause full yielding in the section of an element. As the SM can be used up to 90% of the yield load, it can be quite a promising tool in argumenting the material capacity to do so, without the need for a non-linear analysis. In case the acting load exceeds 90% of the yield load, the problems with respect to ductility are no longer so much concerned with stress concentrations and the ability of the material to yield locally, but rather with the overall behaviour of the structure. For this case an IFEA based on the material non-linear behaviour should be carried out.

Another issue with respect to the ability of the material to yield locally and redistribute stresses is the  $f_u/f_y$  ratio. Most design codes use a limitation for this value in order to ensure ductility (see section 3.3). The strains at the notch-tip (where the largest strains occur) at the load level of  $0.9q_y$  for WoSH ( $f_u/f_y=1$ ) and WSH ( $f_u/f_y=1.4$ ) are compared (Table 37).

Table 37 – IFEA: Equivalent strains at a load level of  $0.9q_y$  for the cases WoSH and WSH

	IFEA		Differences in strain at the notch tip [%]
	$\epsilon_{NL}$ [WoSH]	$\epsilon_{NL}$ [WSH]	
Plate A	0.0065	0.0062	-4.84
Plate B	0.007	0.0065	-7.69
Plate C	0.0074	0.0069	-7.25
Plate D	0.0081	0.0076	-6.58
Plate E	0.0102	0.0097	-5.15

 Table 38 – SM: Equivalent strains at a load level of  $0.9q_y$  for the cases WoSH and WSH

	SM		Differences in strain at the notch tip [%]
	$\epsilon_{NL}$ [WoSH]	$\epsilon_{NL}$ [WSH]	
Plate A	0.0063	0.0063	0.00
Plate B	0.0072	0.007	-2.86
Plate C	0.0078	0.0075	-4.00
Plate D	0.0085	0.0082	-3.66
Plate E	0.0097	0.0095	-2.11

The differences in the strains that occur between the two cases (WoSH and WSH) and the strain values are quite small (the highest is 1%, far from the 5% limit). In the case of the IFEA the differences in results go up to about 7.7% while in the case of the SM approach the ultimate to yield strength ratio has a lower influence, with differences in strains only up to 4%. Perhaps a better way to quantify ductility with respect to stress concentrations would be to ensure a minimum elongation at rupture instead of a minimum ultimate to yield strength ratio. The later seems to be rather a minimum requirement when high demands for ductility are required (as for example in structures subject to high seismic or accidental loadings), in cases where for certain loads large deformations are expected and such a ratio would ensure a global redistribution of stresses through the structure.

In the next section of this work the applicability of the SM method will be investigated in a more complex case (a bridge joint). Also on the same connection the influence of the  $f_u/f_y$  ratio will be further looked into.

## 5 APPLICATION OF THE SM AND THE INFLUENCE OF THE TENSILE-YIELD RATIO

In steel structures stress concentrations occur due to rapid geometric changes in the cross section. The questions that arise are related to the material ductility. Some examples of stress concentrations occurring in structures are presented in Figure 1.1.

In practice, the real issue is that the designer has to prove that the deformation capacity which is available is sufficient with respect to what is necessary for a certain structure. This check can be omitted provided that the requirements with regards to ductility as presented in section 3.3 are met.

The question that arises is whether or not these values are too conservative and in the case when these requirements are not met, what would be a simple and straightforward method of solving such issues. Usually when such complications occur a nonlinear analysis is performed. The material nonlinear behaviour is used as input in order to understand the real strain development in the area of interest and check whether it fulfils the ductility requirements. Such tasks however raise certain difficulties in the development of a project due to time issues. This is a time consuming operation which raises costs and problems with respect to project deadlines. A possible solution would be to relate the results of the much simpler linear analysis to the nonlinear behaviour of the material, thus avoiding a time consuming nonlinear analysis. For this purpose the SM applicability will be researched more into depth in this chapter and also the influence of the  $f_u/f_y$  ratio in the strain developments in a detail.

### 5.1 Description of Connection

In order to have a better understanding of the ductility problems that stress concentrations pose in steel joints, a real life project is chosen, namely the A1/A6 Diemen-Almere Havendreef steel railway arch bridge developed by Iv-Infra. The bridge will carry a double lane railway track, having a width of 17.2 meters, 50.2 meters high and a span of 255 meters. The geometry of the structure is presented in the figure below.

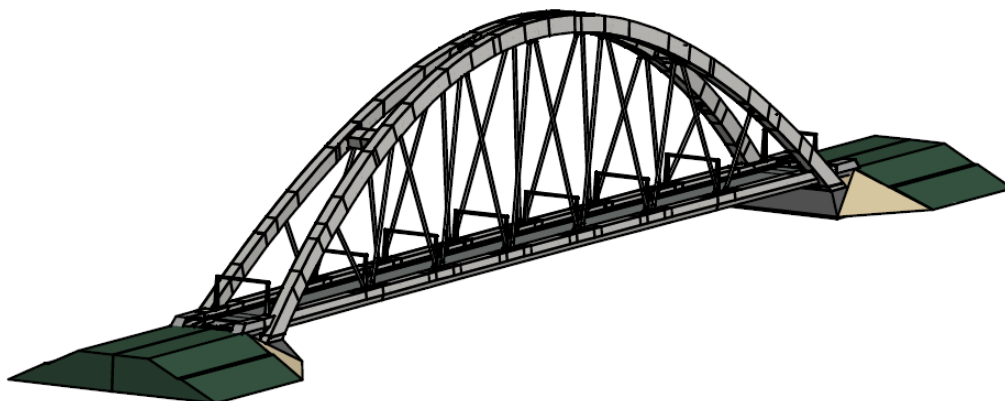


Figure 5.1 – Steel Structure Isometry [Iv-Infra]

From the bridge project, a particular joint is chosen for this study. The location of the connection, entitled as “Knoop 6”, is illustrated in Figure 4.2.

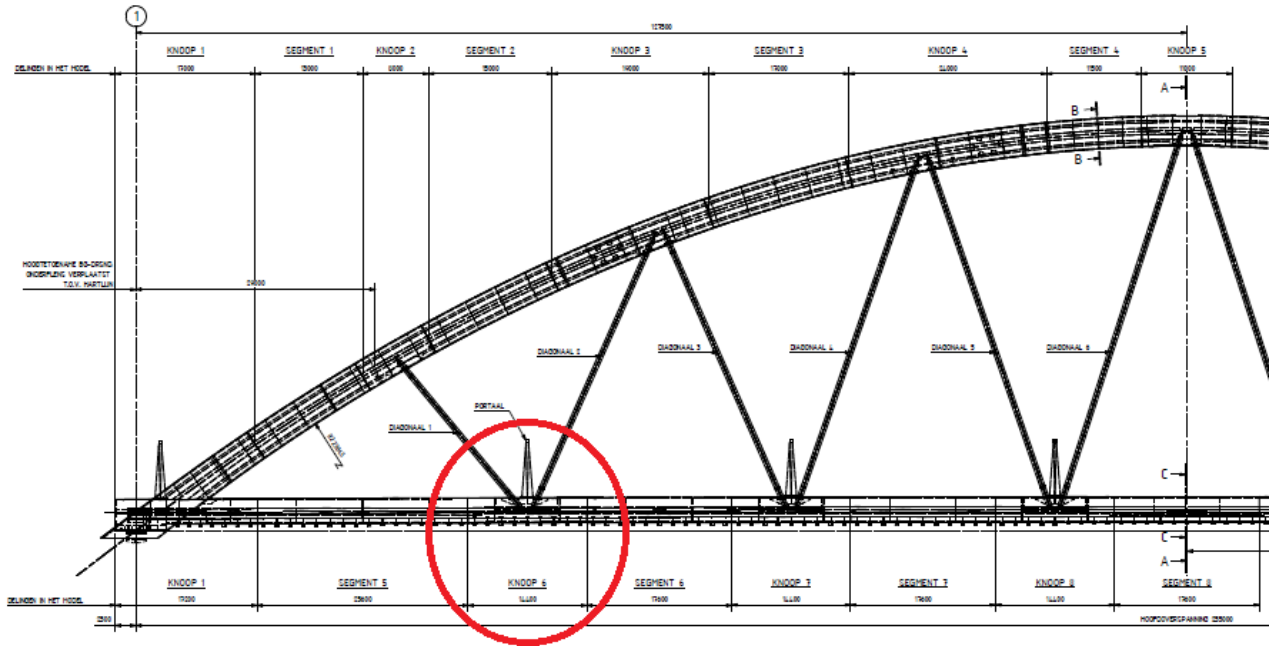


Figure 5.2 – Side View K050 [Iv-Infra]

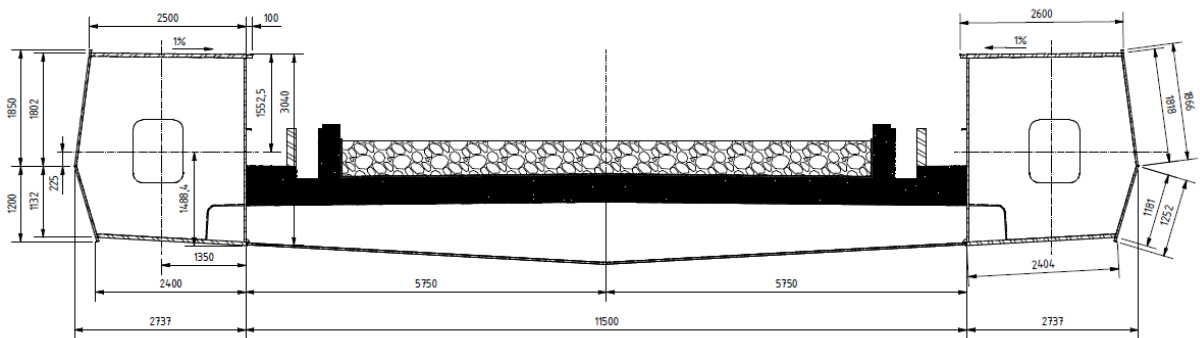


Figure 5.3 – Section C-C [Iv-Infra]

The detailed geometry of the joint is presented in the following figures.

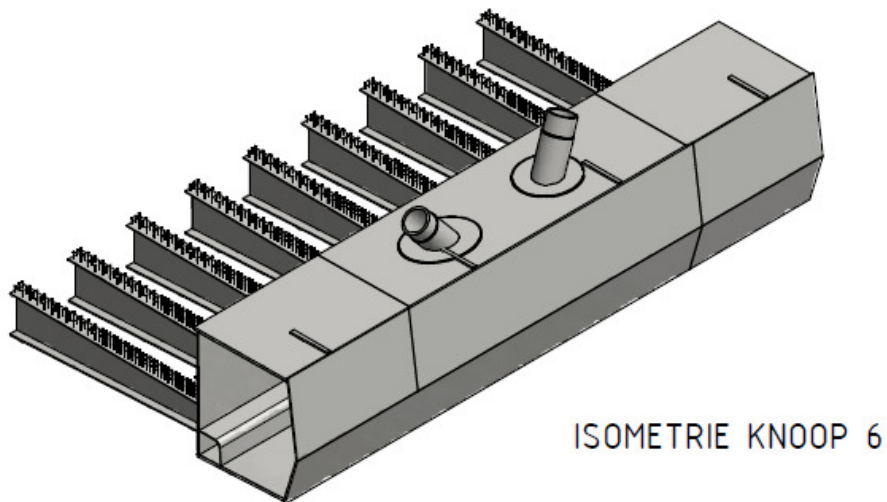


Figure 5.4 – Joint Isometry [Iv-Infra]

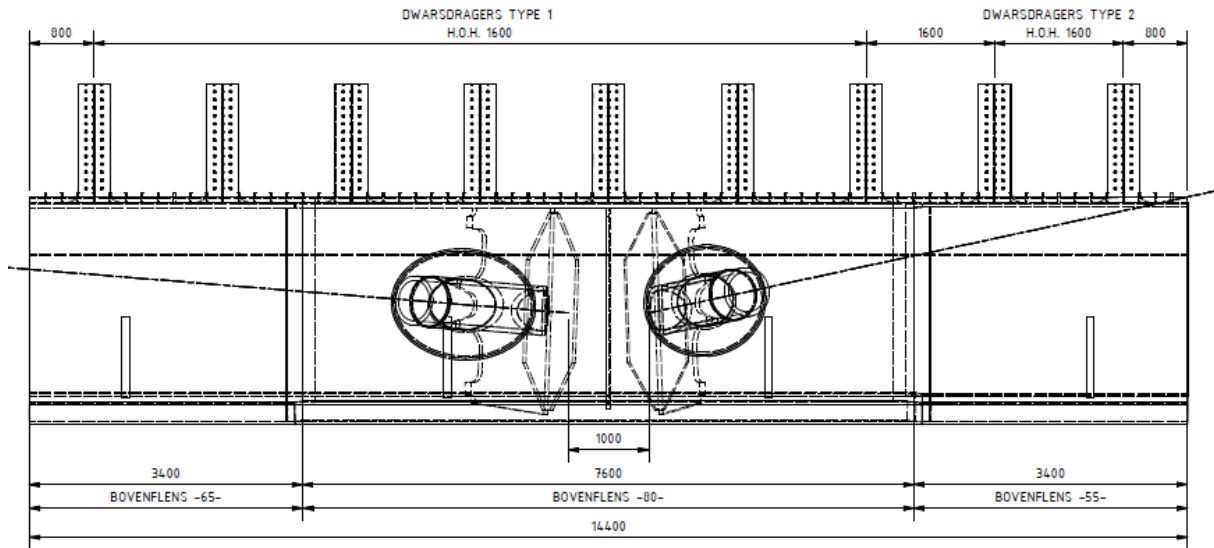


Figure 5.5 – Joint Top View [Iv-Infra]

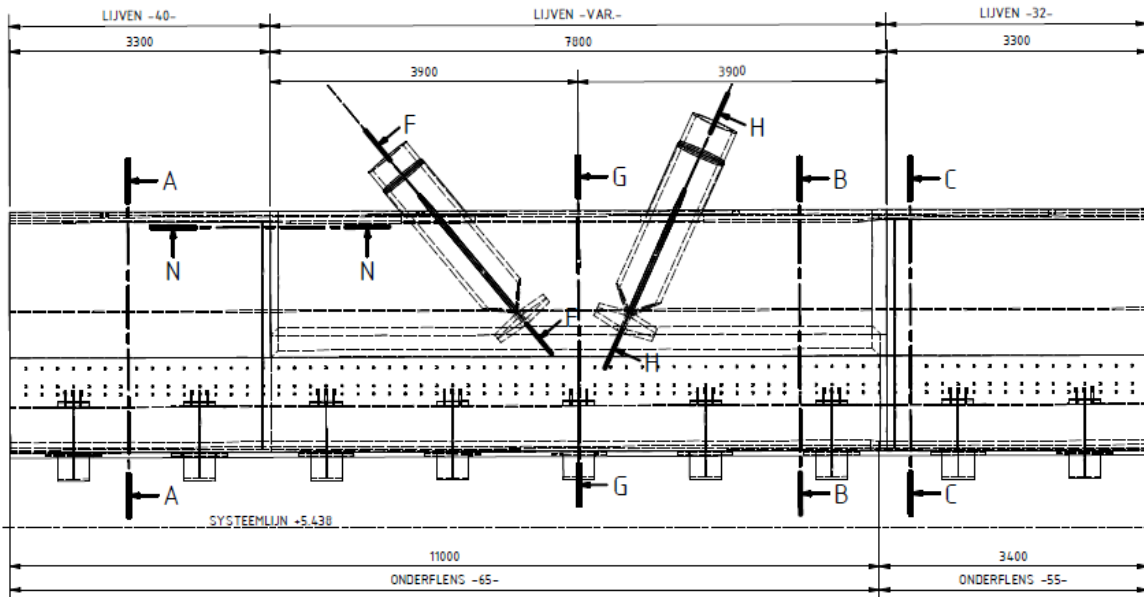


Figure 5.6 – Joint Side View [Iv-Infra]

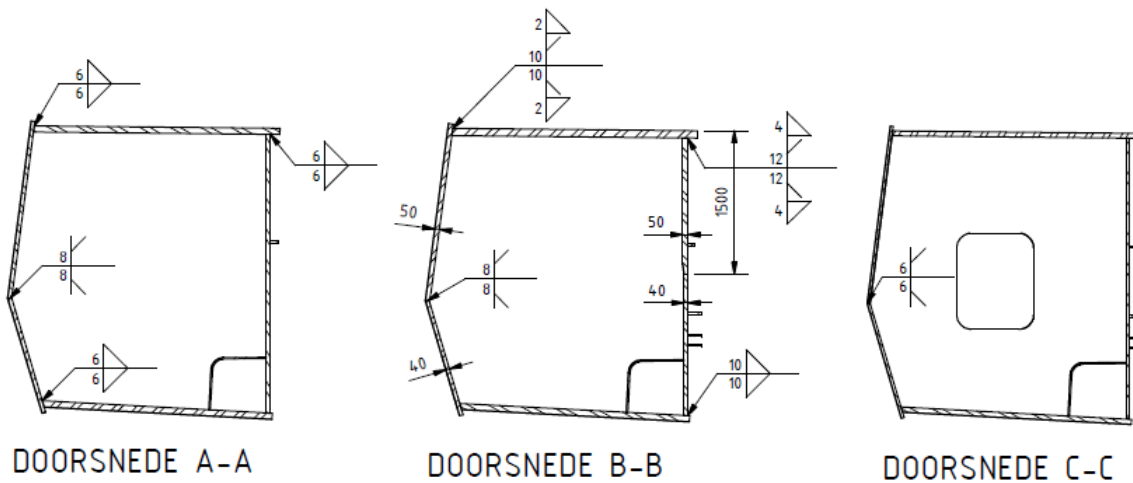


Figure 5.7 – Sections A-A, B-B and C-C [Iv-Infra]

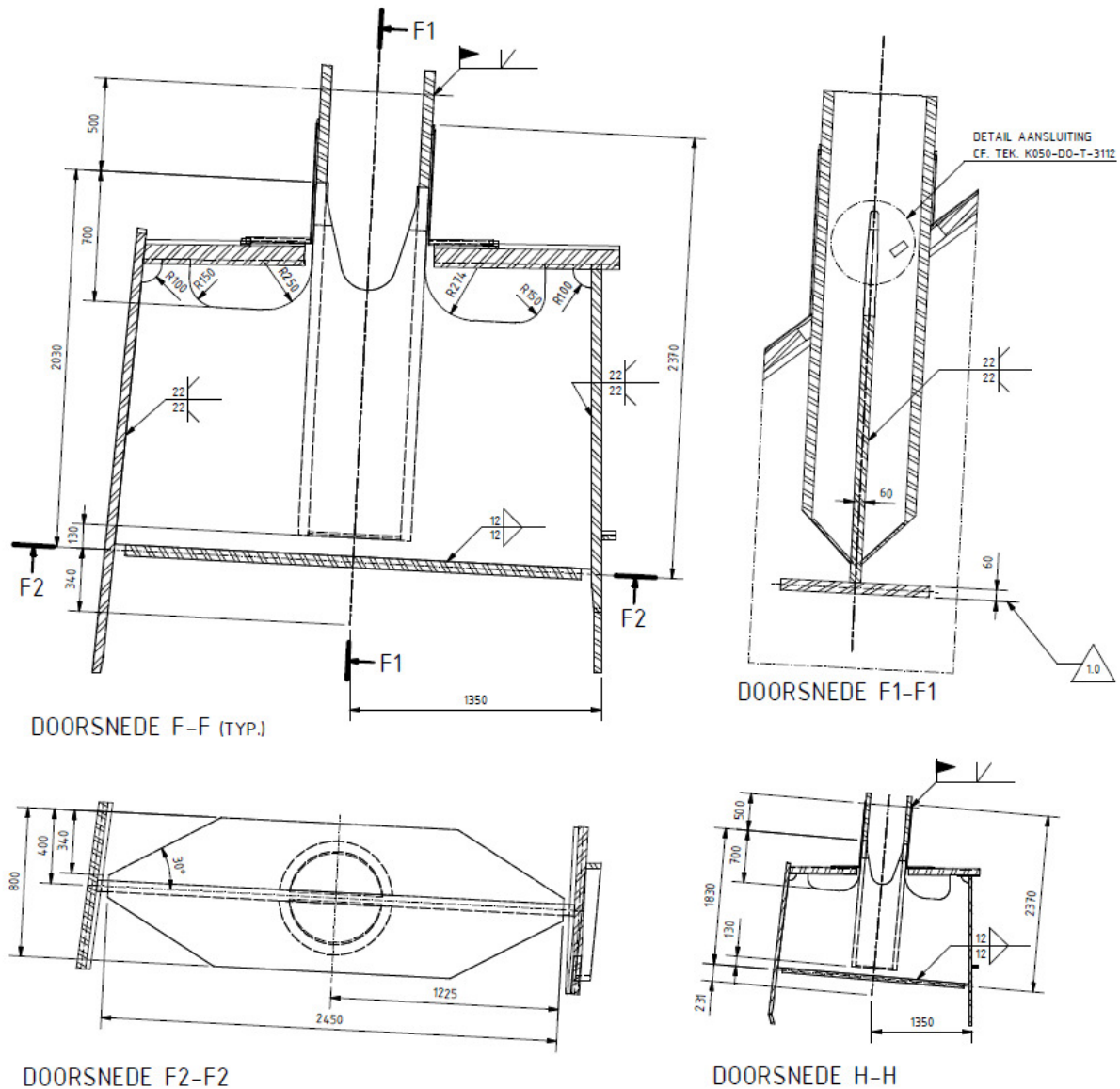


Figure 5.8 – Sections F-F and H-H [Iv-Infra]

In this project ductility issues were raised related to the requirements of the Rijkswaterstaat. S355 and S460 steel grades were used in the design of the bridge. Due to the client's stricter ductility requirements, the designer needed to prove that the available deformation capacity is sufficient with respect to what was necessary (this raised problems in the connections where it was necessary to calculate the plastic strain due to the high stress concentrations occurring there).

One of the recommendations to deal with the stress concentrations was provided by BouwQ. This was to limit the peak stress to  $f_u/f_y(\text{guaranteed}) \times f_y$ . At some locations this might be achieved through geometric changes, but there are still areas where the stresses are still too high and require a nonlinear analysis to understand the real strain development and study whether it is acceptable or not.

For the top flange, in order to solve the ductility issues, the designer chose to develop a single plate model in tension created with the same stress magnitude in the elastic analysis as in the real model. Afterwards a plastic analysis is carried out on the plate and the resulting

stresses and plastic strains are compared to an acceptable limit. The different models are presented in the figures below.

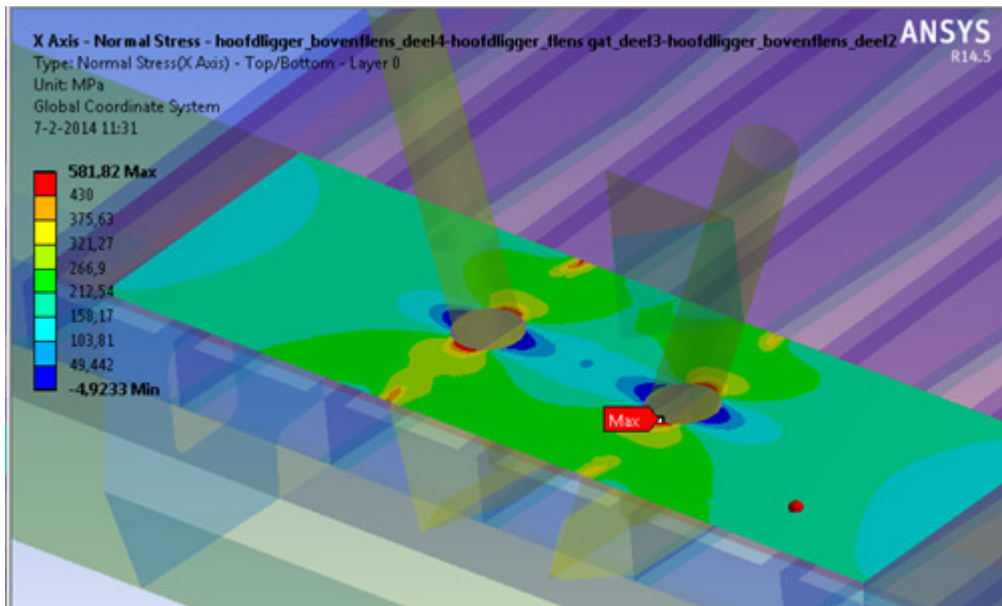


Figure 5.9 – Original tension in upper flange of global model [Iv-Infra]

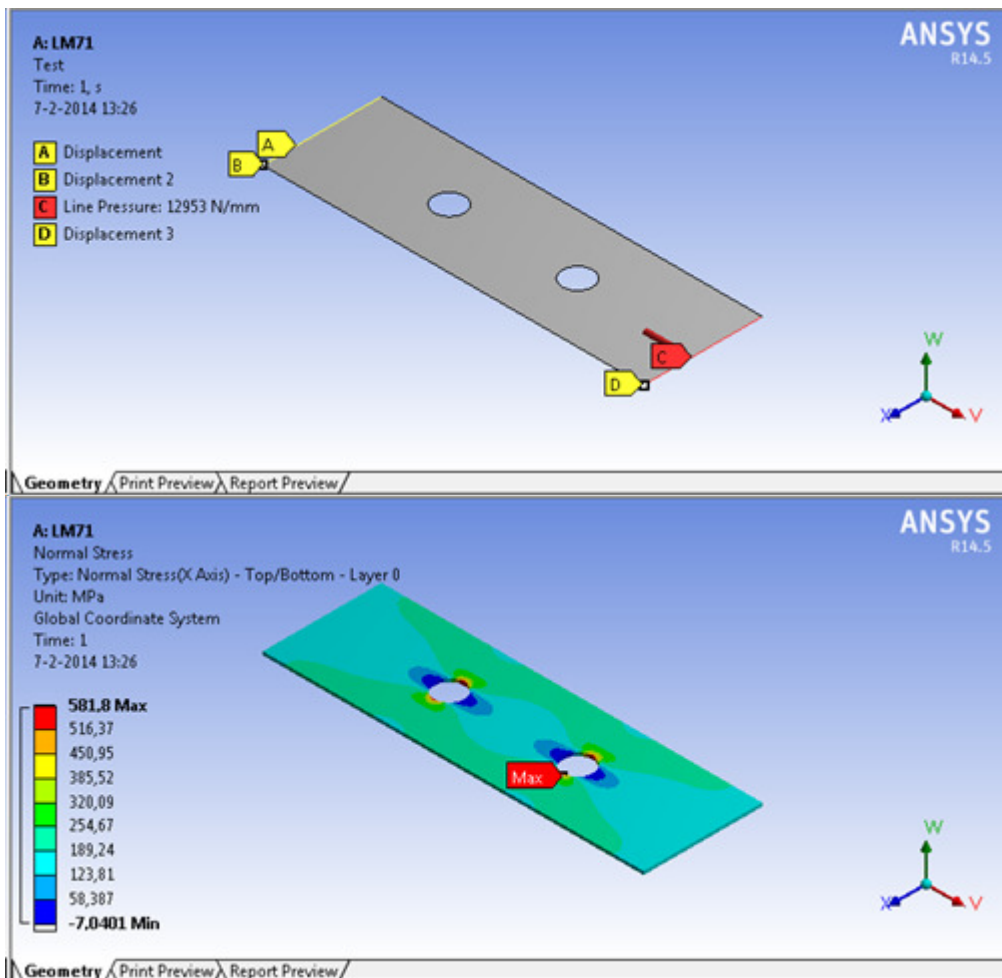


Figure 5.10 – Single plate model, elastic analysis [Iv-Infra]

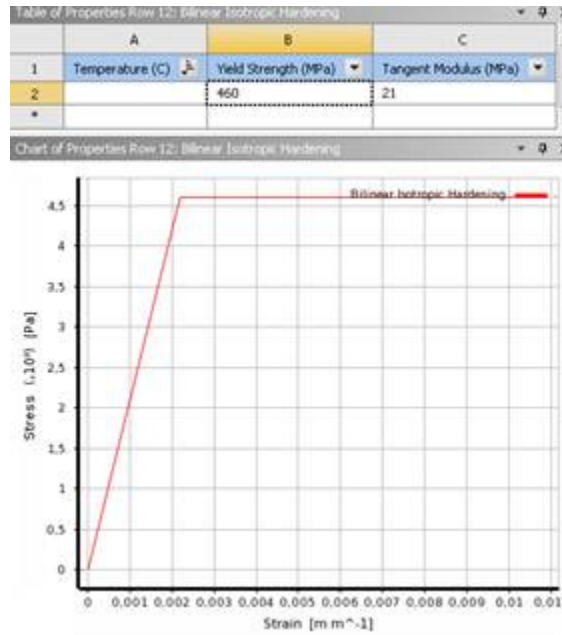


Figure 5.11 – Single plate model, plastic analysis, material properties input [Iv-Infra]

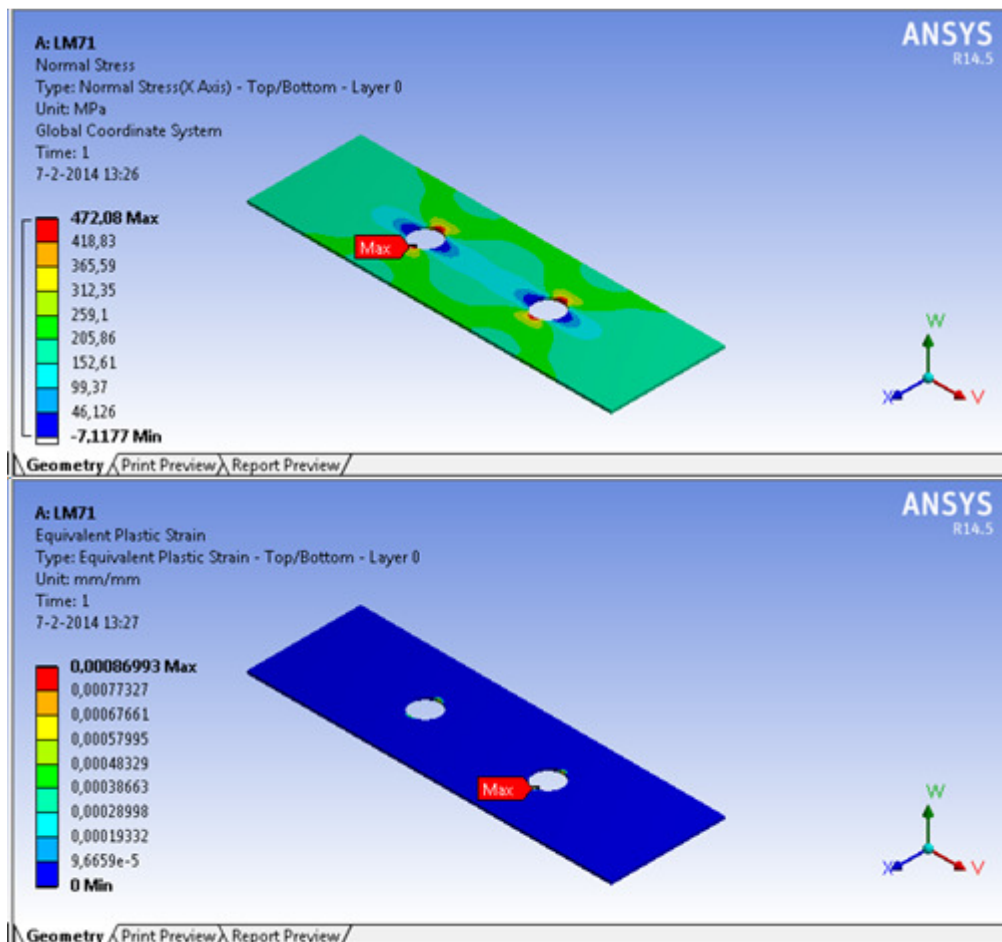


Figure 5.12 – Single plate model, plastic analysis [Iv-Infra]

It can be concluded from the case presented above that such an approach is quite long and time consuming. In the following pages the SM method will be applied to the bridge connection.

## 5.2 Finite Element Modelling

To obtain a better understanding of the stress and stress concentration development inside of the connection a finite element model has been developed. This was done in Ansys Workbench 14. The “DO Hoofddetailering K050” report and bridge drawings (some of which are presented in Figure 5.1 to Figure 5.8) provided by Iv-Infra were used in the build-up of the model. In Appendix B a detailed description of how the finite element input and analysis was carried out is presented. Throughout this process the mm, kg, N metric system is used. In this section only the general layout of the model and the results are illustrated.

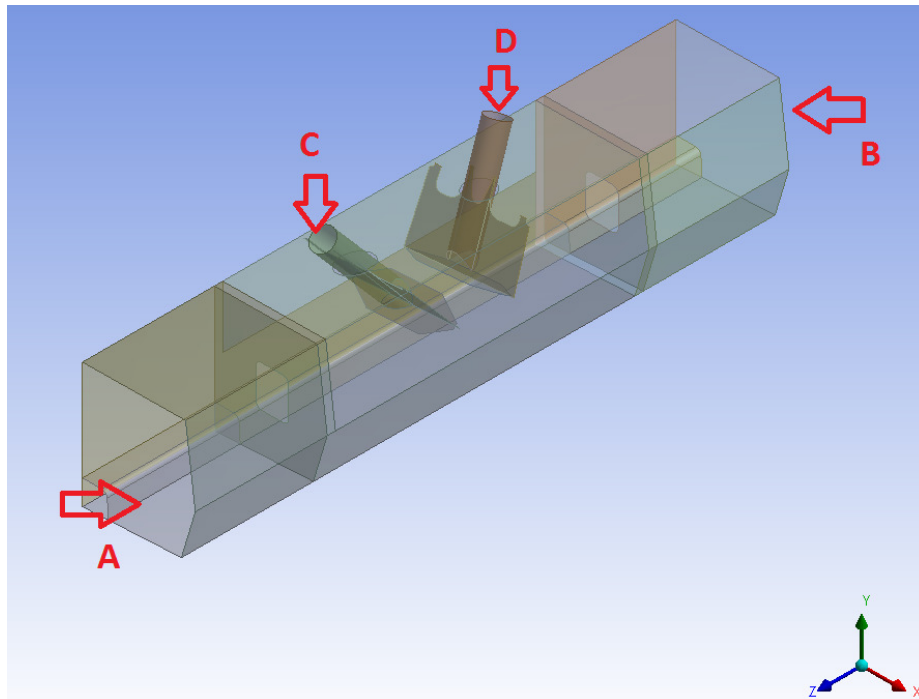


Figure 5.13 – Geometry of the joint with notations

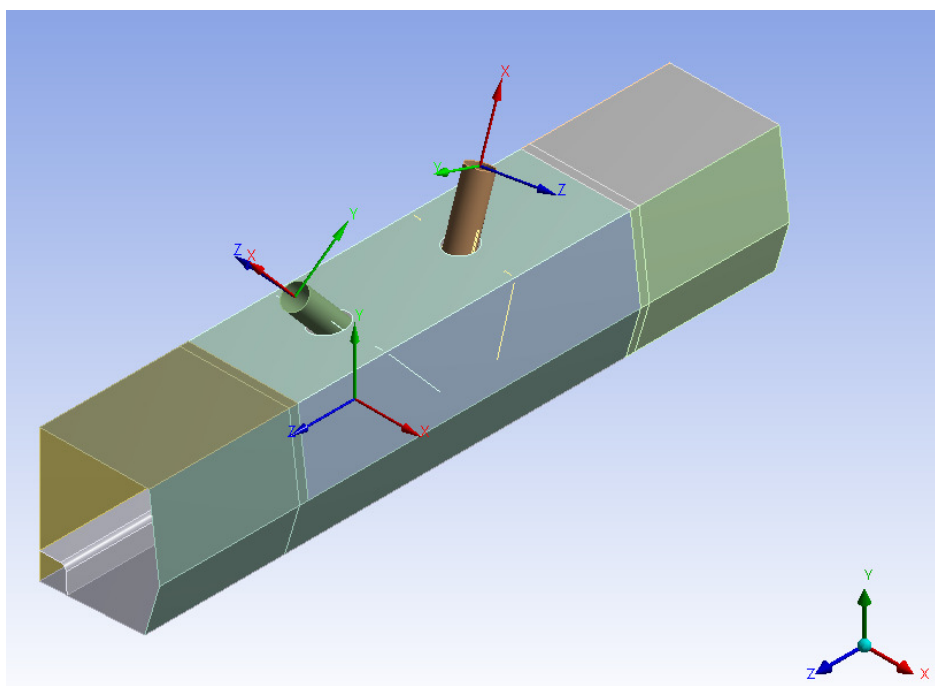


Figure 5.14 – Global and local coordinate axis directions

The model was constructed in S355 in order to match the real project. The steel grade has the properties as presented in section 2.5:  $f_y=355\text{N/mm}^2$ ,  $f_u=470\text{N/mm}^2$ ,  $E=210000\text{MPa}$  and  $\varepsilon_u=15\%$ . In Figure 5.15 and Figure 5.16 the boundary conditions and loads acting on the bridge connection are illustrated.

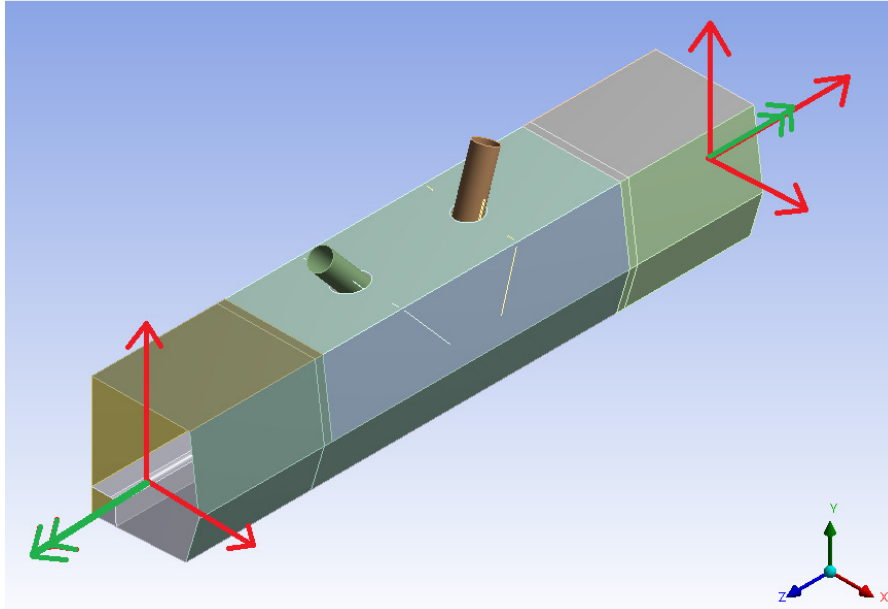


Figure 5.15 – Boundary conditions

Where: the red arrows represent the displacement blocked in the direction of the respective axis and the green arrows the rotation blocked about the respective axis

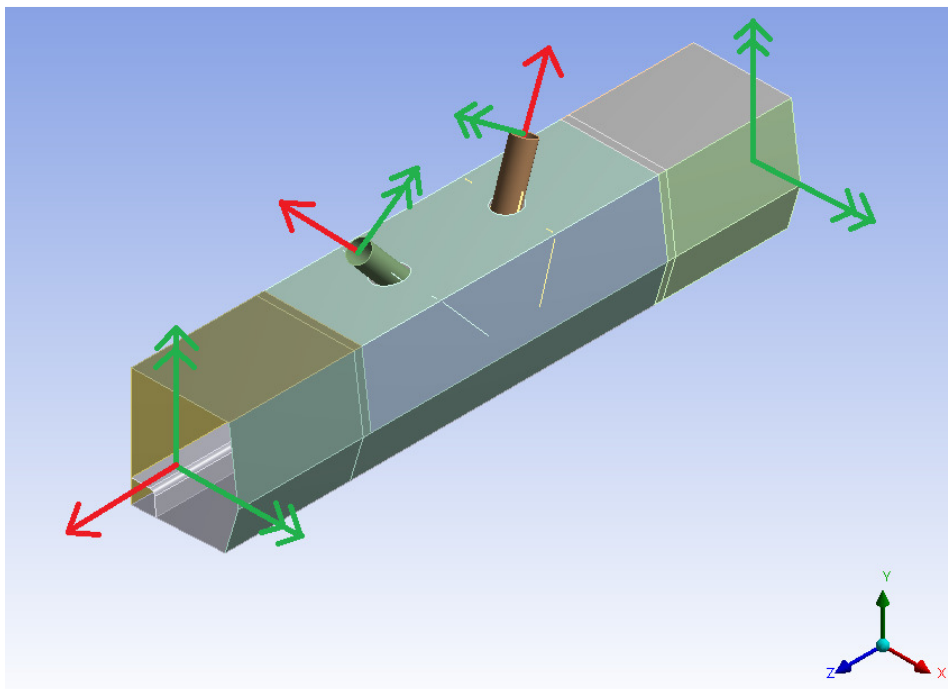


Figure 5.16 – Loads acting on the bridge connection

Where: the red arrows represent the force acting in the direction of the respective axis and the green arrows the bending moment acting about the respective axis

### 5.2.1 Mesh

The mesh must balance two requirements: too many elements and this will result in long solver runs, and too few might lead to inaccurate results.

As the element midsize nodes are kept the surface bodies are meshed using SHELL281 which is a 3D 8-node second-order structural shell. Each node has 3 translational and 3 rotational degrees of freedom. In its natural shape the element is quadrilateral but can also degenerate to a triangle.

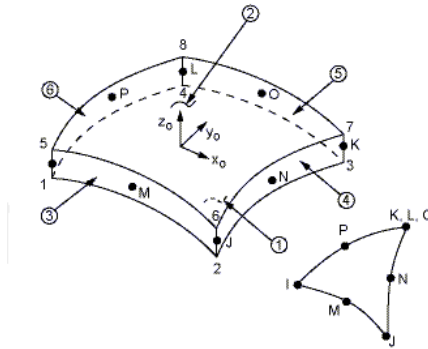


Figure 5.17 – SHELL281 geometry [ANSYS 14.5 Help]

A detailed explanation of the chosen mesh is presented in Appendix B. The final mesh used in the bridge connection model is illustrated in Figure 5.18.

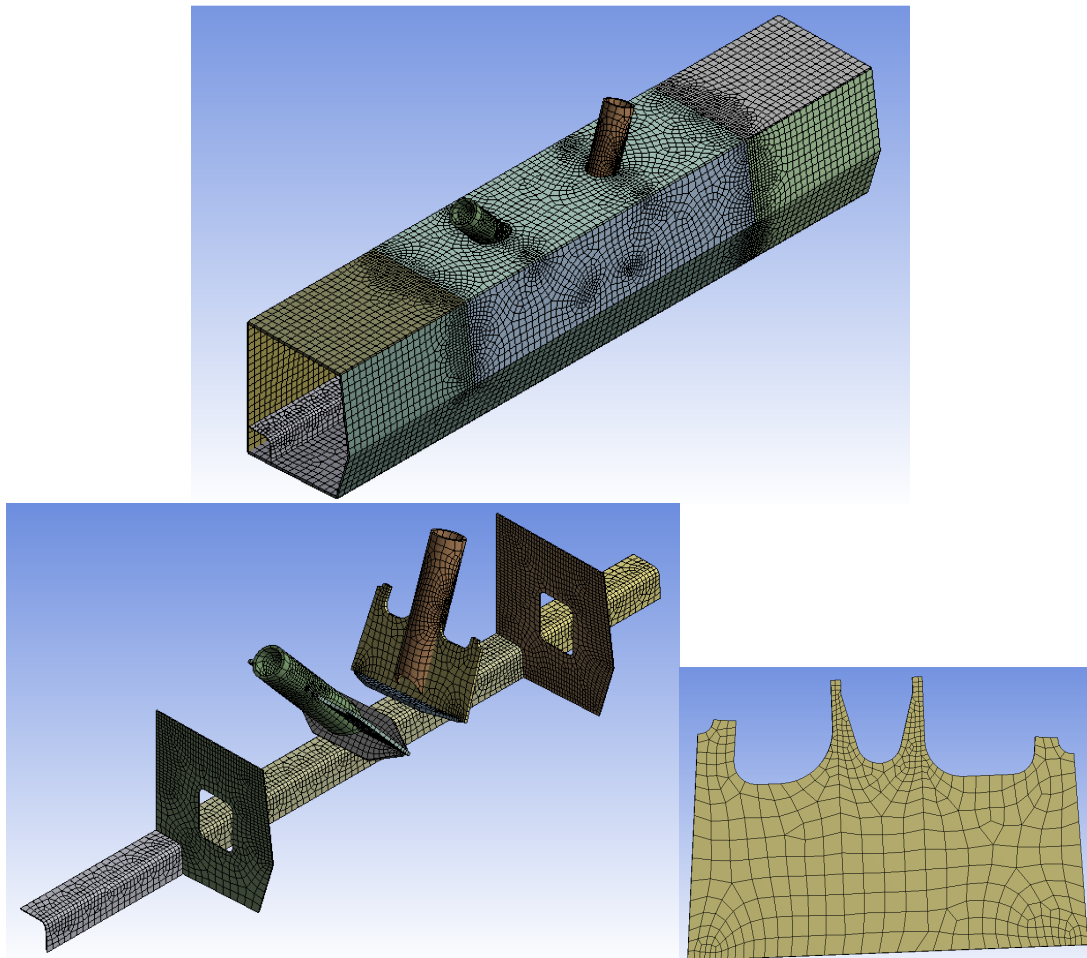
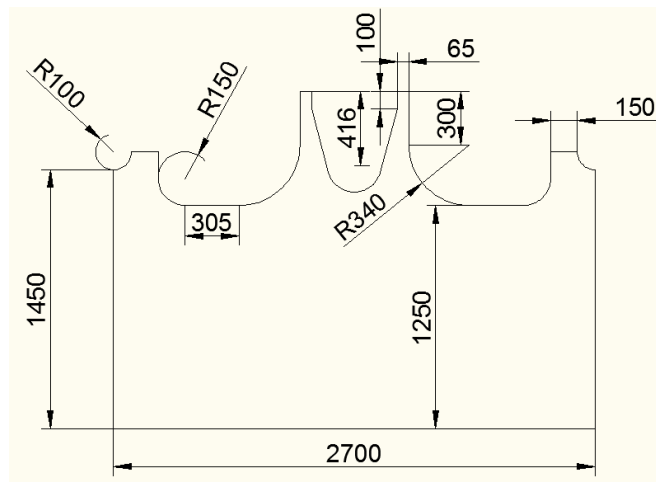


Figure 5.18 – Mesh used in the bridge connection modelling

### 5.3 Application of the SM Correlation Method to the Gusset Plate

The first step in applying the SM method to the bridge connection would be to check the method's applicability on a simplified model of the gusset plate. The gusset plate in the actual bridge connection has a complicated geometry which does not offer clear insight on the stress development. For this purpose the gusset plate from the bridge connection presented in section 5.1 is used together with the diagonal. The geometry is modified in order to have symmetry and simplify the plate as illustrated in the figure below:



The finite element model used for the calculation is illustrated in Figure 5.19

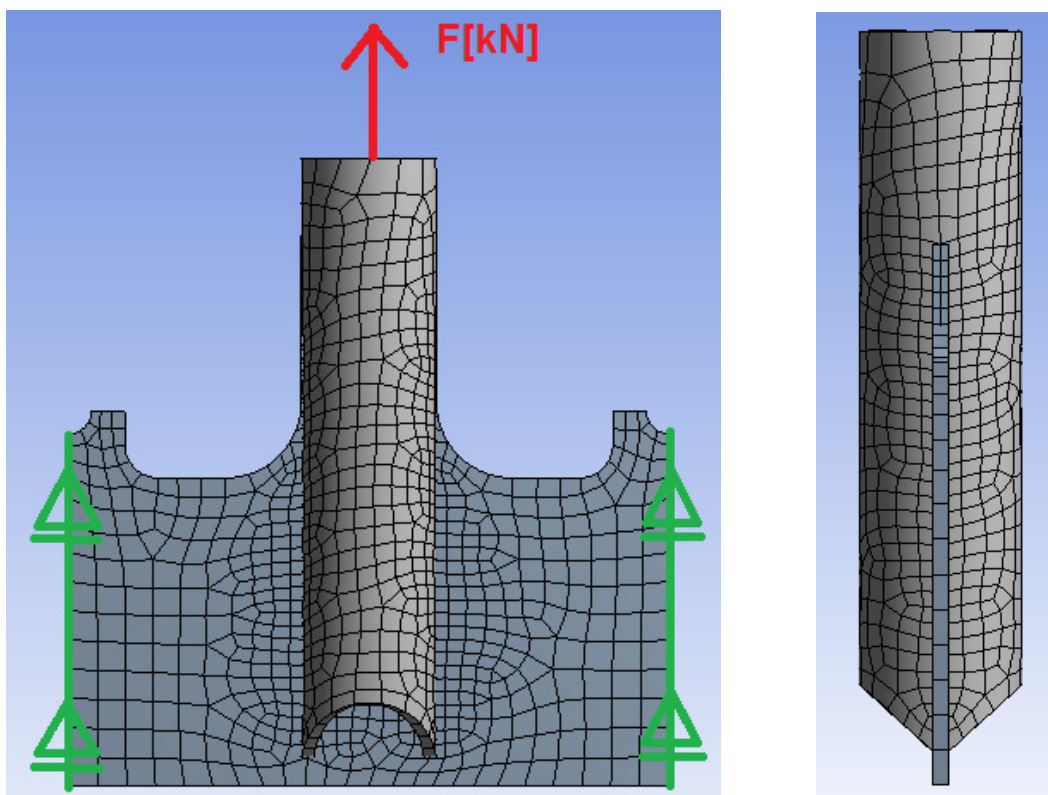


Figure 5.19 – Gusset plate model used in the finite element analysis

The bridge connection presented earlier is modelled in steel grade S690 with three different  $f_u/f_y$  ratios. Based on [50] where the authors investigate the strain hardening properties of HSS, the true stress-strain curves as illustrated in the work will be used. The material properties are listed in Table 39. The  $\epsilon_u=5\%$  and  $f_u/f_y=1.05$  and 1.10 values correspond to the Eurocode requirements presented in section 3.3.1.

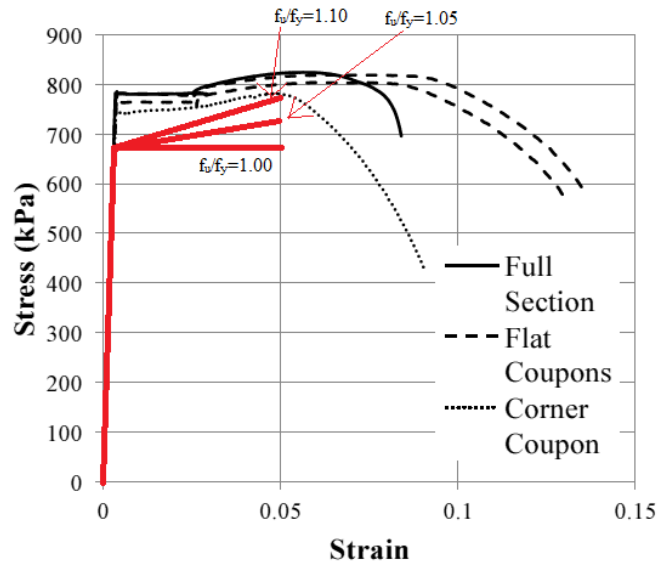


Figure 5.20 – Stress-strain curves used based on test results from [50]

Table 39 – Material properties for different  $f_u/f_y$  ratios

	E [N/mm <sup>2</sup> ]	$f_y$ [N/mm <sup>2</sup> ]	$f_u$ [N/mm <sup>2</sup> ]	$\epsilon_u$ [%]	$E_2$ (strain hardening) [N/mm <sup>2</sup> ]
$f_u/f_y=1.00$	210000	690	690	5	0
$f_u/f_y=1.05$	210000	690	725	5	739
$f_u/f_y=1.10$	210000	690	759	5	1477

In order to understand how the SM can be applied, the equivalent strain and the displacement are measured at locations illustrated in Figure 5.21 and plotted versus the load. The displacement location is chosen as it coincides with the maximum total displacement occurring in the plate, and the strain locations coincides with the location of the highest stress concentrations occurring in the gusset plate.

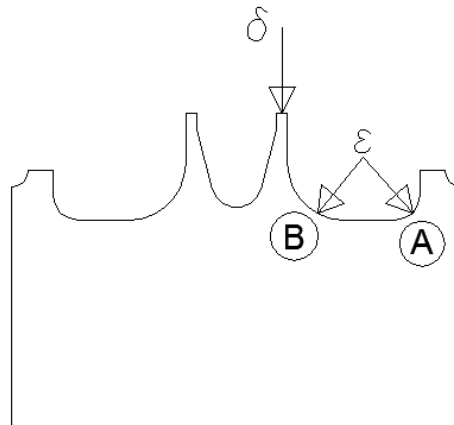
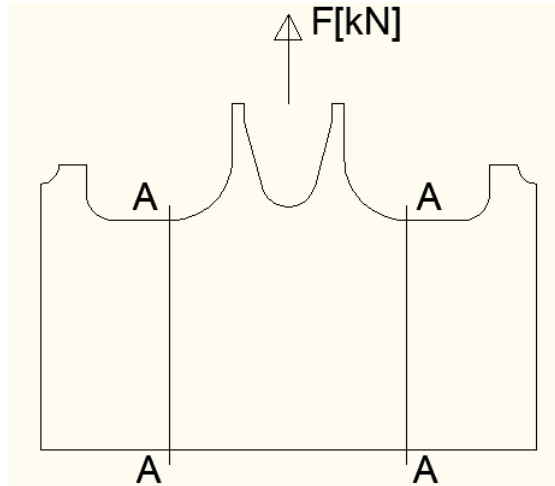


Figure 5.21 – Measured displacement and equivalent strain locations

The load acting on the gusset plate is an axial force through the diagonal. Of interest is how the SM can be used to predict the strains at the notch-tips. As in section 4 it was proven that the method can work only up to 90% of the lowest value of the load that is expected to cause yielding in the net section, in the case of the gusset plate the same limit criteria will be used. This means that the load used in the model is only up to the value for which yielding is expected in the sections A-A.



The value of the axial force for which yielding is expected to occur in the net section of the gusset plate (sections A-A) can easily be calculated as the thickness of the plate is known. There are 2 planes of the gusset plate which are expected to yield at the same time, the lowest load for which yielding is first expected to occur is:

$$\left( \frac{f_y * 1250\text{mm} * 60\text{mm}}{\sqrt{3} * 1000} \right) * 2 = 59750\text{kN}$$

However when applying this load to the case with a  $f_u/f_y$  ratio of 1.00 the finite element analysis does not converge. This can be explained by the fact that the mesh of the model influences the calculation and the plate does not yield due to shear only. The force calculated by hand is based on the assumption that the plate will yield only due to shear force. However the stress development in the plate is more complex and in order to be more accurate the calculation should be based on an equivalent Von-Mises stress and continuum damage mechanics theory developed by Lemaitre. The load that was used in the finite element calculation was equal to 58000kN. For higher values the model would not converge. Also, just as in the cases from section 4.1, the gusset plate yielded for slightly lower values of around 57800kN. These values are quite close to the one calculated by hand. Also the value of the load has influence on determining the load limit for which the SM should be replaced by an inelastic finite element analysis and the behaviour of the gusset plate is quite complex without previous knowledge (i.e. stress concentration factors and nominal stresses) available. For this reason the exact method of calculating the load for which yielding occurs in the net section is not pursued any further.

The displacement and strains measured at the locations specified earlier are plotted with respect to the load and compared for the case of the SM with that of an IFEA. Based on the results the applicability and the load limit up to which the SM can be used are investigated. For more detailed information plots of the displacement and stress contour plots on the three gusset plate examples at different load levels are illustrated in Appendix B.

### 5.3.1 Gusset plate with $f_u/f_y=1.00$

In order to understand the behaviour of the plate under the current load conditions, the first step is to plot the load-displacement diagram based on the inelastic finite element analysis (Figure 5.22).

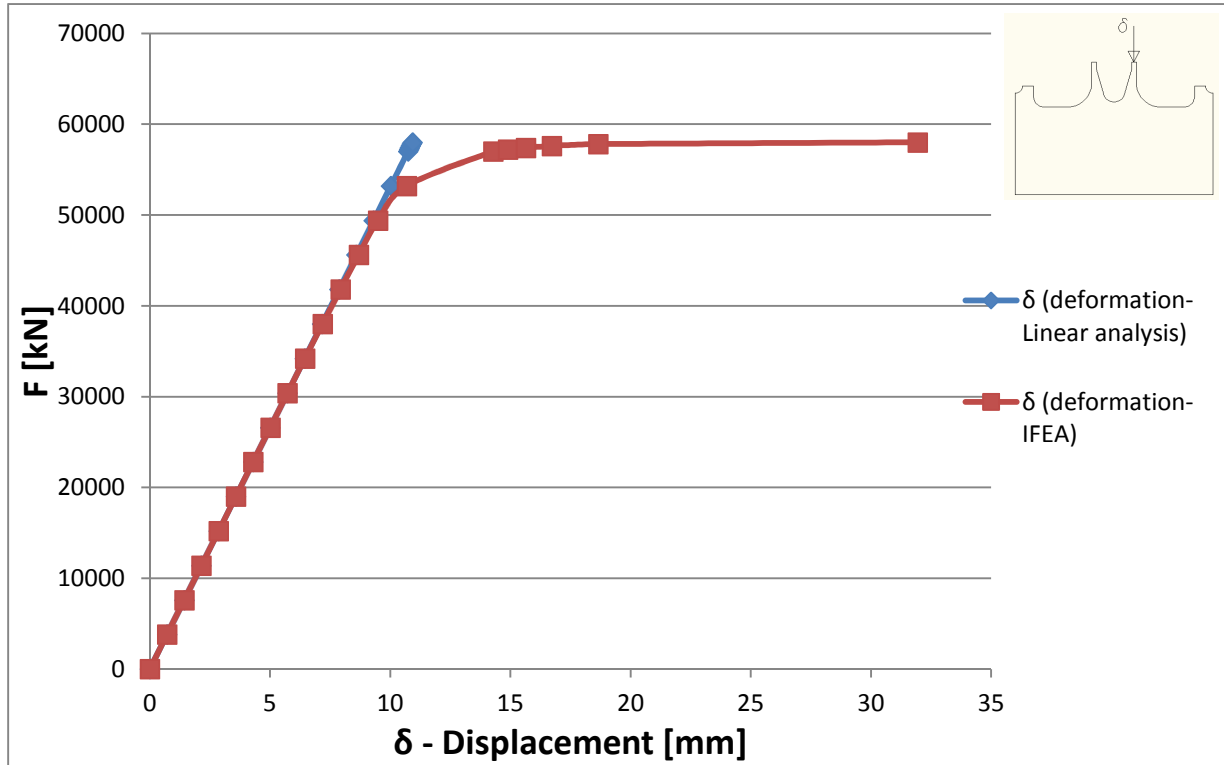


Figure 5.22 – Gusset plate with  $f_u/f_y=1.00$ : Load-displacement diagram

The maximum displacement corresponding to the ultimate load is  $\delta_u = 32\text{mm}$ . From Figure 5.22 it can be noticed that once the load reaches approximately the value of 57600kN, full yielding of the net section occurs and the material deforms linear under the same load. The equivalent strains of the gusset plate at a load level of 57600kN as calculated with the inelastic finite element analysis are illustrated in Figure 5.23.

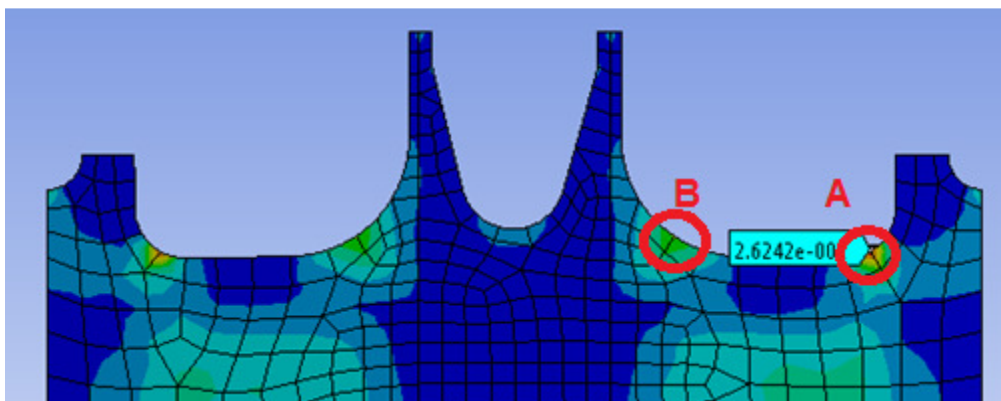


Figure 5.23 - Gusset plate with  $f_u/f_y=1.00$ : location of the stress concentrations

In order to estimate the applicability of the SM method to the gusset plate, the equivalent strain at the curvatures of the gusset plate (where stress concentrations occur, positions A and B) are plotted versus the load. The results of the SM are compared to those

obtained from the inelastic finite element analysis based on the material's nonlinear behaviour.

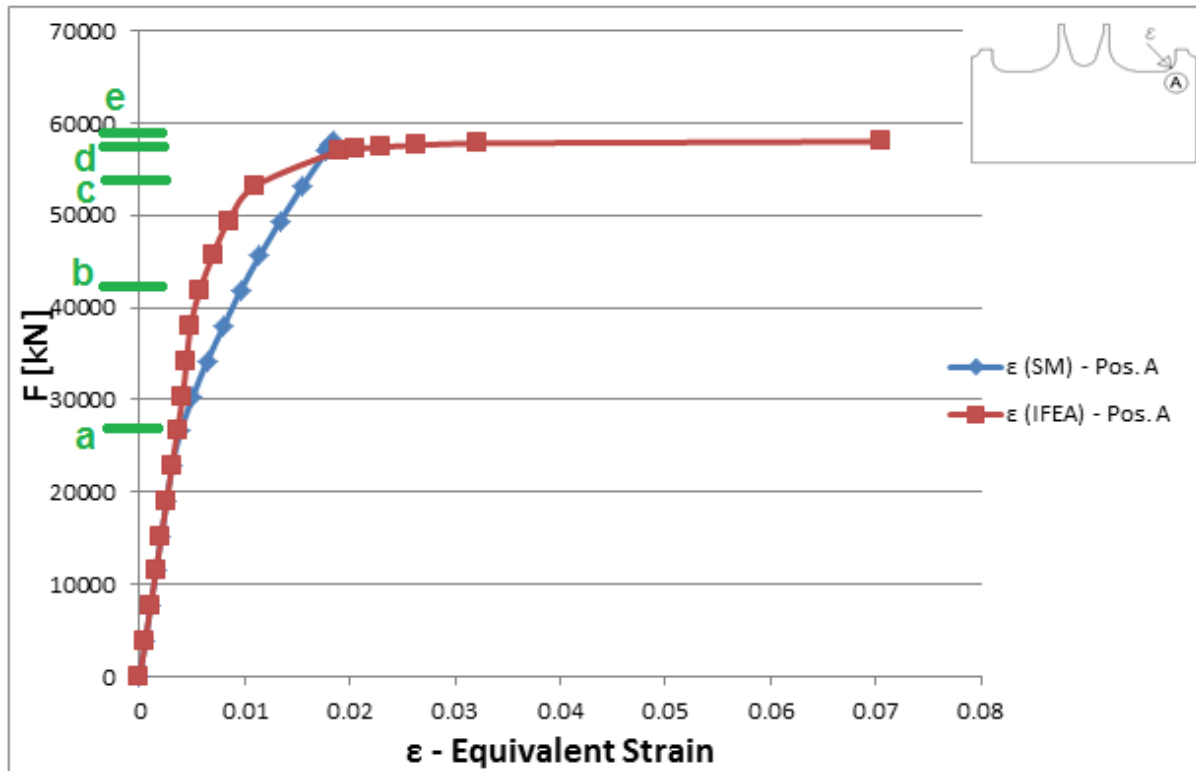
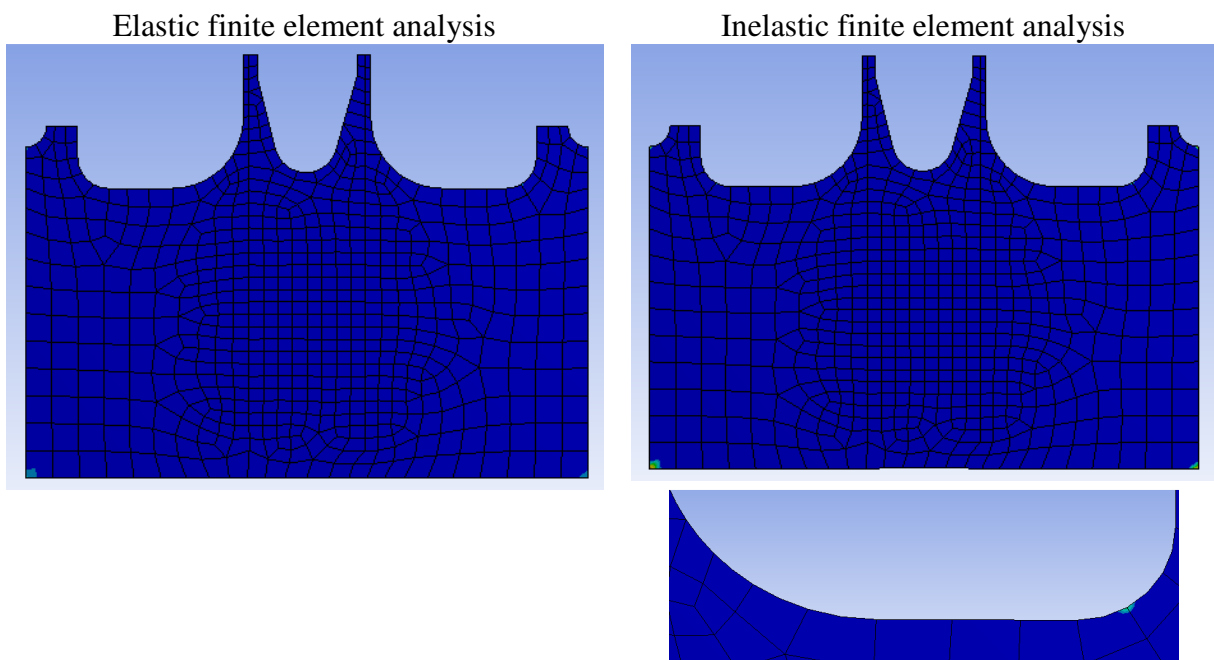


Figure 5.24 - Gusset plate with  $f_u/f_y=1.00$ : Load-Equivalent strain diagram at pos. A

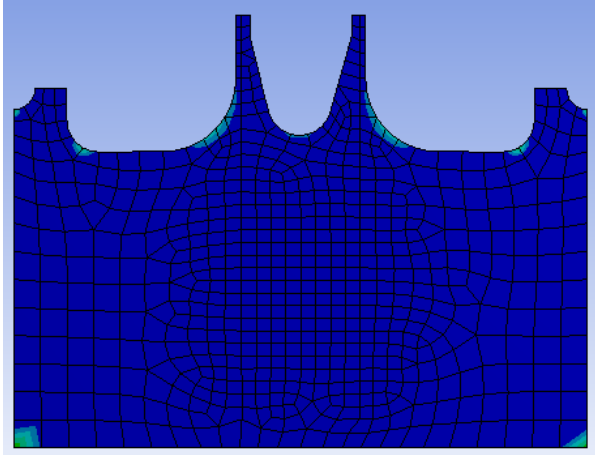
To have a better understanding of how the stresses develop in the gusset plate in the linear and inelastic finite element analysis, the equivalent strain contours are plotted for the two analyses at the 5 load levels illustrated in Figure 5.24. In the following figures the dark-blue contour represents the material that has not reached yielding.

- Equivalent strains at load level a (26600kN):

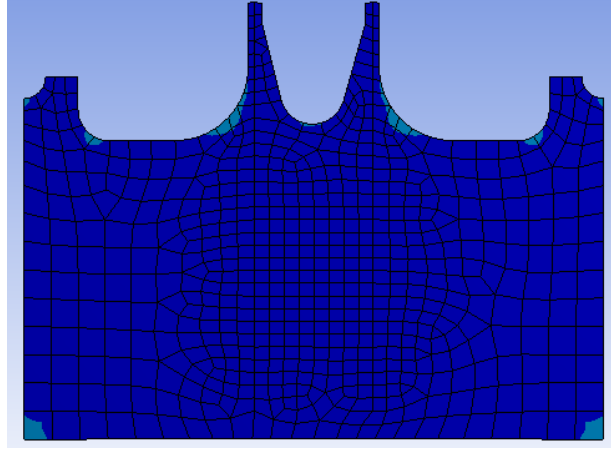


- Equivalent strains at load level b (41800kN):

Elastic finite element analysis

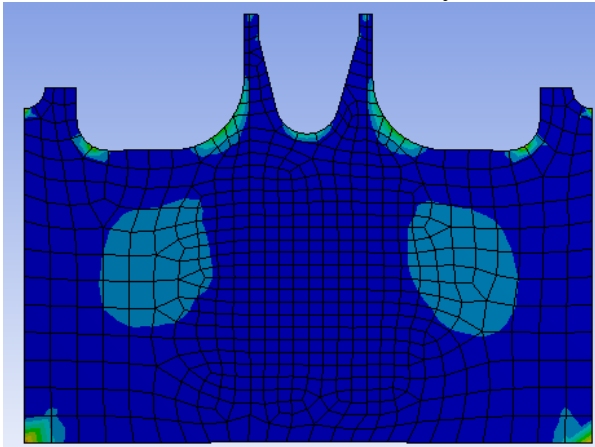


Inelastic finite element analysis

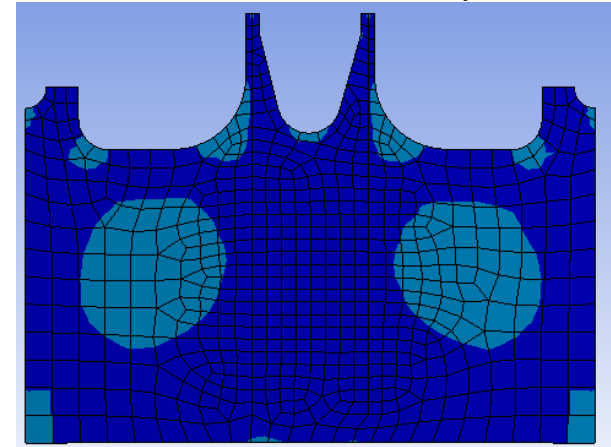


- Equivalent strains at load level c (53200kN):

Elastic finite element analysis

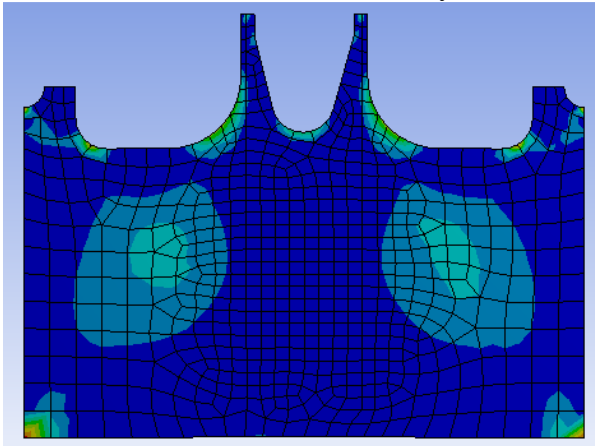


Inelastic finite element analysis

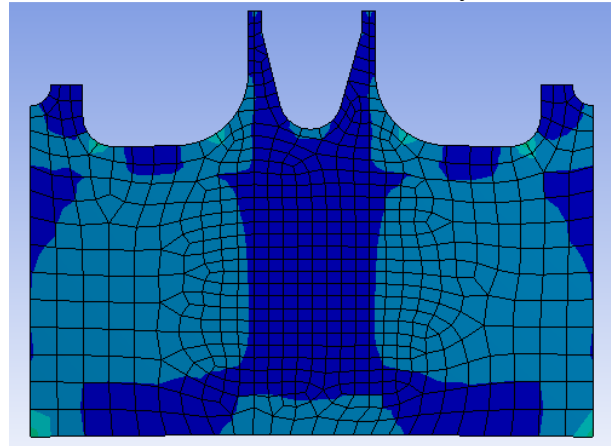


- Equivalent strains at load level d (57600kN):

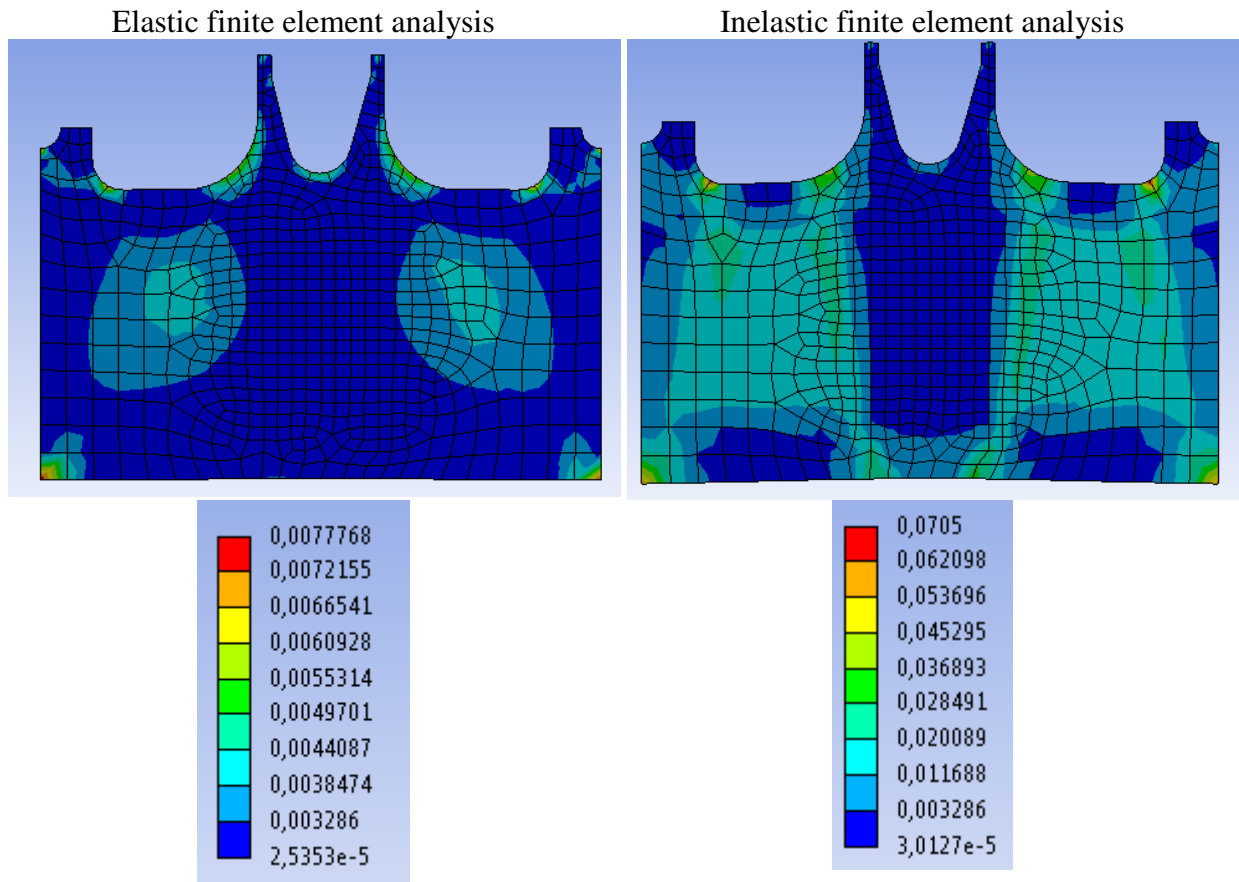
Elastic finite element analysis



Inelastic finite element analysis



- Equivalent strains at load level e (58000kN):



The colours illustrated above represent the values of the equivalent strain plots used in the EFEA and IFEA illustrations.

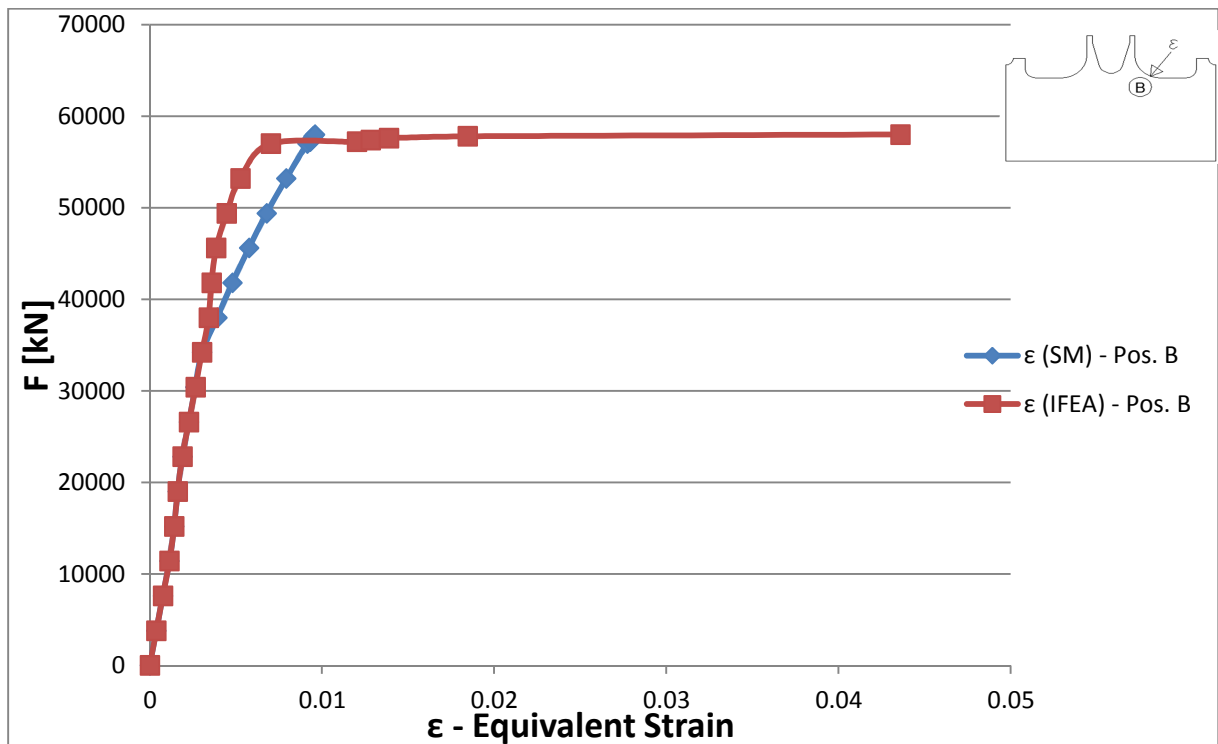


Figure 5.25 - Gusset plate with  $f_u/f_y=1.00$ : Load-Equivalent strain diagram at pos. B

Just as in the case studied in section 4.1, it can be noticed that once the section goes into yielding, the results of the linear analysis can no longer be used in the SM approach to give estimates of the strain. This can be explained by the same logic as in the case of the plate with a hole. However, the difference between the SM and IFEA seems to occur at a lower value of the load. For this purpose the load versus ratio in equivalent strains as calculated with the SM and IFEA are plotted in Figure 5.26.

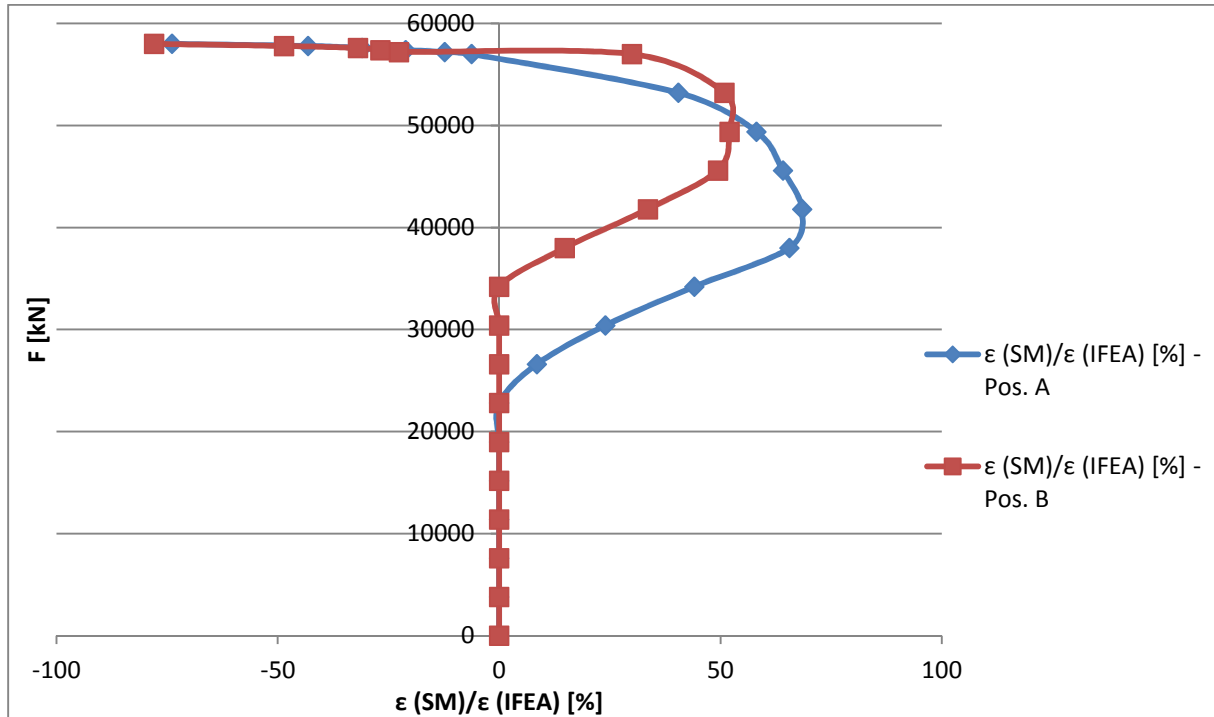


Figure 5.26 - Gusset plate with  $f_u/f_y=1.00$ : Differences in equivalent strains from SM and IFEA versus load

From Figure 5.26 it can be noticed that the SM offers good, quite conservative estimates of the strains at the locations of the stress concentrations. The differences between the strains calculated with the IFEA and the new method can be as high as 68%. This can be explained by the fact that due to the gusset plates more complex geometry, due to localized yielding a higher stress redistribution occurs, leading to lower strain values at the notch-tips compared to the ones estimated based on the linear finite element analysis.

The SM method gives conservative estimates of the strains at the notch-tips up to a load value of about 56000kN. However, in section 4.1, for the case of a plate with a hole, the load up to which the method could be applied was equal to 90% of the lowest value of the load for which yielding is expected to occur in the net section. In order to have consistency in the SM applicability the same criteria will be applied to the gusset plate. This is translated into the fact that for the example illustrated here the SM method should be considered as a valid solution only up to a value of 90% of the calculated load that is expected to cause yielding in the net section (i.e.  $0.9F_y=0.9*59750\text{kN}=53775\text{kN}$ ).

### 5.3.2 Gusset plate with $f_u/f_y=1.05$

Just as for the case with the  $f_u/f_y$  ratio of 1.00, the gusset plate is loaded with an axial force of 58000kN. A higher load is not of interest as the main threshold is the load for which yielding is expected to occur in the net section of the plate. The first step is to plot the load displacement diagram. Illustration of the stress contour plots at different load levels are shown in Appendix B.

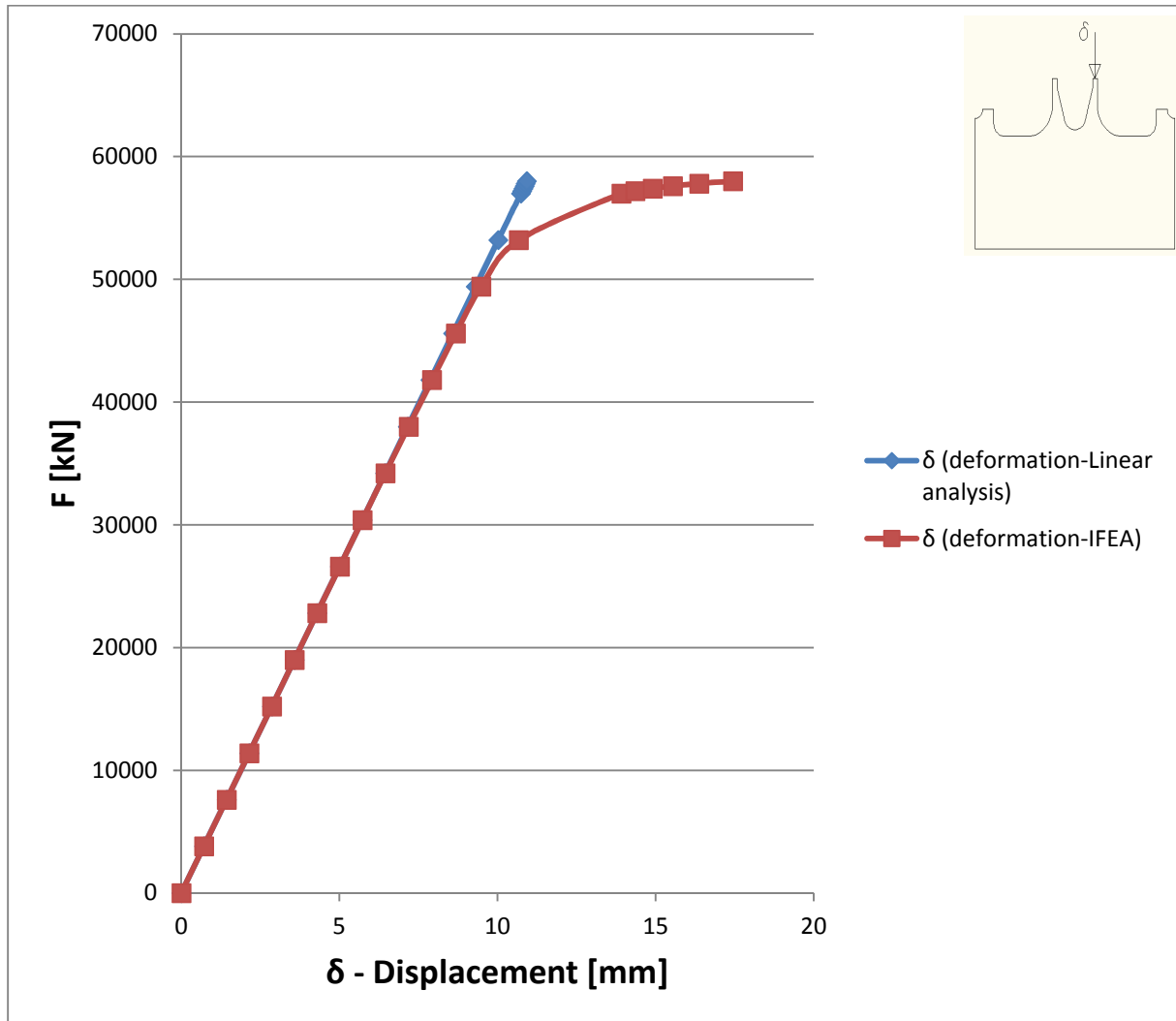


Figure 5.27 – Gusset plate with  $f_u/f_y=1.05$ : Load-displacement diagram

The maximum displacement corresponding to the ultimate load is  $\delta_u = 17.5\text{mm}$ . The value of the displacement is significantly smaller than compared to the case with a  $f_u/f_y$  ratio of 1.00. This seems to indicate the fact that the presence of strain hardening significantly enhances the capacity of the element.

In order to estimate the applicability of the SM method to the gusset plate, the equivalent strain at the curvatures of the gusset plate (where stress concentrations occur, positions A and B) are plotted versus the load. The results of the SM are compared to those obtained from the inelastic finite element analysis based on the material's nonlinear behaviour.

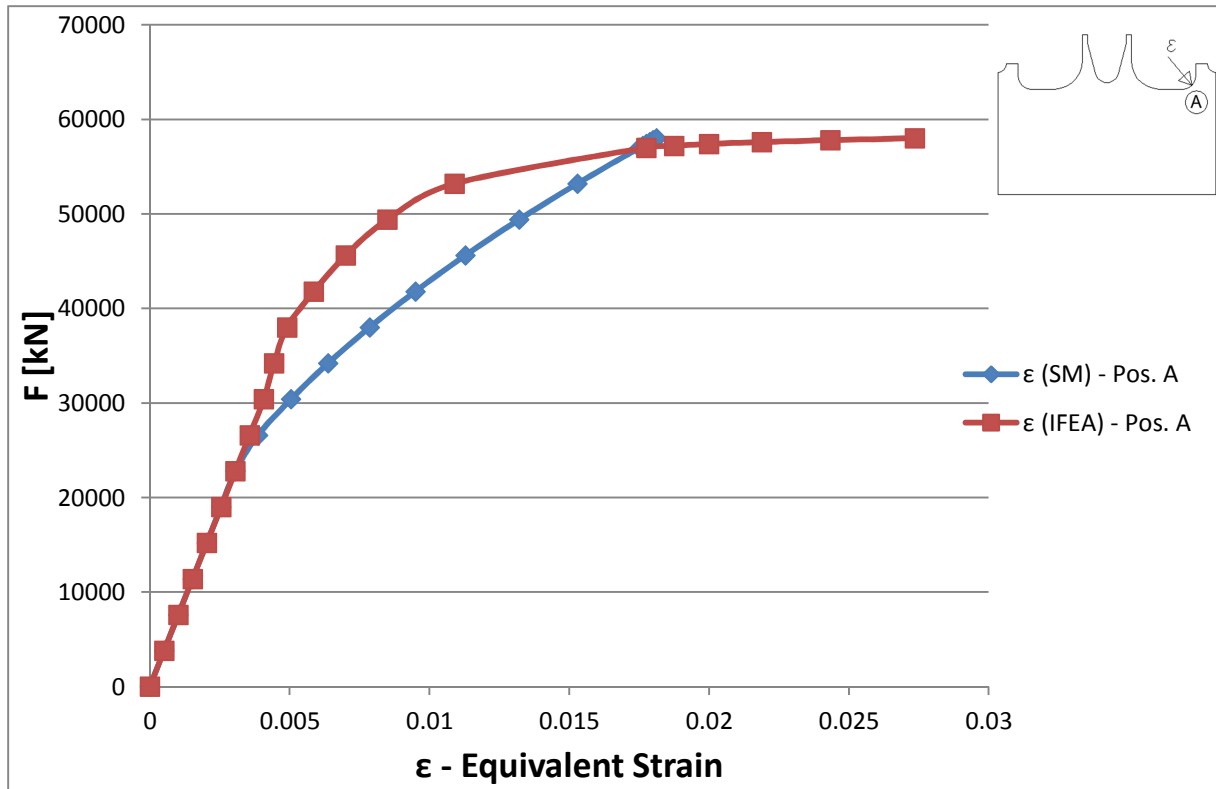


Figure 5.28 - Gusset plate with  $f_u/f_y=1.05$ : Load-Equivalent strain diagram at pos. A

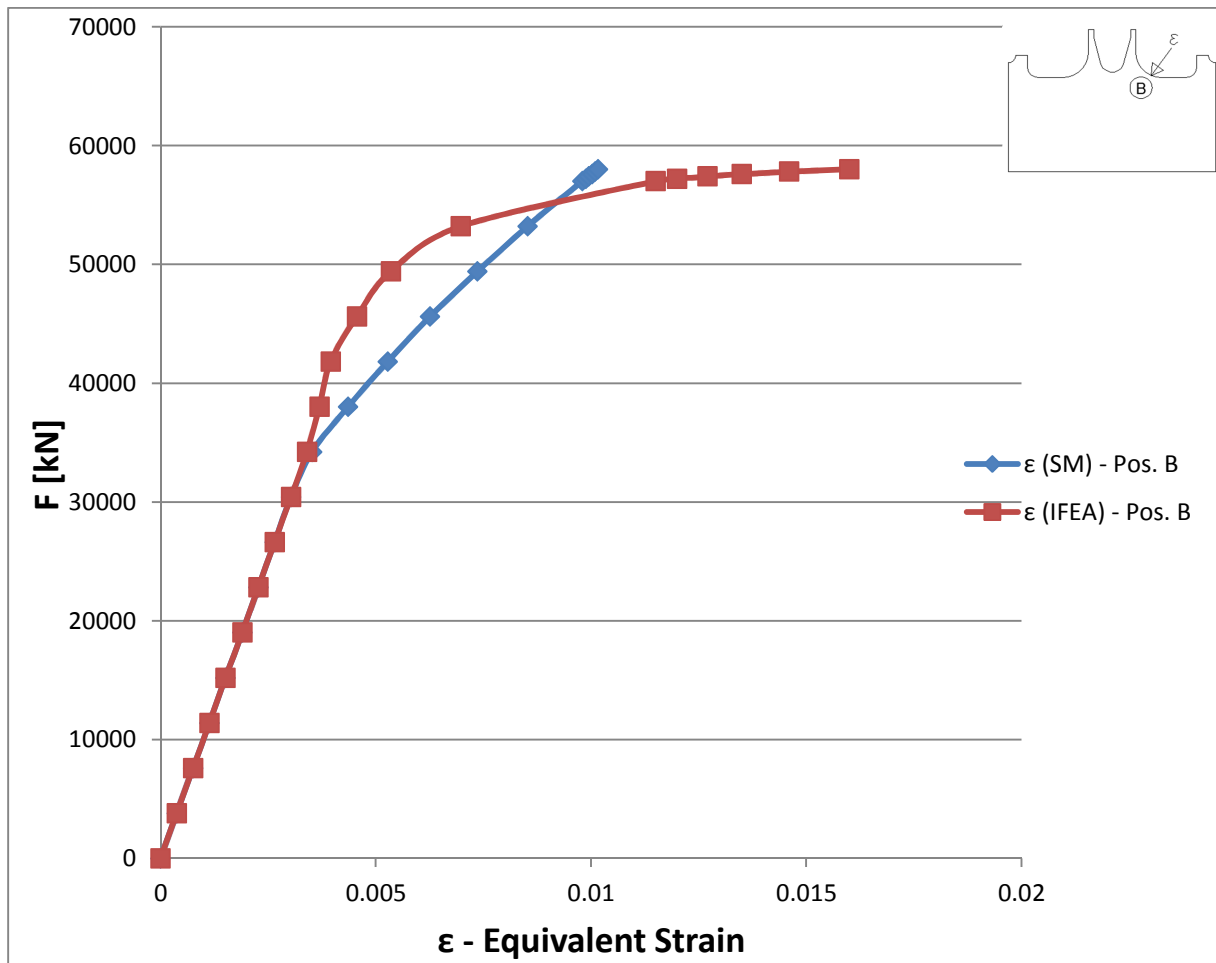


Figure 5.29 - Gusset plate with  $f_u/f_y=1.05$ : Load-Equivalent strain diagram at pos. B

Just as in the previous cases studied, it can be noticed that once the section approaches yielding, the results of the linear analysis can no longer be used in the SM approach to give estimates of the strain. This can be explained by the same logic as before, the fact that the linear finite element analysis does not offer accurate results when the load approaches the yield value. In order to have a better overview of the new method's applicability to this case the load versus ratio in equivalent strains as calculated with the SM and IFEA are plotted in Figure 5.30.

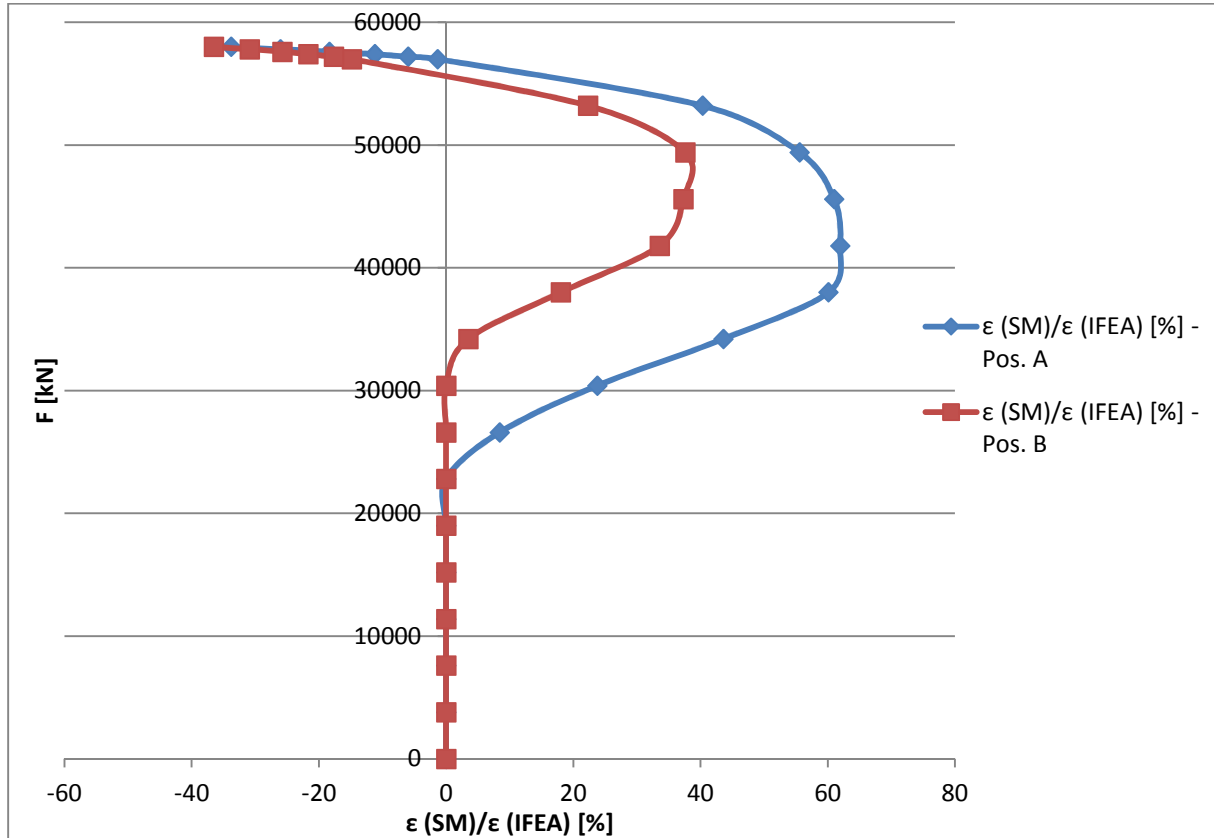


Figure 5.30 - Gusset plate with  $f_u/f_y=1.05$ : Differences in equivalent strains from SM and IFEA versus load

Based on Figure 5.30 it can be stated that for this case the SM offers good, quite conservative estimates of the strains at the locations of the stress concentrations. The differences between the strains calculated with the IFEA and the new method can be as high as 61%. However, it can be noticed that the difference between the strains calculated with the new method and the IFEA have reduced. The presence of strain hardening leads to lower estimates of the strains compared to the case where the  $f_u/f_y$  ratio equalled 1.00. This leads to lower differences between the strains calculated with the SM method and the IFEA. Thus the presence of strain hardening seems to increase the accuracy of the new approach in calculating strains at the notch-tips.

Just as in the case with a  $f_u/f_y$  ratio of 1.00, the method gives conservative estimates of the strains at the notch-tips up to a load value of about 56000kN. This load is higher than the 90% yield load limit. Thus, for the example illustrated here the SM method should be considered as a valid solution only up to a value of 90% of the calculated load that is expected to cause yielding in the net section (i.e.  $0.9F_y=0.9*59750\text{kN}=53775\text{kN}$ ).

### 5.3.3 Gusset plate with $f_u/f_y=1.10$

Just as for the previous two cases, the gusset plate is loaded with an axial force of 58000kN. A higher load is not of interest as the main threshold is the load for which yielding is expected to occur in the net section of the plate. The first step is to plot the load displacement diagram. Illustration of the stress contour plots at different load levels are shown in Appendix B.

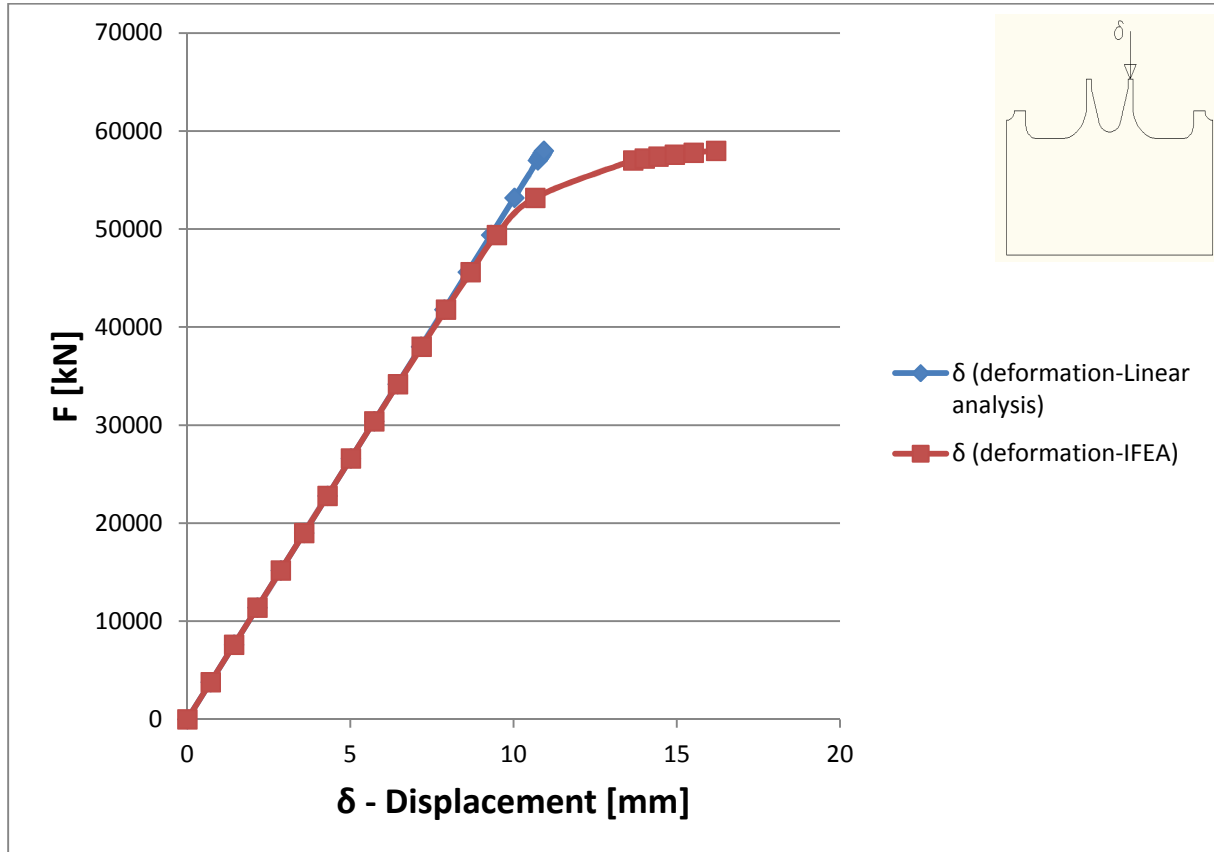


Figure 5.31 – Gusset plate with  $f_u/f_y=1.10$ : Load-displacement diagram

The maximum displacement corresponding to the ultimate load is  $\delta_u = 16.2mm$ . The value of the displacement is significantly smaller than compared to the case with a  $f_u/f_y$  ratio of 1.00. However the difference is not that high when comparing it to the displacement of 17.5mm of the  $f_u/f_y=1.05$ . This seems to indicate the fact that the simple presence of strain hardening significantly enhances the capacity of the element.

In order to estimate the applicability of the SM method to the gusset plate, the equivalent strain at the curvatures of the gusset plate (where stress concentrations occur, positions A and B) are plotted versus the load. The results of the SM are compared to those obtained from the inelastic finite element analysis based on the material's nonlinear behaviour.

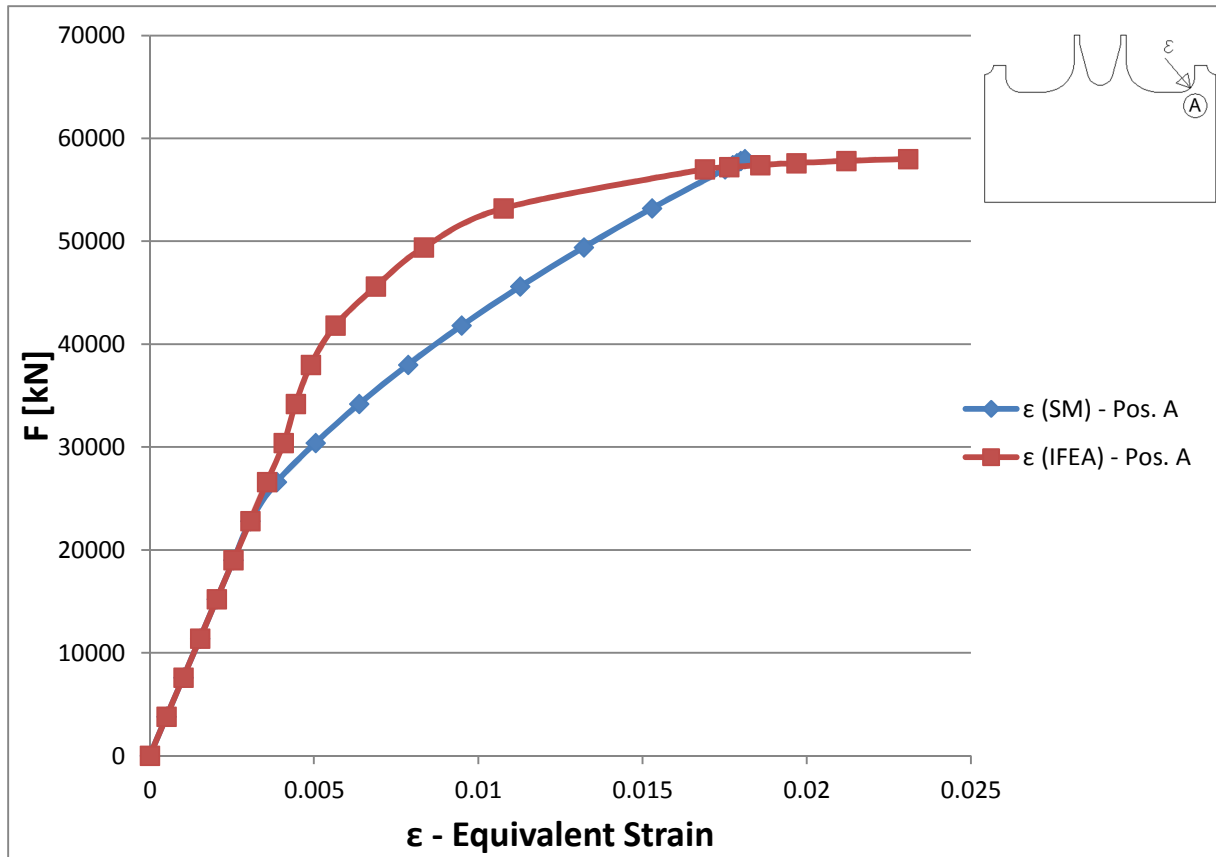


Figure 5.32 - Gusset plate with  $f_u/f_y=1.10$ : Load-Equivalent strain diagram at pos. A

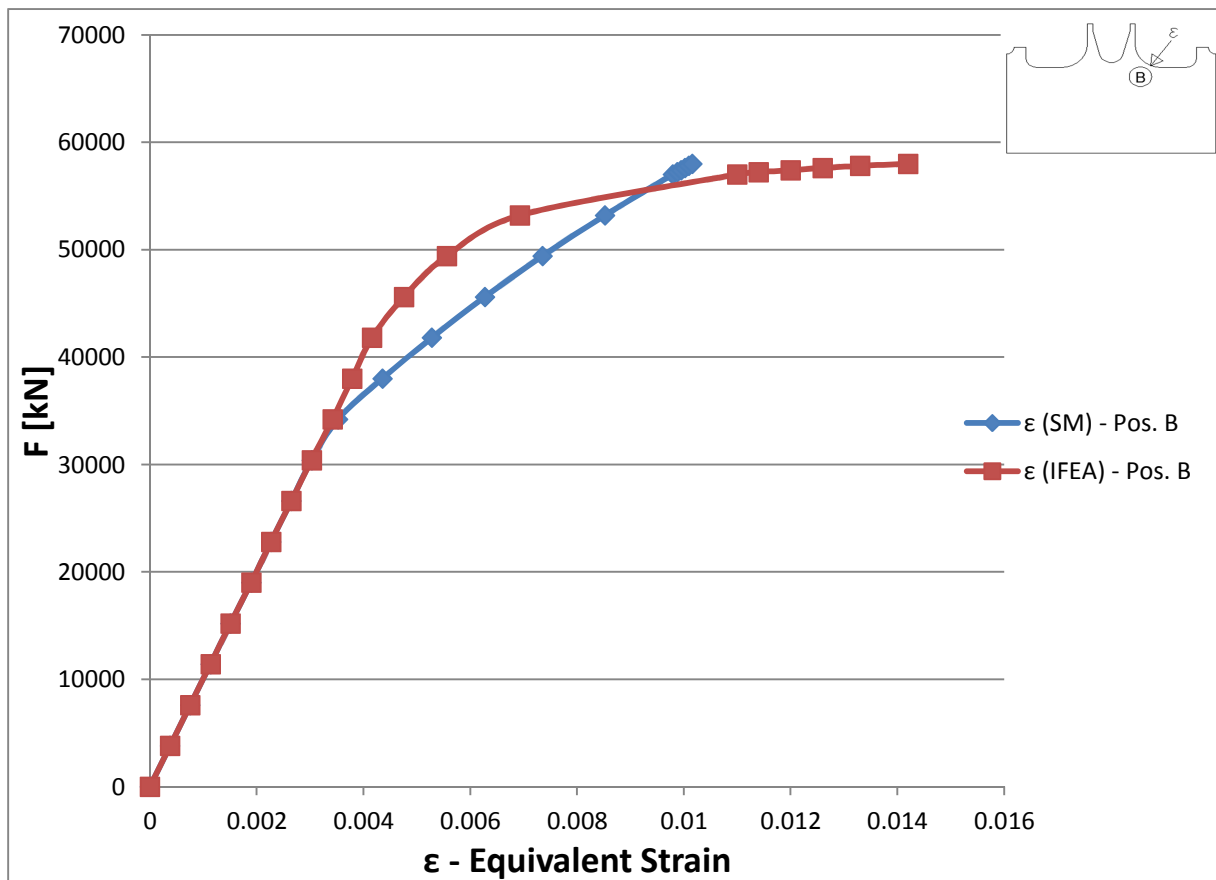


Figure 5.33 - Gusset plate with  $f_u/f_y=1.10$ : Load-Equivalent strain diagram at pos. B

Just as in the previous cases studied, it can be noticed that once the section approaches yielding, the results of the linear analysis can no longer be used in the SM approach to give estimates of the strain. This can be explained by the same logic as before, the fact that the linear finite element analysis does not offer accurate results when the load approaches the yield value. In order to have a better overview of the new method's applicability to this case the load versus ratio in equivalent strains as calculated with the SM and IFEA are plotted in Figure 5.34.

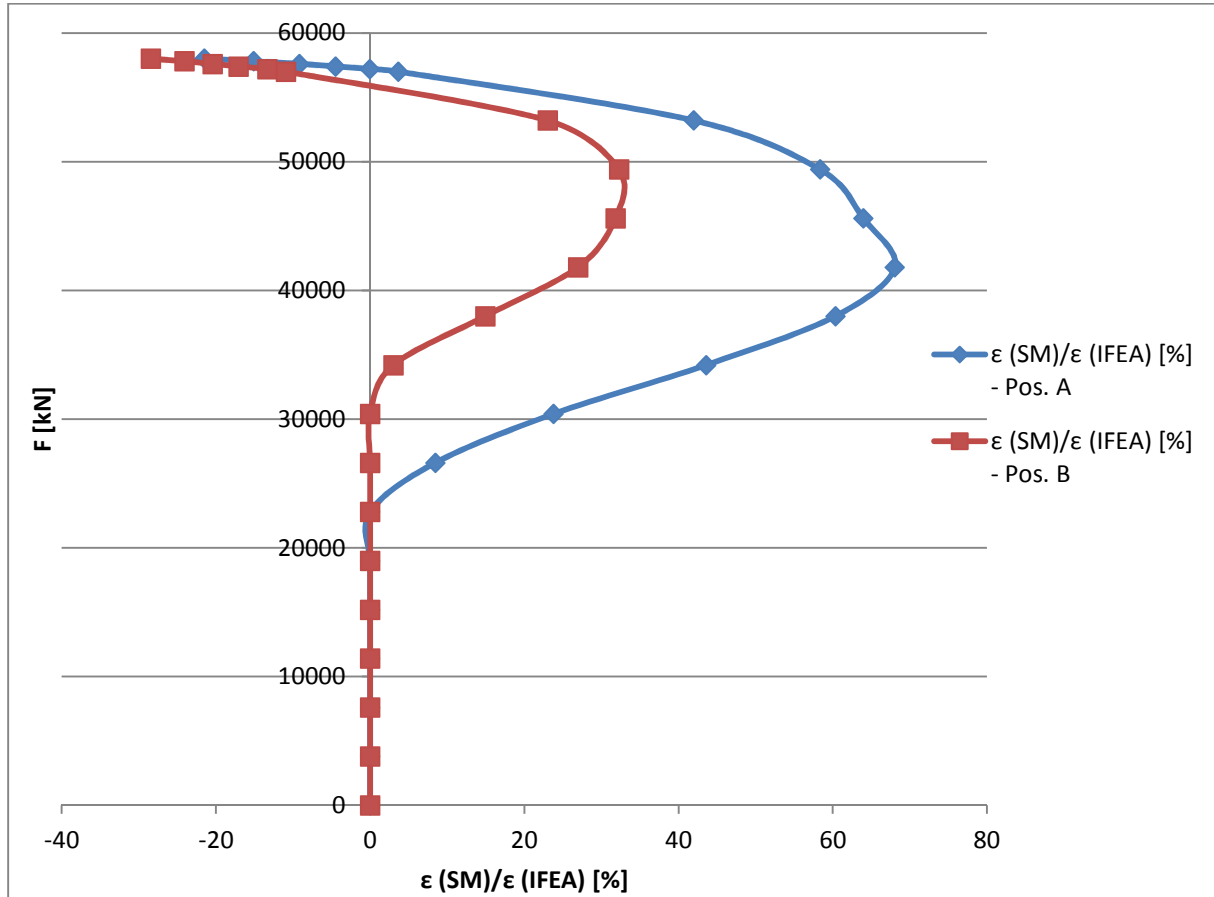


Figure 5.34 - Gusset plate with  $f_u/f_y=1.10$ : Differences in equivalent strains from SM and IFEA versus load

Based on Figure 5.34 it can be stated that for this case the SM offers good, quite conservative estimates of the strains at the locations of the stress concentrations. The differences between the strains calculated with the IFEA and the new method can be as high as 68%. Compared to the previous two cases the differences in the strains calculated with the two methods are quite similar. Thus the presence of strain hardening does not appear to influence the accuracy of the new approach in calculating strains at the notch-tips.

Just as in the previous two cases, the method gives conservative estimates of the strains at the notch-tips up to a load value of about 56000kN. This load is higher than the 90% yield load limit. Thus, for the example illustrated here the SM method should be considered as a valid solution only up to a value of 90% of the calculated load that is expected to cause yielding in the net section (i.e.  $0.9F_y=0.9*59750\text{kN}=53775\text{kN}$ ).

### 5.3.4 Conclusions on the simplified gusset plate

Most modern-day design codes use a  $f_u/f_y$  (or  $f_y/f_u$ ) ratio limitation to ensure the material has sufficient ductility. However, with respect to stress concentrations, it's the materials' ability to yield locally and redistribute stresses that appears to be more significant. In this section the influence of the ultimate to yield tensile strength ratio is investigated up to the lowest load that is expected to cause yielding of a section. The purpose is to gain a better insight of what would be the best parameter ( $f_u/f_y$  or  $\epsilon_u$ ) to define ductility when stress concentrations are an issue. In order to understand how the  $f_u/f_y$  ratio influences ductility, the equivalent strain at location A and the displacement are measured. The displacement location is chosen as it coincides with the maximum total displacement occurring in the plate, and the strain location coincides with the location of the highest stress concentration occurring in the gusset plate. The displacement and strains measured at the locations specified earlier are plotted with respect to the load in Figure 5.35 and Figure 5.36.

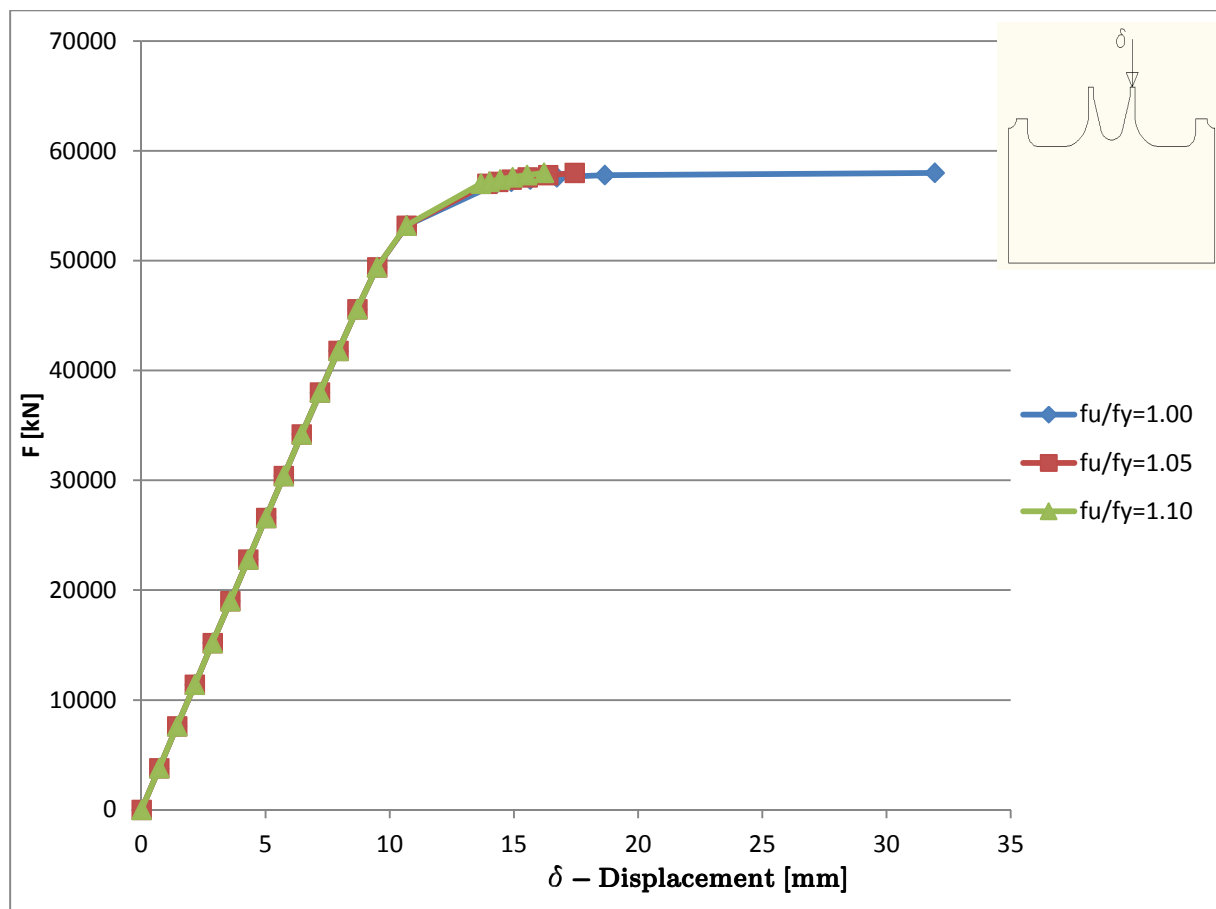


Figure 5.35 – Load-Displacement diagram for the three ultimate-yield ratios

From Figure 5.35 it is easy to notice that the ultimate to yield strength ratio has influence on the displacement of the gusset plate. The values of the displacement measured on the gusset plate at a load level of 58000kN are listed in Table 40.

Table 40 – Displacement values at a load of 58000kN for the three  $f_u/f_y$  ratios

$f_u/f_y=1.00$	$f_u/f_y=1.05$	Displacement difference [%]	$f_u/f_y=1.05$	$f_u/f_y=1.10$	Displacement difference [%]	$f_u/f_y=1.00$	$f_u/f_y=1.10$	Displacement difference [%]
$\delta$ [mm]	$\delta$ [mm]		$\delta$ [mm]	$\delta$ [mm]		$\delta$ [mm]	$\delta$ [mm]	
31.94	17.446	-45.38	17.446	16.208	-7.10	31.94	16.208	-49.25

In the case of  $f_u/f_y=1.00$ , at a load level of 58000kN, yielding of the net sections of the gusset plate has occurred while in the other two cases where strain hardening was used, yielding did not occur at the same load level. This means that the  $f_u/f_y$  ratio appears to be a good parameter in increasing the capacity of the plate for which yielding occurs in the net section. However at values of the load below those that would cause yielding, the ratio does not have any influence in the displacement of the gusset plate. The equivalent strain at the notch-tip is also plotted with respect to the axial force in Figure 5.36

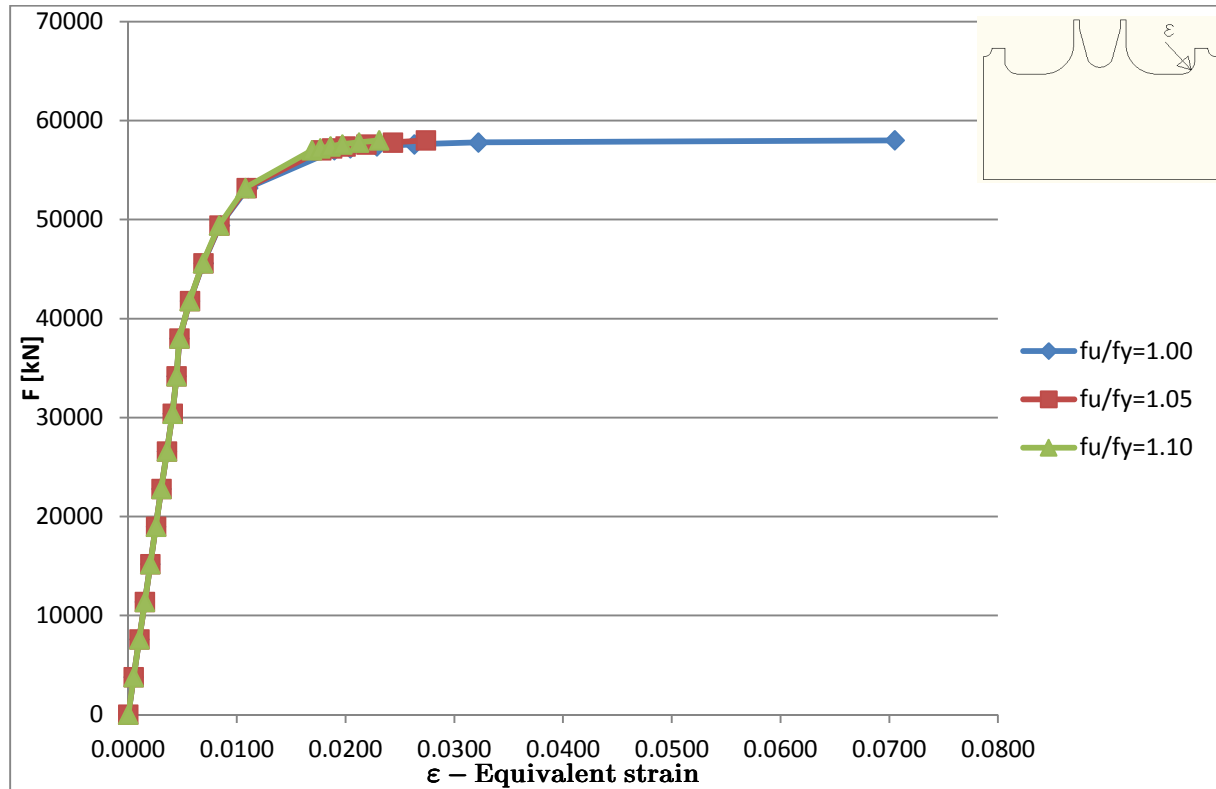


Figure 5.36 – Load-Equivalent strain diagram for the three ultimate-yield ratios

From Figure 5.36 it can be noticed that the different  $f_u/f_y$  ratios affect the values of the equivalent strains at the location of the highest stress concentration. In order to have a better understanding of the difference the value of the strains at the load of 58000kN are compared in Table 41.

Table 41 – Equivalent strains at the notch-tip at 58000kN axial force in the diagonal

$f_u/f_y=1.00$	$f_u/f_y=1.05$	Strain difference [%]	$f_u/f_y=1.05$	$f_u/f_y=1.10$	Strain difference [%]	$f_u/f_y=1.00$	$f_u/f_y=1.10$	Strain difference [%]
$\epsilon_{NL}$	$\epsilon_{NL}$		$\epsilon_{NL}$	$\epsilon_{NL}$		$\epsilon_{NL}$	$\epsilon_{NL}$	
0.0705	0.0274	-61.19	0.0274	0.0231	-15.62	0.0705	0.0231	-67.26

The presence of strain hardening significantly reduces the value of the strain at the notch-tip and also that of the displacement at a load level close to the yield capacity of the plate. This is due to the fact that while in the case of the  $f_u/f_y=1.00$  yielding of the net section occurs at a load level of 57800kN, the same does not happen in the other two examples. However in the case when the force is below that which would cause yielding of the net section, the  $f_u/f_y$  ratio does not have any influence on the development of strains or displacements. Thus, in the case of structures that are designed in the elastic range and the only stresses exceeding that of the yield strength are those at notch-tips, it would be advisable

to focus on ensuring a minimum elongation at fracture  $\varepsilon_u$  first, rather than a minimum  $f_u/f_y$  ratio, in order to ensure the local redistribution of stresses. The later should be of more importance in the cases when the load is expected to exceed the yield capacity of an elements section, as there very high ductility requirements are needed in order to ensure the redistribution of stresses in the structure. However a minimum  $f_u/f_y$  ratio should be ensured as this parameter significantly enhances the ductility capacity of the elements. Based on the results of the gusset plate, it can be stated that a minimum ratio of 1.05 for the  $f_u/f_y$  parameter can be used in design as long as calculations are carried out to prove that this satisfies the ductility requirements with respect to the respective structure.

With respect to the SM approach, the method gives promising results. Compared to the IFEA, the strains estimated with the SM are quite conservative. Unlike the case of the plate with a hole, the applicability of the new method seems to go up to around 95% of the lowest value that is expected to cause yielding in the net section of the plate. However, as the stress development is more complex and the load that causes yielding is lower than the theoretical calculated one, the 90% limit for the load should still be used. This also ensures a certain consistency in the applicability of the SM. The method gives quite conservative results along the load path of the gusset plate. If the SM is used to estimate strains, these values can easily be calculated and compared to design code requirements in order to state whether the material has sufficient ductility or will fracture. However, as the method can give quite high over predictions of the strains, in the cases when these exceed the design code requirements, an IFEA should still be carried out.

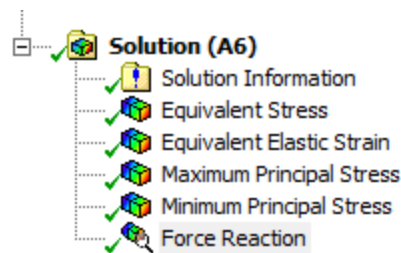
## 5.4 Application of the SM Correlation Method to the Bridge Joint

In this section the applicability of the SM method in estimating strains to more complex examples is verified. The bridge connection model is used for this purpose. A linear analysis is run on the model and the output is used to pin-point the locations of the stress concentrations and their respective stresses. With the results from this analysis, the SM method is applied in order to estimate the real non-linear strains at those locations. Afterwards the results calculated are checked using a non-linear finite element calculation on the bridge connection model using the non-linear material behaviour. Just as in the case of a plate with a hole, the equivalent Von-Mises strains and stresses are used.

### 5.4.1 Linear static structural analysis

Linear static structural analysis is carried out. The output of interest is the equivalent stress and strain.

The solutions of interest comprise: Equivalent (von-Mises) Stress, Equivalent Elastic Strain, Maximum Principal Stress, Minimum Principal Stress and the Force Reaction at B location. All these solutions are taken as output in order to have a better insight on the behaviour of the joint under the acting load conditions



The maximum and minimum principal stresses are usually positive and negative values corresponding to tension and compression respectively. In the resulting output from the analysis on the joint model, the highest maximum principal stress occurs in the girder, more specifically in the top flange. This is due to the high tension forces acting on the upper part of the girder. The geometric irregularity introduced by the hole results in high tension stress peaks adjacent to the openings.

The highest minimum principal stress (representing compression) is located in the gusset plate. This is a result of the geometry and the high axial force acting on the diagonal and pulling on the gusset plate upward.

Due to the big difference between the maximum and minimum principal stresses the highest Von-Mises stress location coincides with that of the minimum principal stress. The results of the analysis on the bridge connection are presented in Figure 5.37.

The reaction force at location B has a magnitude of 103230kN which is almost the same as the expect value of 104650kN (value taken from the K050-DO-B-005 report of the A1/A6 Diemene-Almere Havendreef project) which gives a confirmation of the accuracy of the built model.

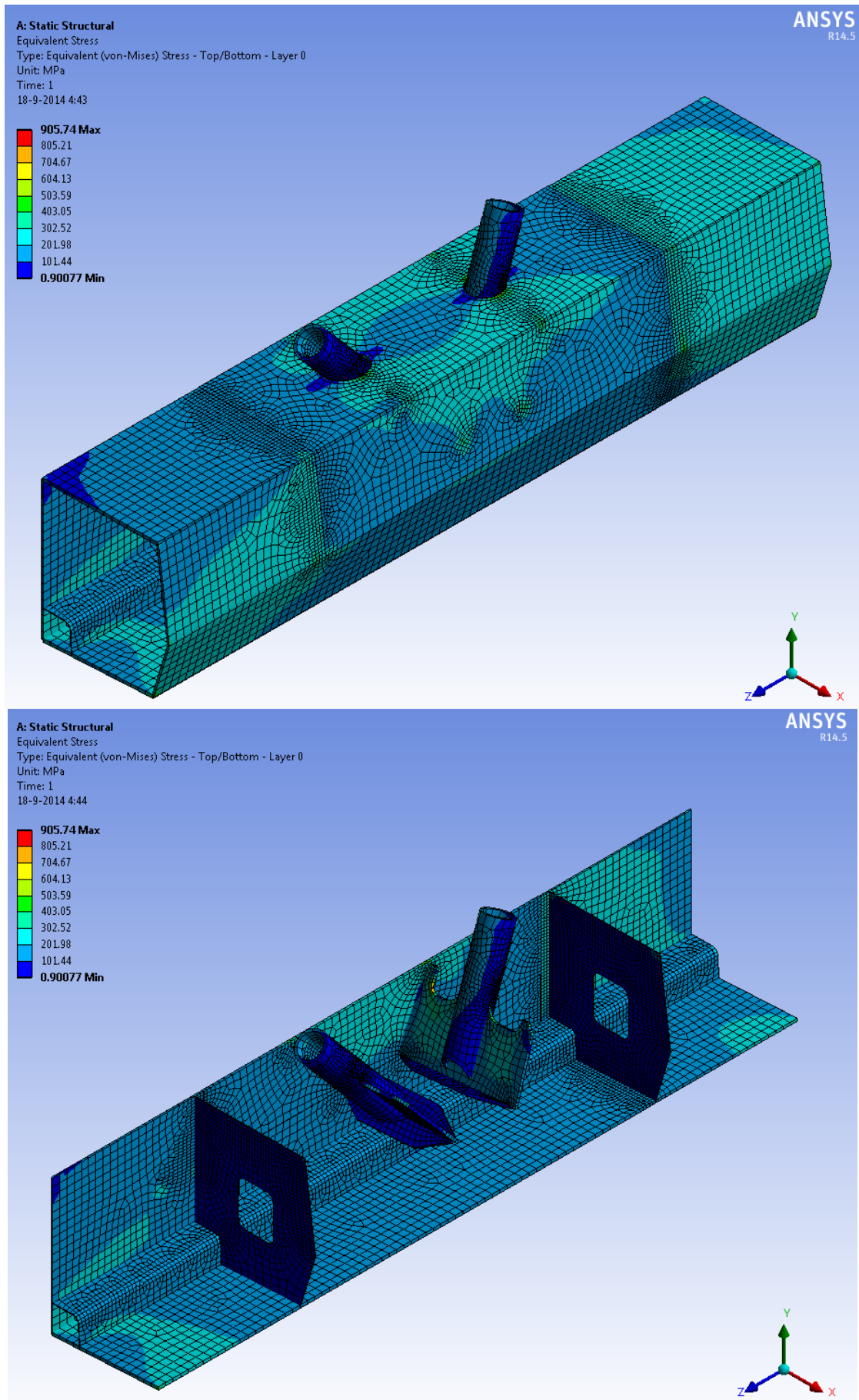


Figure 5.37 – The equivalent (Von-Mises) stress in the joint

From Figure 5.37 the location of the stress concentrations can be pinpointed in the bridge connection. It is easy to notice that the peak stresses occur in the top flange of the box beam and in the gusset plates connecting the diagonals to the girder. In the following figures the dark-blue contour or the bright-red contour (in the case of minimum principal stresses) represents the area that has not reached the yield stress.

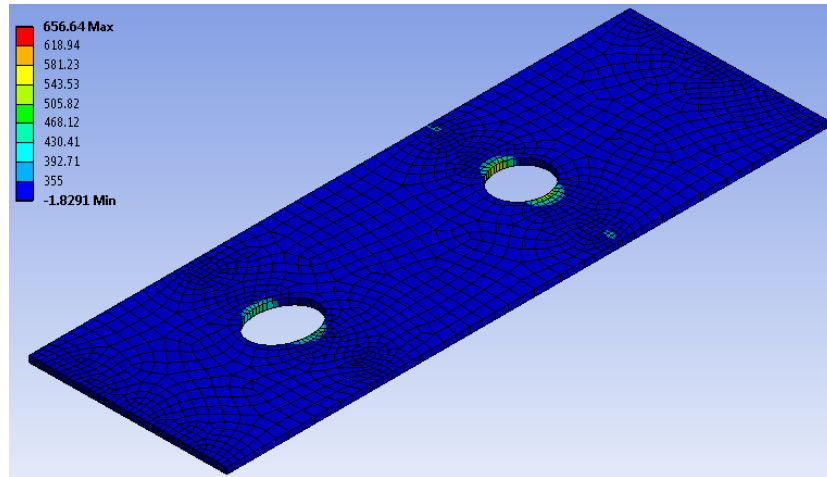


Figure 5.38 – Maximum principal stress in the top flange

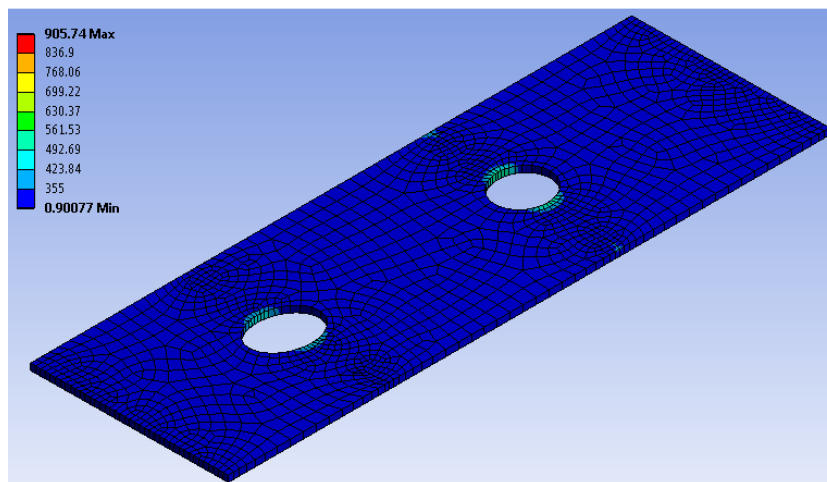


Figure 5.39 – Equivalent stress in the top flange

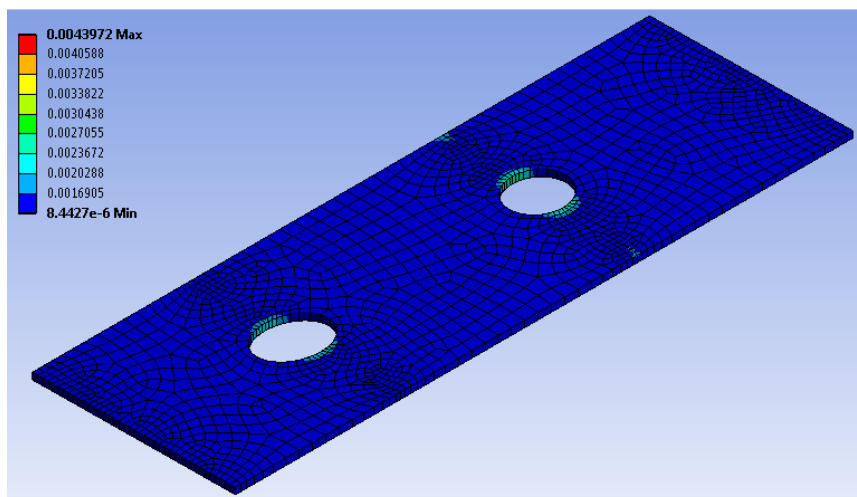


Figure 5.40 – Equivalent strain in the top flange

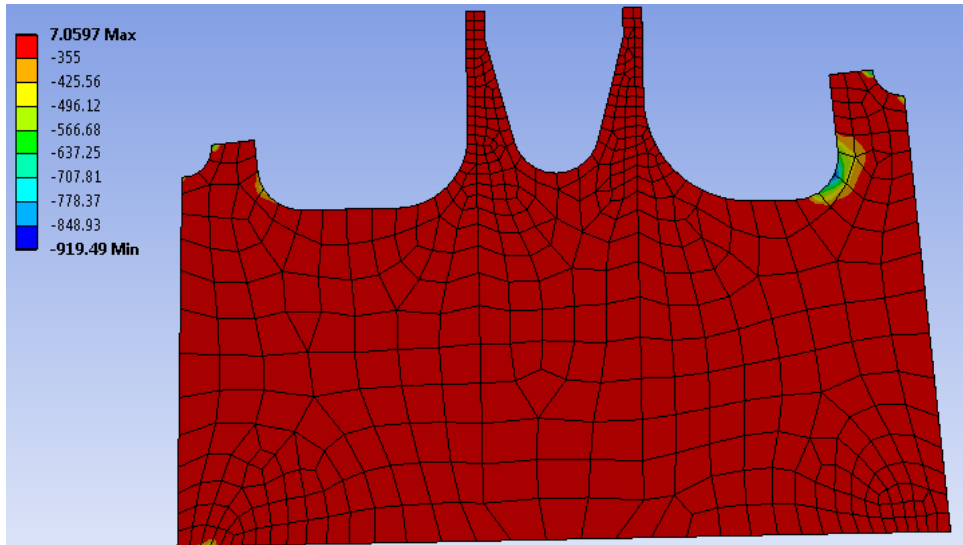


Figure 5.41 – Minimum principal stress in the gusset plate at diagonal D

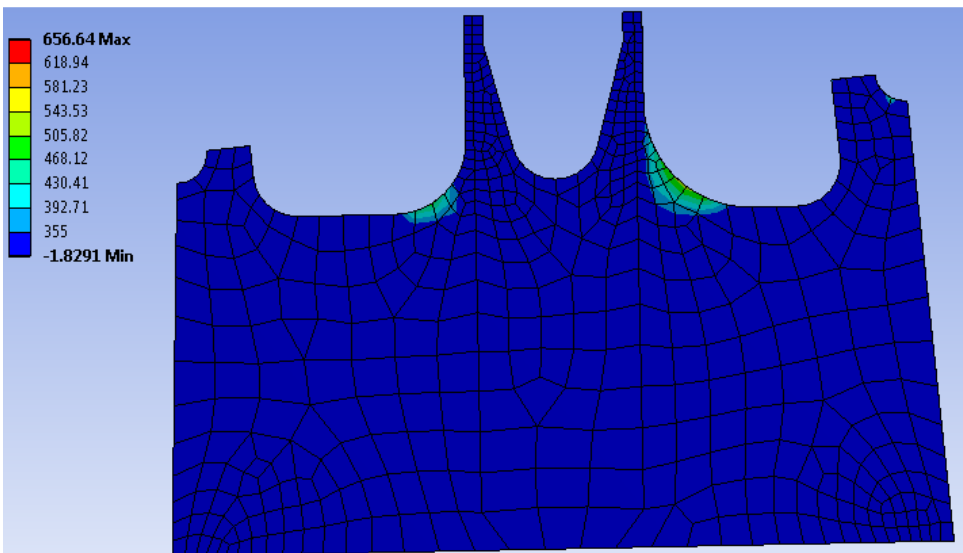


Figure 5.42 – Maximum principal stress in the gusset plate at diagonal D

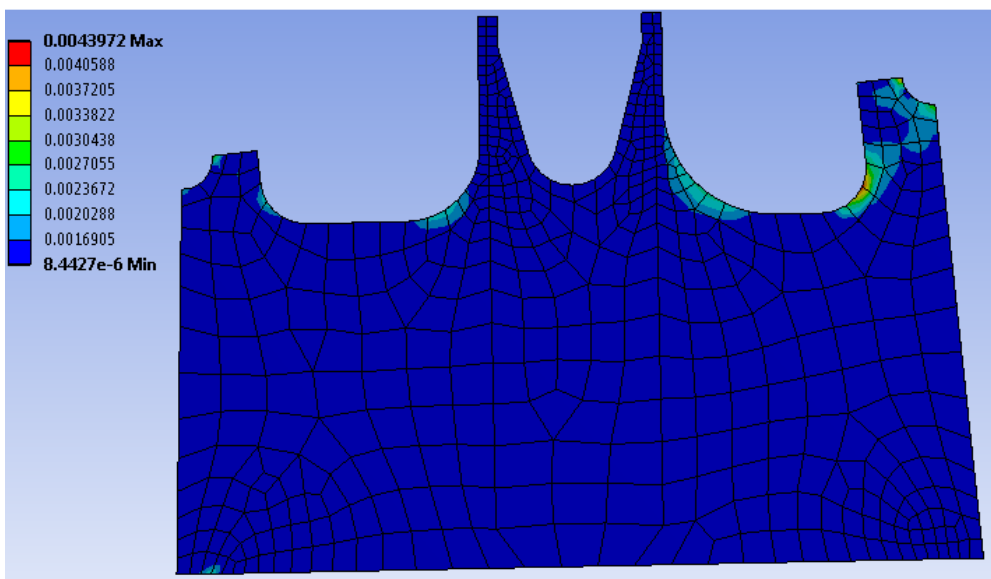


Figure 5.43 – Equivalent stress in the gusset plate at diagonal D

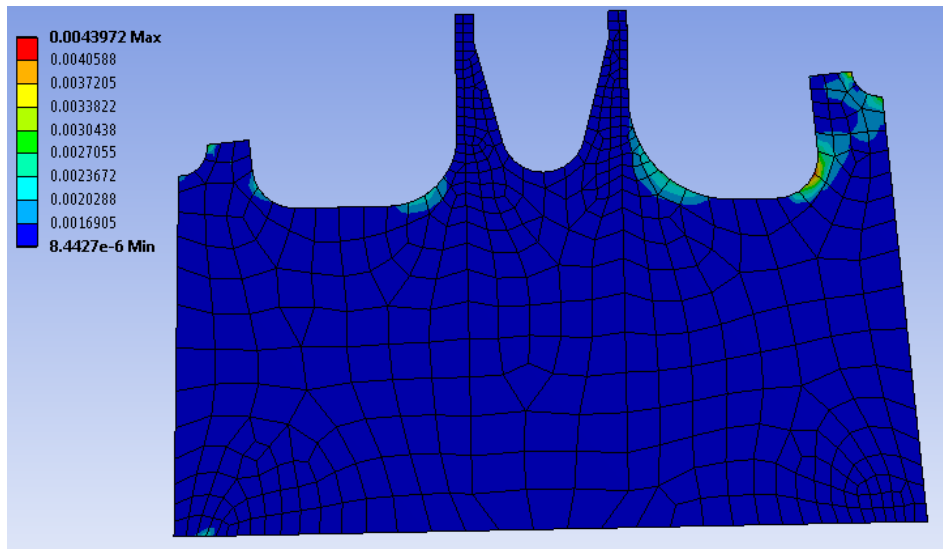


Figure 5.44 – Equivalent strain in the gusset plate at diagonal D

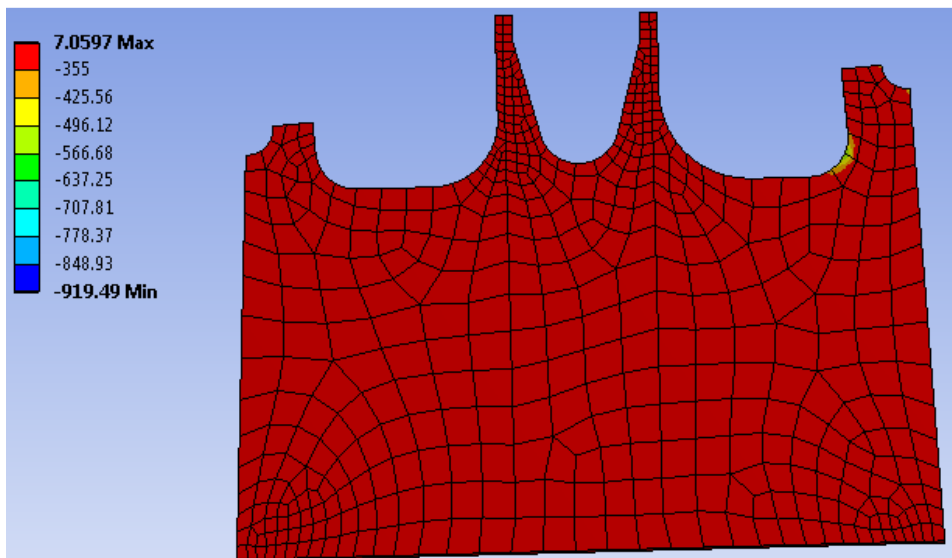


Figure 5.45 – Minimum principal stress in the gusset plate at diagonal C

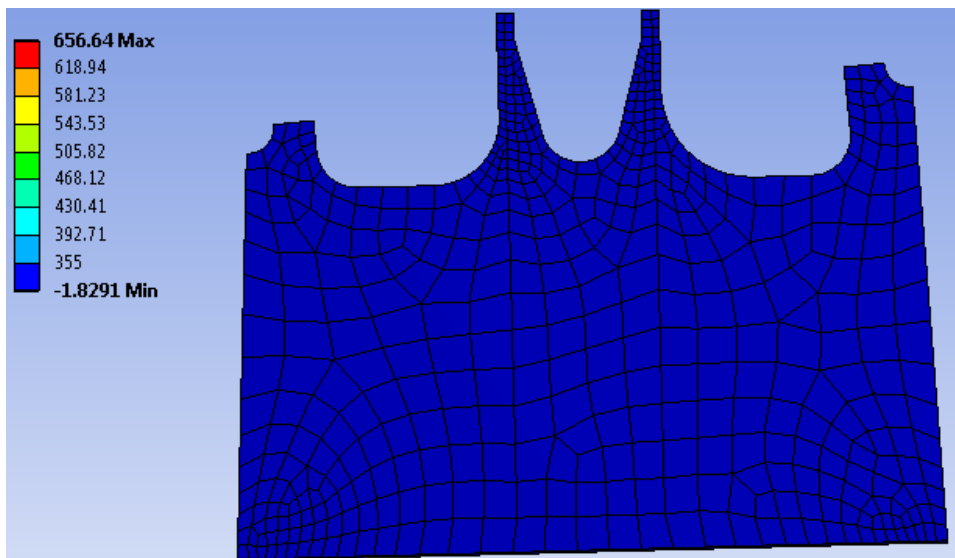


Figure 5.46 – Maximum principal stress in the gusset plate at diagonal C

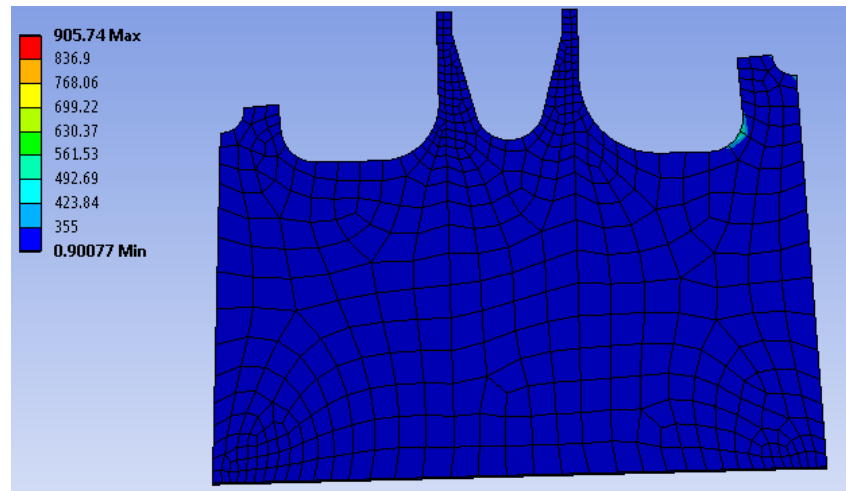


Figure 5.47 – Equivalent stress in the gusset plate at diagonal C

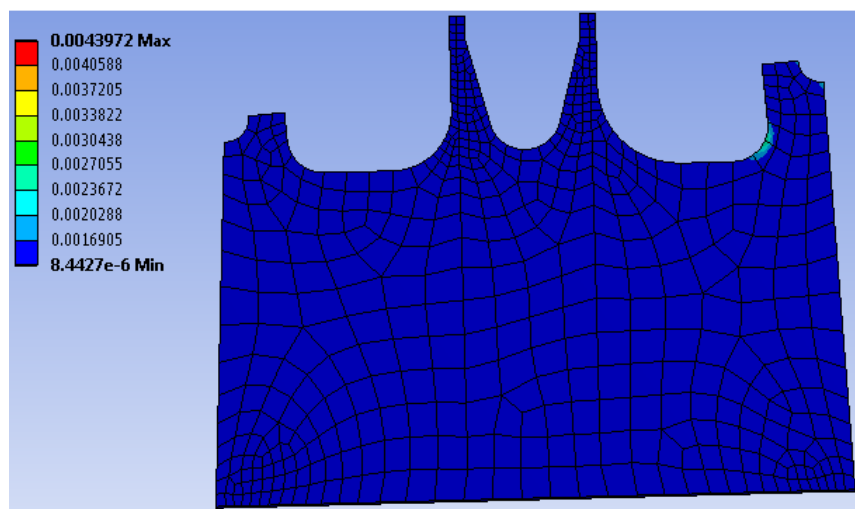


Figure 5.48 – Equivalent strain in the gusset plate at diagonal C

With respect to the top flange, the magnitude of the stress concentrations is higher at the opening of diagonal D. As the purpose is to study the applicability of the SM, only the stresses at part D of the top flange will be taken into account as they are higher than the ones occurring at opening C and the behaviour of the plate at the two opening is quite similar.

In the case of the gusset plates, only the one corresponding to diagonal D is checked for the applicability of the SM. This is due to the fact that the behaviour of the 2 elements (gusset plate at C and D) is similar; the only difference is that at the location of diagonal D the magnitude of the loads is higher which results in larger stress peaks.

In Figure 5.49 and Figure 5.52 the equivalent Von-Mises stresses are plotted for the top flange and gusset plate at diagonal D. The dark-blue contour represents the material that has not reached the yield stress. The peak stresses occurring at the location of the stress concentrations are illustrated.

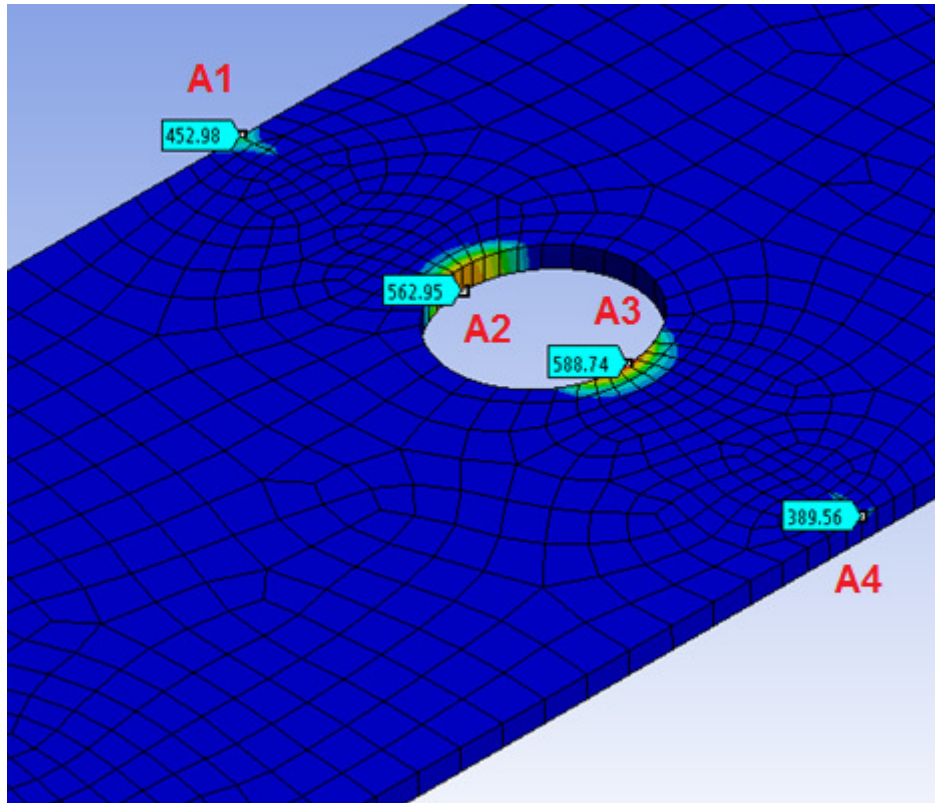


Figure 5.49 – Equivalent stresses at the stress concentration locations in the top flange at diagonal D:  $\sigma_{el}$

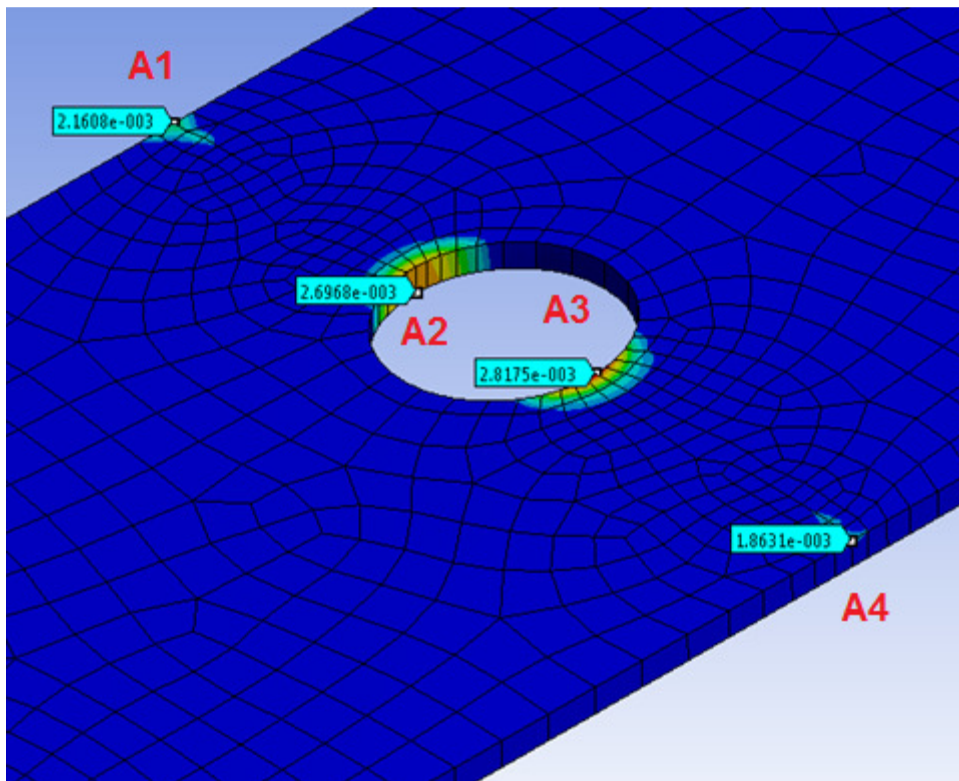


Figure 5.50 – Equivalent strains at the stress concentration locations in the top flange at diagonal D:  $\varepsilon_{el}$

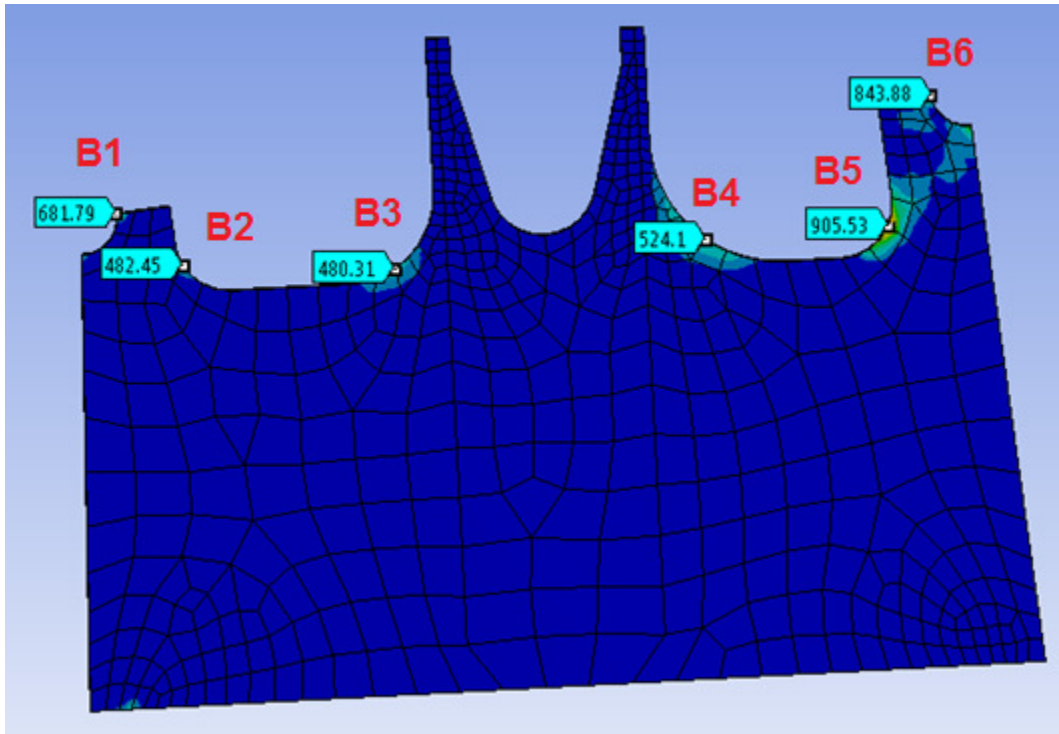


Figure 5.51 – Equivalent stresses at the stress concentration locations in the gusset plate at diagonal D:  $\sigma_{el}$

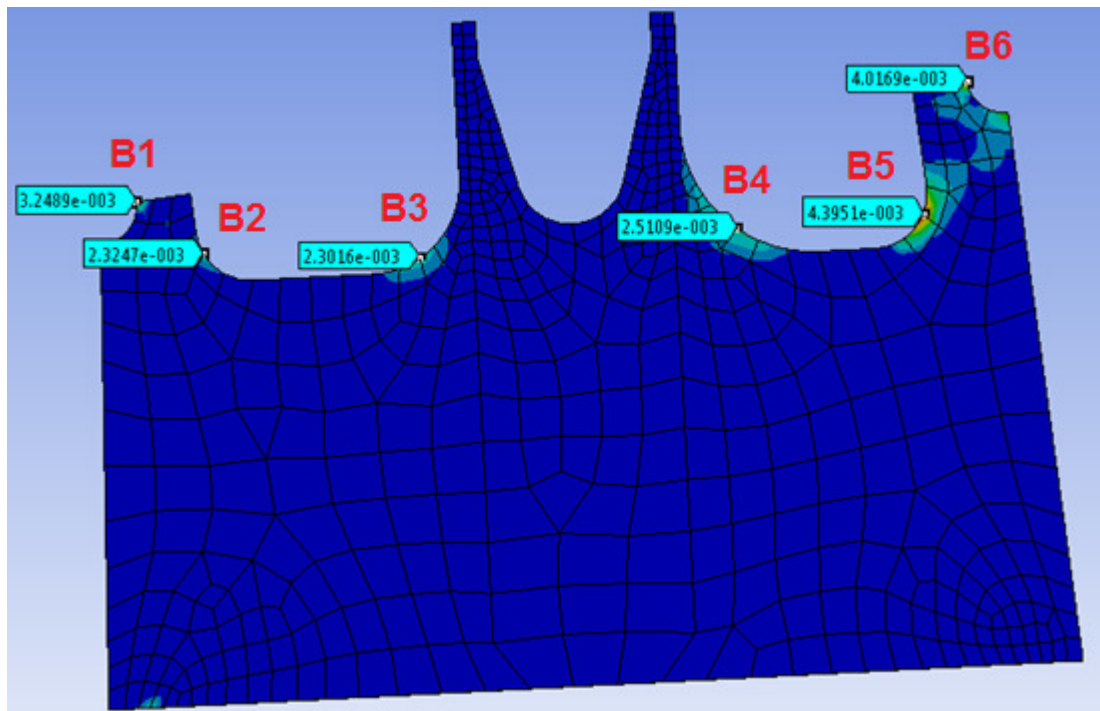


Figure 5.52 - Equivalent strains at the stress concentration locations in the gusset plate at diagonal D:  $\epsilon_{el}$

Table 42 – Peak stresses in the top flange at diagonal D

Top Flange - Peak stresses [N/mm <sup>2</sup> ]			
A1	A2	A3	A4
453	563	589	390

Table 43 – Peak stresses in the gusset plate at diagonal D

Gusset Plate - Peak stresses [N/mm <sup>2</sup> ]					
B1	B2	B3	B4	B5	B6
682	483	481	525	906	844

### 5.4.2 Estimation of strains using the SM approach

As stated in section 4.1.11 and 5.3.4, in order to be able to apply the SM method to the results of the linear analysis one must first make sure that full yielding has not occurred in any full section of the studied plates. In other words, the acting loads should lead to an average stress lower than  $0.9f_y$  in the weakest section of the plate (nominal section in the case of the top flange).

- *Top flange*

In the case of the top flange, the bending moments and axial force acting at end B of the connection are known. The stresses induced in the girder cross-section can be easily calculated and averaged over the nominal section. The forces and cross-section properties of the girder are presented in Table 44.

Table 44 – Girder: acting forces, bending moments and cross-sectional characteristics

F [kN]	M <sub>x</sub> [kNm]	M <sub>y</sub> [kNm]	A [mm <sup>2</sup> ]	I <sub>x</sub> [mm <sup>4</sup> ]	I <sub>y</sub> [mm <sup>4</sup> ]
103230	2103	4187	631163	9.8631E+11	6.463E+11

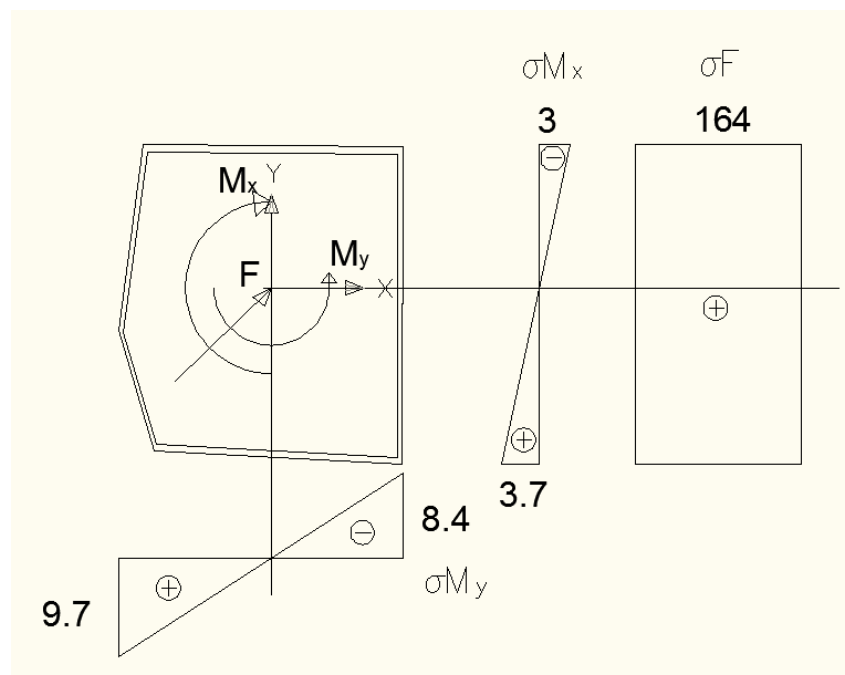


Figure 5.53 – Stresses in the girder cross-section

Where “+” represents tension and “-“ compression and the values are displayed in N/mm<sup>2</sup>.

Of interest is the stress occurring in the top flange. For this purpose the stresses over the width of the plate are calculated (Figure 5.54 – Averaged stress in the nominal section)

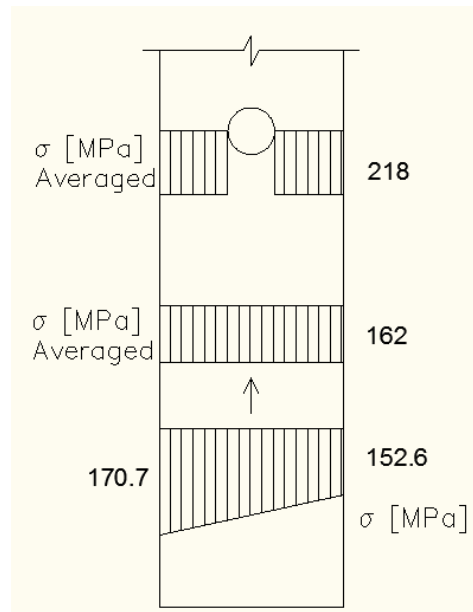


Figure 5.54 – Averaged stress in the nominal section

The stress averaged over the net section of the top flange has a value of 218MPa which is lower than  $0.9f_y=322\text{MPa}$ . This means that the SM approach can be attempted on the plate to estimate the real strains, as the stress state of the element is below that which causes full yielding of the section and the results of the linear analysis are still usable.

- *Gusset plate*

In the case of the gusset plate, the loads acting on diagonal D and transmitted through the plate are known. The gusset plate as working in the bridge connection can be modelled as illustrated in Figure 5.55.

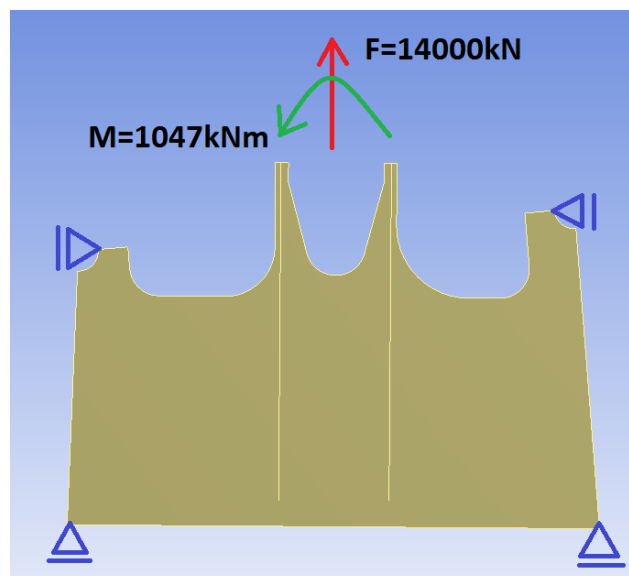


Figure 5.55 – Loads and boundary conditions of the gusset plate

Based on the loads and boundary conditions, the gusset plate is expected to yield due to the shear force acting on it. The bending moment can be expressed as two equivalent axial forces which combined with the axial force results in the following efforts.

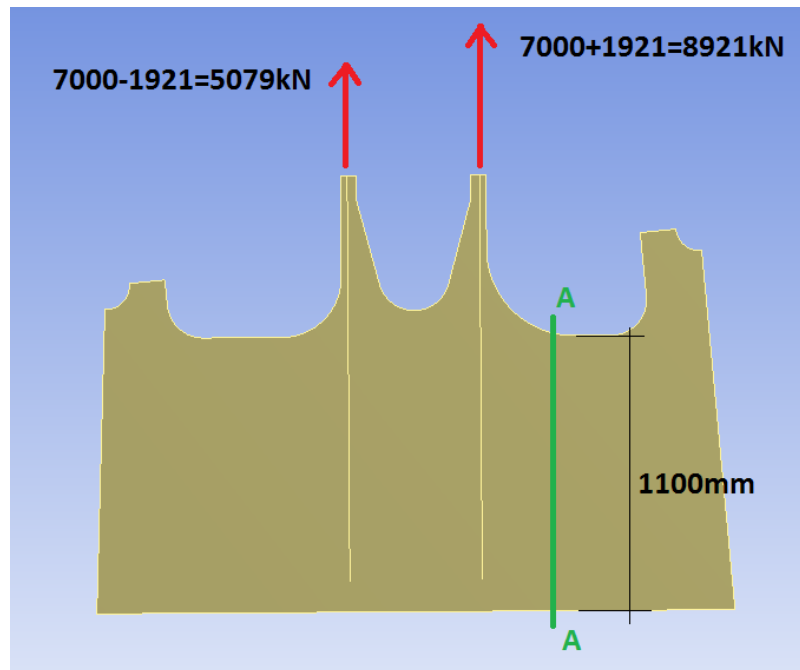


Figure 5.56 – Expected shear plane and equivalent loads on the gusset plate

The thickness of the plate is 60mm. The stress induced in the expected shear plane A-A can be calculated:

$$\frac{8921\text{kN}}{1100\text{mm} * 60\text{mm}} = \frac{135\text{N}}{\text{mm}^2} < \frac{0.9 * f_y}{\sqrt{3}} = 185\text{N}/\text{mm}^2$$

The forces acting on the gusset plate do not cause yielding through the entire section which means that the SM can be applied to the results of the linear analysis to estimate the strains. The real notch-tip strains estimated using the SM are listed in Table 45 and Table 46.

Table 45 – Notch-tip elastic-plastic strain calculated using the SM approach for the top flange

Top Flange			
Positon	$\sigma_{el}$ [N/mm <sup>2</sup> ]	$D_m$	$\epsilon_{NL}$
A1	453	1.28	0.0027
A2	563	1.59	0.0042
A3	589	1.66	0.0046
A4	390	1.10	0.0020

Table 46 - Notch-tip elastic-plastic strain calculated using the SM approach for the gusset plate

Gusset Plate			
Position	$\sigma_{el}$ [N/mm <sup>2</sup> ]	$D_m$	$\varepsilon_{NL}$
B1	682	1.92	0.0062
B2	483	1.36	0.0031
B3	481	1.35	0.0031
B4	525	1.48	0.0037
B5	906	2.55	0.0108
B6	844	2.38	0.0094

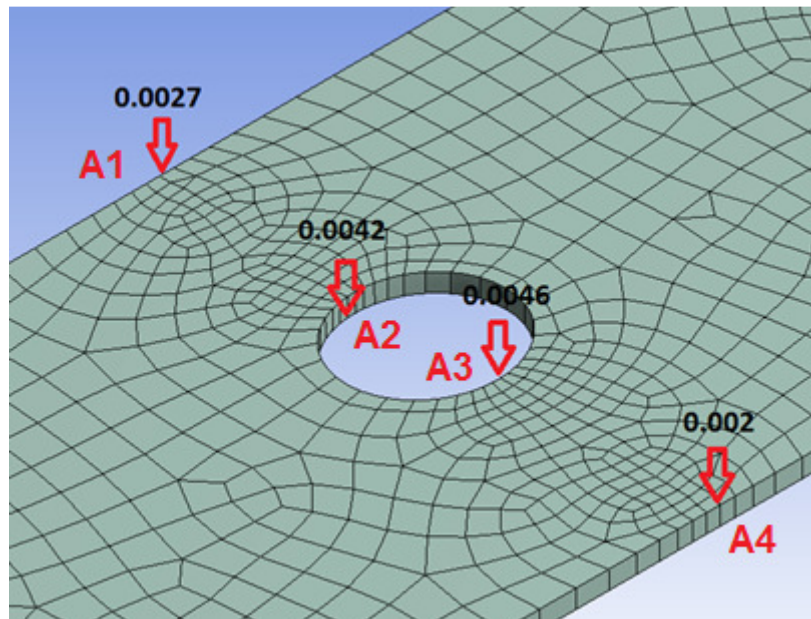


Figure 5.57 – Elastic-plastic strains in the top flange calculated with the SM

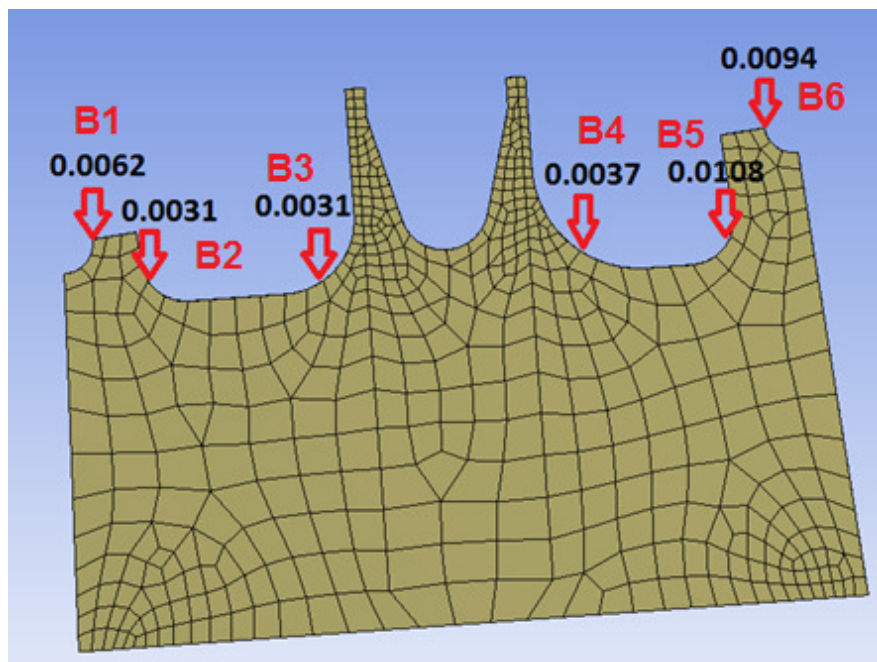


Figure 5.58 - Elastic-plastic strains in the gusset plate calculated with the SM

### 5.4.3 IFEA

In order to check the validity of the results calculated with the SM approach, a non-linear analysis is carried out on the joint model using the non-linear material behaviour. The value of the equivalent strain at the location of the stress concentrations are illustrated in Figure 5.59 and Figure 5.60.

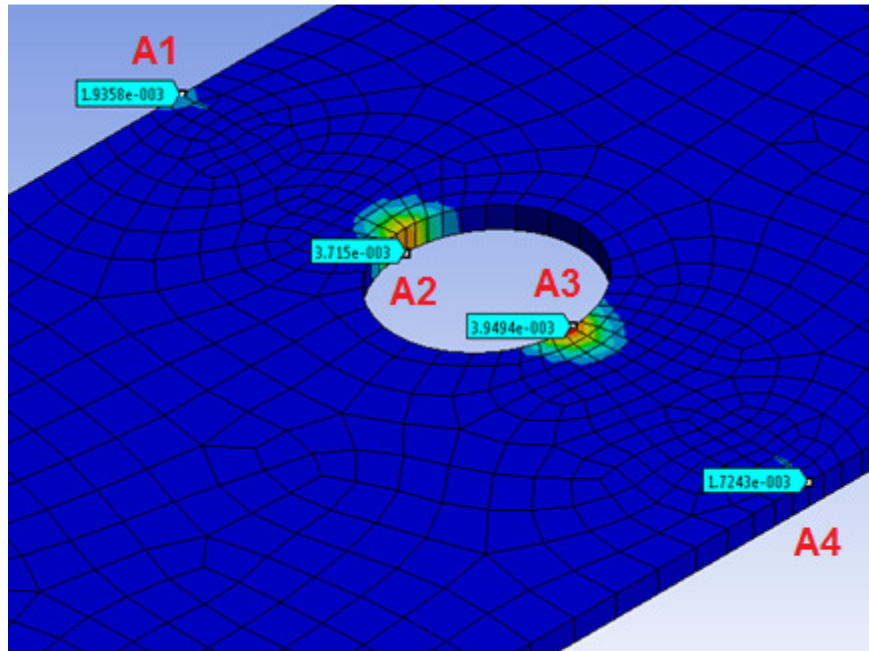


Figure 5.59 - Elastic-plastic strains in the top flange calculated with the IFEA

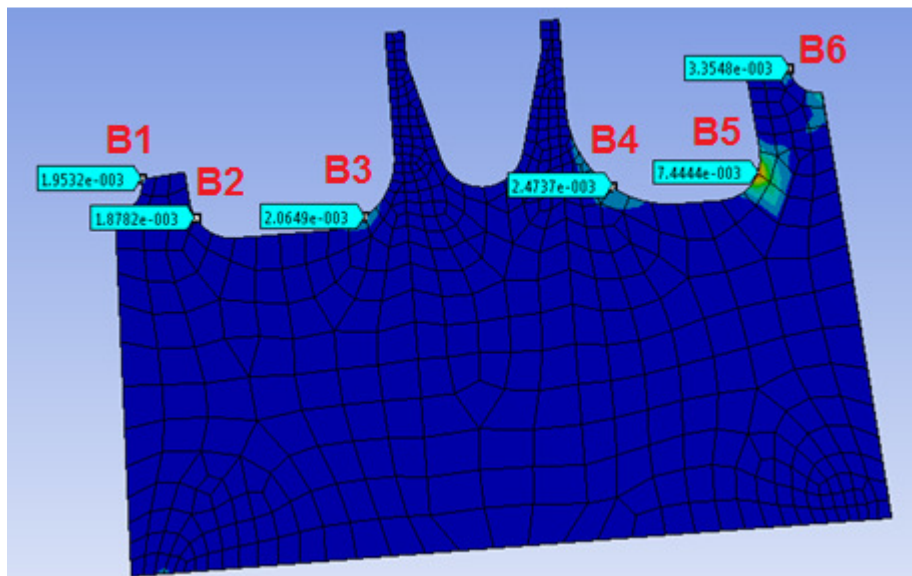


Figure 5.60 - Elastic-plastic strains in the gusset plate calculated with the IFEA

The values are transferred to a table and compared to the strain values computed using the SM approach. The difference between the two is expressed in percentage.

Table 47 – Difference between the IFEA and SM strains in the top flange

Top Flange			
Position	$\epsilon_{NL}$ [LNA]	$\epsilon_{NL}$ [IFEA]	Strain difference [%]
A1	0.0027	0.00194	39.2
A2	0.0042	0.00372	12.9
A3	0.0046	0.00395	16.5
A4	0.0020	0.00173	15.6

Table 48 – Difference between the IFEA and SM strains in the gusset plate

Gusset Plate			
Position	$\epsilon_{NL}$ [LNA]	$\epsilon_{NL}$ [IFEA]	Strain difference [%]
B1	0.00620	0.002	210.0
B2	0.00310	0.0019	63.2
B3	0.00310	0.0021	47.6
B4	0.00370	0.0025	48.0
B5	0.01080	0.0075	44.0
B6	0.00940	0.0034	176.5

The results of the SM compared to the IFEA give conservative predictions of the strains. All the results are on the conservative side, however considering the magnitude of the strains this is not a problem as the values are way below the ones that would pose problems with respect to the capacity of the plates.

In the case of the gusset plate the SM method gives strain estimates which differ quite significantly from the ones calculated with the IFEA. This is especially noticed at the top flange-gusset plate connection (positions B1 and B6). The explanation behind this is the fact that in the IFEA, once yielding occurs at the location of the notch-tips, stresses redistribute in the plate leading to internal force equilibrium and thus lower strains than expected. As the SM method is based on the results of the linear finite element analysis, the estimates are higher than the real ones due to the fact that the linear analysis cannot take into account the complex stress redistribution and for the increased load it simply increases the magnitude of the stresses at the notch-tips leading to the higher differences in the results. This is more noticeable in the gusset plate than the top flange because of the higher complexity of the geometry influencing the redistribution of stresses and thus the strain developments.

#### 5.4.4 Conclusions on the SM application to the bridge connection

The SM application to the bridge connection offered an easy and straight-forward procedure and the results are comparable to the ones from the IFEA. The SM proves to be a very promising tool in predicting the strains at the location of the stress concentrations up to 90% of the lowest values of the load that is expected to cause yielding in the net section of the studied plate (and thus to help in design to prove that the stresses at the notch-tips will not lead to structural failure). With the load conditions and material parameters known it is very easy to apply the SM to the results of the linear elastic analysis and estimate the strains at stress concentration location. The results can be compared with code requirements and thus argument that the material has sufficient ductility to yield locally and redistribute stresses. In the case where the code requirements are exceeded a nonlinear analysis should still be used as the SM was proven to sometimes give quite high overestimates of the strain values.

## 6 RECOMMENDATIONS WITH RESPECT TO THE SM APPROACH

Based on the examples studied in this paper, it can be stated that the SM approach has proven to give good estimates of the strains at the notch-tip based only on the results of the linear finite element. The method, due to its simple and straight-forward applicability, seems to be a useful tool in proving that the material at stress concentrations yields locally and ensure redistribution of stresses prior to fracture. However the method should only be used to predict strains based on known loading condition. In order to apply the SM the following recommendations are given:

- The loading conditions should be known: prior knowledge of the forces acting on the structure should be available. Based on these actions, the sections of the elements under consideration should be checked for yielding. In other words one should check that the acting loading conditions are below 90% of the lowest value of the forces that would cause full yielding in a section. This is a lower bound condition for the applicability of the SM method. If this condition is not fulfilled and yielding occurs through the entire section of an element, than the method cannot be applied anymore as the results of the linear finite element analysis cannot account for the large development of strains;
- Finite element analysis: based on the results of a linear finite element analysis, the location of the stress concentrations and their magnitude can easily be established. This point's to the locations in the structure where problems arise with respect to ductility. As the stresses at the notch-tips are known, the SM method can be applied to predict the strains at those locations. In order to do this, the stress-strain diagram of the steel grade used must be known;
- SM estimates: the SM results, based on the examples studied in this paper, show to give conservative results. As the purpose of this method is to estimate the strains at notch-tips and compare these values to design code limits, this is not a problem as long as the limits are not exceeded. In the latter case a nonlinear finite element analysis based on the material's nonlinear behaviour should still be carried out as the value of the strains might be lower than the ones predicted with the SM.

## 7 CONCLUDING REMARKS

Due to rapid geometric changes in the cross section, stress concentrations occur in details of steel structures. If the material has sufficient ductility then, due to plastic deformations, forces are redistributed so there will be equilibrium in the internal forces. However it is not often clear how to deal with these stress concentrations for a ULS check, especially in relation to the approach of a hand calculation or based on a linear elastic analysis. The present paper offers a possible solution to this problem through the application of the SM method. Based on the examples studied in this paper (plate with a hole and gusset plate), the results of the linear finite element analysis together with a lower boundary condition for yielding of the section can be used to predict the strains at the notch-tips and prove that the material has sufficient capacity to yield locally and redistribute stresses. As illustrated in the examples of this work, the SM method can be applied (independent of the steel grade used) to the results of the linear finite element analysis and used to give estimates of the strains at the stress concentration locations. These values can be easily compared with the design code requirements and checked whether it fulfils the requirements or not. In case the estimated strains exceed the code limits, a nonlinear finite element analysis based on the materials nonlinear behaviour should be carried out as the SM method, based on the examples studied in this paper, appears to be a conservative approach and leads to overestimates of the strains.

Another issue addressed in this paper is with respect to code requirements for ductility. In order for the material to yield and redistribute stresses that result in equilibrium, the material must have sufficient deformation capacity which is translated in most cases as: tensile strength higher than the yield strength. However, in the case of stress concentrations, the material only needs to yield locally in order to redistribute stresses. High requirements with respect to the  $f_u/f_y$  ratio would be more necessary in the case of structures subject to exceptional loading conditions (as for example earthquakes) where plastic hinges are designed to occur through the structure and such a ratio would ensure a stress redistribution prior to collapse of one section. In the case when the only ductility requirements are related to stress concentrations, based on the examples illustrated in this work, lower values of this parameter seem acceptable. For the case studied in this paper (the bridge connection) a  $f_u/f_y$  ratio of 1.05 fulfils such requirements under the stated loading conditions. However such a ratio should only be used in design as long as a refined calculation is carried out in order to prove that this value ensures adequate stress redistributions and thus meets the ductility requirements of the structure under the loading conditions it is subject to. A lower value of the  $f_u/f_y$  ratio (below 1.05) does not appear to be acceptable as it leads to low stress redistributions and failure at quite low capacities compared to the examples with strain hardening. This parameter ( $f_u/f_y$ ) should always be considered together with ensuring a minimum elongation at fracture ( $\epsilon_u$ ). Based on the examples modelled in this paper, these two ductility parameters can significantly enhance the capacity of the plate ( $f_u/f_y$ ) while ensuring stress redistribution in the element and avoidance of fracture at the location of the stress concentration ( $\epsilon_u$ ).

Finally, with respect to repair and maintenance of HSSs: these steel grades show very good weldability. Using high-quality filler metals with low hydrogen content HSSs have a very high safety against cold cracking due to their low carbon equivalent. Together with preheating for the hydrogen effusion and delay of the cooling in the weld the occurrence of cold cracking can be avoided.

## 7.1 Future Research

The current work was only able to address a few of the challenges that ductility poses. However, numerous other questions still need investigation. A few of the possible research topics that can be developed in the future based on the current paper are listed below:

- Minimum elongation at failure: As it was shown in this paper that this parameter can significantly enhance the capacity with respect to ductility at stress concentrations, further research into this topic should be carried out in order to establish what would be an acceptable value;
- Stefanescu method: The applicability of this new approach should be studied on other types of geometries and connections where stress concentrations occur in order to determine the methods possible extension to a more general approach;
- Fatigue: As the SM method is used to estimate strains at notch-tips, further investigation on this method and its applicability to low-cycle fatigue calculations should be studied;
- Hydrogen embrittlement: further research should be carried out on simpler methods that can be used to avoid this in order to make HSS a more attractive alternative.

## BIBLIOGRAPHY

- [1] British Standards Institution, *BS EN 10020:2000 Definition and Classification of Grades of Steel*, London: BSI, 2000.
- [2] *ESDEP WG 2 "APPLIED METALLURGY", Lecture 2.4: Steel Grades and Qualities*.
- [3] Nederlands Normalisatie-instituut, *NEN-EN 10025-2 Hot Rolled Products of Structural Steels - Part 2: Technical Delivery Conditions for Non-Alloy Structural Steels*, Delft: NEN, 2004.
- [4] Nederlands Normalisatie-instituut, *NEN-EN 10025-6 Hot Rolled Products of Structural Steels - Part 6: Technical Delivery Conditions for Flat Products of High Yield Strength Structural Steels in the Quenched and Tempered Condition*, Delft: NEN, 2004.
- [5] R. Willms, "High Strength Steel for Steel Constructions," in *Nordic Steel Construction Conference*, Malmo, 2009.
- [6] F. Schröter, "Trends of using high-strength steel for heavy steel structures," 2004. [Online]. Available: [http://www.dillinger.de/imperia/md/content/dillinger/publikationen/stahlbau/technische\\_literatur/dh\\_trends\\_of\\_using\\_high-strength.pdf](http://www.dillinger.de/imperia/md/content/dillinger/publikationen/stahlbau/technische_literatur/dh_trends_of_using_high-strength.pdf). [Accessed 19 March 2014].
- [7] Nederlands Normalisatie-instituut, *NEN-EN 10025-3 Hot Rolled Products of Structural Steels - Part 3: Technical Delivery Conditions for Normalized/Normalized Rolled Weldable Fine Grain Structural Steels*, Delft: NEN, 2004.
- [8] Nederlands Normalisatie-instituut, *NEN-EN 10025-4 Hot Rolled Products of Structural Steels - Part 4: Technical Delivery Conditions for Thermomechanical Rolled Weldable Fine Grain Structural Steels*, Delft: NEN, 2004.
- [9] Nederlands Normalisatie-instituut, *NEN-EN 10025-5 Hot Rolled Products of Structural Steels - Part 5: Technical Delivery Conditions for Structural Steels With Improved Atmospheric Corrosion Resistance*, Delft: NEN, 2004.
- [10] European Committee for Standardization, *EN 1993-1-1 Design of steel structures - Part 1-1: General rules and rules for buildings*, Brussels: CEN, 2005.
- [11] Nederlands Normalisatie-instituut, *NEN-EN 1993-1-12 Design of steel structures - Part 1-12: Additional rules for the extension of EN 1993 up to steel grades S700*, Delft: NEN, 2007.
- [12] European Committee for Standardization, *EN 1993-1-10 Design of steel structures - Part 1-10: Material toughness and through-thickness properties*, Brussels: CEN, 2005.
- [13] L. F. e. a. Geschwindner, "Load and Resistance Factor Design of Steel Structures," Prentice Hall, Englewood Cliffs, 1994.
- [14] R. BJORHOVDE, M. F. ENGSTROM, G. G. LARRY, L. A. KLOIBER and J. O. MALLEY, *Structural Steel Selection Considerations - A Guide for Students, Educators, Designers and Builders*, American Society of Civil Engineers, 2001.
- [15] Metal Pass, "Structural steel Metallurgical Characteristics and Properties," [Online]. Available: <http://www.metalpass.com/metaldoc/paper.aspx?docID=705>. [Accessed 6 March 2014].
- [16] F. Schröter and T. Lehnert, "Trends in the Application of High-Performance Steel in European Bridge Building," in *The Eight International Conference "Bridges in Danube Basin": New Trends in Bridge Engineering and Efficient Solutions for Large and Medium Span Bridges*, Timișoara, 2013.
- [17] F. Schröter and A. Samuelsson, "High Performance Steels in Europe - Production Processes, Mechanical and Chemical Properties, Fabrication Properties," in *Use and*

- Application of High-performance Steels for Steel Structures*, Zürich, Günther H.-P., 2005, pp. 99-109.
- [18] British Standards Institution, *BS EN 10164:2004 Steel products with improved deformation properties perpendicular to the surface of the product. Technical delivery conditions*, London: BSI, 2004.
- [19] British Standards Institution, *BS EN 1011-1:2009 Welding. Recommendations for welding of metallic materials. General guidance for arc welding*, London: BSI, 2009.
- [20] T.-Y. Yoon, "Korean High Performance Steel for Bridges," in *Proceedings of Korea-China-Japan Symposium on Structural Steel Construction*, 2009.
- [21] P. Collin and B. Johansson, "Bridges in High Strength Steel," International Association for Bridge and Structural Engineering, Budapest, 2006.
- [22] Dillinger Hütte GTS, "Bridges in the Netherlands," [Online]. Available: [https://www.dillinger.de/imperia/md/content/dillinger/publikationen/stahlbau/referenzolder/brueckenniederlande\\_e.pdf](https://www.dillinger.de/imperia/md/content/dillinger/publikationen/stahlbau/referenzolder/brueckenniederlande_e.pdf). [Accessed 7 March 2014].
- [23] F. Schröter, "High-strength heavy plates for modern European medium and large span bridges," [Online]. Available: [http://www.dillinger.de/imperia/md/content/dillinger/publikationen/stahlbau/technische\\_literatur/dh\\_high\\_strength\\_heavy\\_plates.pdf](http://www.dillinger.de/imperia/md/content/dillinger/publikationen/stahlbau/technische_literatur/dh_high_strength_heavy_plates.pdf). [Accessed 25 March 2014].
- [24] U.S. Department of Transportation, "High Performance Steel Designers' Guide - HPS Design Experience," [Online]. Available: <http://www.fhwa.dot.gov/bridge/guide03.cfm>. [Accessed 27 March 2014].
- [25] L. N. Triandafilou and W. Wright, "Welding Advantages with High Performance Steel," [Online]. Available: <http://www.structuremag.org/article.aspx?articleID=740>. [Accessed 2 April 2014].
- [26] Nippon Steel & Sumitomo Metal, "High-yield-point steel plates for bridges (SBHS)," [Online]. Available: <http://www.nssmc.com/en/product/plate/SBHS.html>. [Accessed 11 March 2014].
- [27] Nippon Steel & Sumitomo Metal, "Bridges-Example of use," [Online]. Available: <http://www.nssmc.com/en/product/use/case/bridge/index.html>. [Accessed 10 April 2014].
- [28] A. C. Bannister, "Yield Stress/Tensile Stress Ratio Results of Experimental Programme," Structural Integrity Assessment Procedures for European Industry, Rotherham, 1999.
- [29] R. L. BROCKENROUGH & ASSOCIATES INC., "Effect of Yield-Tensile Ratio on Structural Behavior - High Performance Steels for Bridge Construction," Pittsburgh, 1995.
- [30] U.S. Department of Transportation, "High Performance Steel Designers' Guide - Material Properties," [Online]. Available: <http://www.fhwa.dot.gov/bridge/guide02.cfm>. [Accessed 27 March 2014].
- [31] R. J. Dexter, S. A. Altstadt and C. A. Gardner, "Strength and Ductility of HPS70W Tension Members and Tension Flanges with Holes," University of Minnesota, Minneapolis, 2002.
- [32] P. Mans, A. J. Yakel and A. Azizinamini, "Full-Scale Testing of Composite Plate Girders Constructed Using 485-MPa High-Performance Steel," *Journal of Bridge Engineering*, vol. 6, pp. 598-604, 2001.
- [33] *ESDEP WG 1B "Steel Construction: Introduction to Design", Lecture 1B.8: Learning from Failures.*

- [34] C. Bevers, “The Latchford Bridge Failure,” [Online]. Available: <http://www.thekingshighway.ca/latchford.html>. [Accessed 9 April 2014].
- [35] S. Hao, “I-35 W Bridge Collapse,” *Journal of Bridge Engineering*, vol. 15, no. 5, pp. 608-614, 2010.
- [36] Toll Bridge Program Oversight Committee (TBPOC), “Report on the A354 Grade BD High-Strength Steel Rods on the New East Span of the San Francisco-Oakland Bay Bridge With Findings and Decisions,” Sacramento, 2013.
- [37] S. Chakrabarti, C. Hendy, N. Adamson and D. Iles, “The UK National Annexes to BS EN 1993-2, BS EN 1993-1-11, and BS EN 1993-1-12”.
- [38] J. Bringas, “Handbook of Comparative World Steel Standards,” 2004. [Online]. Available: [http://kmcenter.rid.go.th/kcresearch/MANUAL\\_OUT/MAEN0006.pdf](http://kmcenter.rid.go.th/kcresearch/MANUAL_OUT/MAEN0006.pdf). [Accessed 4 March 2014].
- [39] European Committee for Standardization, *EN 1993-1-5 Design of steel structures - Part 1-5: Plated structural elements*, Brussels: CEN, 2006.
- [40] European Committee for Standardization, *EN 1993-1-8 Design of steel structures - Part 1-8: Design of joints*, Brussels: CEN, 2005.
- [41] W. C. Young and R. G. Budynas, *Roark's Formulas for Stress and Strain*, New York: McGraw-Hill, 2002.
- [42] R. G. Budynas, *Advanced Strength and Applied Stress Analysis*, McGraw-Hill, 1999.
- [43] H. Neuber, “Theory of Stress Concentration for Shear-Strained Prismatical Bodies With Arbitrary Nonlinear Stress-Strain Law,” *Journal of Applied Mechanics*, vol. 28, no. 4, pp. 544-550, 1961.
- [44] M. Hoffmann and T. Seeger, “A Generalized Method for Estimating Multiaxial Elastic-Plastic Notch Stresses and Strains, Part 1: Theory,” *Journal of Engineering Materials and Technology*, vol. 107, no. 4, pp. 250-254, 1985.
- [45] M. Hoffmann and T. Seeger, “A Generalized Method for Estimating Multiaxial Elastic-Plastic Notch Stresses and Strains, Part 2: Application and General Discussion,” *Journal of Engineering Materials and Technology*, vol. 107, no. 4, pp. 225-260, 1985.
- [46] K. Molski and G. Glinka, “A Method of Elastic-Plastic Stress and Strain Calculation at a Notch Root,” *Materials Science and Engineering*, vol. 50, no. 1, pp. 93-100, 1981.
- [47] W. N. Sharpe, C. H. Yang and R. L. Tregoning, “An Evaluation of the Neuber and Glinka Relations for Monotonic Loading,” *Journal of Applied Mechanics*, vol. 59, no. 2S, pp. S50-S56, 1992.
- [48] S. K. Visvanatha, “A Study on the Use of Neuber's Rule in Fatigue Crack Initiation Predictions,” Department of Mechanical and Aerospace Engineering, Carleton University, Ottawa, 1998.
- [49] Wikipedia, “von Mises yield criterion,” [Online]. Available: [http://en.wikipedia.org/wiki/Von\\_Mises\\_yield\\_criterion](http://en.wikipedia.org/wiki/Von_Mises_yield_criterion).
- [50] H. Y. G. Lee, “Strain Hardening Properties of High Strength Steel SHS and RHS,” Imperial College London, London.
- [51] A. Moftakhar, A. Buczynski and G. Glinka, “Calculation of Elasto-Plastic Strain and Stresses in Notches Under Multiaxial Loading,” *International Journal of Fracture*, vol. 70, no. 4, pp. 357-373, 1995.
- [52] A. C. d. O. Miranda, A. Lopes, M. A. Meggiolaro, J. T. P. d. Castro and L. F. Martha, “Finite Element Analysis of Notch-Root Stress and Strain Concentration Factors Under Large Deformations,” in *Congressi Nacional de Engenharia Mecanica*, Belem, 2004.

- [53] R. J. McDonald and D. F. Socie, "A Technique to Estimate the Local Multiaxial Elastic-Plastic Behavior from a Purely Elastic Solution," *Engineering Fracture Mechanics*, vol. 78, no. 8, pp. 1696-1704, 2011.
- [54] L. Jianhui, W. Shengnan and S. Yi, "A New Method for Calculating Notch Tip Stresses and Strains Based on Neuber Method and ESED Method under Multiaxial Loading," *Jordan Journal of Mechanical and Industrial Engineering*, vol. 8, no. 1, pp. 21-26, 2014.
- [55] G. Glinka, "Energy Density Approach to Calculation of Inelastic Strain-Stress Near Notches and Cracks," *Engineering Fracture Mechanics*, vol. 22, no. 3, pp. 485-508, 1985.
- [56] P. S. Ferreira, J. Pinho-da-Cruz and F. Teixeira-Dias, "Finite Element and Local Strain Approach Stress-Strain Predictions in Notched AlCu4.5Mn Specimens," in *XXI Encuentro Del Grupo Espanol de Fractura*, Punta Umbria, 2004.
- [57] R. Adibi-Asl and R. Seshadri, "Improved Prediction Method for Estimating Notch Elastic-Plastic Strains," in *International Association for Structural Mechanics in Reactor Technology*, Toronto, 2007.
- [58] G. Eleni, "Use of High Strength Steel Grades for Economical Bridge Design," Delft University of Technology, Delft, 2012.
- [59] G. Ozkula, "High Strength Steel for Seismic Resistance of Beam-to-Column Connections," University of Illinois, Urbana, 2011.
- [60] A. M. Coelho and F. S. Bijlaard, "Behaviour of High Strength Steel Moment Joints," Delft University of Technology, Delft, 2010.
- [61] B. Åkesson, *Understanding Bridge Collapses*, London: Taylor & Francis Group, 2008.
- [62] C. Miki, K. Homma and T. Tominaga, "High strength and high performance steels and their use in bridge structures," *Journal of Constructional Steel Research*, vol. 58, pp. 3-20, 2002.
- [63] Nederlands Normalisatie-instituut, *NEN-EN 10025-1 Hot Rolled Products of Structural Steels - Part 1: General Technical Delivery Conditions*, Delft: NEN, 2004.
- [64] European Committee for Standardization, *EN 1990 Basis of structural design*, Brussels: CEN, 2002.
- [65] R. Adibi-Asl and R. Seshadri, "Variational Method for Limit Load Analysis of Inhomogeneous Media," in *Proceedings of the ASME 2009 Pressure Vessels and Piping Division Conference*, Prague, 2009.
- [66] R. Adibi-Asl and W. Reinhardt, "Ratchet Boundary of a Beam with Arbitrary Cross Section," in *Proceedings of the ASME 2013 Pressure Vessels and Piping Conference*, Paris, 2013.
- [67] R. Adibi-Asl and W. Reinhardt, "Shakedown/Ratcheting Boundary Determination Using Iterative Linear Elastic Schemes," in *Proceedings of the ASME 2009 Pressure Vessels and Piping Division Conference*, Prague, 2009.
- [68] M. Noban and R. Adibi-Asl, "A Unified Approach for Comparison of Multiaxial Fatigue Models," in *Proceedings of the ASME 2013 Pressure Vessels and Piping Conference*, Paris, 2013.
- [69] W. Fricke, "Guideline for the Fatigue Assessment by Notch Stress Analysis for Welded Structures," International Institute of Welding, Hamburg, 2010.
- [70] A. Hobbacher, "Recommendations for Fatigue Design of Welded Joints and Components," International Institute of Welding, Paris, 2013.

- [71] W. Fricke, "Guideline for the Assessment of Weld Root Fatigue," International Institute of Welding, Hamburg, 2011.
- [72] M. Jirasek and Z. P. Bazant, *Inelastic Analysis of Structures*, Chichester: John Wiley & Sons, Ltd, 2002.
- [73] W. Han and B. D. Reddy, *Plasticity Mathematical Theory and Numerical Analysis*, New York: Springer, 1999.
- [74] F. Dunne and N. Petrinic, *Introduction to Computational Plasticity*, Oxford: Oxford University Press, 2005.
- [75] E. d. S. Neto, D. Peric and D. Owen, *Computational Methods for Plasticity Theory and Applications*, Chichester: John Wiley & Sons Ltd, 2008.

### A. APPENDIX A

In this section the load, boundary conditions and results from the finite element modelling of the plate with a hole are presented.

In creating the mesh element midsize nodes are kept and the surface bodies were meshed using SHELL281 which is a 3D 8-node second-order structural shell. Each node has 3 translational and 3 rotational degrees of freedom. In its natural shape the element is quadrilateral but can also degenerate to a triangle.

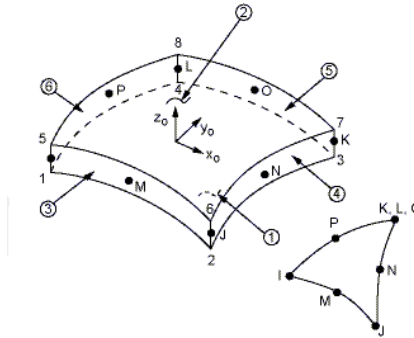


Figure A.1 – SHELL281 element

For the finite element analysis only one quarter of the plate was modelled due to symmetry conditions. The mesh of geometries with the boundary conditions and loads are presented below. Also the equivalent strains and stresses from the non-linear and linear finite element analysis at  $q_u$  (for both WoSH and WSH) and  $0.9q_y$  are plotted. In all the plots the dark-blue contour of the plate represents the material that has not reached yielding ( $\epsilon_e < \epsilon_y = \frac{f_y}{E} = 0.0016905$  or  $\sigma_e < f_y$ ).

#### Plate A

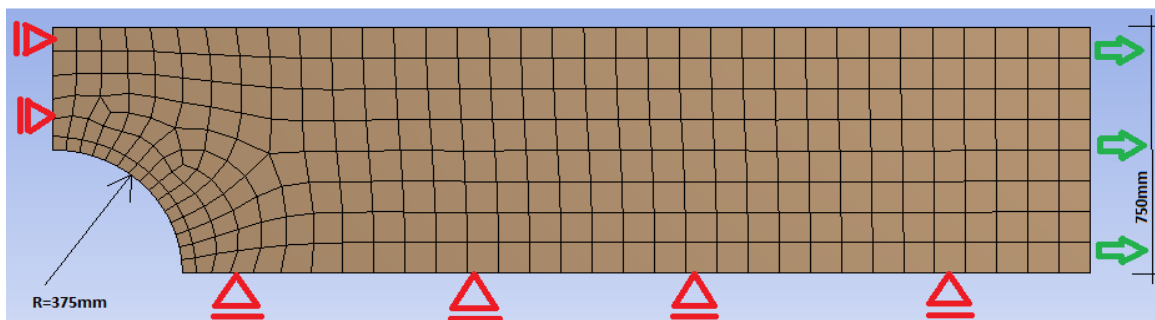


Figure A.2 – Plate A: Mesh geometry, load and boundary conditions of the finite element model

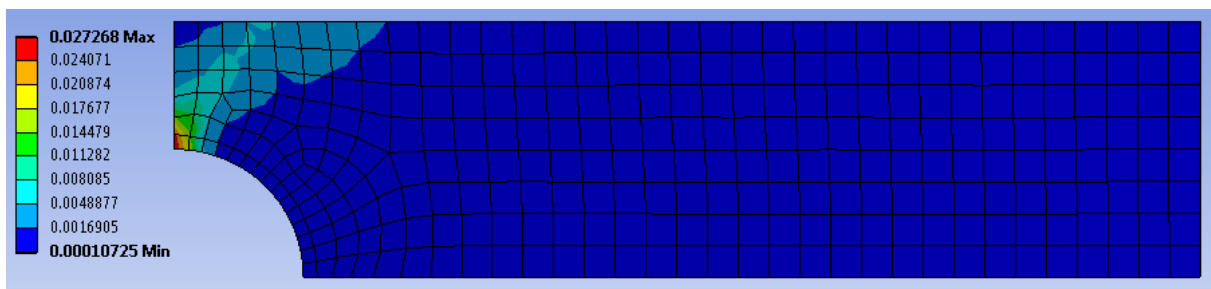


Figure A.3 – Plate A (WoSH): Equivalent strain at  $q_u = 7060N/mm$  (non-linear analysis)

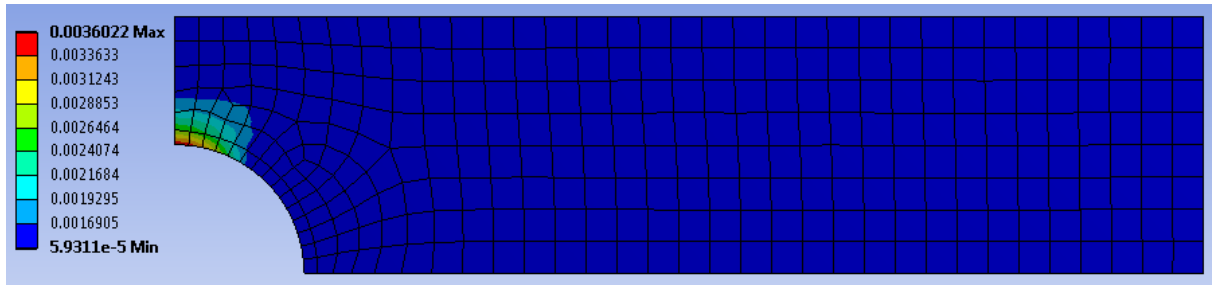


Figure A.4 – Plate A (WoSH): Equivalent strain at  $q_u = 7060 \text{ N/mm}$  (linear analysis)

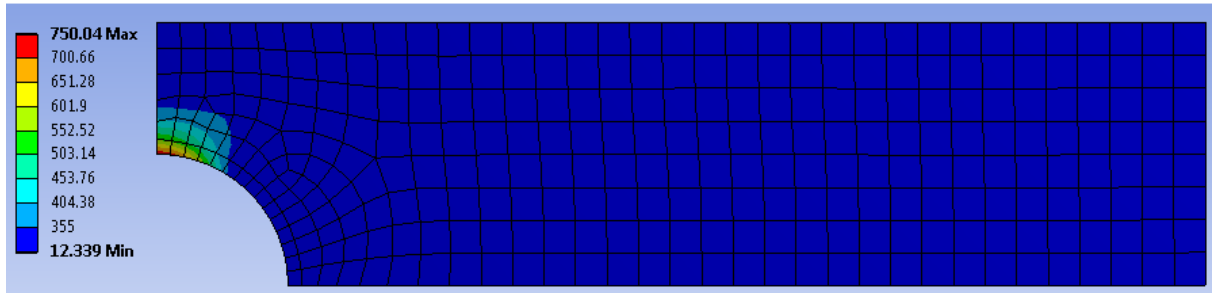


Figure A.5 – Plate A (WoSH): Equivalent stress at  $q_u = 7060 \text{ N/mm}$  (linear analysis)

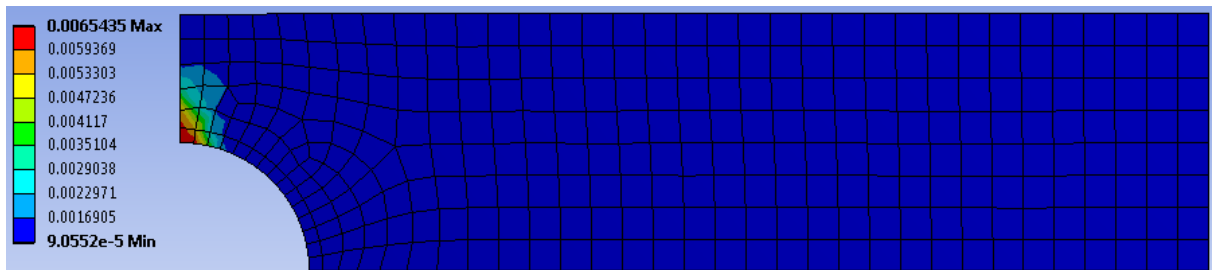


Figure A.6 – Plate A (WoSH): Equivalent strain at  $0.9q_y = 6390 \text{ N/mm}$  (non-linear analysis)

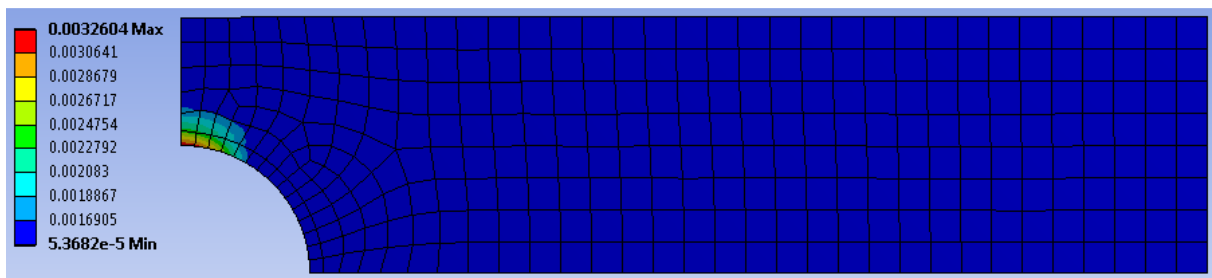


Figure A.7 – Plate A (WoSH): Equivalent strain at  $0.9q_y = 6390 \text{ N/mm}$  (linear analysis)

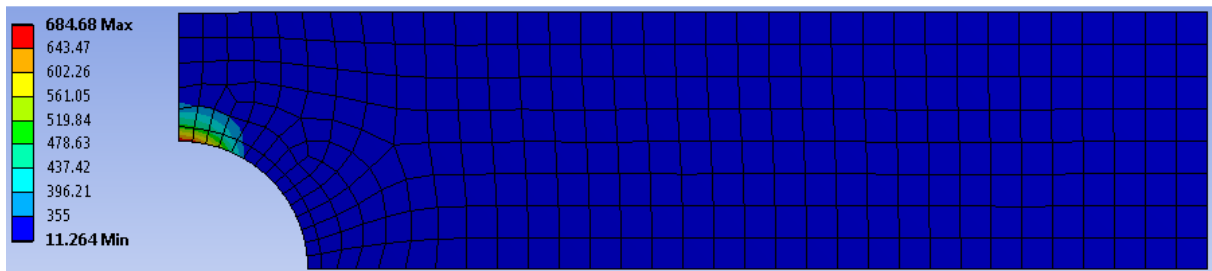


Figure A.8 – Plate A (WoSH): Equivalent stress at  $0.9q_y = 6390 \text{ N/mm}$  (linear analysis)

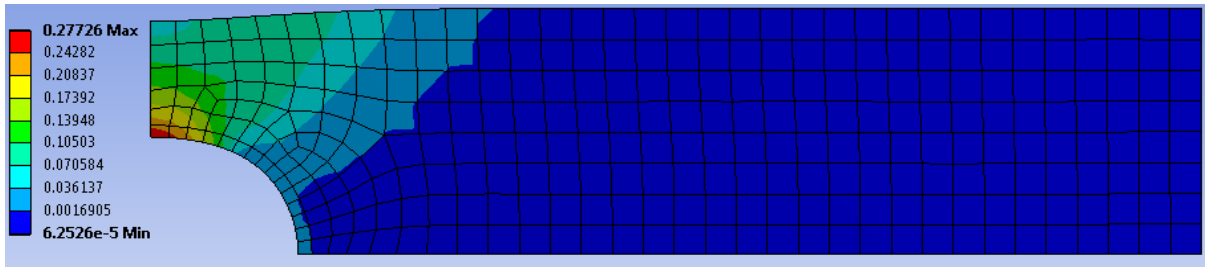


Figure A.9 – Plate A (WSH): Equivalent strain at  $q_u = 10200N/mm$  (non-linear analysis)

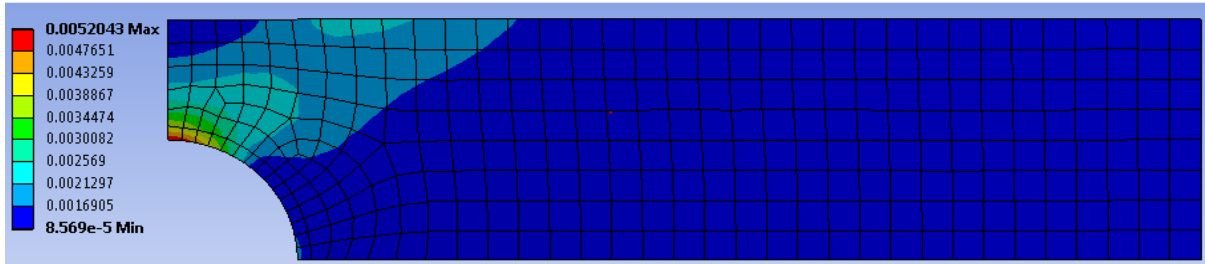


Figure A.10 – Plate A (WSH): Equivalent strain at  $q_u = 10200N/mm$  (linear analysis)

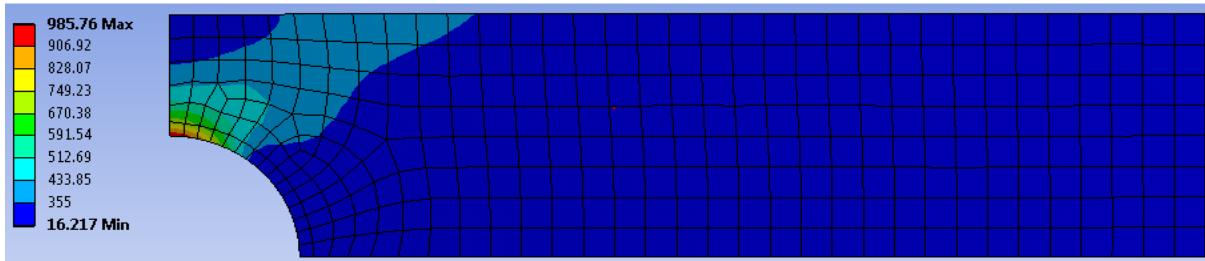


Figure A.11 – Plate A (WSH): Equivalent stress at  $q_u = 10200N/mm$  (linear analysis)

**Plate B**

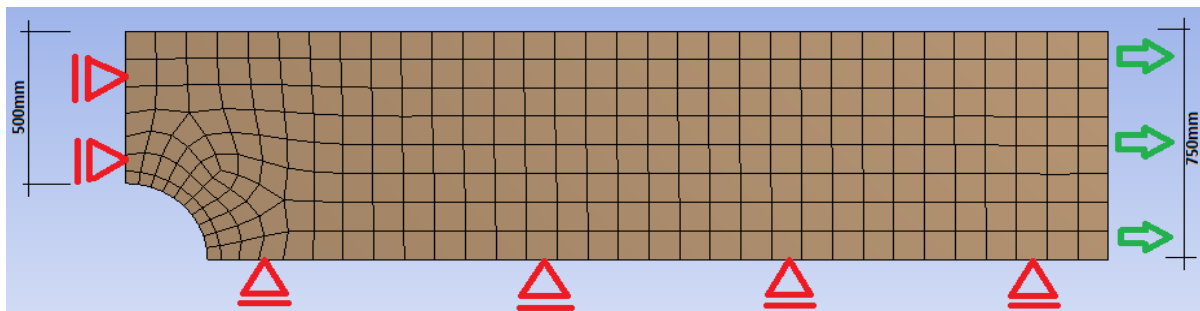


Figure A.12 – Plate B: Mesh geometry, load and boundary conditions of the finite element model

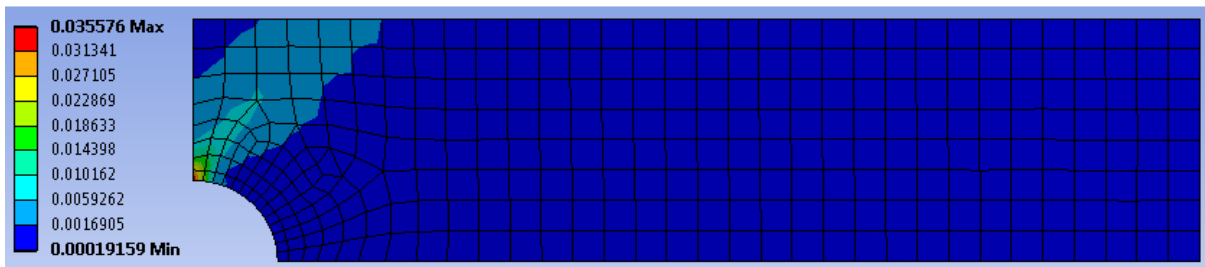


Figure A.13 – Plate B (WoSH): Equivalent strain at  $q_u = 9425N/mm$  (non-linear analysis)

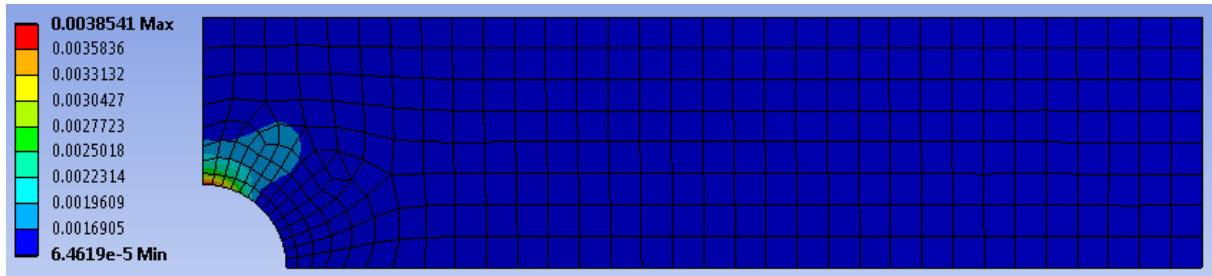


Figure A.14 – Plate B (WoSH): Equivalent strain at  $q_u = 9425N/mm$  (linear analysis)

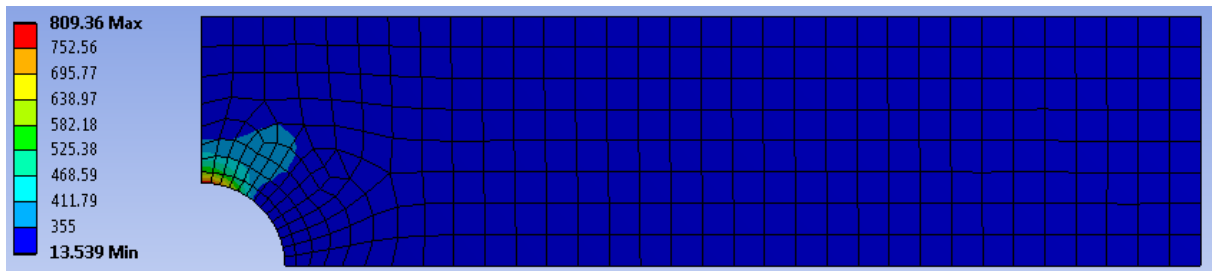


Figure A.15 – Plate B (WoSH): Equivalent stress at  $q_u = 9425N/mm$  (linear analysis)

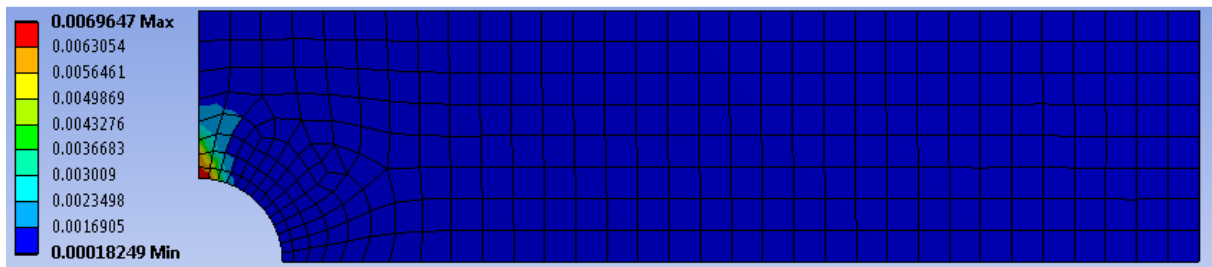


Figure A.16 - Plate B (WoSH): Equivalent strain at  $0.9q_y = 8520N/mm$  (non-linear analysis)

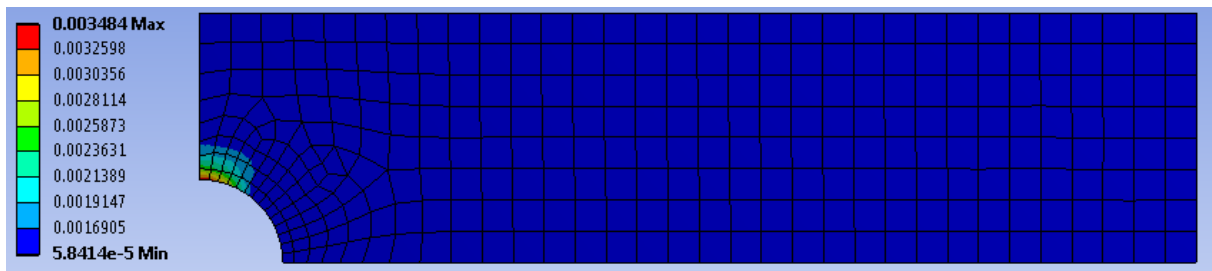


Figure A.17 – Plate B (WoSH): Equivalent strain at  $0.9q_y = 8520N/mm$  (linear analysis)

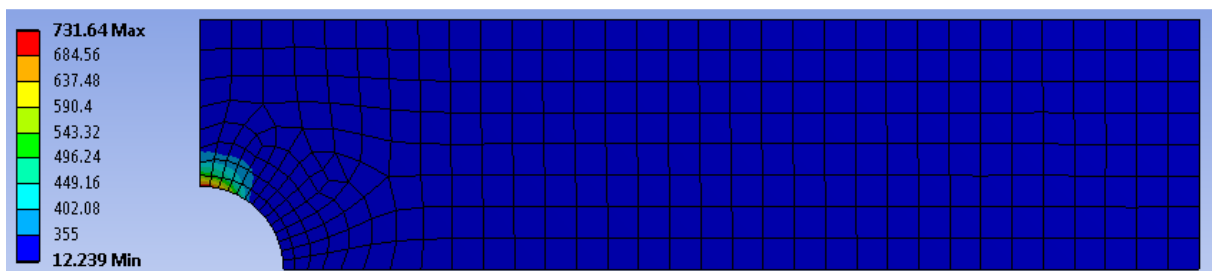


Figure A.18 – Plate B (WoSH): Equivalent stress at  $0.9q_y = 8520N/mm$  (linear analysis)

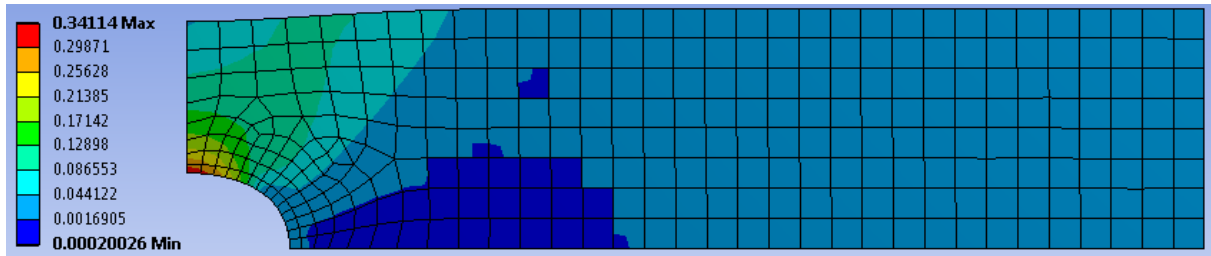


Figure A.19 – Plate B (WSH): Equivalent strain at  $q_u = 13600N/mm$  (non-linear analysis)

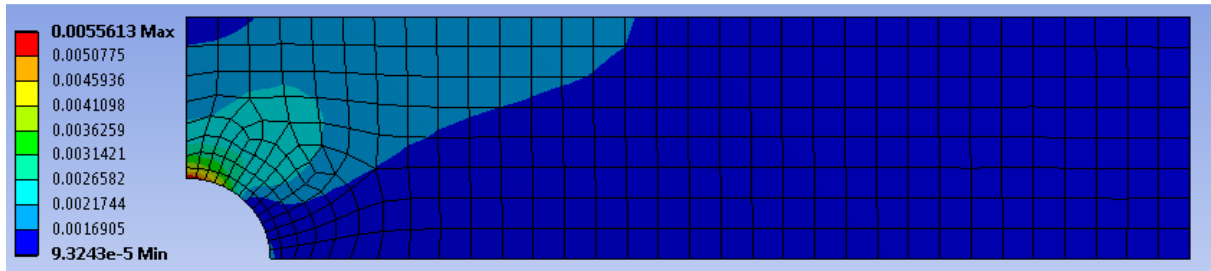


Figure A.20 – Plate B (WSH): Equivalent strain at  $q_u = 13600N/mm$  (linear analysis)

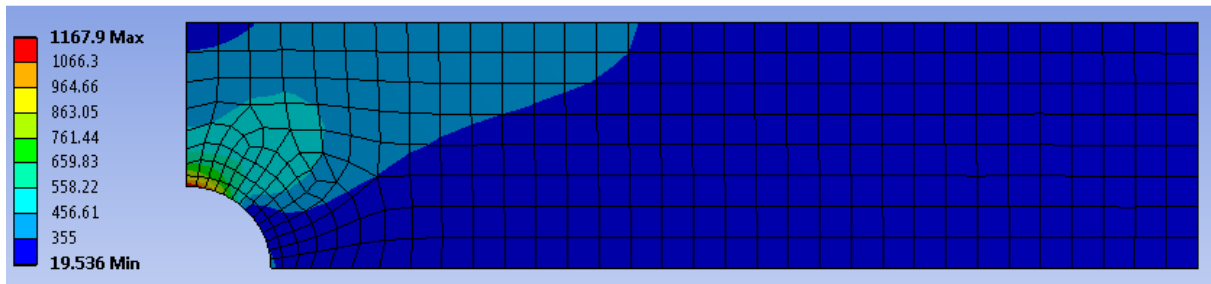


Figure A.21 – Plate B (WSH): Equivalent stress at  $q_u = 13600N/mm$  (linear analysis)

**Plate C**

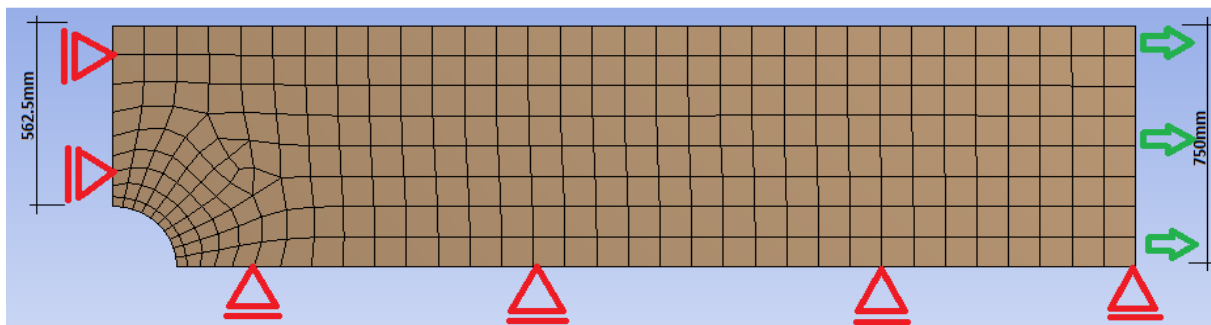


Figure A.22 – Plate C: Mesh geometry, load and boundary conditions of the finite element model

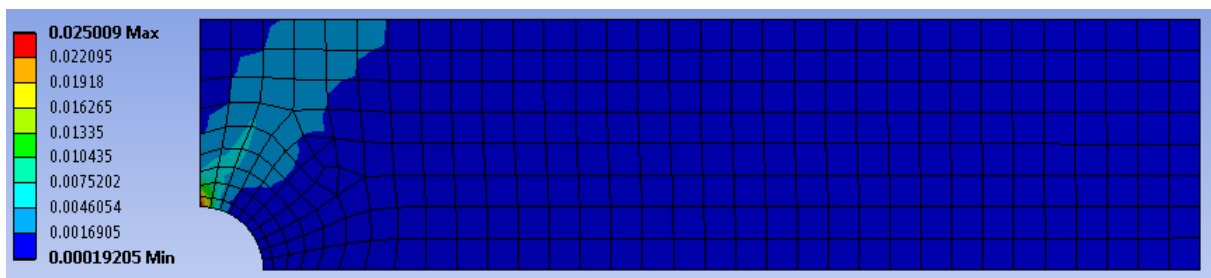


Figure A.23 – Plate C (WoSH): Equivalent strain at  $q_u = 10610N/mm$  (non-linear analysis)

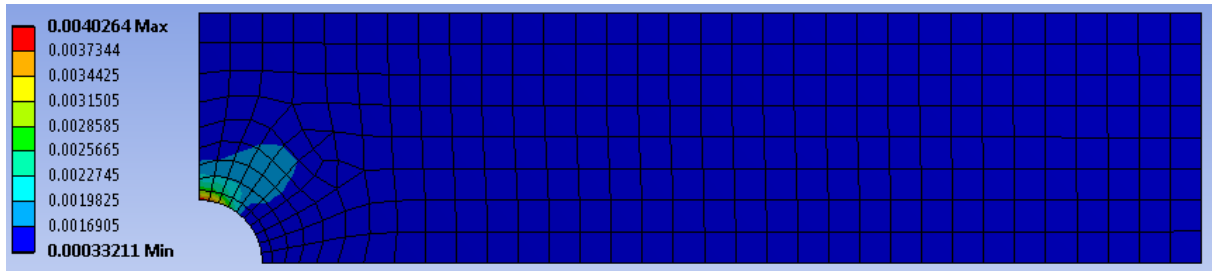


Figure A.24 – Plate C (WoSH): Equivalent strain at  $q_u = 10610N/mm$  (linear analysis)

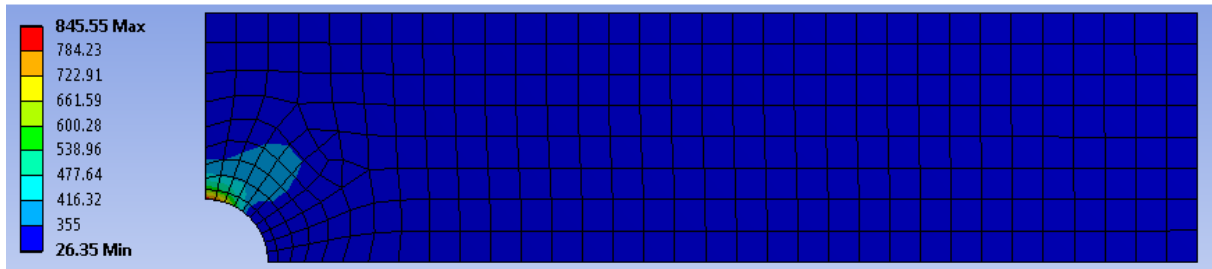


Figure A.25 – Plate C (WoSH): Equivalent stress at  $q_u = 10610N/mm$  (linear analysis)

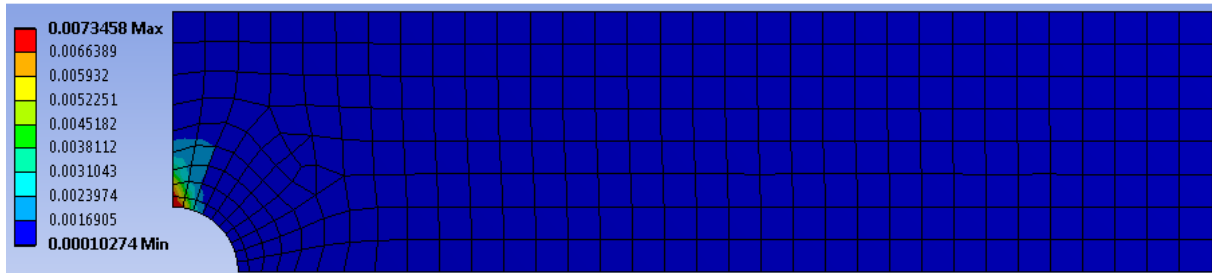


Figure A.26 - Plate C (WoSH): Equivalent strain at  $0.9q_y = 9585N/mm$  (non-linear analysis)

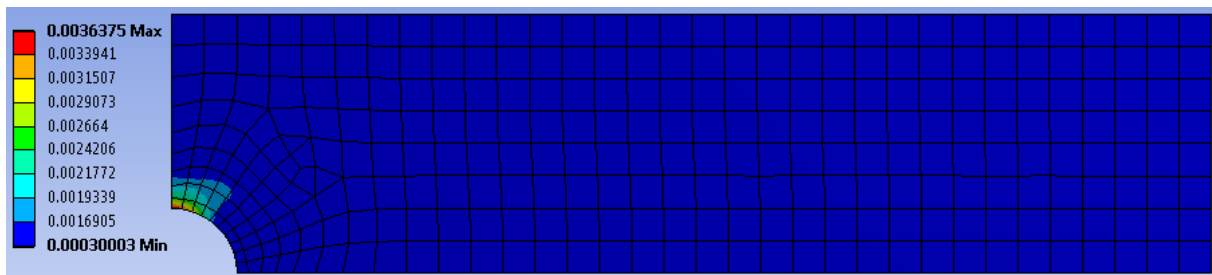


Figure A.27 – Plate C (WoSH): Equivalent strain at  $0.9q_y = 9585N/mm$  (linear analysis)

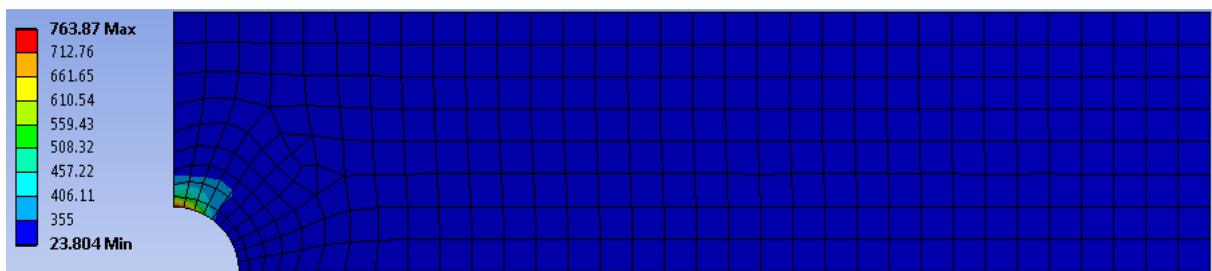


Figure A.28 – Plate C (WoSH): Equivalent stress at  $0.9q_y = 9585N/mm$  (linear analysis)

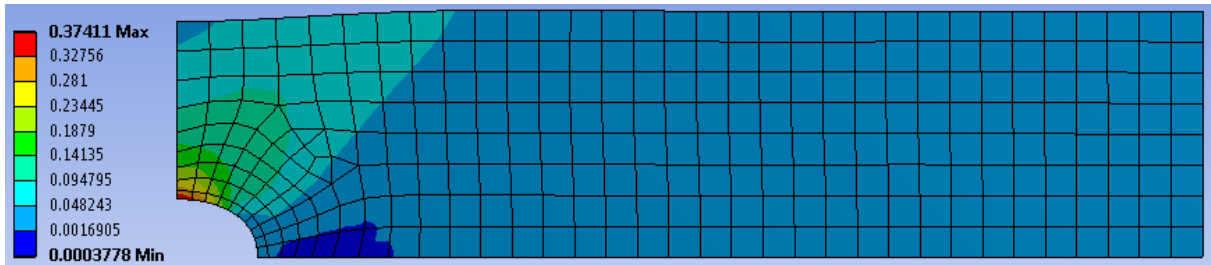


Figure A.29 – Plate C (WSH): Equivalent strain at  $q_u = 15300N/mm$  (non-linear analysis)

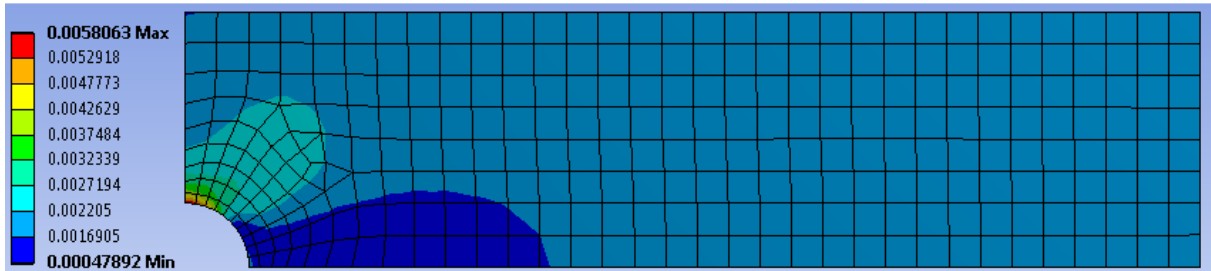


Figure A.30 – Plate C (WSH): Equivalent strain at  $q_u = 15300N/mm$  (linear analysis)

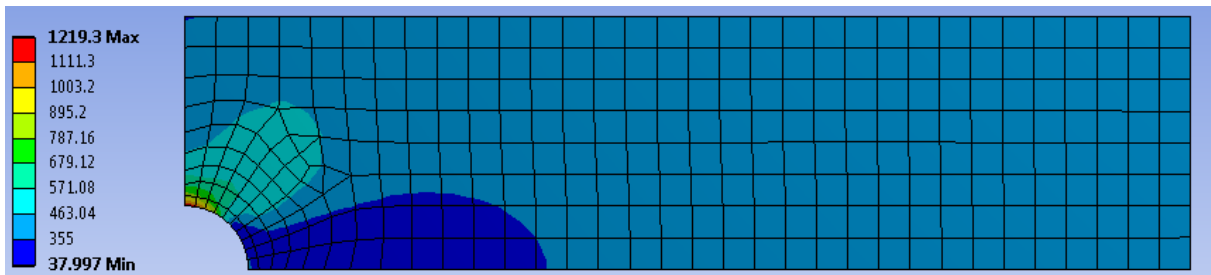


Figure A.31 – Plate C (WSH): Equivalent stress at  $q_u = 15300N/mm$  (linear analysis)

**Plate D**

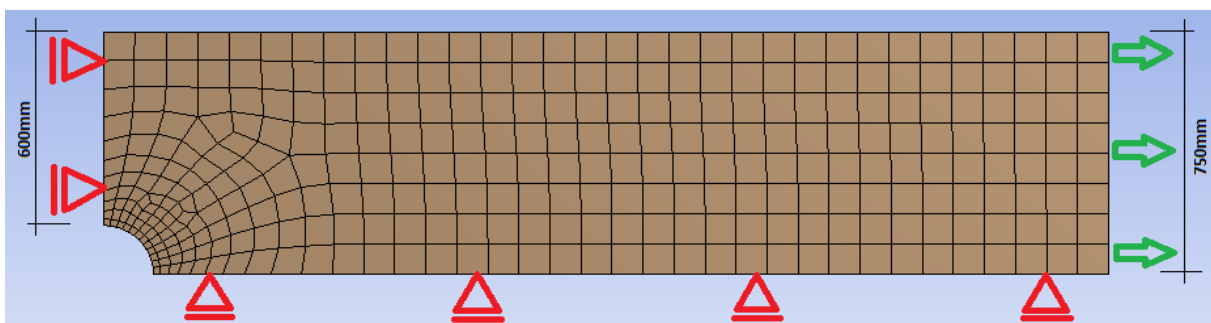


Figure A.32 – Plate D: Mesh geometry, load and boundary conditions of the finite element model

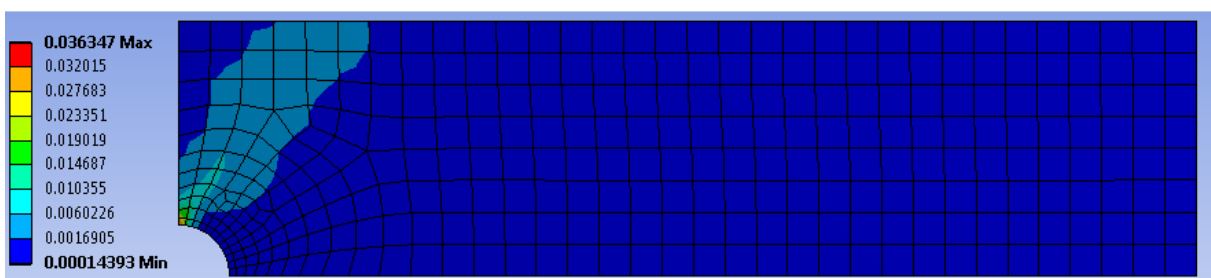


Figure A.33 – Plate D (WoSH): Equivalent strain at  $q_u = 11340N/mm$  (non-linear analysis)

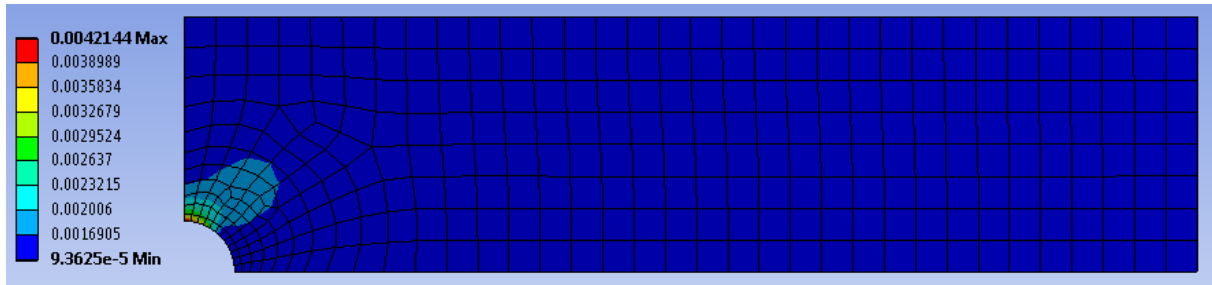


Figure A.34 – Plate D (WoSH): Equivalent strain at  $q_u = 11340N/mm$  (linear analysis)

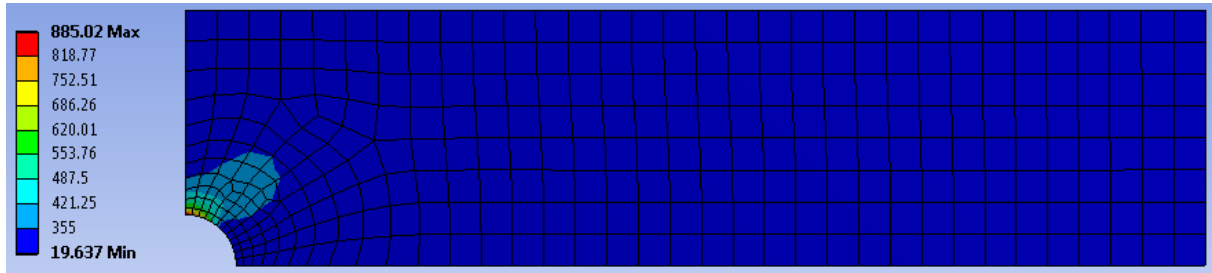


Figure A.35 – Plate D (WoSH): Equivalent stress at  $q_u = 11340N/mm$  (linear analysis)

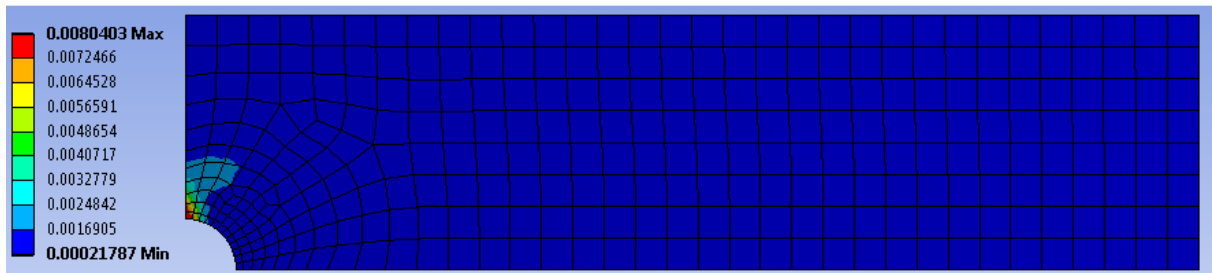


Figure A.36 - Plate D (WoSH): Equivalent strain at  $0.9q_y = 10224N/mm$  (non-linear analysis)

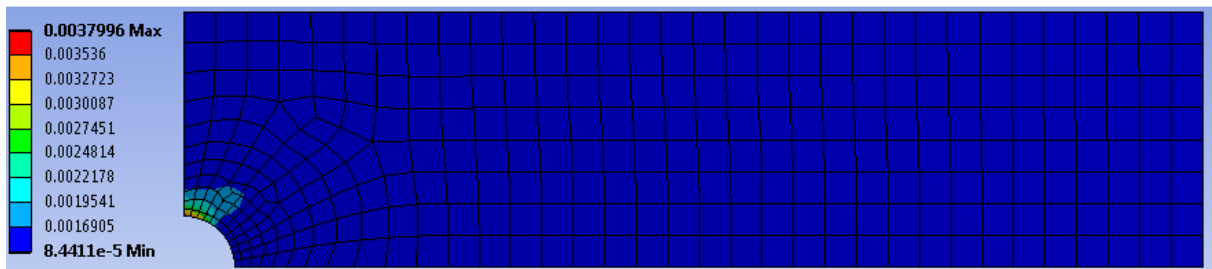


Figure A.37 – Plate D (WoSH): Equivalent strain at  $0.9q_y = 10224N/mm$  (linear analysis)

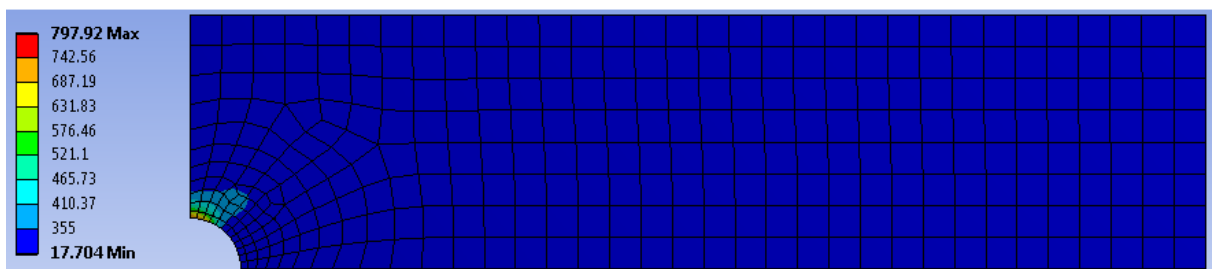


Figure A.38 – Plate D (WoSH): Equivalent stress at  $0.9q_y = 10224N/mm$  (linear analysis)

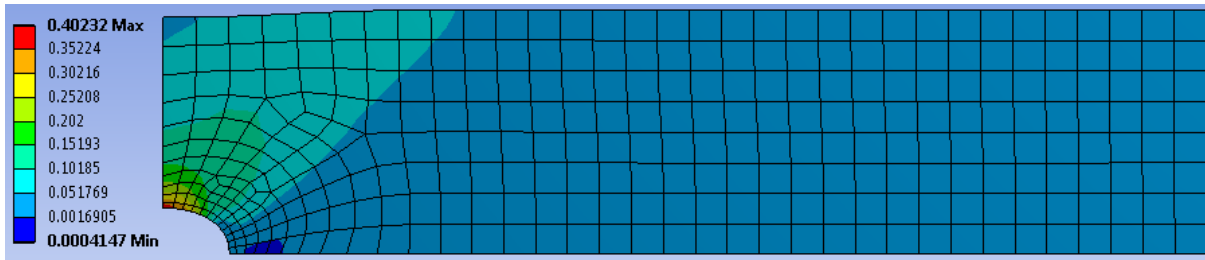


Figure A.39 – Plate D (WSH): Equivalent strain at  $q_u = 16320N/mm$  (non-linear analysis)

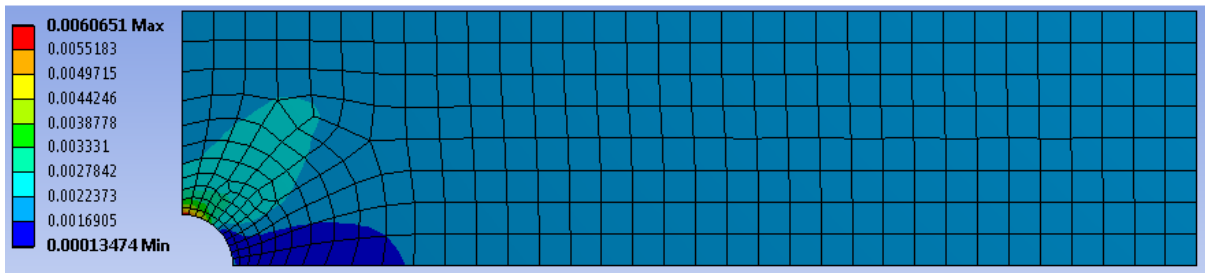


Figure A.40 – Plate D (WSH): Equivalent strain at  $q_u = 16320N/mm$  (linear analysis)

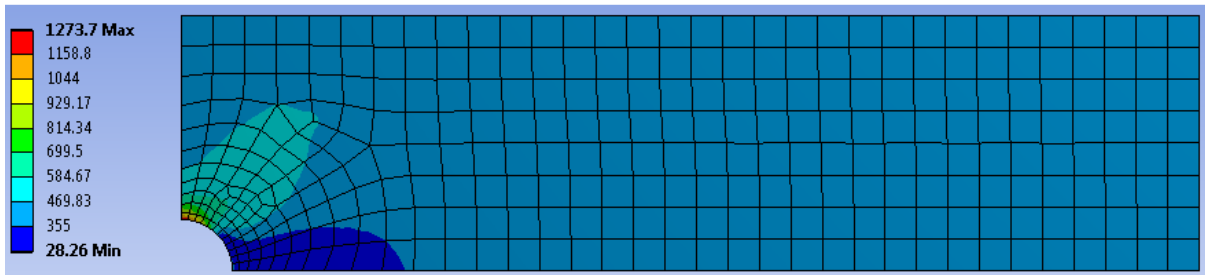


Figure A.41 – Plate D (WSH): Equivalent stress at  $q_u = 16320N/mm$  (linear analysis)

**Plate E**

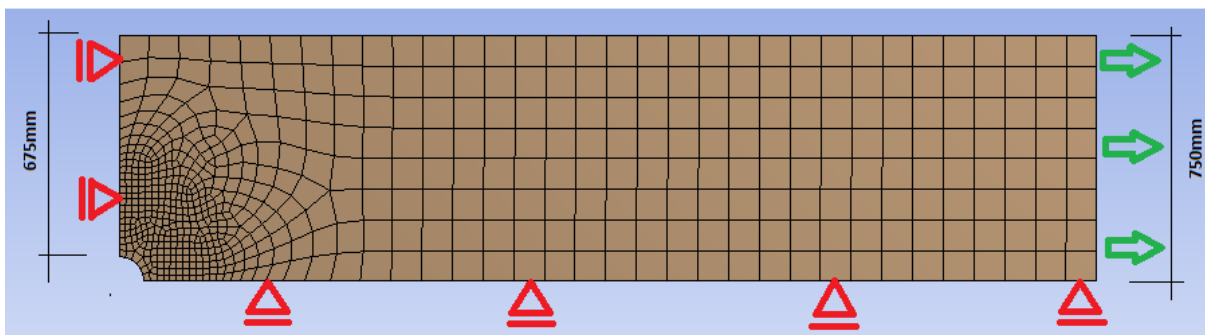


Figure A.42 – Plate E: Mesh geometry, load and boundary conditions of the finite element model

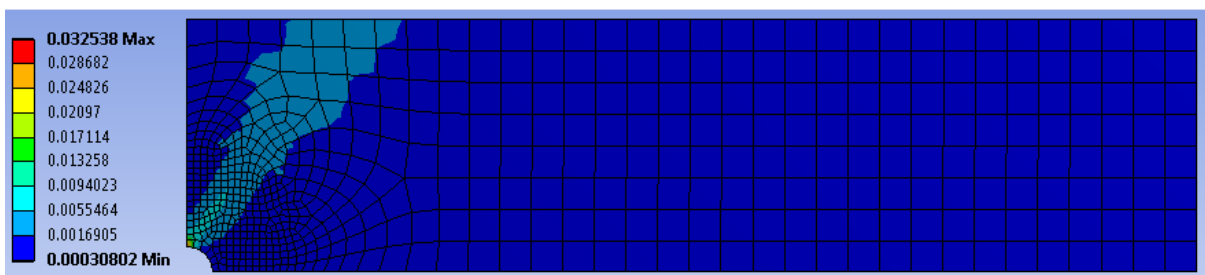


Figure A.43 – Plate E (WoSH): Equivalent strain at  $q_u = 12780N/mm$  (non-linear analysis)

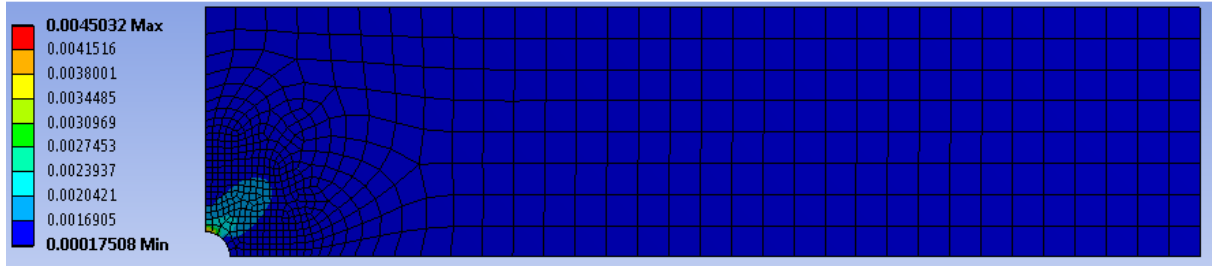


Figure A.44 – Plate E (WoSH): Equivalent strain at  $q_u = 12780N/mm$  (linear analysis)

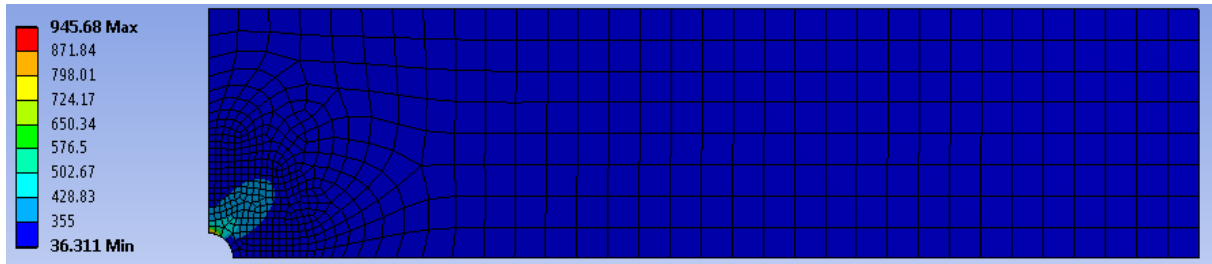


Figure A.45 – Plate E (WoSH): Equivalent stress at  $q_u = 12780N/mm$  (linear analysis)

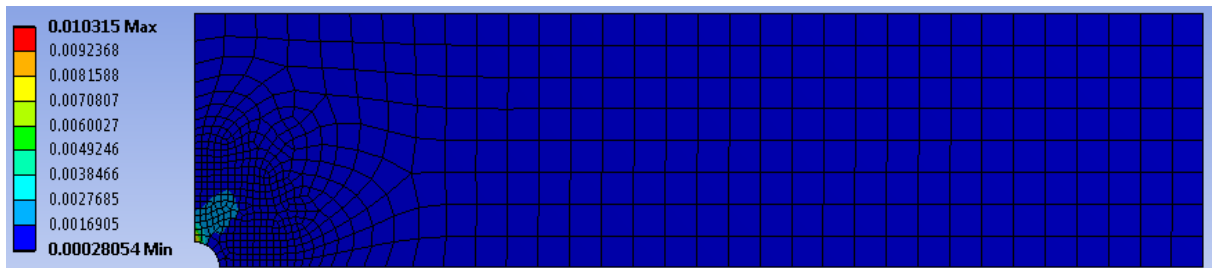


Figure A.46 - Plate E (WoSH): Equivalent strain at  $0.9q_y = 11502N/mm$  (non-linear analysis)

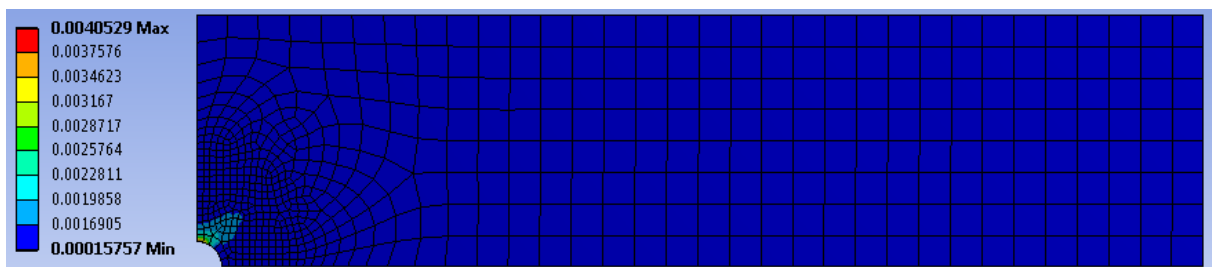


Figure A.47 – Plate E (WoSH): Equivalent strain at  $0.9q_y = 11502N/mm$  (linear analysis)

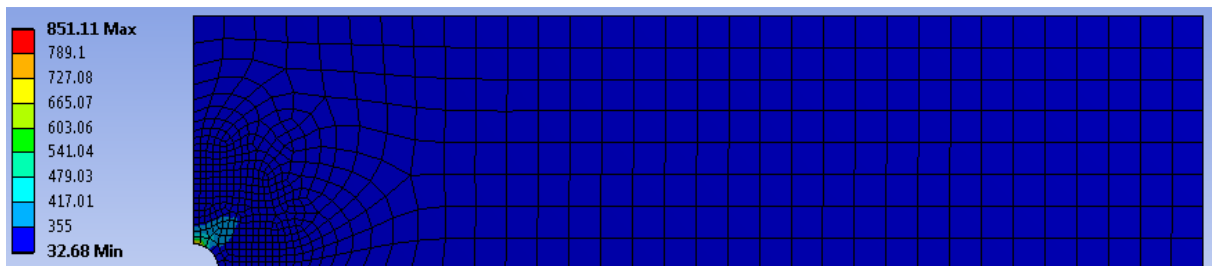


Figure A.48 – Plate E (WoSH): Equivalent stress at  $0.9q_y = 11502N/mm$  (linear analysis)

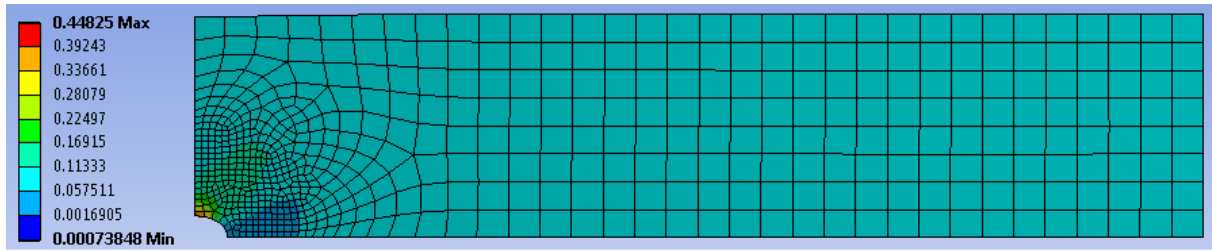


Figure A.49 – Plate E (WSH): Equivalent strain at  $q_u = 18360N/mm$  (non-linear analysis)

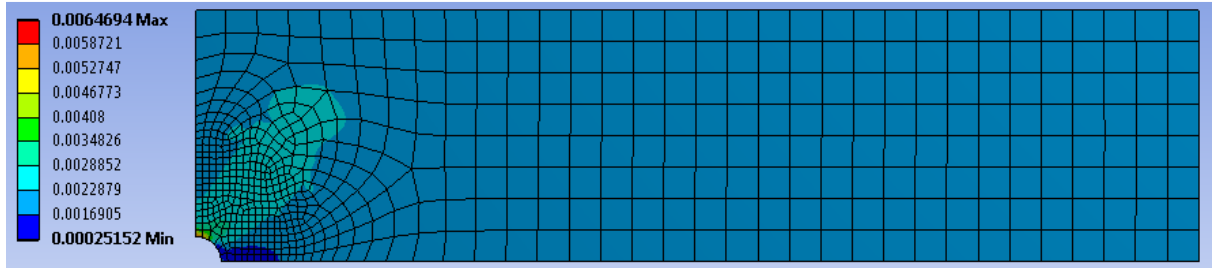


Figure A.50 – Plate E (WSH): Equivalent strain at  $q_u = 18360N/mm$  (linear analysis)

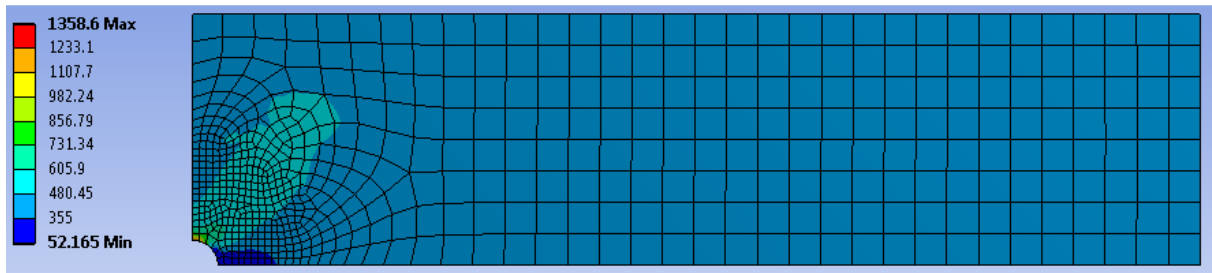


Figure A.51 – Plate E (WSH): Equivalent stress at  $q_u = 18360N/mm$  (linear analysis)

## B. APPENDIX B

In this section a full description of the finite element model of the connection is described.

### Material Properties

Material properties are taken according to Tables 7 to 10 and section 2.5.5. The model is built up only using steel grade S355M with the material parameters as inputted in Ansys illustrated in Table 49

Table 49 – Material properties bridge connection

Outline of Schematic A2: Engineering Data			
	A	B	C
1	Contents of Engineering Data	Source	Description
2	Material		
3	S355M		Fatigue Data at zero mean stress comes from 1998 ASME BPV Code, Section 8, Div 2, Table 5-110.1
*	Click here to add a new material		

Table of Properties Row 12: Bilinear Isotropic Hardening			
	A	B	C
1	Temperature (C)	Yield Strength (Pa)	Tangent Modulus (Pa)
2	22	3.55E+08	7.755E+08
*			

Properties of Outline Row 3: S355M					
	A	B	C	D	E
1	Property	Value	Unit		
2	Density	7850	kg m^-3		
3	Isotropic Secant Coefficient of Thermal Expansion				
4	Coefficient of Thermal Expansion	1.2E-05	C^-1		
5	Reference Temperature	22	C		
6	Isotropic Elasticity				
7	Derive from	Young's Modulus and Po...			
8	Young's Modulus	2.1E+11	Pa		
9	Poisson's Ratio	0.3			
10	Bulk Modulus	1.75E+11	Pa		
11	Shear Modulus	8.0769E+10	Pa		
12	Bilinear Isotropic Hardening				
13	Yield Strength	3.55E+08	Pa		
14	Tangent Modulus	7.755E+08	Pa		
15	Alternating Stress Mean Stress	Tabular			
19	Strain-Life Parameters				
27	Tensile Yield Strength	3.55E+08	Pa		
28	Compressive Yield Strength	3.55E+08	Pa		
29	Tensile Ultimate Strength	4.7E+08	Pa		
30	Compressive Ultimate Strength	0	Pa		

### Geometry

The geometry of the connection was built in DesignModeler making use of the drawings from the A1/A6 Diemen-Almere Havendreef bridge project provided by Iv-Infra. The development of the model geometry is described in the following figures step by step. In order to avoid the occurrence of trivial mistakes and allow later changes in the geometry each step is dependent on the previous one. This means that any data which will be changed in a later phase will result in an automatic update of the geometry, without having to trace step by step where further modifications must be made.

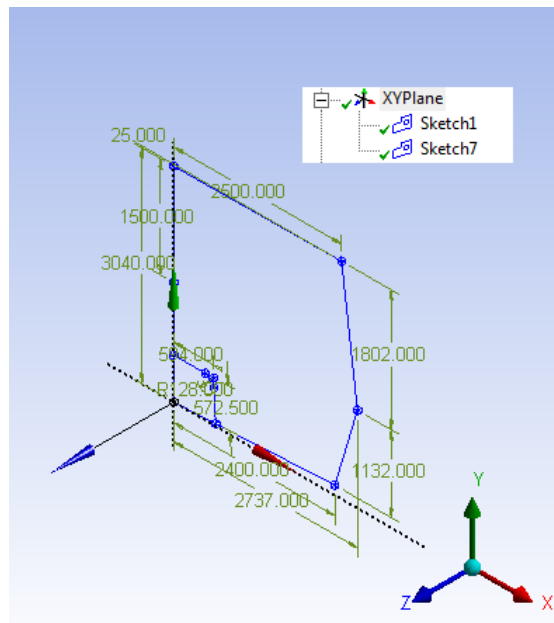


Figure B.1 – Girder Sketch

Two separate sketches are drawn of the girder and longitudinal stiffener with the dimensions taken according to Figure 5.3. This is done in the XY Global Plane at coordinate zero on the Z Global axis.

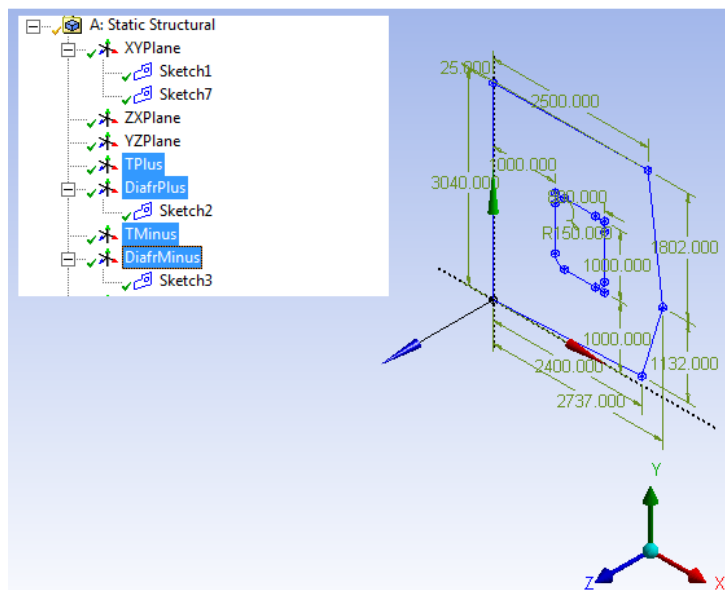


Figure B.2 – Section and diaphragm planes with diaphragm sketch

The TPlus and Tminus planes are placed at a distance of 3800mm and -3800mm respectively along the Z Global axis. They will be later used for sectioning the geometry of the girder in order to be able to define different thicknesses for the plates.

The DiafrPlus and DiafrMinus planes are placed at 4000mm and -4000 millimetres, respectively on the Z Global axis. A sketch of the diaphragm is drawn in both these planes, which will be later defined as a surface representing the real diaphragms from the structure.

All of these four planes are parallel to the XY Global Plane.  
 After the inclination angles of the diagonals was determined from the drawings, the planes normal to these could be drawn at the exact location of the stiffness plates.

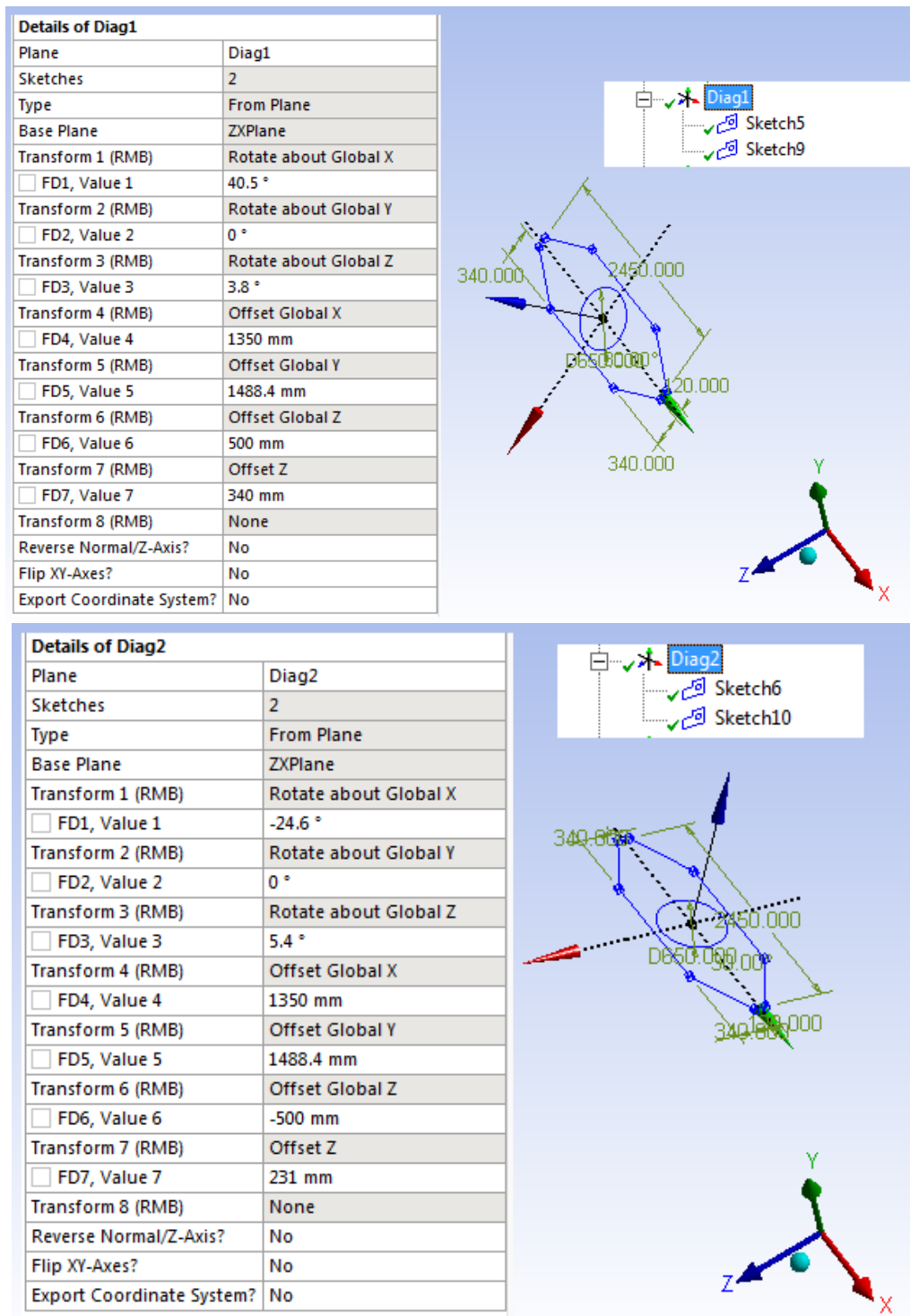


Figure B.3 – Stiffness plate sketch

The offset value along the local Z axis represents the distance to the girder centroid. Two sketches are drawn in both cases, the first representing the stiffener plate while the second (the circle in the images above) will be later used to cut through the upper flange to create the openings through which the diagonals pass.

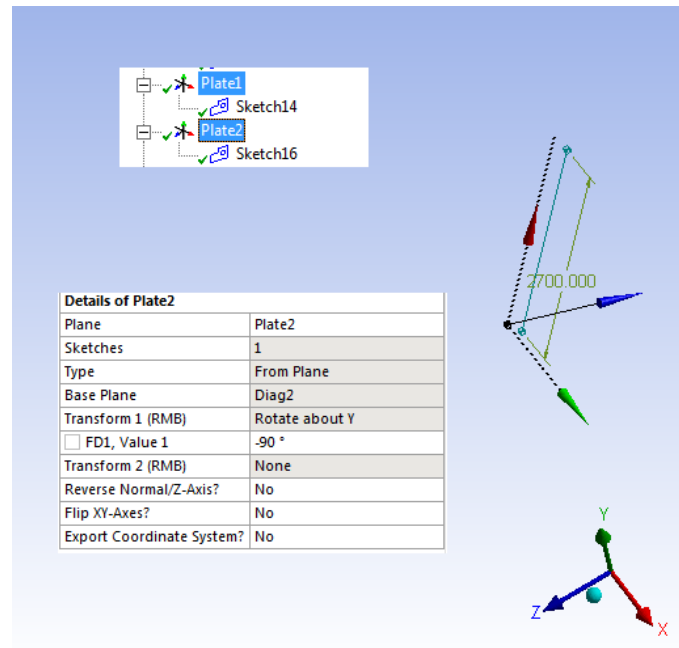


Figure B.4 – Diagonal sketch

In order to build up the geometry of the diagonals, two additional planes are created from the Diag1 and Diag2 planes mentioned earlier. These two new planes, Plate1 and Plate2 are rotated by 90° around the local Y axis in order to be in the same plane as the diagonal. A sketch is drawn in both cases, a line of 2700mm length at a distance of 130mm from the origin along the local X axis and 277.5mm along the local Y axis.

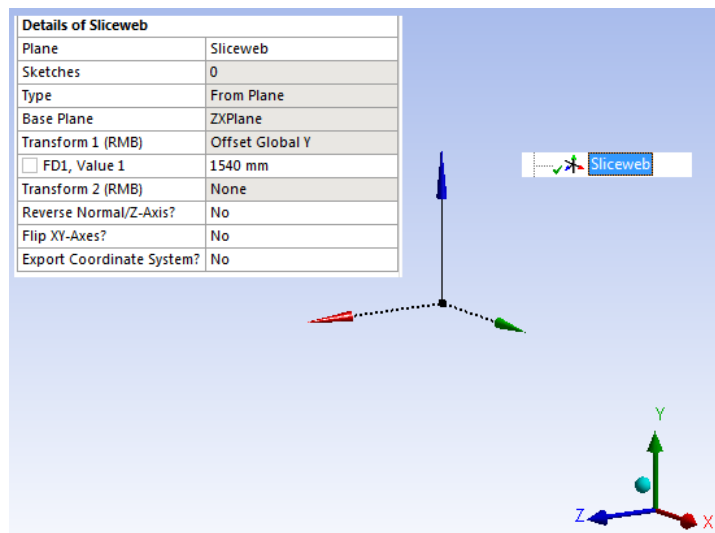


Figure B.5 – Sliceweb plane

The Sliceweb plane, placed at a distance of 1540mm from the Global Coordinate Origin along the Y Global axis, is parallel to the XZ Global plane and will be used in a later step to slice the web in order to define different thicknesses on the section as depicted in Figure 5.7.

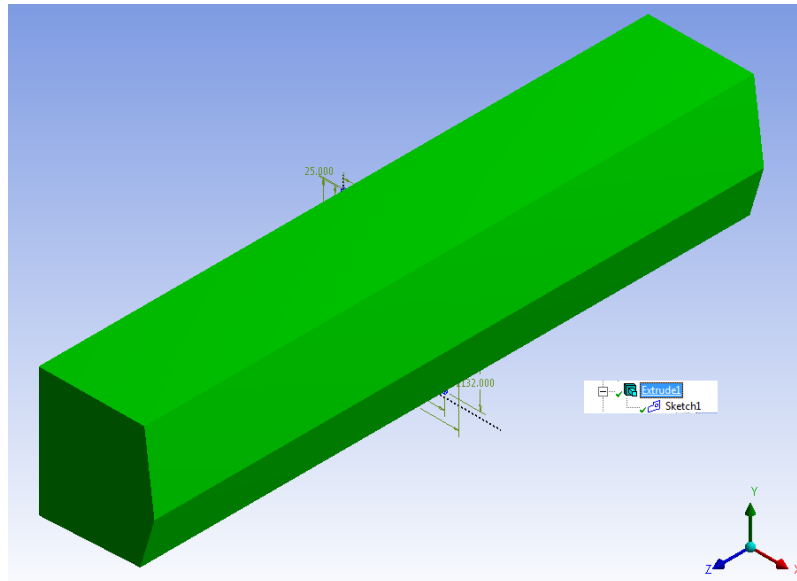


Figure B.6 – Girder extrusion

Using “Extrude” on the girder sketch a body of the beam is created. Using “Surfaces from faces” on the extruded element the girder geometry is created. Afterwards using “Slice”, the geometry is divided so as to be able to define different thicknesses of the elements corresponding to Figure 5.5, Figure 5.6 and Figure 5.8.



Slice 1, 2 and 3 correspond to plane Tplus, Tminus and Sliceweb in order to define different surfaces and assign different thicknesses.

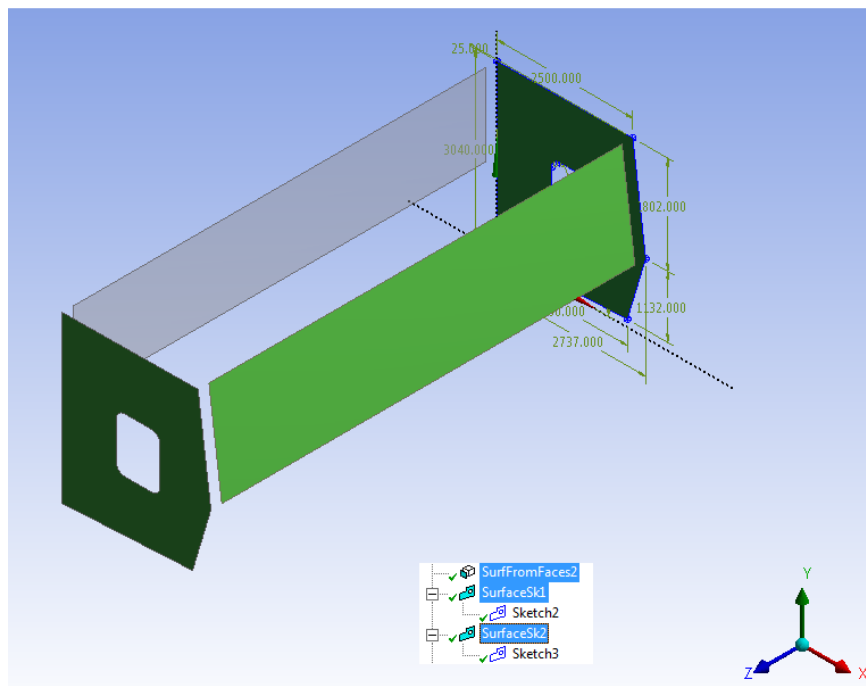


Figure B.7 – Diaphragm geometry

“Surface from sketches” is used to define the geometry of the two diaphragms.

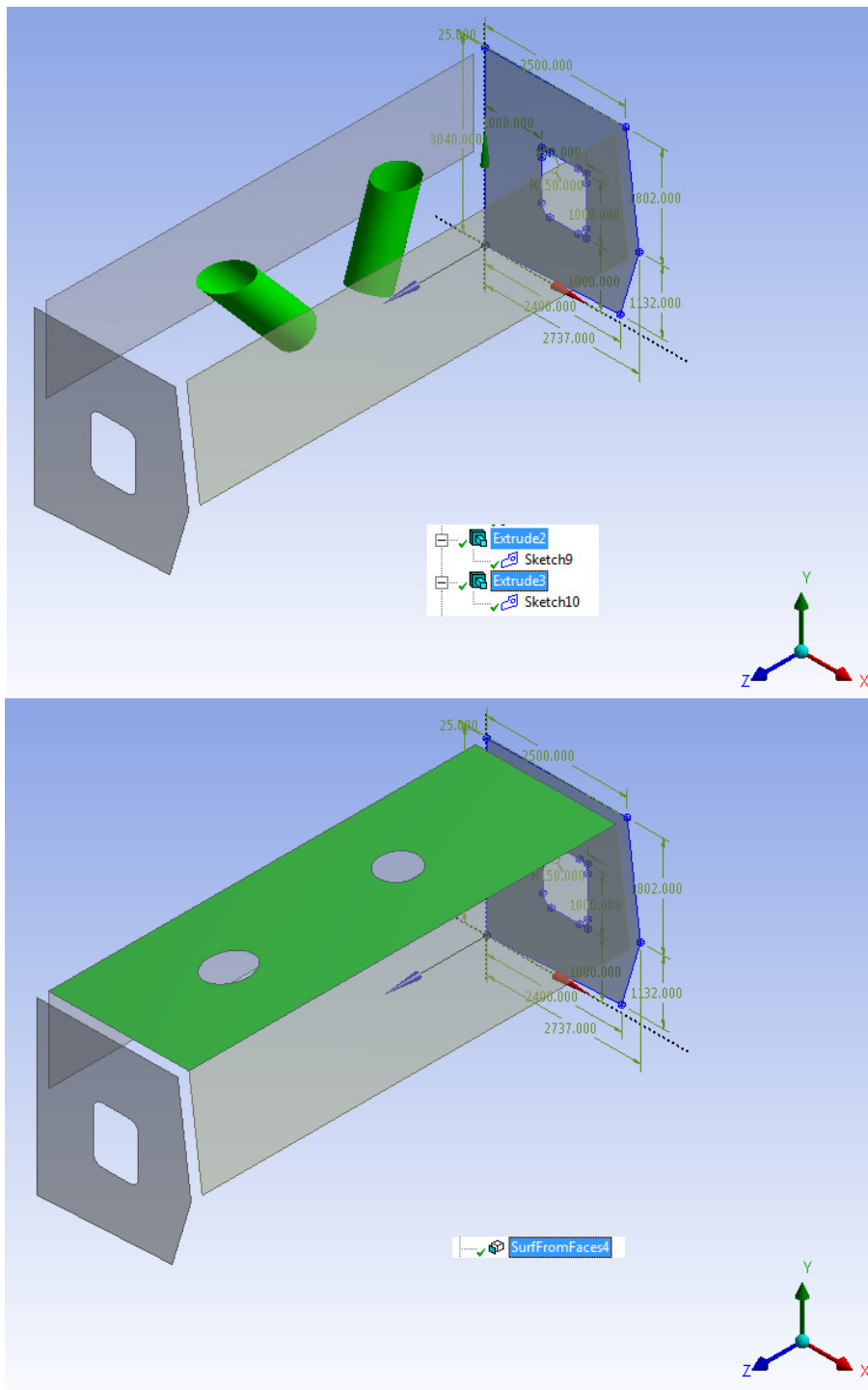


Figure B.8 – Geometry of upper flange

“Extrude” is used to project the Sketches (circles) presented in Figure B.3 the holes in the upper flange are generated. The upper flange was already defined as a surface when assigning the “surface from faces” on the extrusion from the girder sketch. The holes in the upper flange allow a clearance of 20mm around the diagonals in order to ensure no contact between the elements.

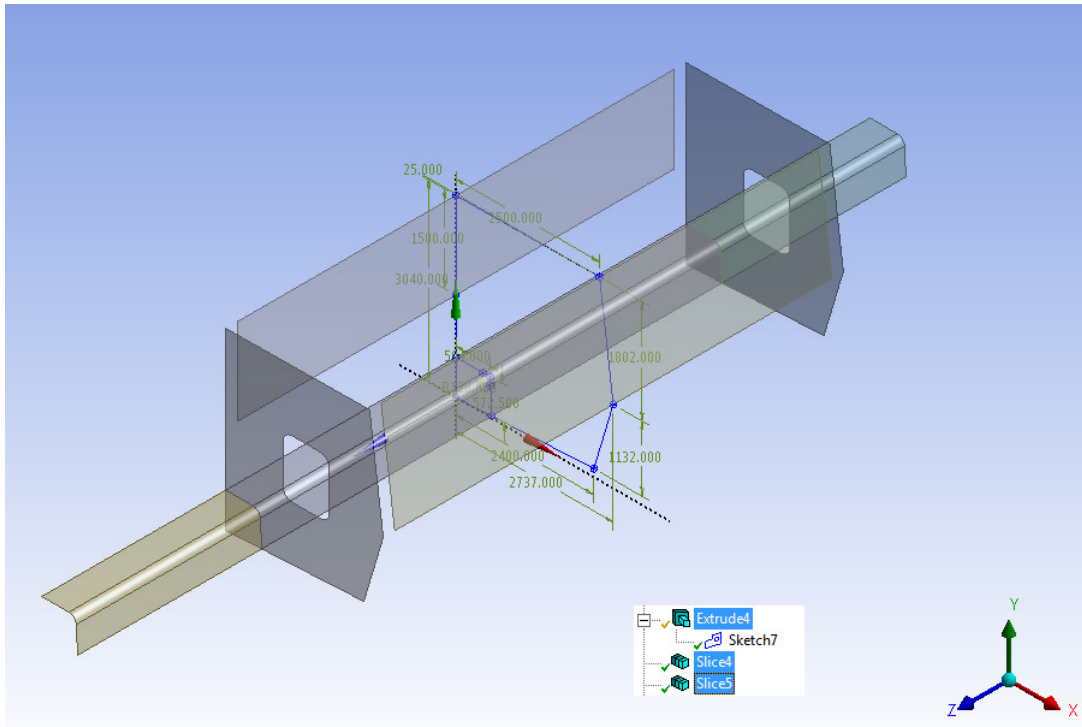


Figure B.9 – Geometry of the longitudinal stiffener

“Extrude” is used on the second sketch from the XY Global plane to create the geometry of the longitudinal stiffener. DiaphragPlus and DiaphragMinus planes are used to slice the newly created element in order to ensure its discontinuity at the diaphragm locations

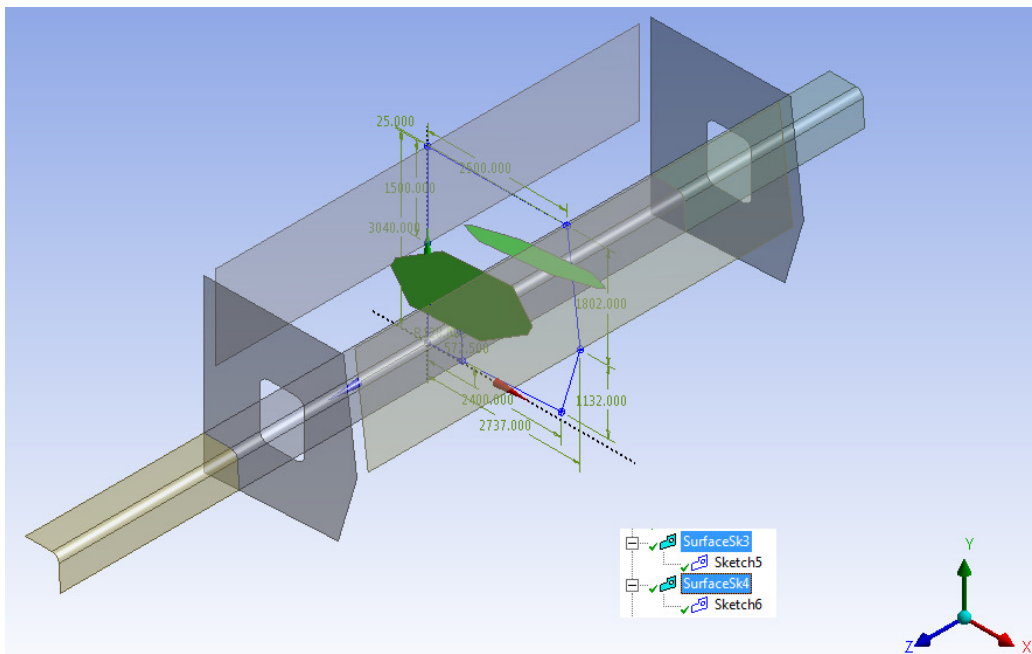


Figure B.10 – Geometry of the diagonal stiffeners

“Surface from sketches” is used on the sketches presented in Figure B.3 in order to create the geometry of the stiffeners of the diagonals.



The planes PlateStifD1 and PlateStifD2 are both normal to the Diag1 and Diag2 planes respectively. Using project sketches and the geometry illustrated in Figure 5.8 new sketches are created of the gusset plates. The geometry of these elements is then defined using “Surface from sketches”.

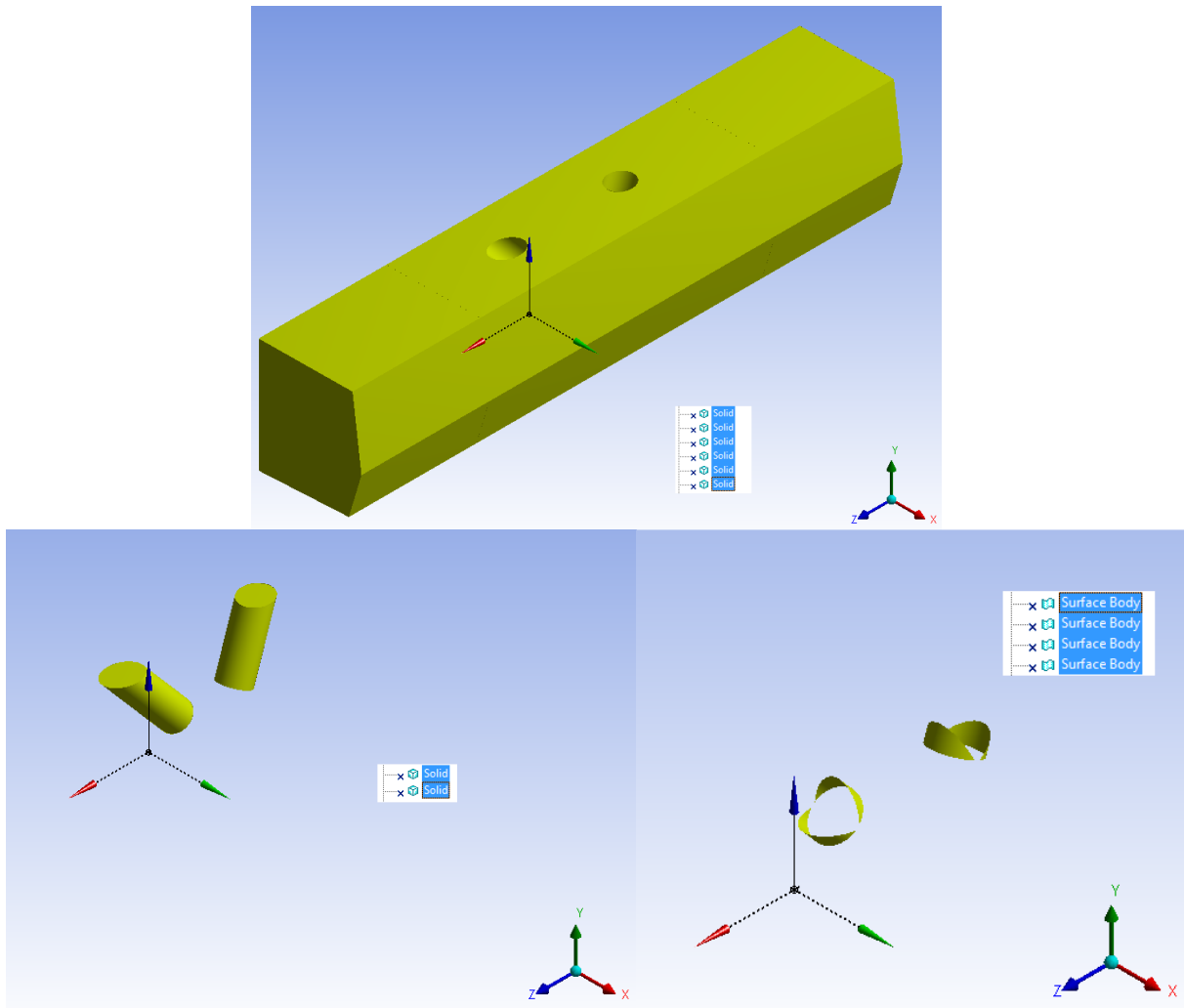


Figure B.12 – Extra solids and surface bodies

The objects presented in Figure B.12 represent the additional solids resulting from the use of “Extrusion” and surface bodies from the use of “Slice” in order to build up the geometry. As they are no longer of any use in the geometry of the joint they are deleted using “Body operation”.



In order to obtain a full working geometry of the connection all the remaining elements are defined as one part and “Share topography” is generated”.



Figure B.13 illustrates the geometry of the joint. The different colours of the surfaces represent separate parts which will be later assigned corresponding thicknesses.

When surfaces are created there are two options for the operation, namely “Add Material” and “Add Frozen”. If the first option is chosen then the material created is added to the existing body forming a union. Each of the elements generated in this geometry are separate parts and interact with each other. This is the reason why in all the cases “Add Frozen” is used. The material created does not add to the existing one and thus they become two separate parts enabling each one of them to be meshed independently. Another detail that can be provided in the “Surface from sketches” is the thickness. In all cases a zero value is defined. If a nonzero value would be provided this would result in the creation of “thin” solid bodies instead of surface bodies. The main difference between the two is that in the first case the parts would be meshed with solid elements while in the latter case the mesh will be created using shell elements, which is the desired outcome.

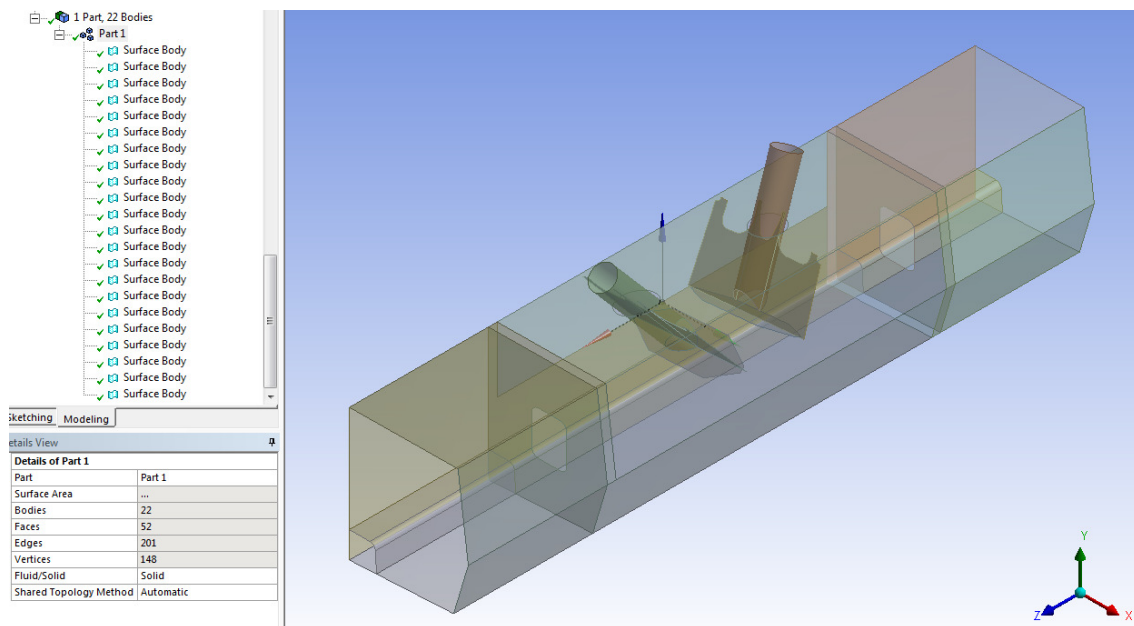


Figure B.13 – Joint geometry

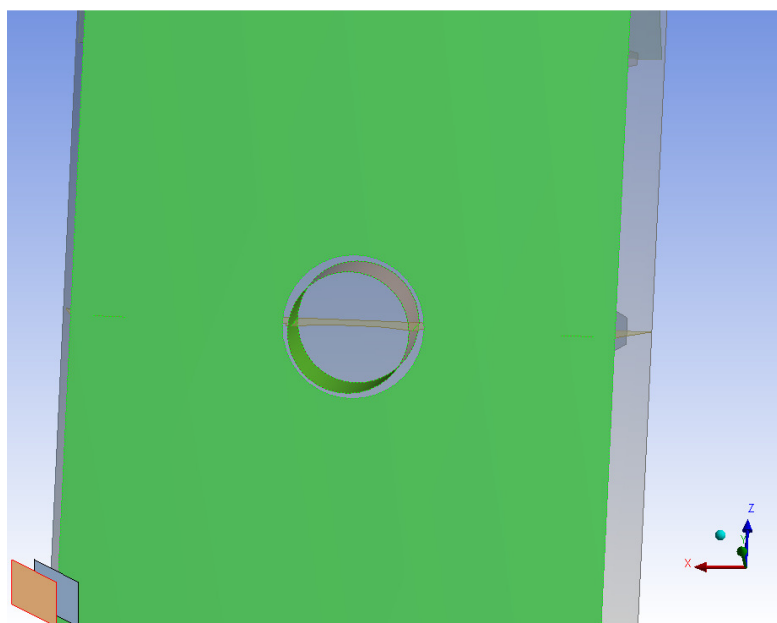


Figure B.14 – Clearance around diagonal

At this stage the geometry of the model is complete in DesignModeler and the next step is to open it in Mechanical under the “Static Structural” Analysis System. In Mechanical under “Geometry” the material and thickness are assigned for each of the surface bodies.

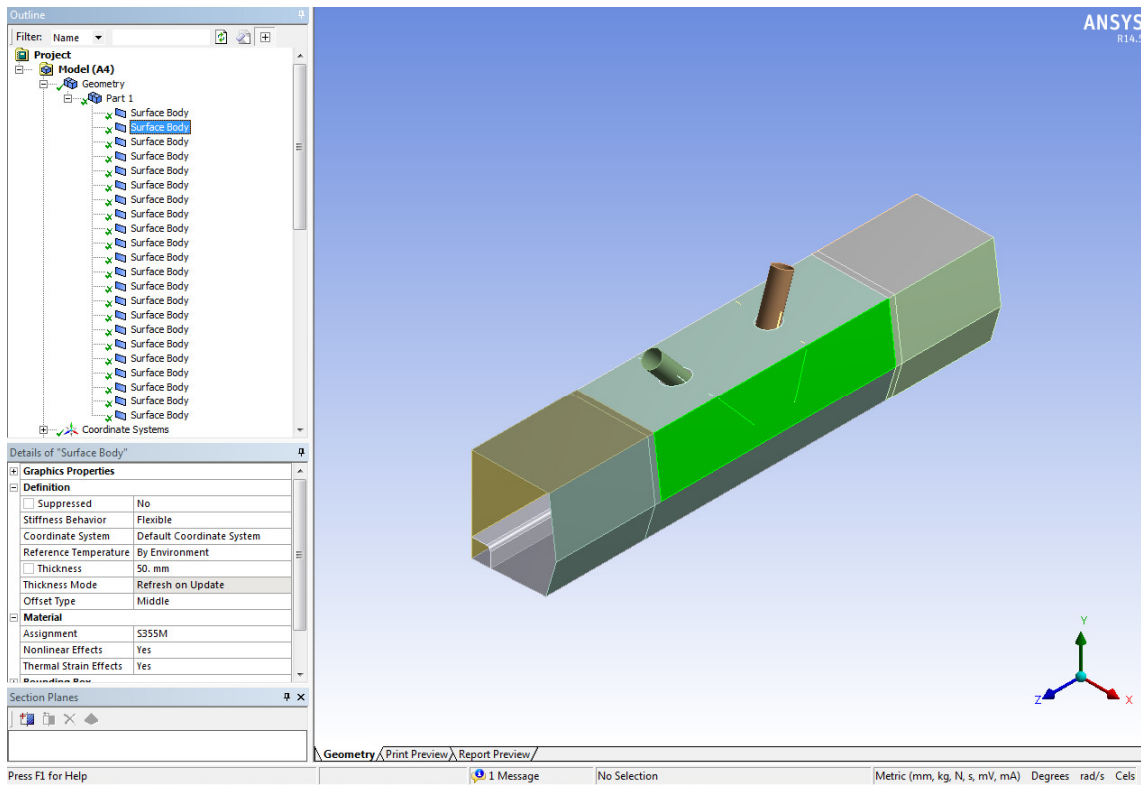


Figure B.15 – Thickness and material assignment in “Mechanical”

In DesignModeler the different thicknesses of the parts can now be displayed. The different colours represent the thicknesses corresponding to each of the surface elements.

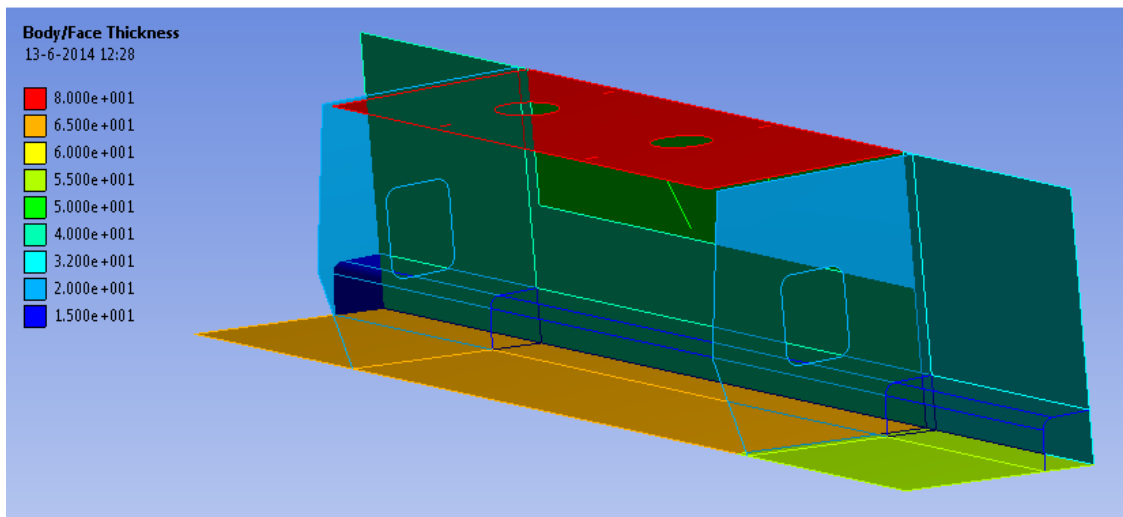


Figure B.16 – Thickness flanges and inner web

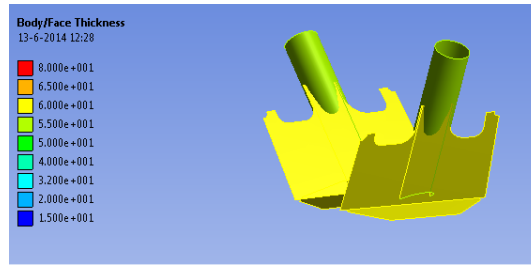


Figure B.17 – Thickness diagonals, gusset plates and stiffeners

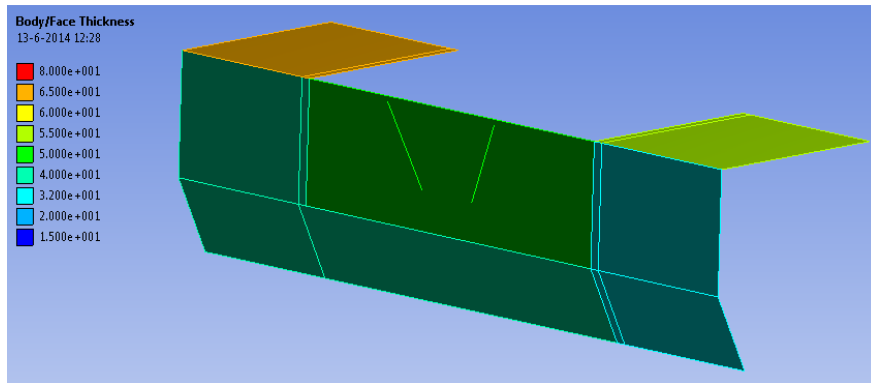


Figure B.18 – Thickness of the outer web

### Boundary Conditions

The boundary conditions are chosen such as to simulate as close as possible the real behaviour of the joint within the bridge structure. Special attention is given to how they would influence the behaviour of the gusset plate and the upper flange as these elements are of main focus due to the stress concentrations occurring there.

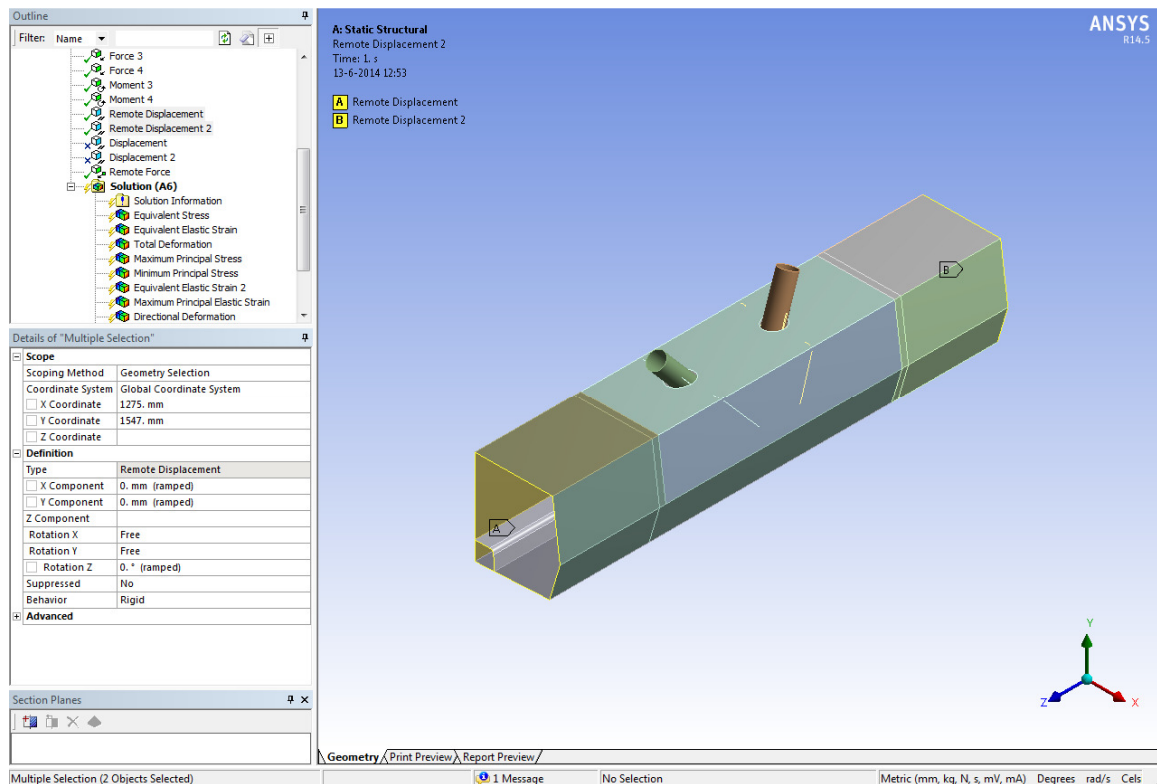


Figure B.19 – Boundary conditions at the joint ends

“Remote Displacement” is applied at the ends of the girder on the cross-section. The advantage is that it can be applied at a location anywhere in space with the equivalent displacement and rotation being calculated and applied on the body by Ansys. When applying the constraint on the edges on the cross-section, the centroid does not coincide with that of the girder as the thickness is not taken into account. Using “Remote Displacement” gives the possibility to manually place it at the exact location of the centroid of the girder. At both A and B location the displacement in the X and Y global directions and rotation about Z global axis are constrained and at location B additional zero displacement along the Z global axis is applied. This means that the vertical shear force, transversal forces and torsion moment are constrained, but all of these have a negligible effect on the stress concentrations development in the connection. Constraint along the global Z axis will result in an axial force at location B which brings the system in equilibrium. Also, for both end constraints the behaviour is chosen to be “Rigid”. This is due to the fact that the surrounding elements (the rest of the bridge structure to which it is connected) significantly stiffens the model at the attachment points and it will maintain its initial shape (the geometry will not deform).

### Loadings

The loading case is implemented from the K050-DO-B-005 report of the A1/A6 Diemene-Almere Havendreef project of Iv-Infra. Thus the real stress behaviour of the joint within the entire bridge structure is simulated. In order to simplify the model the loading from the transversal beams is neglected as this will mainly introduce shear force and torsion moment which have a negligible effect on the stress concentration development in the gusset plates and upper flange, the locations of highest concern with respect to stress concentrations.

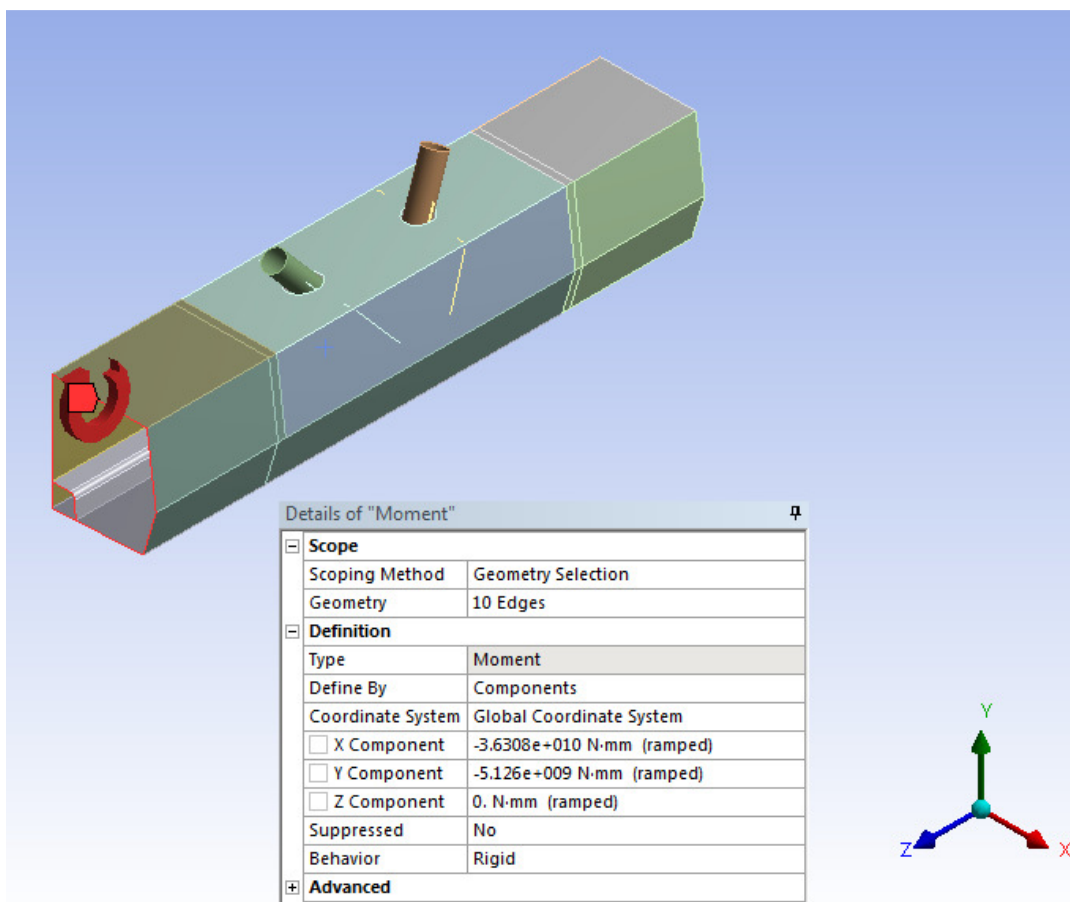


Figure B.20 – Bending moment at A

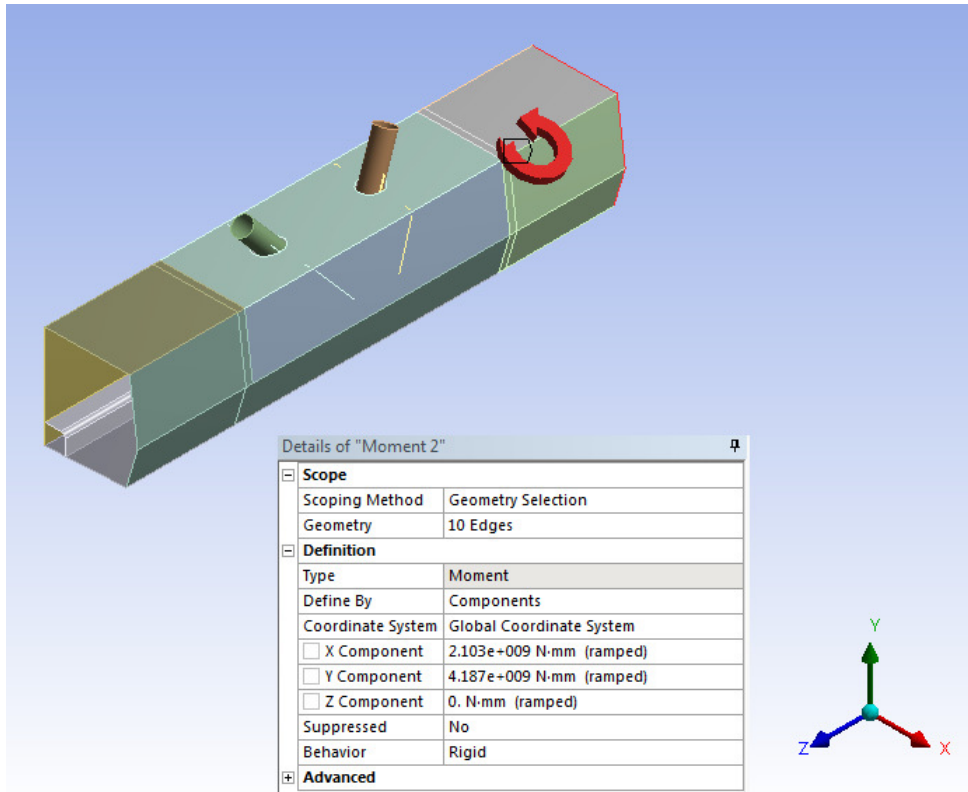


Figure B.21 – Bending moment at B

The bending moments at the girder ends are shown in Figure B.20 and Figure B.21. In both cases the torsional bending moment is not taken into consideration due to its negligible effect on the stress concentrations in the gusset and top flange.

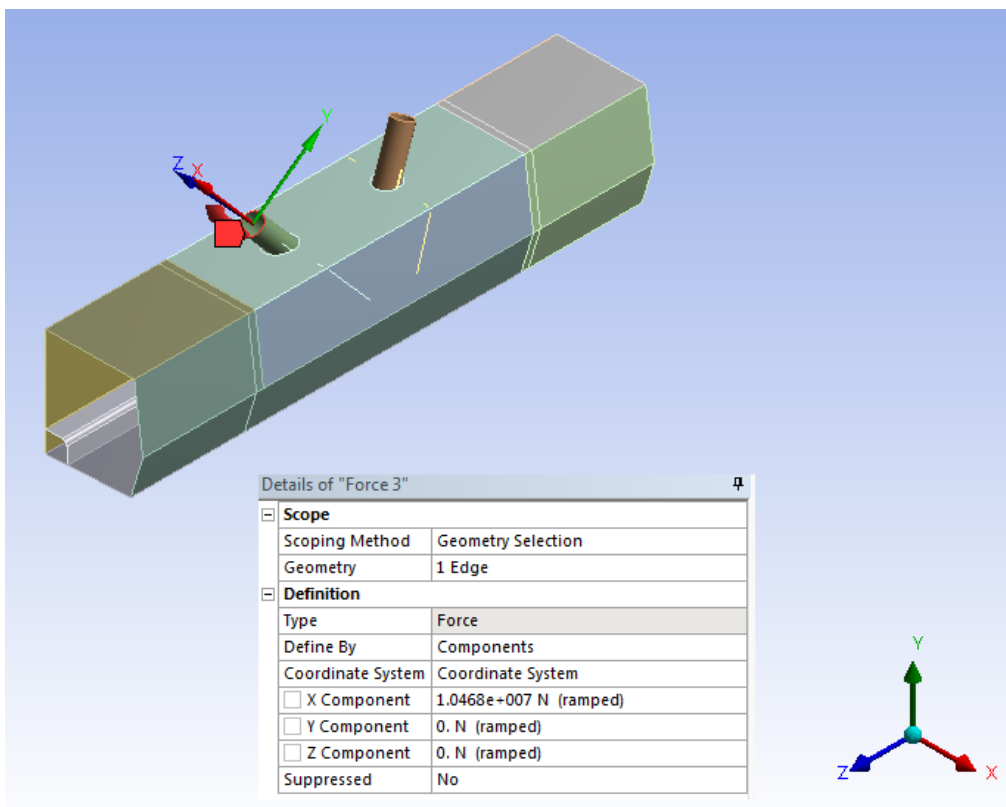


Figure B.22 – Axial force in Diagonal C

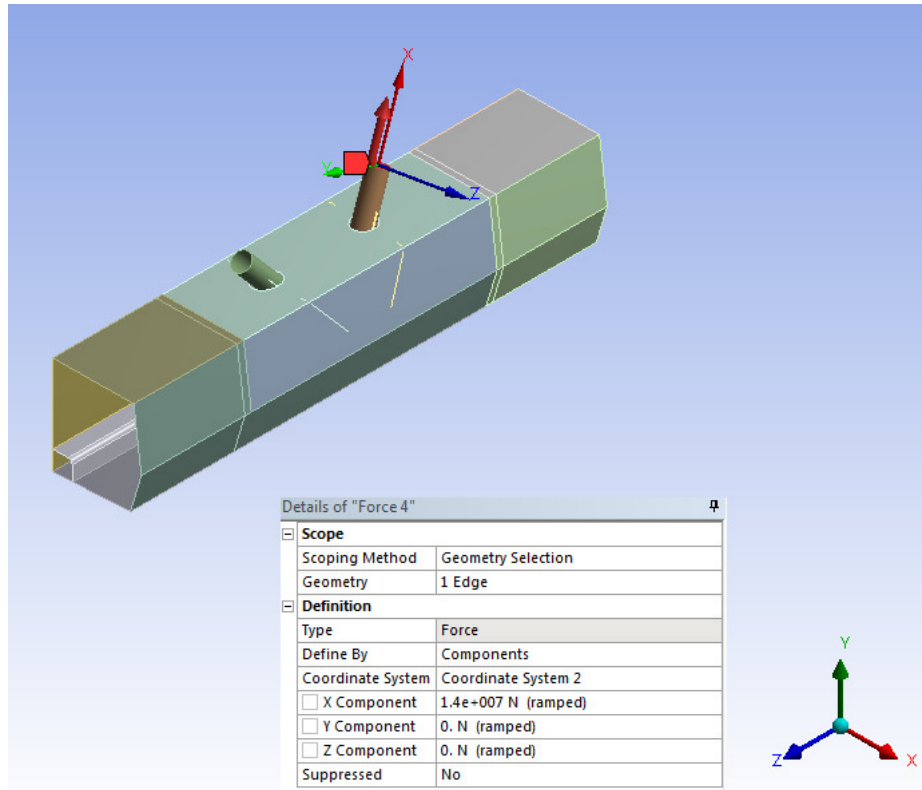


Figure B.23 – Axial force in Diagonal D

In the case of the forces acting on the diagonals only the axial force is taken into account. The shear forces are two order of magnitudes lower(223kN and 26kN compared to 10468kN and 150kN and 37kN compared to 14000kN respectively) and the stress development resulting from them is negligible.

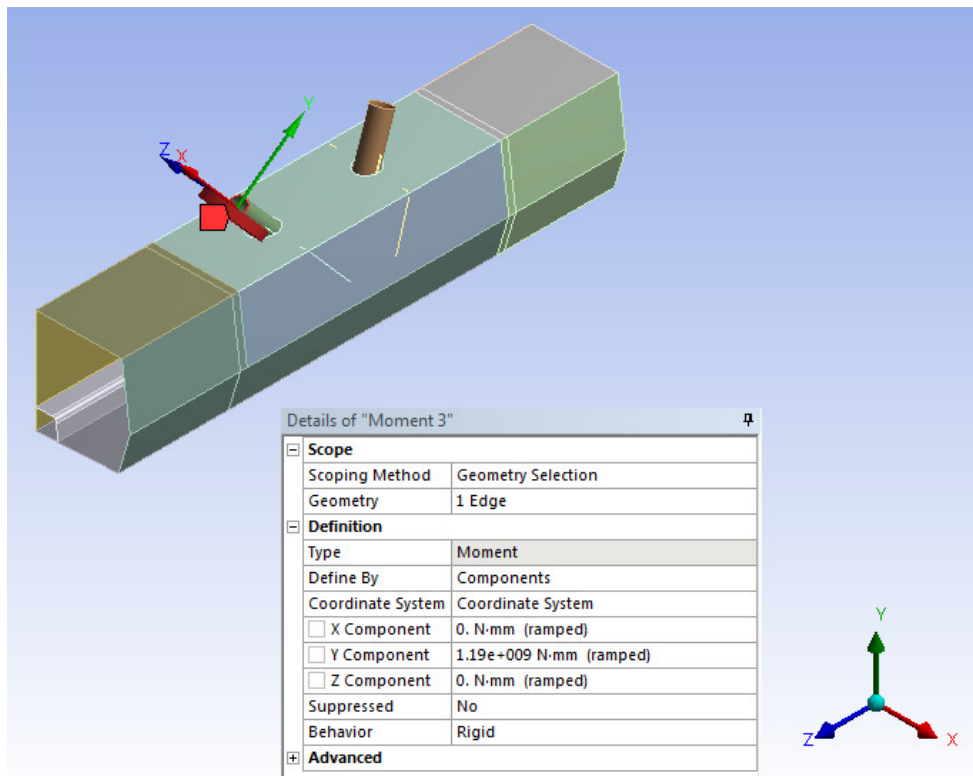


Figure B.24 – Bending moment in Diagonal C

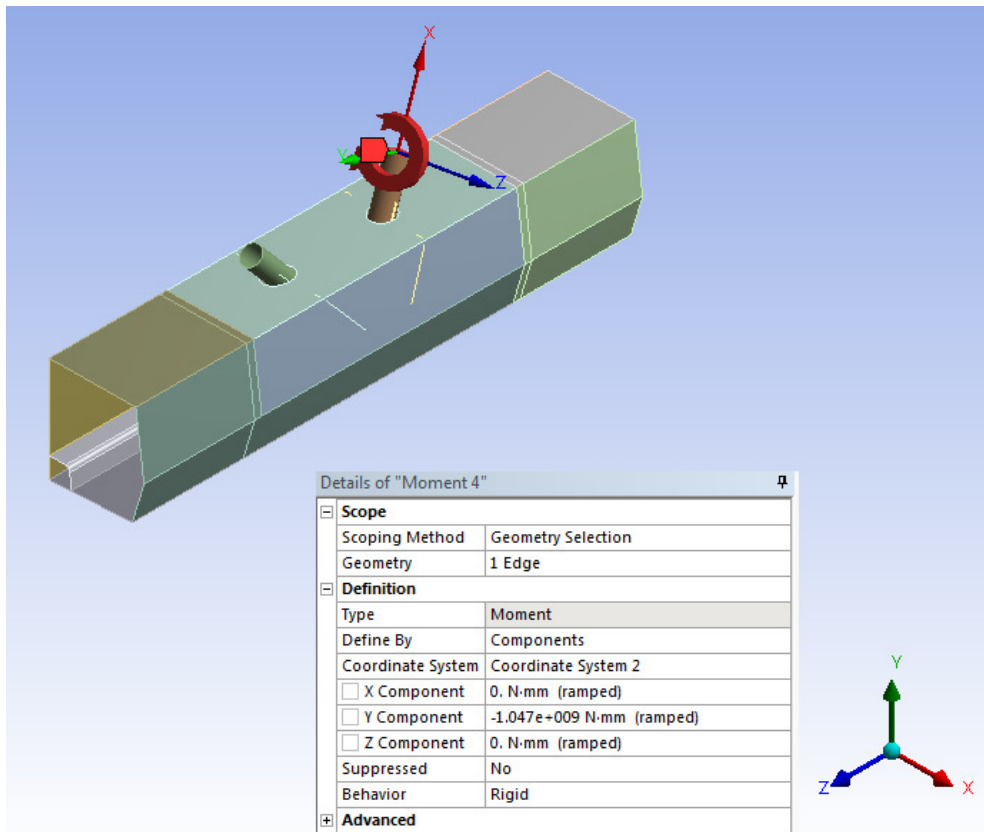


Figure B.25 – Bending moment in Diagonal D

The bending moment about the local Y axis is taken into consideration. The torsional bending moment and the one about the local Z axis are neglected as they are two orders of magnitude lower, corresponding to values of around 50kNm.

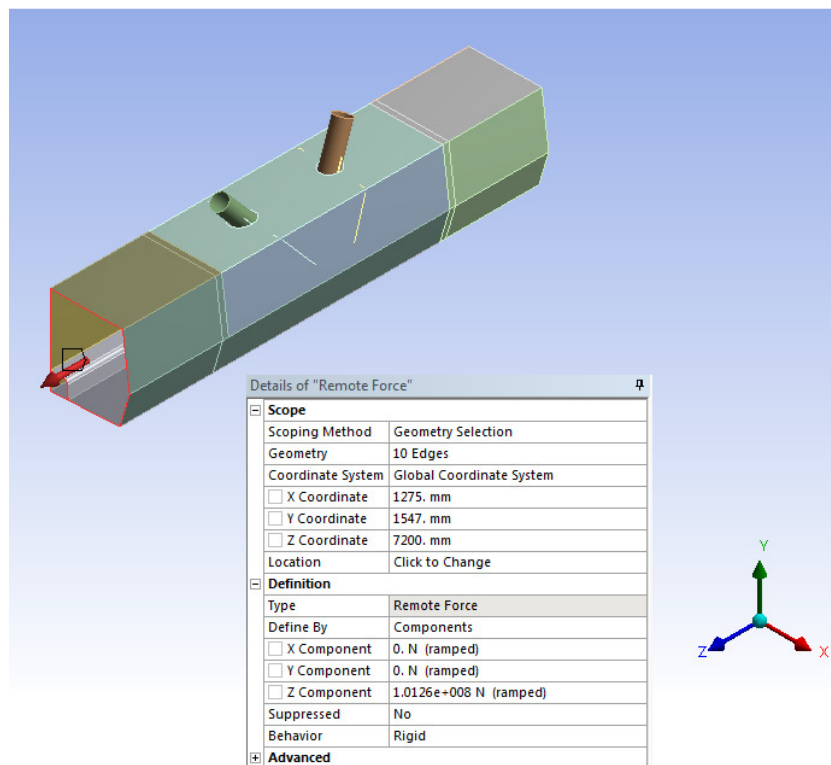


Figure B.26 – Axial force at A

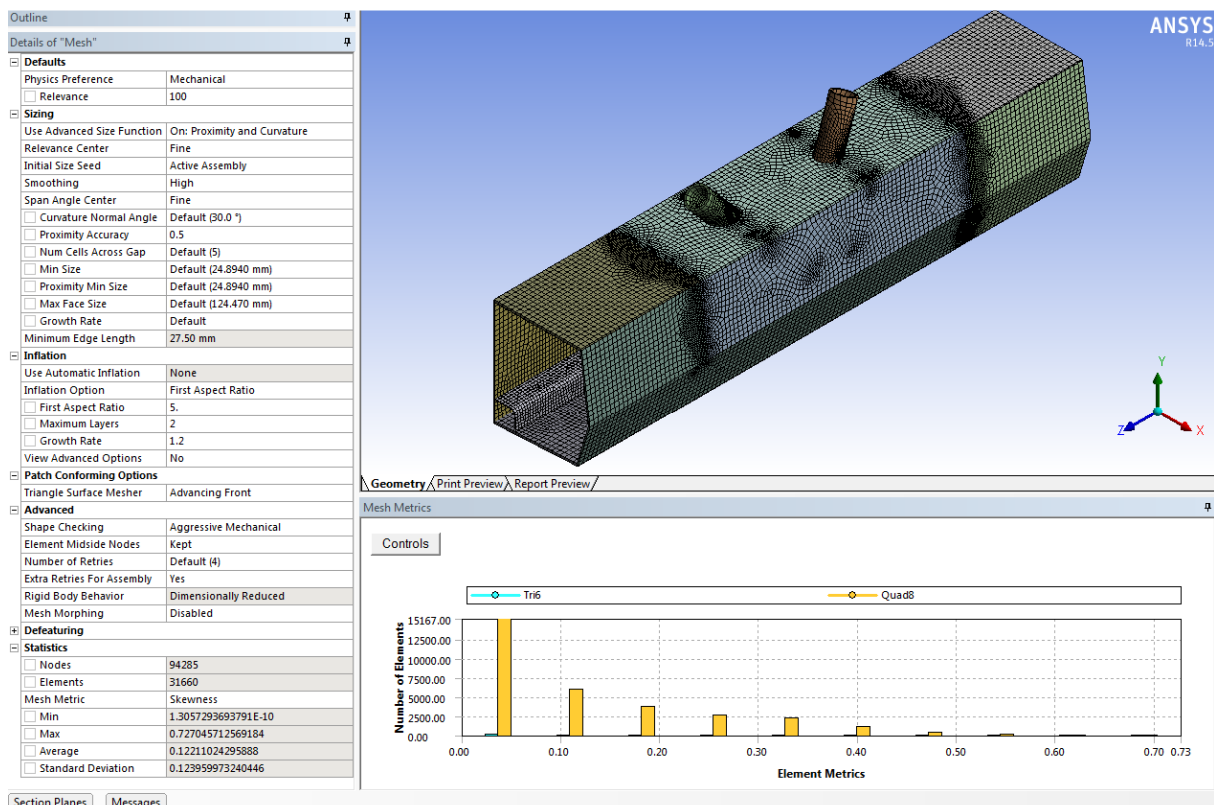
In the case of forces acting on the girder, only the axial force at the A location is inputted into the model. The shear force in X and Y global axis directions are not considered in the development of the stress concentrations as their effect is negligible and their order of magnitude is 3 and 4 times lower respectively. In order to have some insight into whether the load input is correct, the resultant force at the B location on the girder should be similar in magnitude to the one at A. “Remote Froce” is preffered for input as it gives the possibility to place the loading at the exact location of the centroid of the cross-section and thuis avoid eccentricities resulting in second order effects.

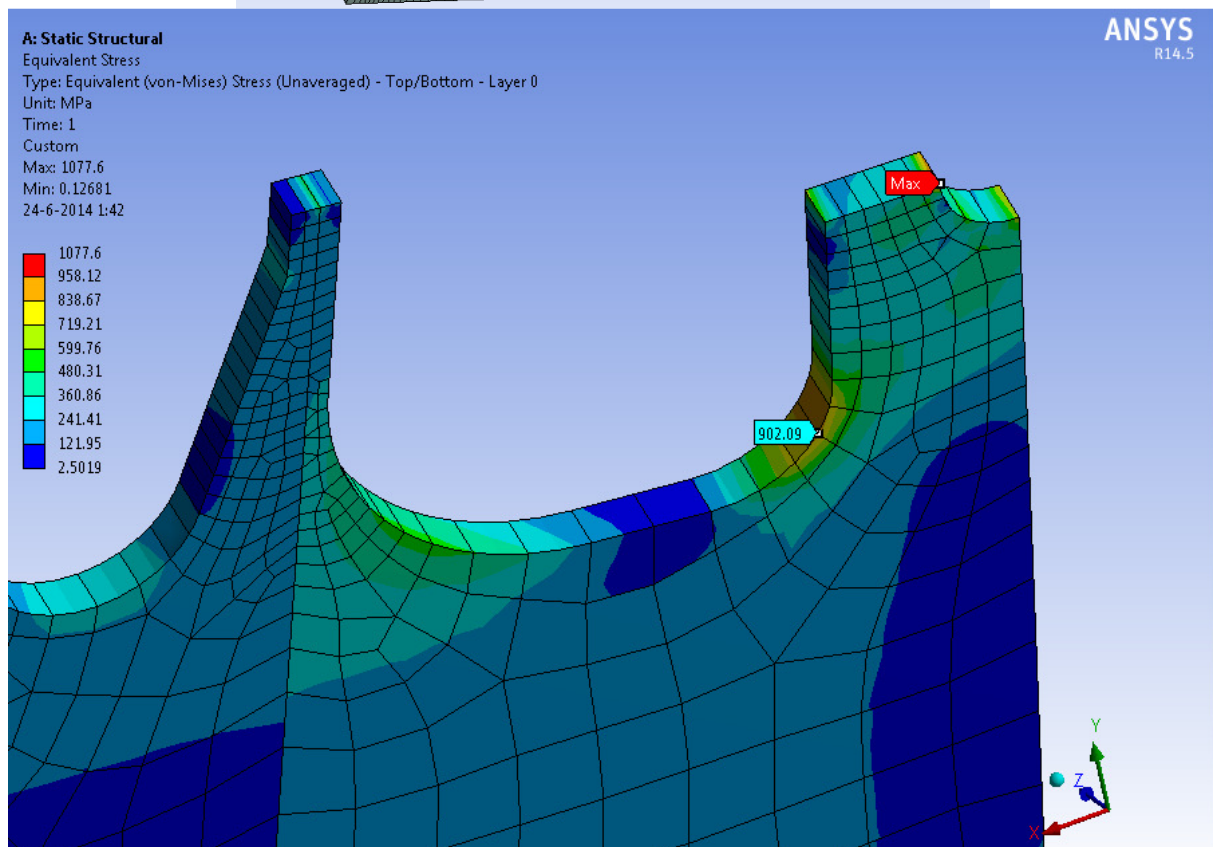
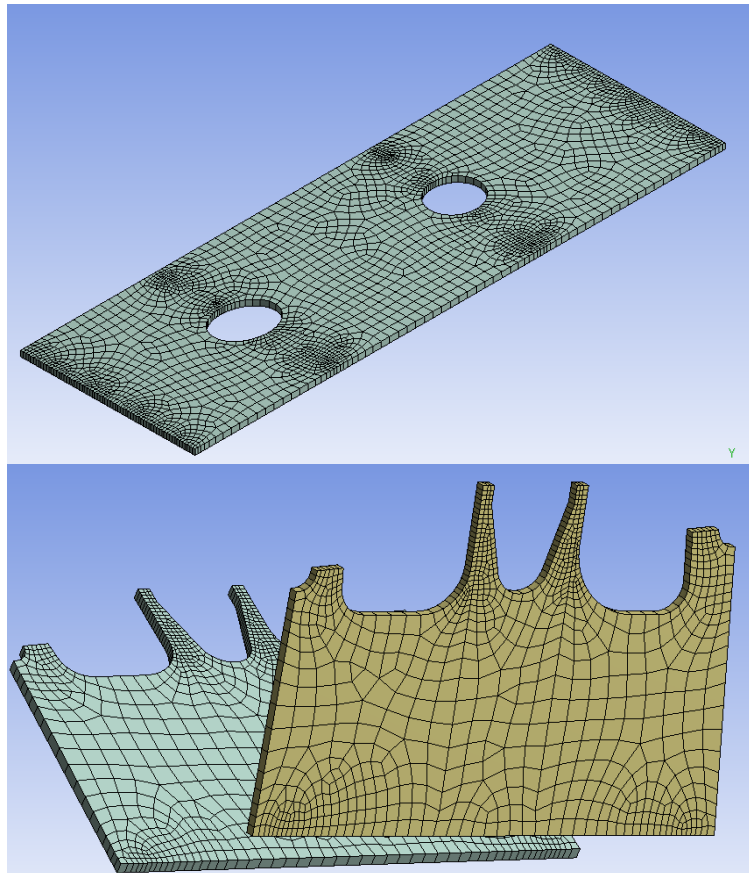
## Mesh

The mesh must balance two requirements: too many elements and this will result in long solver runs, and too few might lead to inaccurate results.

As the element midsize nodes are kept the surface bodies are meshed using SHELL281 which is a 3D 8-node second-order structural shell. Each node has 3 translational and 3 rotational degrees of freedom. In its natural shape the element is quadrilateral but can also degenerate to a triangle (Figure 5.17).

In order to arrive at an optimal mesh a step by step procedure is carried out analysing different mesh results. In the first case presented below the mesh is constructed as fine as possible.





In this situation a maximum stress occurs at the location corresponding to “Max” in the figure above. The second largest stress concentration occurs at the curvature with a value of 902.09MPa. The problem is which of the two values should be used. Looking at the mesh

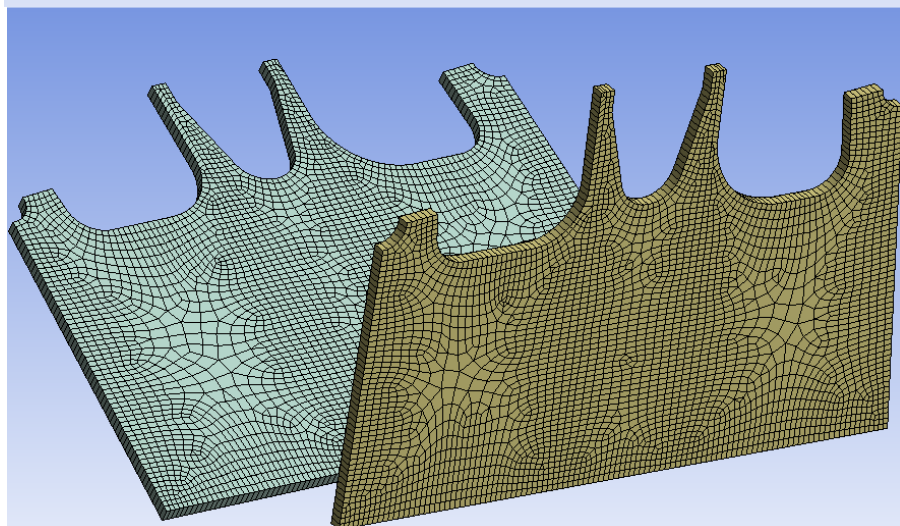
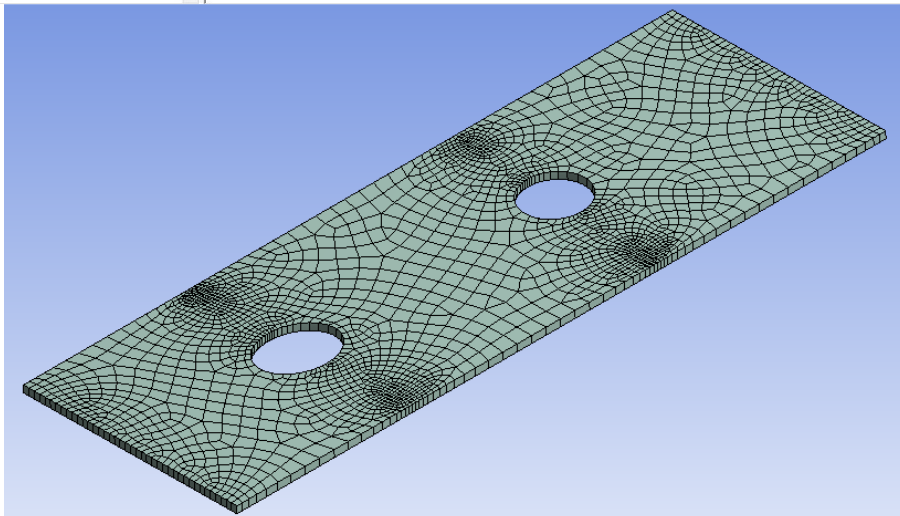
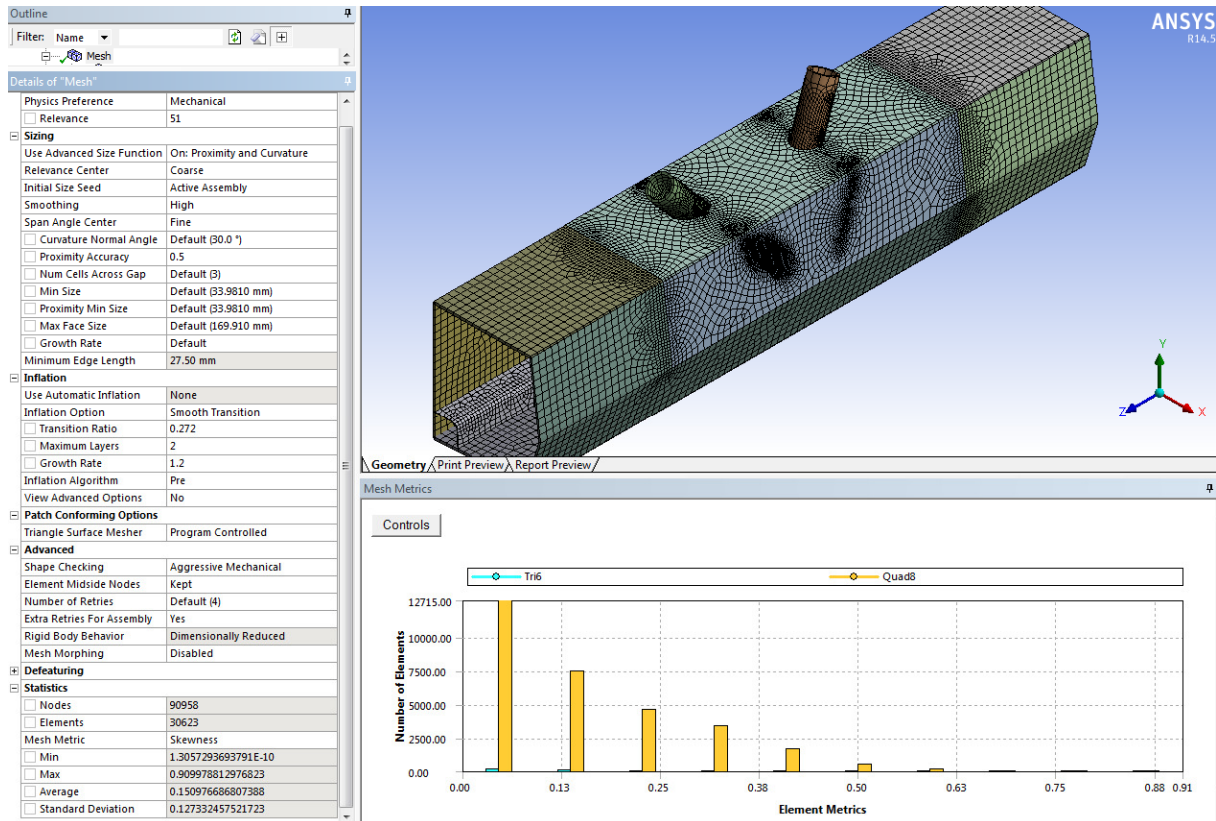
next to the “Max” location, the element dimensions there are smaller than the thickness which might lead to unusable results. In order to have a better insight at the true stress development some simplification steps are carried out:

- The “Relevance Center” can be switched to “Coarse” as midsize nodes are kept;
- The “Inflation Option” can be switched to “Smooth Transition”;
- In the “Patch Conforming Options” the “Triangle Surface Mesher” is set to Program Controlled. This option determines which triangle surface meshing strategy will be used. The mesher determines whether to use the Delaunay or advancing front algorithm based on a variety of factors such as surface type, face topology, and defeatured boundaries;
- In the “Advanced” tab, Aggressive Mechanical is kept for the “Shape Checking”. This uses a criterion based on Jacobian ratio at nodes with a tighter limit on both Jacobian ratio and ANSYS Workbench metric. This is a recommended option for the case when large deformations or material nonlinear analyses are carried out. The “Number of Retries” option which specifies how many times the mesher will try to remesh if meshing fails is kept at a default value of 4. The “Rigid Body Behavior” is Dimensionally Reduced which means that it generates a surface contact mesh only rather than a full mesh. “Mesh Morphing”, which updates changes in nodes coordinates (but is not designed to accommodate severely deformed geometries) is kept Disabled.
- In the “Defeaturing” tab the “Automatic Mesh Based Defeaturing” is kept on. This has the purpose of automatically defeating small features and dirty geometry according to the “Defeaturing Tolerance” specified there.

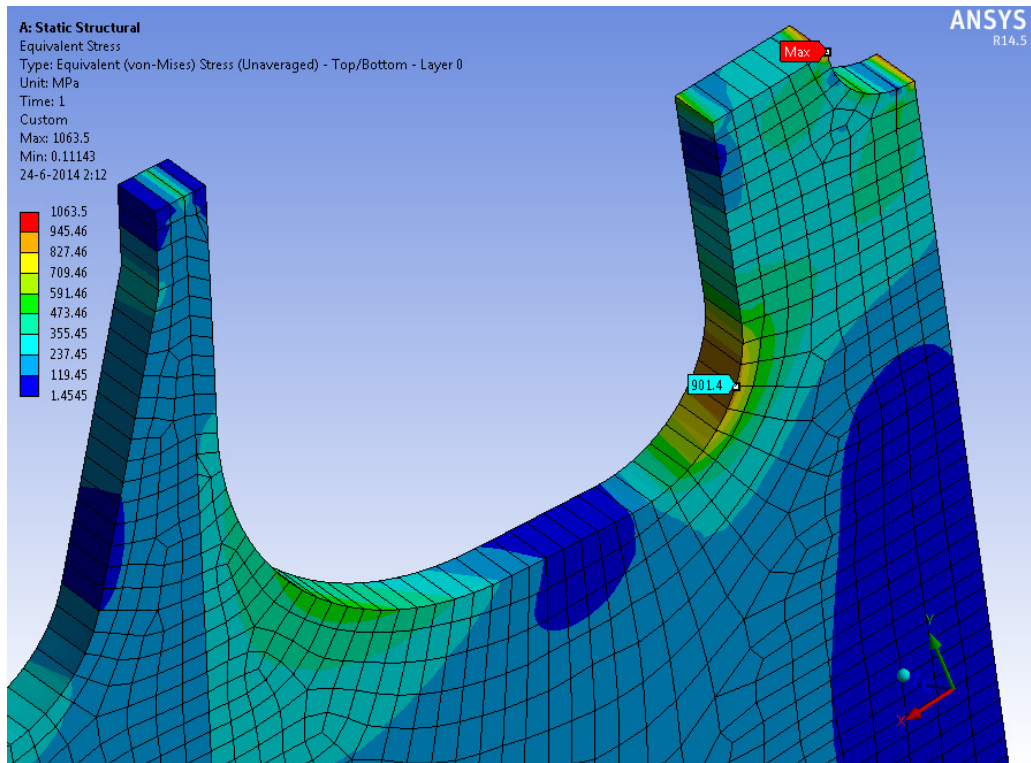
<b>Inflation</b>			
Use Automatic Inflation	None		
Inflation Option	Smooth Transition		
<input type="checkbox"/> Transition Ratio	0.272		
<input type="checkbox"/> Maximum Layers	2		
<input type="checkbox"/> Growth Rate	1.2		
Inflation Algorithm	Pre		
View Advanced Options	No		
<b>Patch Conforming Options</b>			
Triangle Surface Mesher	Program Controlled		
<b>Advanced</b>		<b>Defeaturing</b>	
Shape Checking	Aggressive Mechanical	Use Sheet Thickness for Pinch	No
Element Midside Nodes	Kept	Pinch Tolerance	Default (29.7140 mm)
Number of Retries	Default (4)	Generate Pinch on Refresh	No
Extra Retries For Assembly	Yes	Sheet Loop Removal	No
Rigid Body Behavior	Dimensionally Reduced	Automatic Mesh Based Defeaturing	On
Mesh Morphing	Disabled	<input type="checkbox"/> Defeaturing Tolerance	Default (24.7620 mm)

In the second model the “Relevance Center” is set to Coarse because the midsize nodes are kept. Edge sizing has been added for the gusset plates with a 25mm element size and a “Hard” behaviour meaning the mesh generated on these edges will be projected on the surrounding elements.

# Influence of Ductility in the Design of (High Strength) Steel Bridges

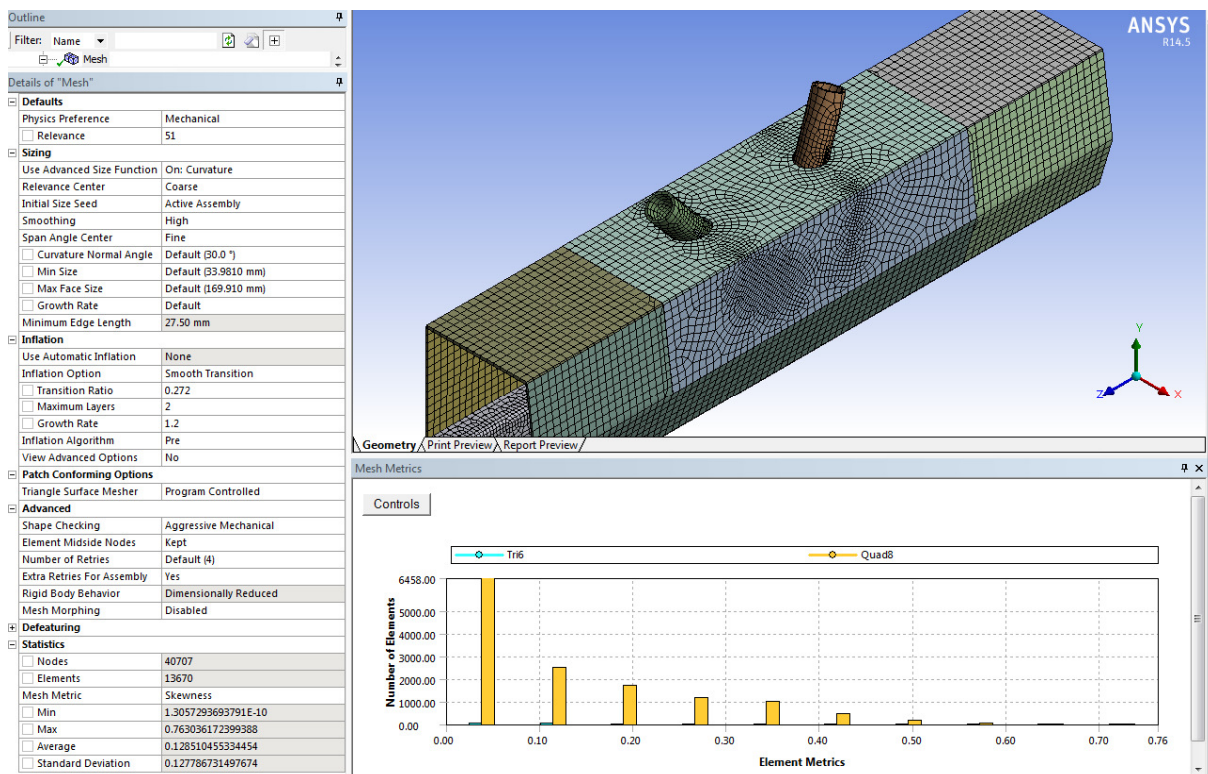


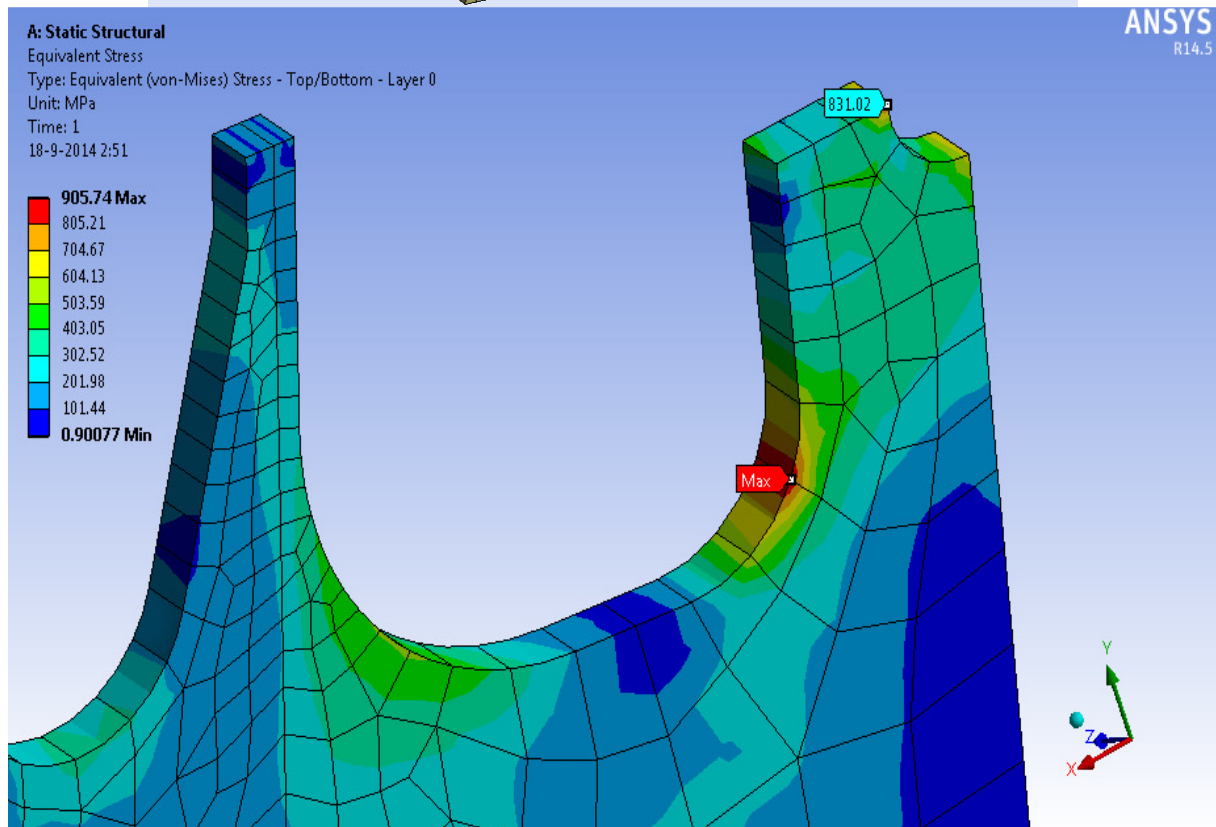
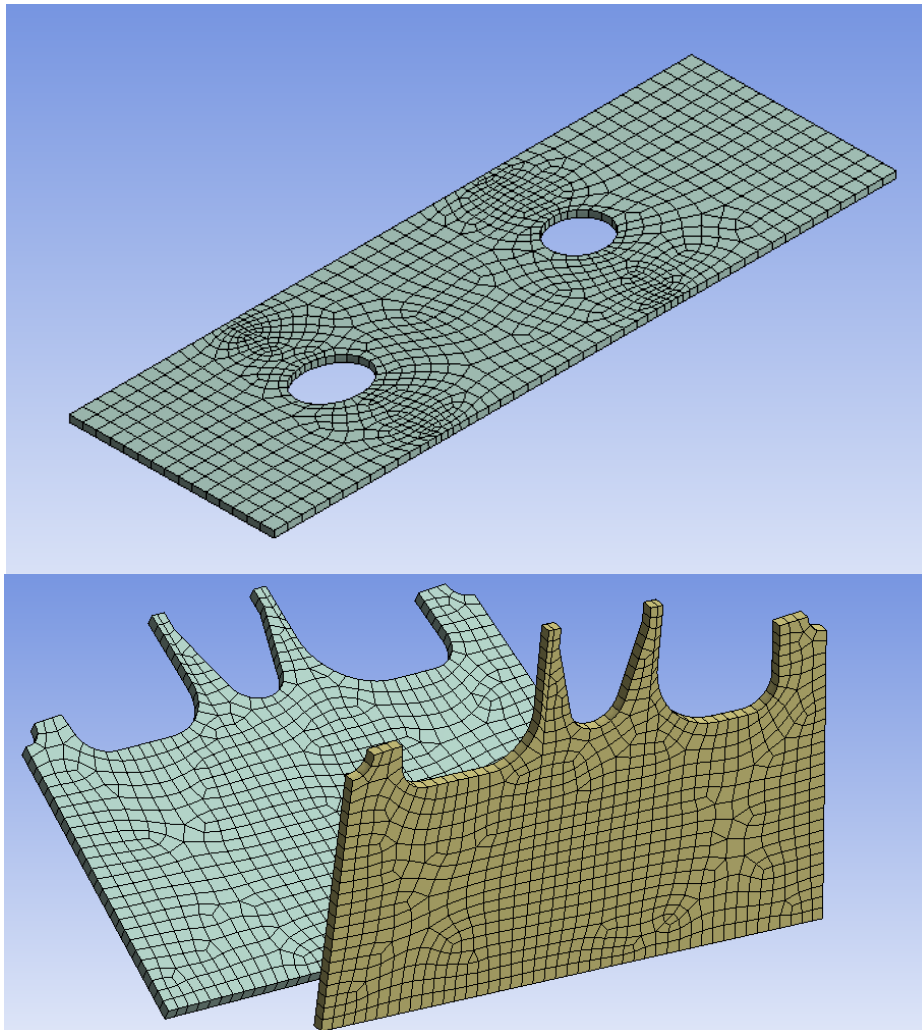
## Influence of Ductility in the Design of (High Strength) Steel Bridges



The mesh elements are still too small and might have led to inaccurate results in different localized parts of the gusset. It can be noticed that at the same locations as in the previous model the stress values are approximately the same. Also the number of elements and mesh quality is roughly the same.

In the third situation the Edge Sizing is set to 60 mm and “Use Advanced Size Function” is set to “On:Curvature”.

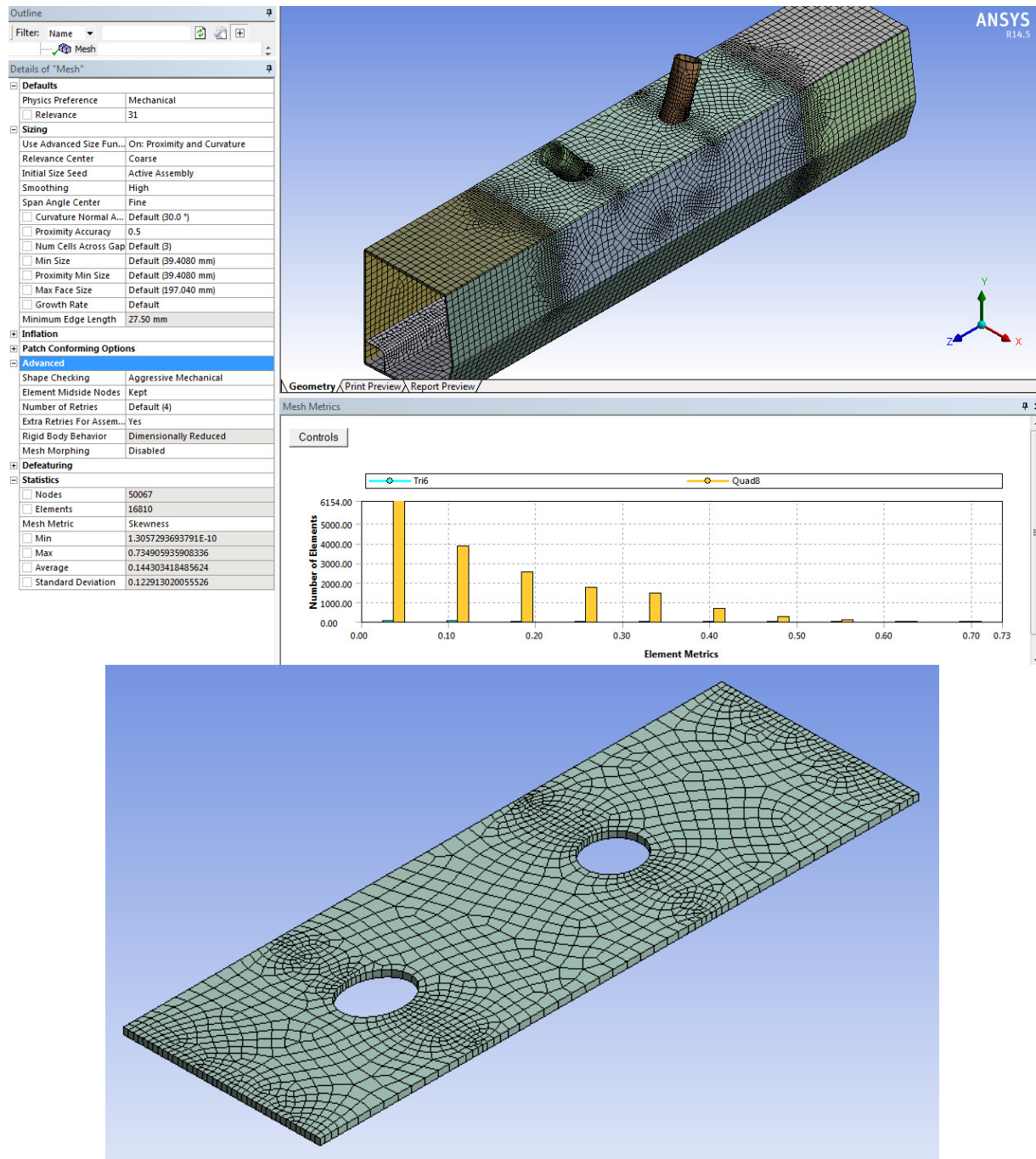


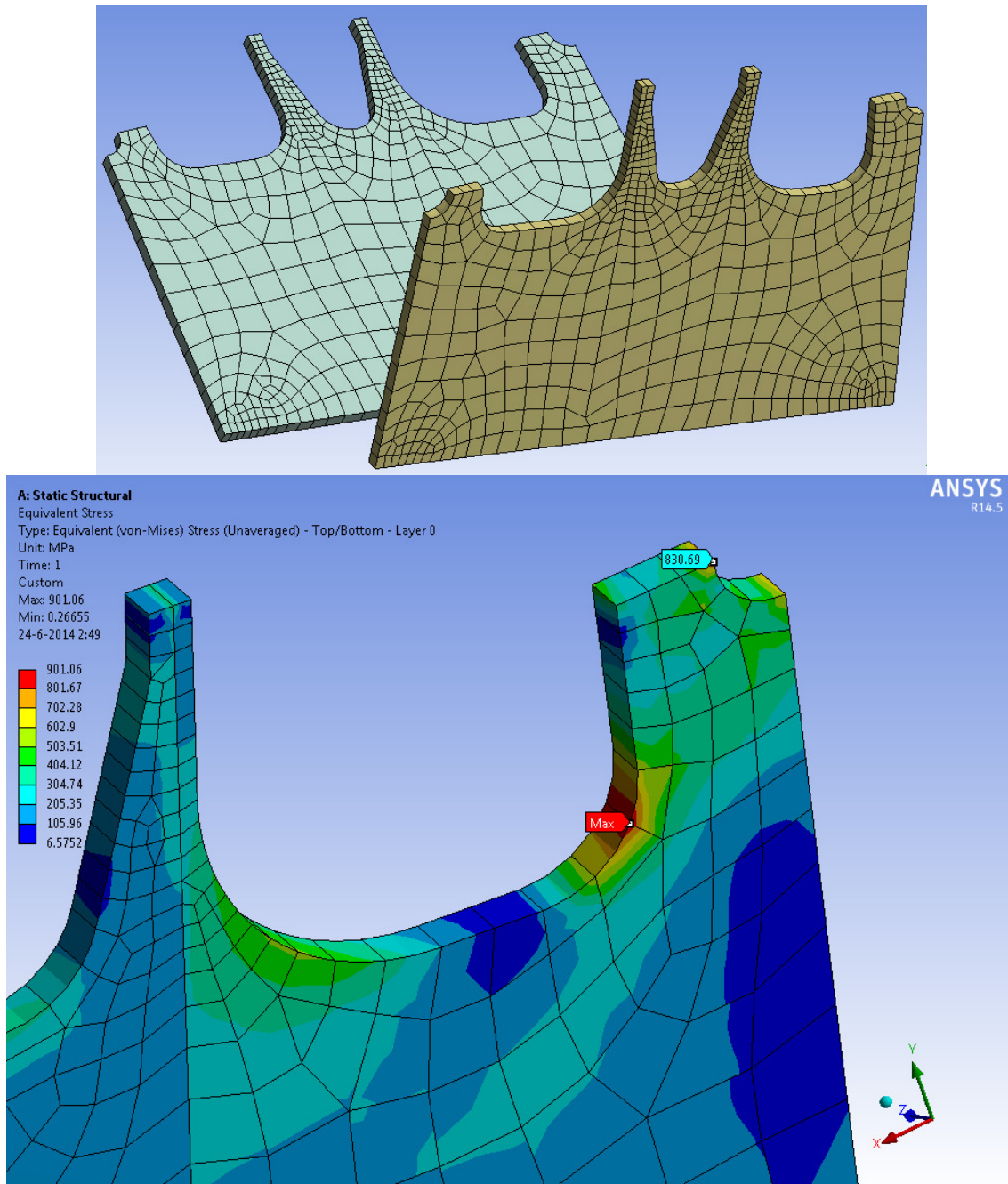


It can be noticed how the number of elements has drastically reduced by over half compared to the previous examples, while the mesh quality has slightly increased with the occurring peak stress shifting to the curvature of the gusset plate.

In order to further understand the mesh influence on the results the following options are changed: the “Use Advanced Size Function” as “On: Proximity and Curvature” and deleting the “Edge Sizing”.

The “Relevance” is set at 31 and at this value the program provides a message stating “The mesher restarted at a higher relevance in order to achieve a successful, quality mesh”. The resulting mesh is presented below.

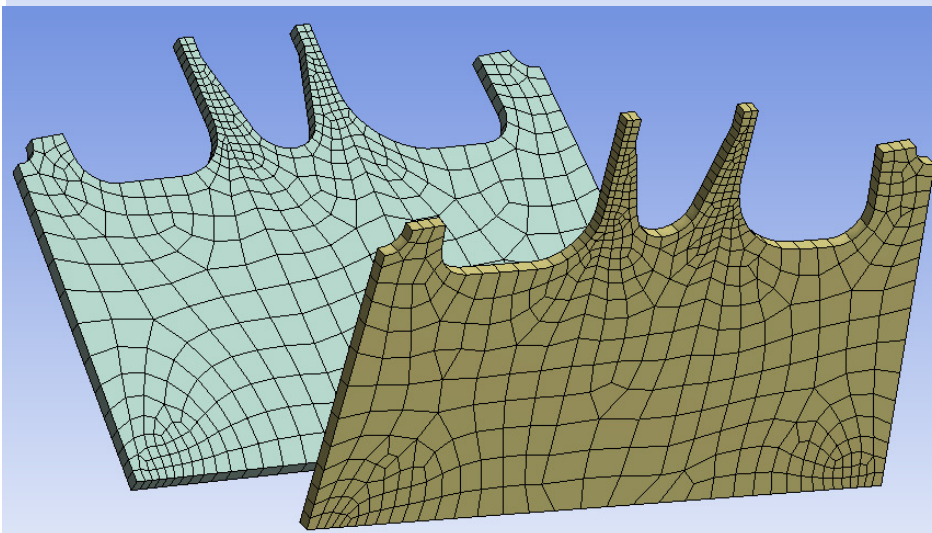
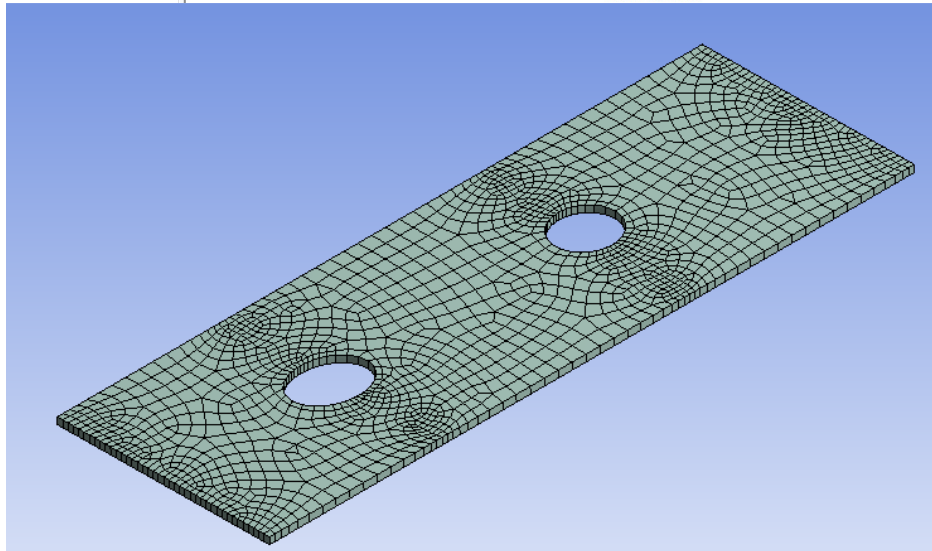
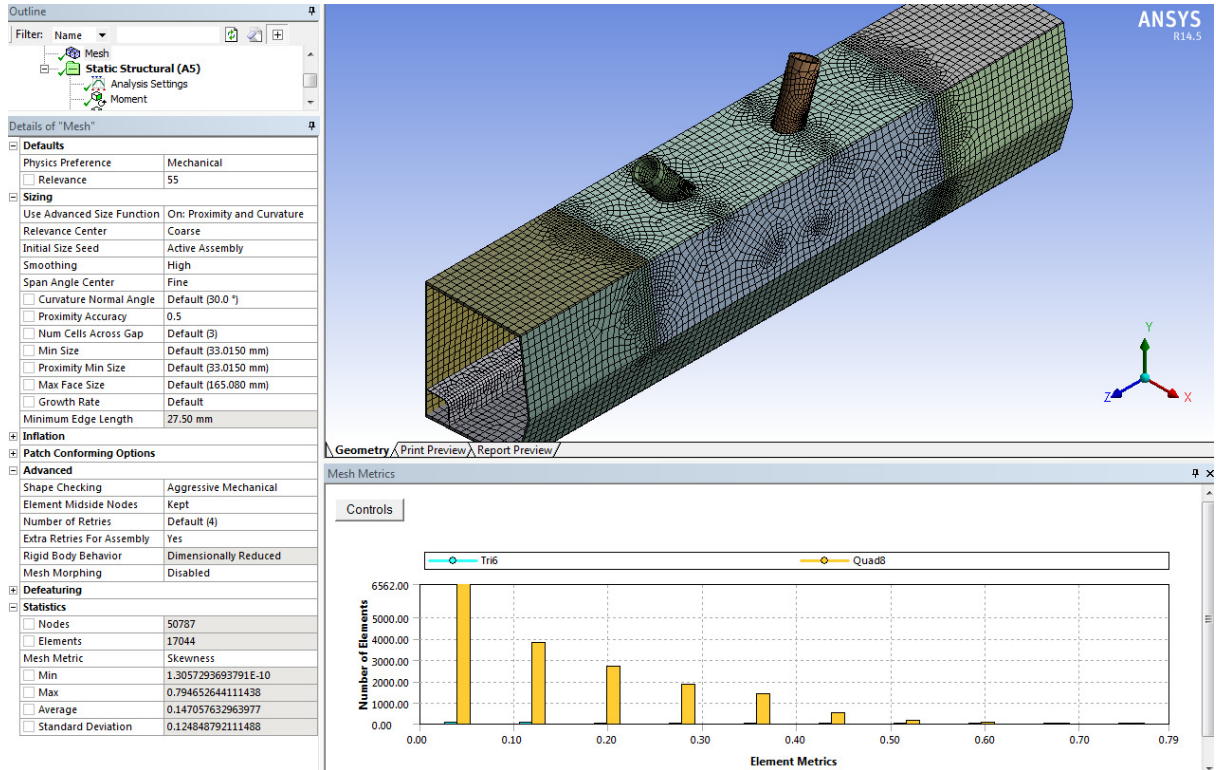




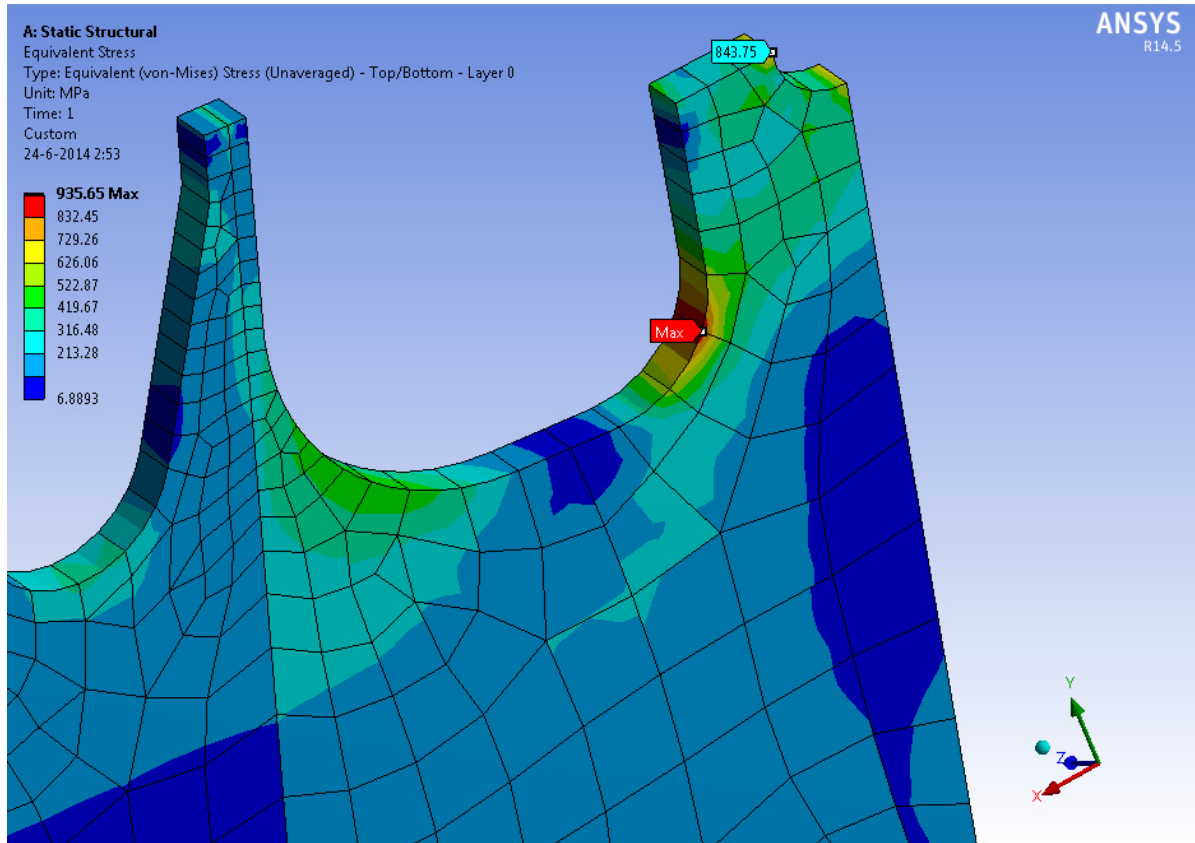
The number of elements has slightly increased compared to the previous two meshes, but the quality of the mesh is roughly the same. The stress concentration locations have yielded the same results as in the previous case. At the previous “Max” location the new value is significantly different from the first two ones, while at the curvature it is roughly the same. This can be translated that the value at the top might be a result due to the mesh size.

A further step to get a better insight of the mesh influence on the stress concentration location is carried out by setting the mesh relevance at 55.

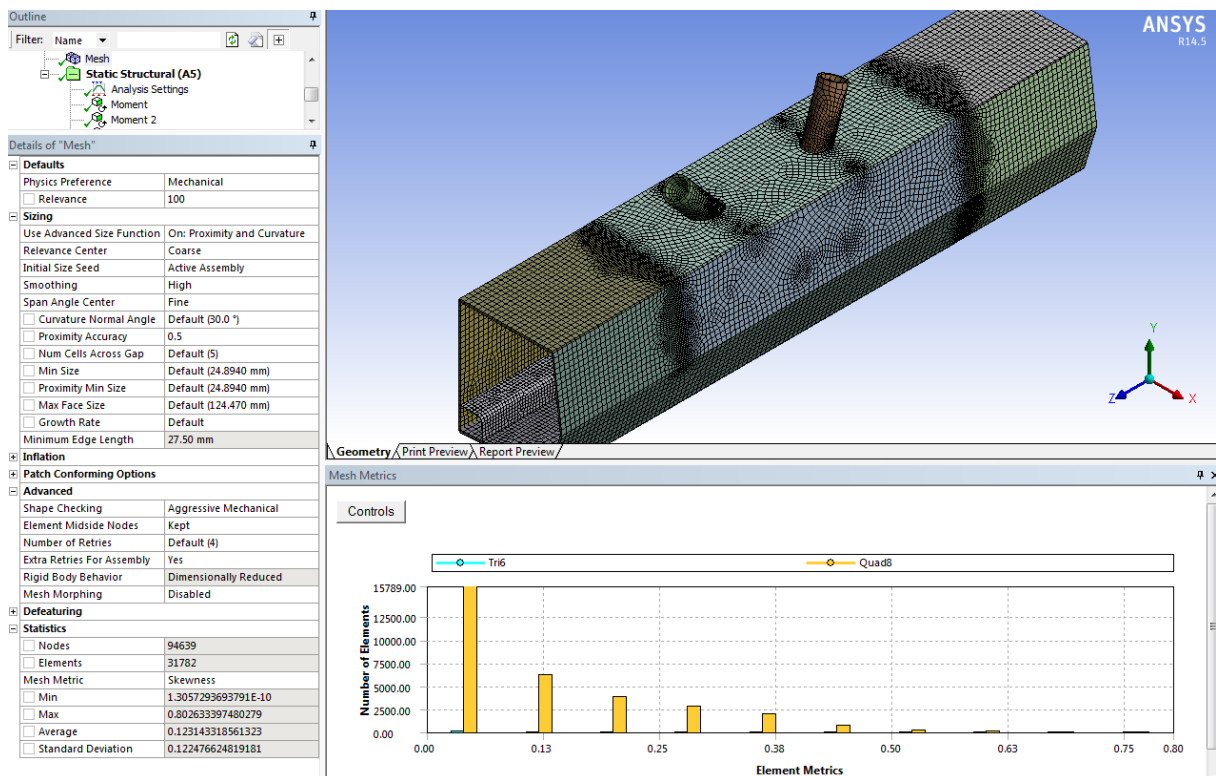
# Influence of Ductility in the Design of (High Strength) Steel Bridges

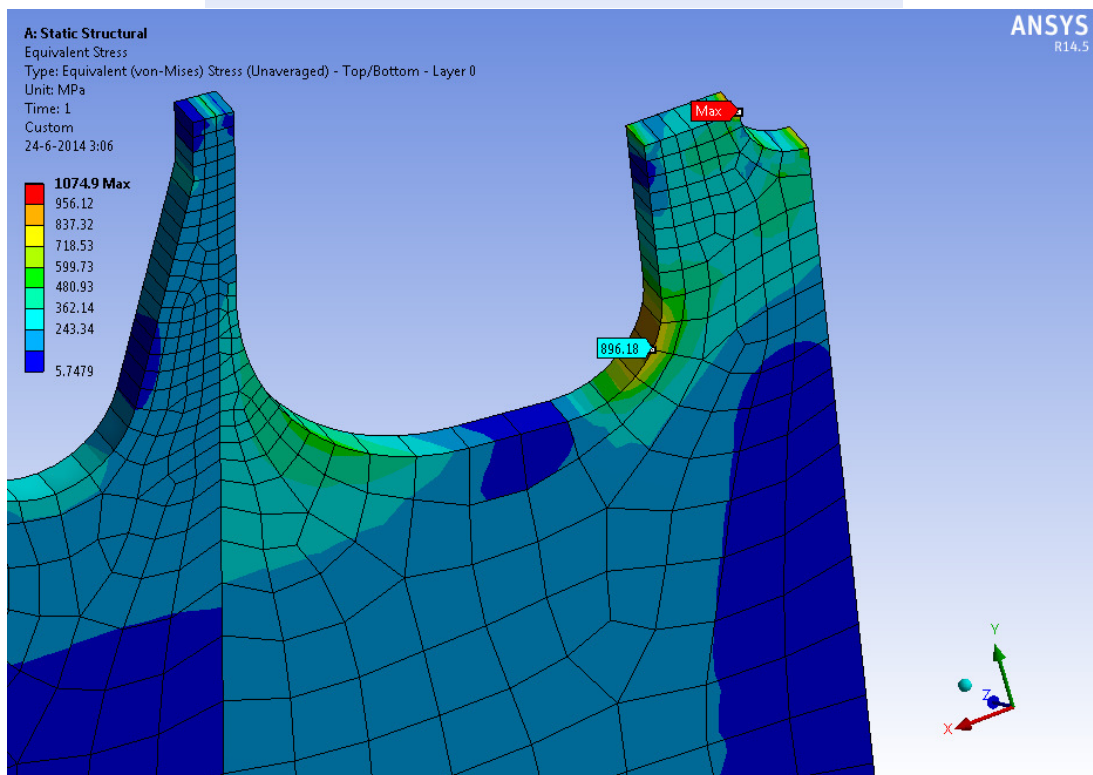
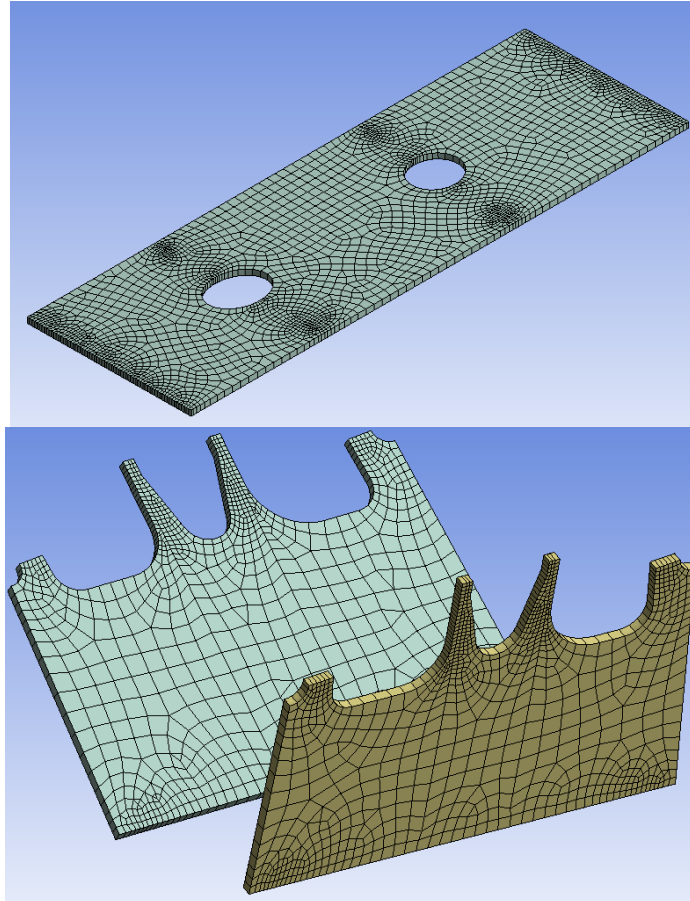


## Influence of Ductility in the Design of (High Strength) Steel Bridges



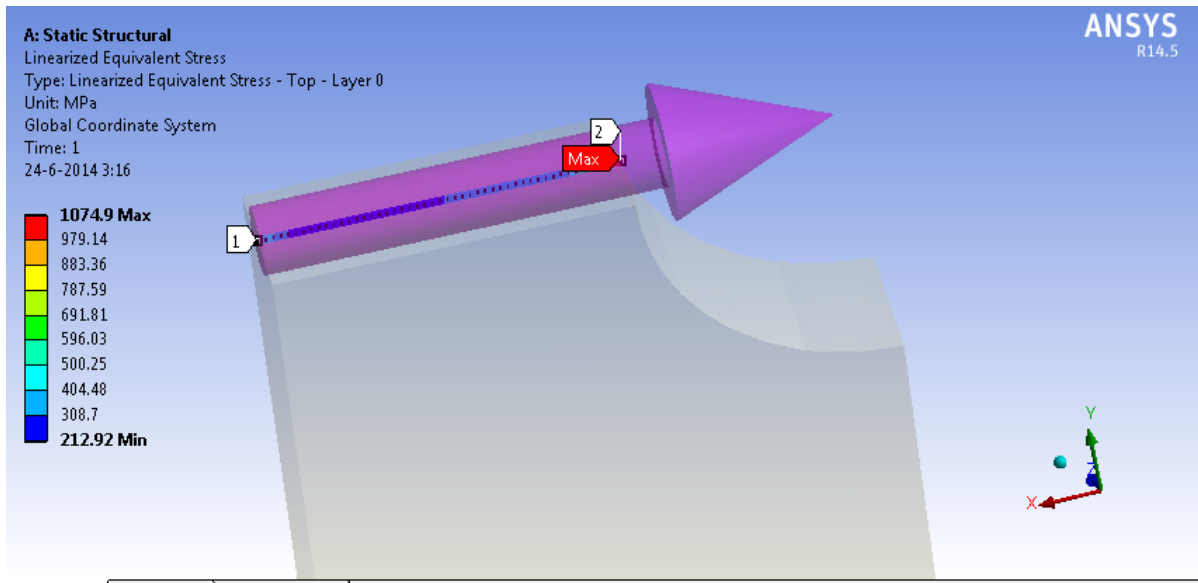
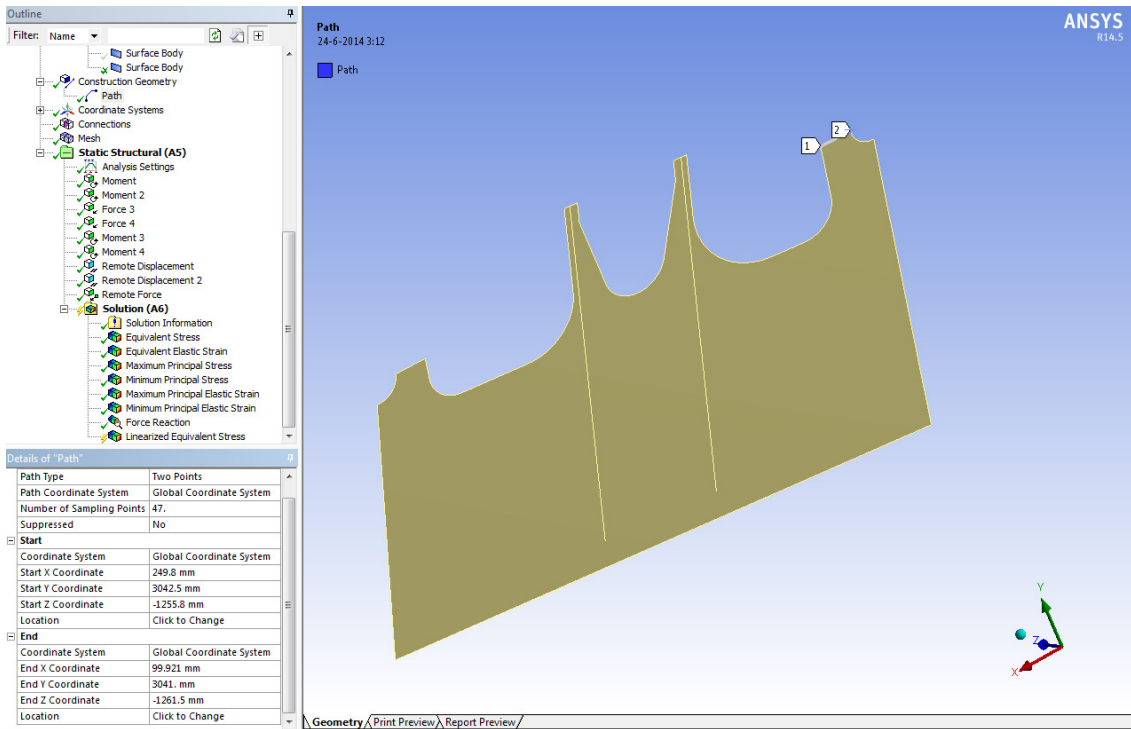
Another step is to set the relevance to 100 to see how the results are affected by such a fine mesh



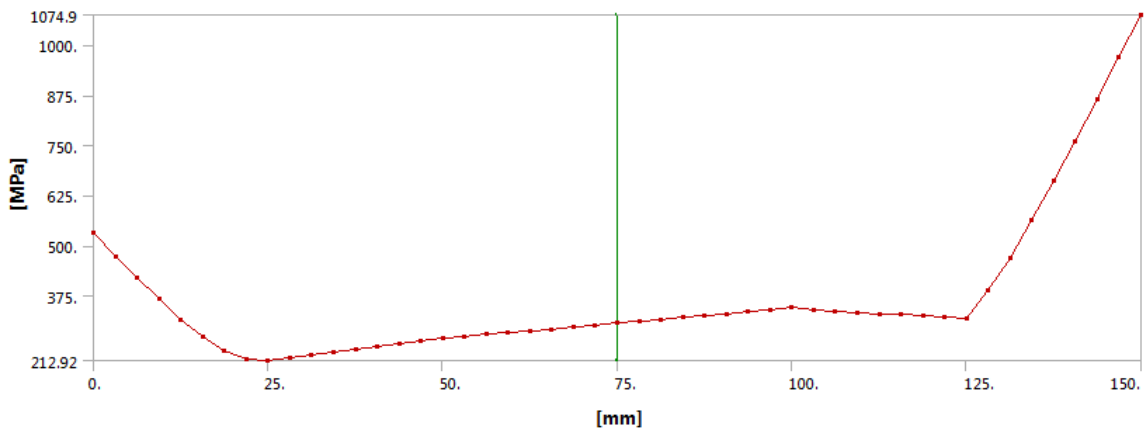


At such a fine mesh the maximum peak stress again shifts from the curvature of the gusset plate to the top part. In order to have a better understanding of how this peak stress is developed there over the area of multiple mesh elements, a linearized equivalent stress is plotted.

# Influence of Ductility in the Design of (High Strength) Steel Bridges



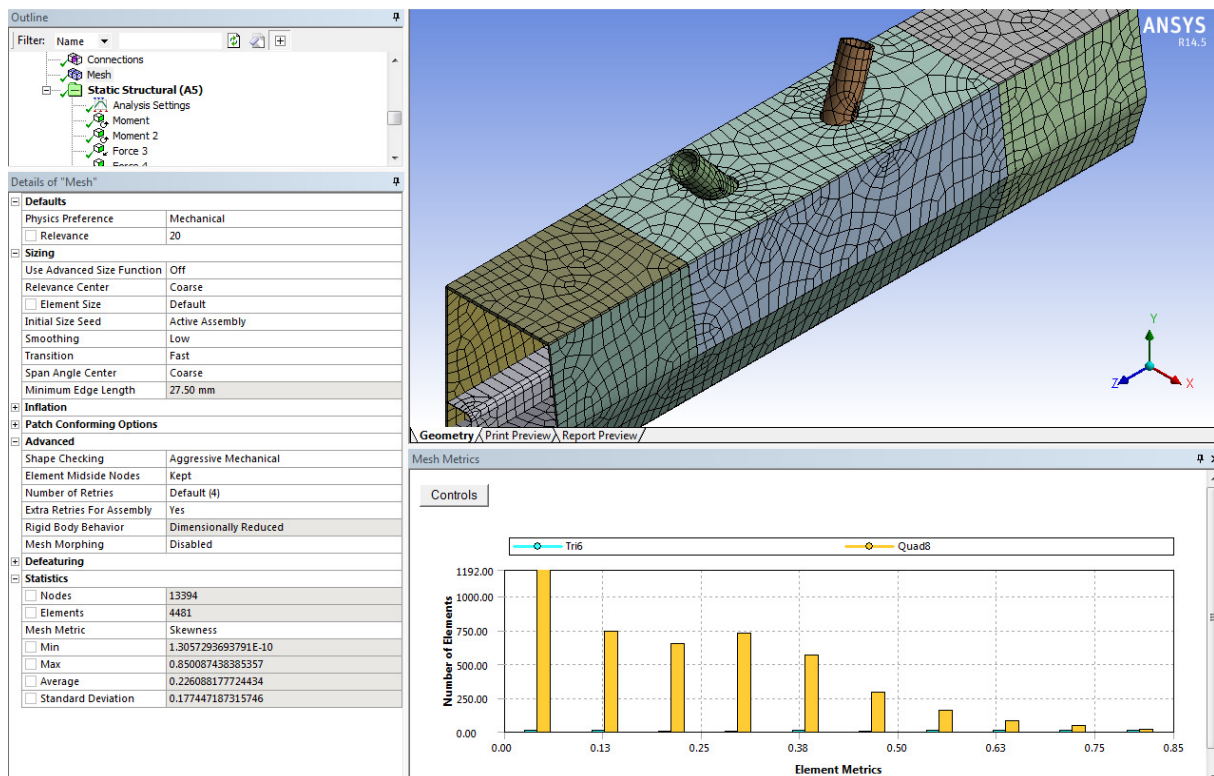
Graph

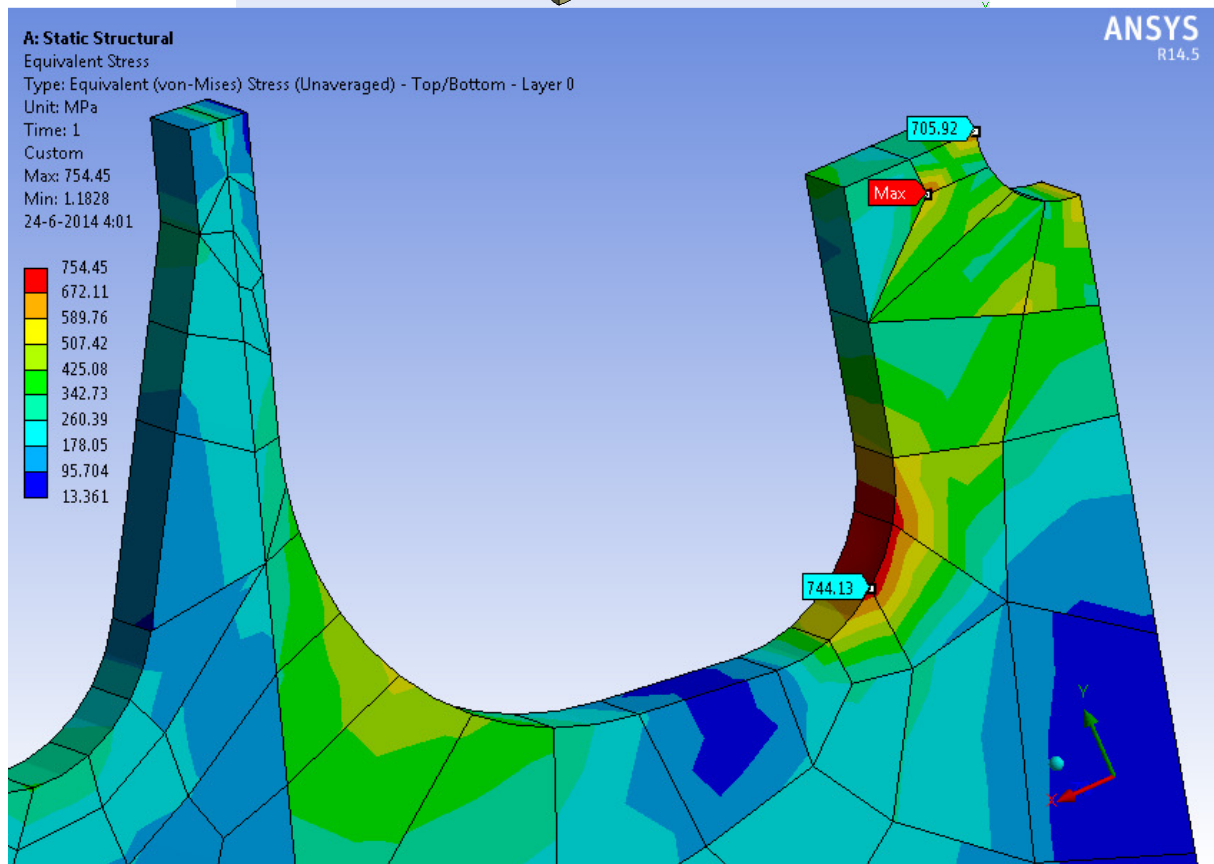
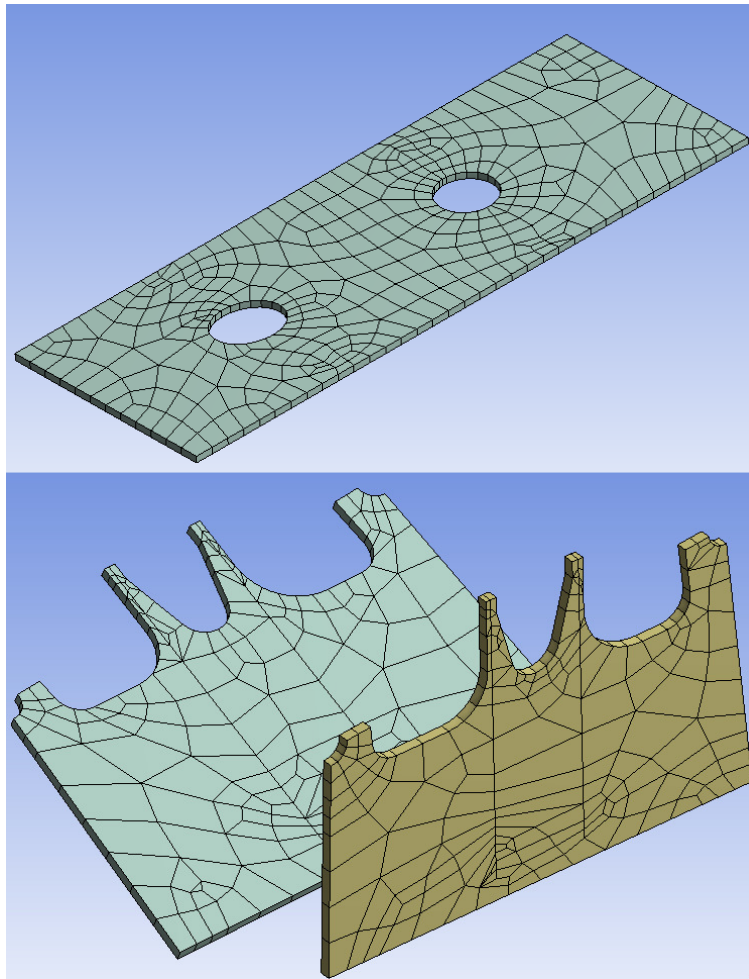


## Influence of Ductility in the Design of (High Strength) Steel Bridges

Tabular Data		
	Length [mm]	Total [MPa]
23	68.75	250.40
24	71.875	301.33
25	75.	306.24
26	78.125	310.72
27	81.25	315.3
28	84.375	319.98
29	87.5	324.75
30	90.625	329.61
31	93.75	334.56
32	96.875	339.59
33	100.	344.45
34	103.12	340.37
35	106.25	336.57
36	109.37	333.04
37	112.5	329.79
38	115.62	326.83
39	118.75	324.17
40	121.88	321.82
41	125.	319.79
42	128.13	386.58
43	131.25	469.59
44	134.37	561.96
45	137.5	659.77
46	140.63	760.93
47	143.75	864.26
48	146.88	969.07
49	150.	1074.9

The peak stress or “Max” occurs only in one of the mesh elements. The width of the elements is 25mm and it can be easily noticed how the stress increases significantly in the last mesh element. A further interesting step in understanding the influence of the mesh on the development of the peak stresses is to choose a very coarse mesh.





Based on the models created with different mesh values it can be concluded that the expected peak stress concentration should occur at the curvature of the plate. In all the cases the value of the stress at the top part of the gusset plate was very sensitive to the chosen mesh, while the values of the stress concentrations occurring at the curvature in all cases were roughly the same.

The final parameters of the mesh used in the modelling are presented below.

Details of "Mesh"	
<b>Defaults</b>	
Physics Preference	Mechanical
<input type="checkbox"/> Relevance	55
<b>Sizing</b>	
Use Advanced Size Function	On: Proximity and Curvature
Relevance Center	Coarse
Initial Size Seed	Active Assembly
Smoothing	High
Span Angle Center	Fine
<input type="checkbox"/> Curvature Normal Angle	Default (30.0 °)
<input type="checkbox"/> Proximity Accuracy	0.5
<input type="checkbox"/> Num Cells Across Gap	Default (3)
<input type="checkbox"/> Min Size	Default (33.0150 mm)
<input type="checkbox"/> Proximity Min Size	Default (33.0150 mm)
<input type="checkbox"/> Max Face Size	Default (165.080 mm)
<input type="checkbox"/> Growth Rate	Default
Minimum Edge Length	27.50 mm
<b>Inflation</b>	
<b>Patch Conforming Options</b>	
<b>Advanced</b>	
Shape Checking	Aggressive Mechanical
Element Midside Nodes	Kept
Number of Retries	Default (4)
Extra Retries For Assembly	Yes
Rigid Body Behavior	Dimensionally Reduced
Mesh Morphing	Disabled
<b>Defeaturing</b>	
<b>Statistics</b>	
<input type="checkbox"/> Nodes	50871
<input type="checkbox"/> Elements	17076
Mesh Metric	Skewness
<input type="checkbox"/> Min	1.3057293693791E-10
<input type="checkbox"/> Max	0.766652062104996
<input type="checkbox"/> Average	0.146074129059595
<input type="checkbox"/> Standard Deviation	0.12459539956615

Figure B.27 – Mesh details

The quality of the mesh can be measured using “Skewness”. This determines how close to ideal (i.e. equilateral or equiangular) a face or cell is.

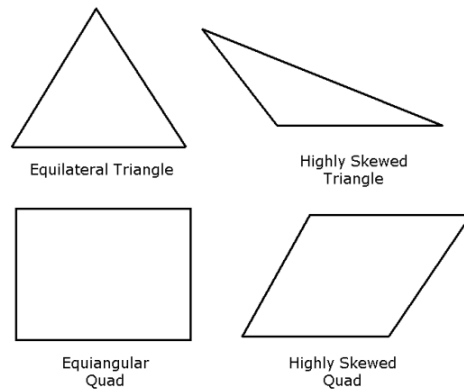


Figure B.28 – Ideal and skewed triangles and quadrilaterals [ANSYS 14.5 Help]

Skewness values range from 0 to 1 with lower values resulting in higher cell quality. Values above 1 are considered invalid. In the chosen mesh the average value is 0.14 which is translated into an excellent cell quality. The mesh metrics are presented in Figure 4.38

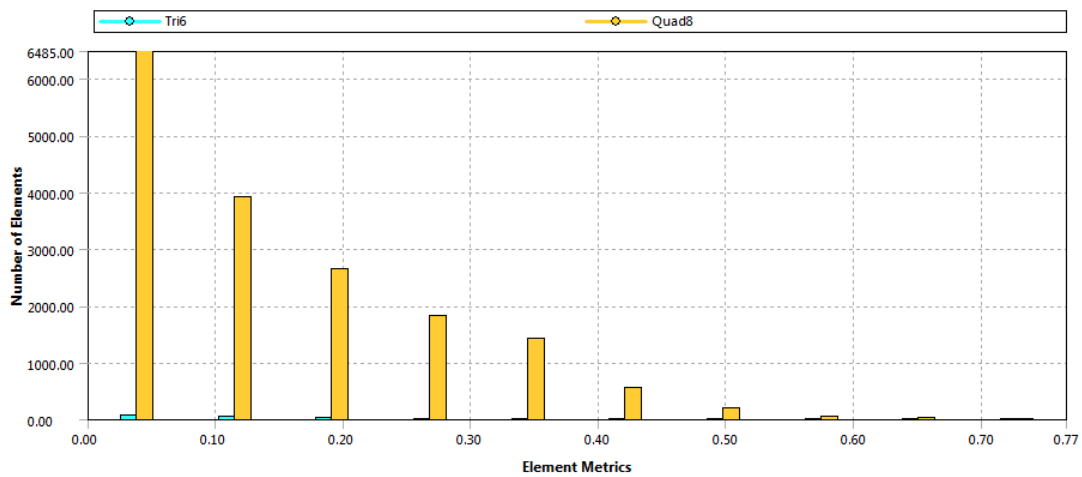


Figure B.29 – Mesh metrics

Advanced size function is used on the proximities and curvatures in order to increase the mesh finesse at these locations. These are the most probable to lead to stress concentrations. Due to the use of midsize nodes the relevance centre can be set to “Coarse”. Smoothing which represents the change in size from one face or cell to the next is set to be “High” in order to ensure a gradual transition as the differential equations being solved assume that the cells shrink or grow smoothly.

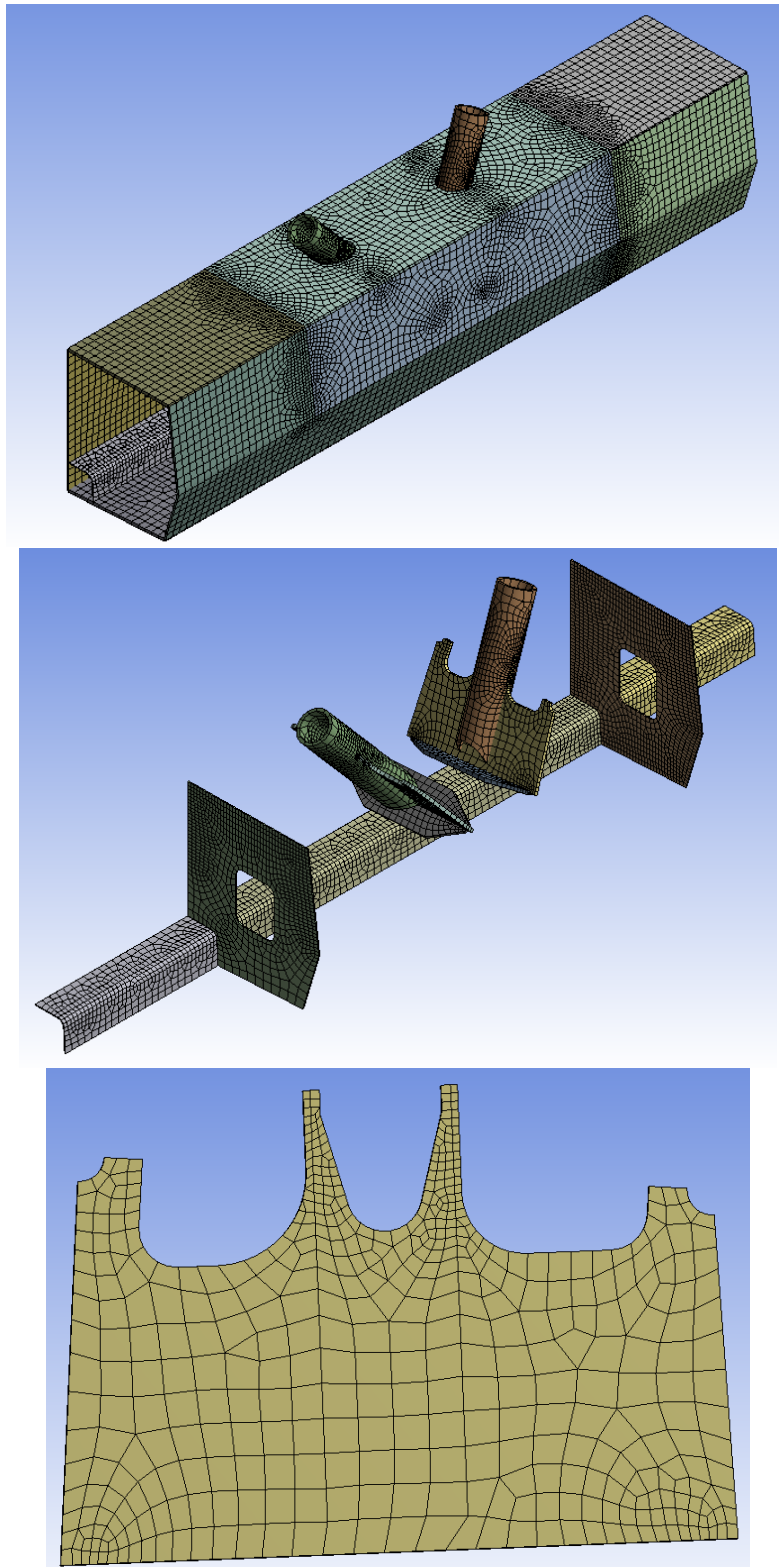


Figure B.30 – Generated mesh

### Simplified Gusset Plate

The values of the displacement and equivalent strain at location A where they were measure are illustrated in the table below for different values of the load and the three different ultimate-yield tensile ratios for comparison.

Table 50 – Equivalent strain and displacement values for different load levels

	$f_u/f_y=1.00$	$f_u/f_y=1.05$	$f_u/f_y=1.10$	$f_u/f_y=1.00$	$f_u/f_y=1.05$	$f_u/f_y=1.10$
F [kN]	$\epsilon_{NL}$	$\epsilon_{NL}$	$\epsilon_{NL}$	$\delta$ [mm]	$\delta$ [mm]	$\delta$ [mm]
0	0.0000	0.0000	0.0000	0	0	0
3800	0.0005	0.0005	0.0005	0.71607	0.71607	0.71607
7600	0.0010	0.0010	0.0010	1.4322	1.4322	1.4322
11400	0.0015	0.0015	0.0015	2.1484	2.1484	2.1484
15200	0.0020	0.0020	0.0020	2.8647	2.8647	2.8647
19000	0.0025	0.0025	0.0025	3.581	3.581	3.581
22800	0.0031	0.0031	0.0031	4.2974	4.2974	4.2974
26600	0.0036	0.0036	0.0036	5.0139	5.0139	5.0139
30400	0.0041	0.0041	0.0041	5.7304	5.7304	5.7304
34200	0.0044	0.0044	0.0044	6.4529	6.4528	6.4528
38000	0.0047	0.0047	0.0047	7.1874	7.1872	7.187
41800	0.0057	0.0057	0.0057	7.9295	7.9291	7.9287
45600	0.0069	0.0069	0.0069	8.6883	8.6874	8.6865
49400	0.0084	0.0084	0.0083	9.4875	9.4851	9.4827
53200	0.0110	0.0109	0.0108	10.692	10.678	10.665
57000	0.0190	0.0177	0.0169	14.292	13.92	13.665
57200	0.0204	0.0188	0.0176	14.893	14.364	14.016
57400	0.0229	0.0200	0.0186	15.65	14.906	14.444
57600	0.0263	0.0219	0.0197	16.727	15.551	14.94
57800	0.0322	0.0243	0.0212	18.656	16.38	15.518
58000	0.0705	0.0274	0.0231	31.94	17.446	16.208

In the following figures the equivalent strain and displacement at different load levels are illustrated. In the case of equivalent strains the dark-blue contour represents the material that has not reached yielding. The colours for the plots are shown for each figure.

The loads used are listed below. An illustration of the physical meaning of the threshold of these forces is shown in section 5.3.

- a 26600kN
- b 41800kN
- c 53200kN
- d 57600kN
- e 58000kN

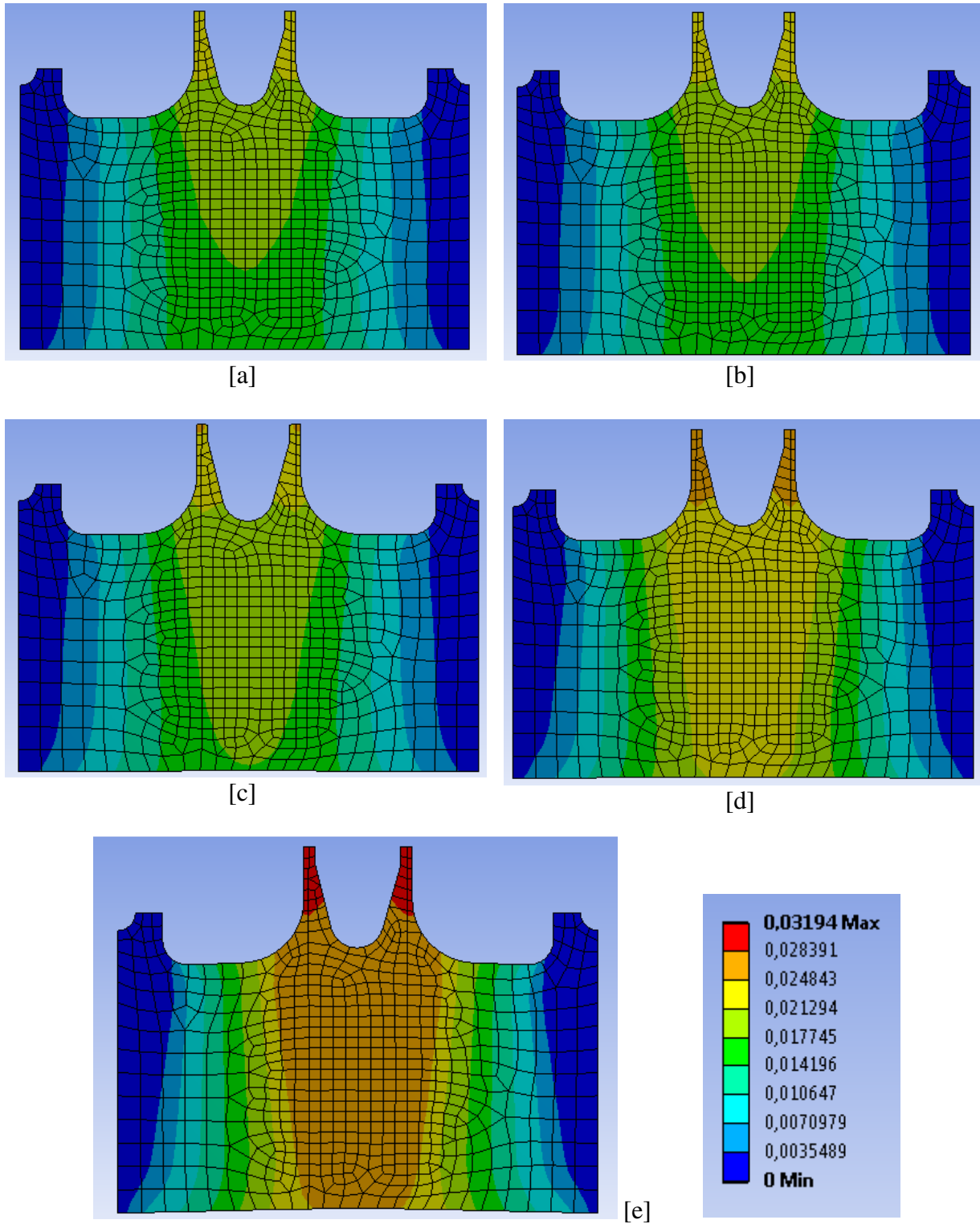


Figure B.31 – Displacement field for  $f_u/f_y=1.00$  (IFEA) at load levels a, b, c, d and e

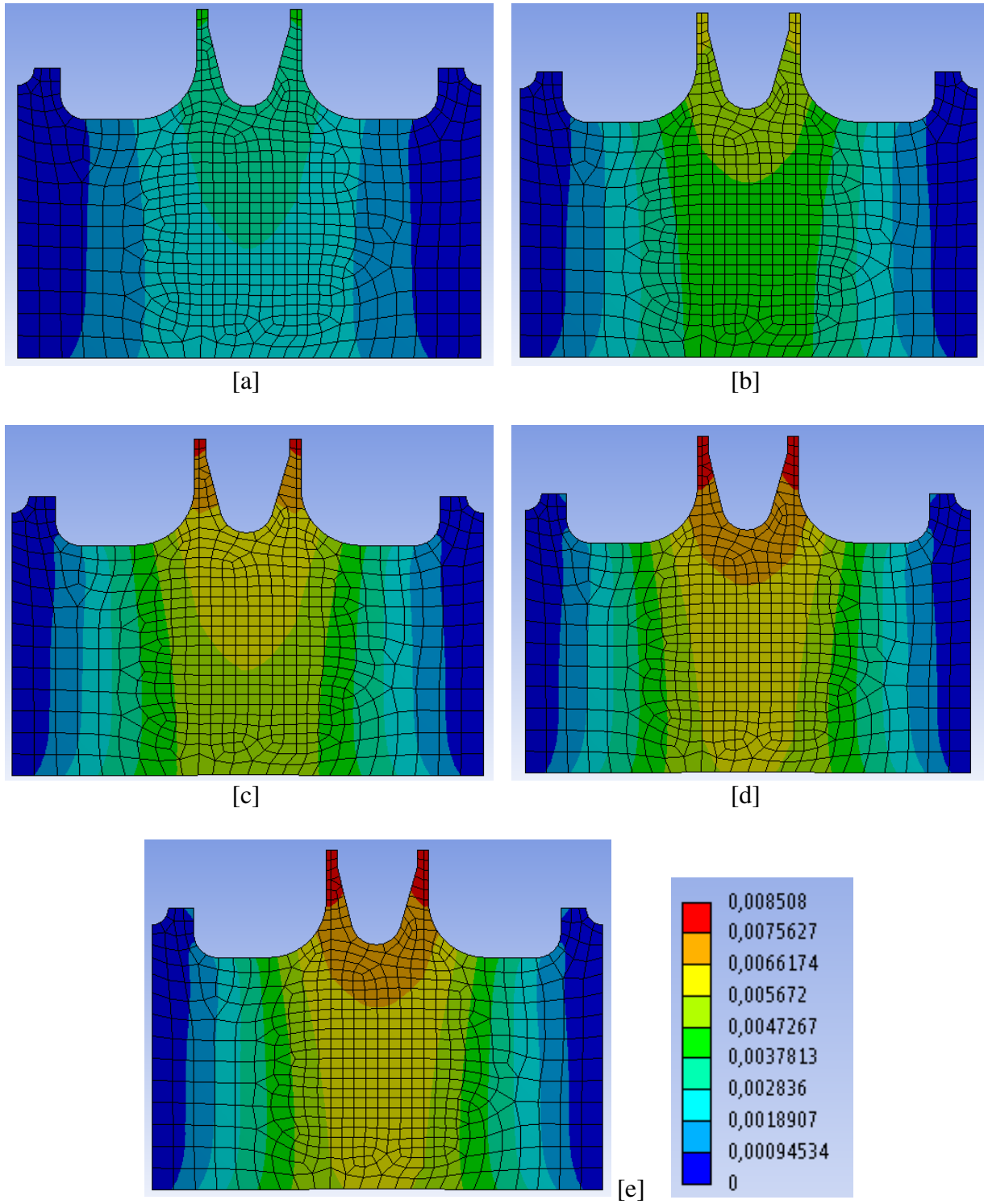


Figure B.32 – Displacement field (EFEA) at load levels a, b, c, d and e

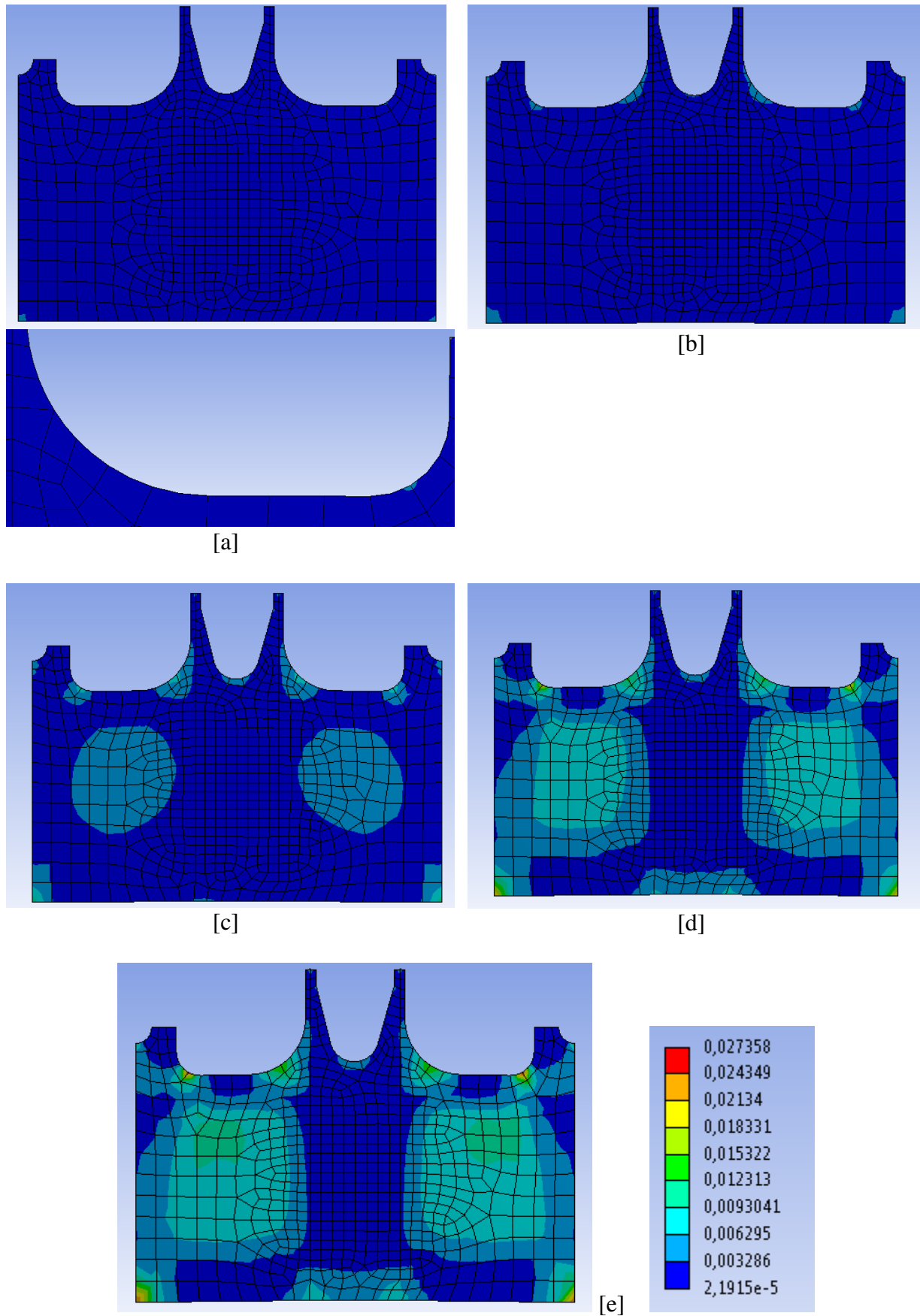


Figure B.33 – Equivalent strain field for  $f_u/f_y=1.05$  (IFEA) at load levels a, b, c, d and e

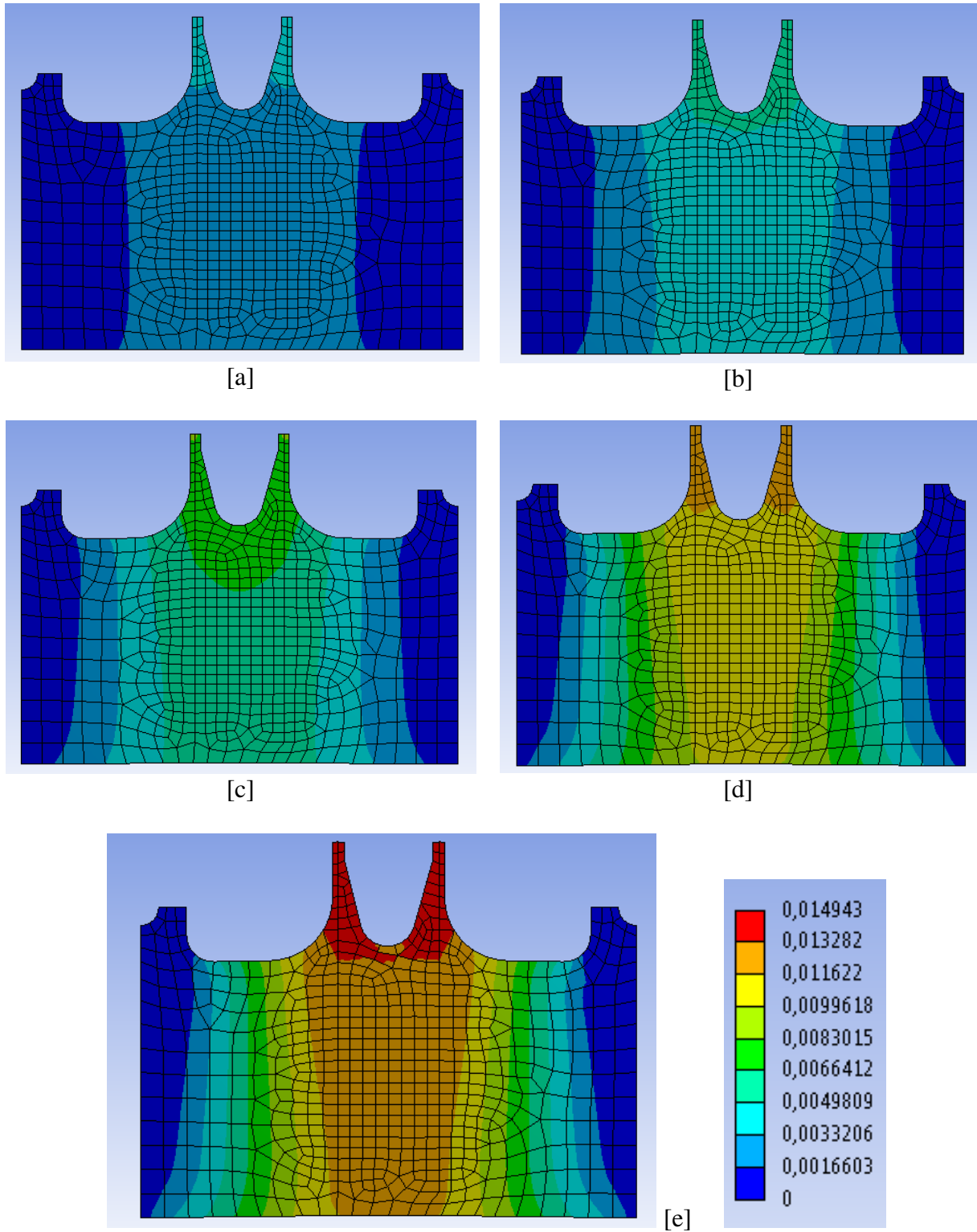


Figure B.34 – Displacement field for  $f_u/f_y=1.05$  (IFEA) at load levels a, b, c, d and e

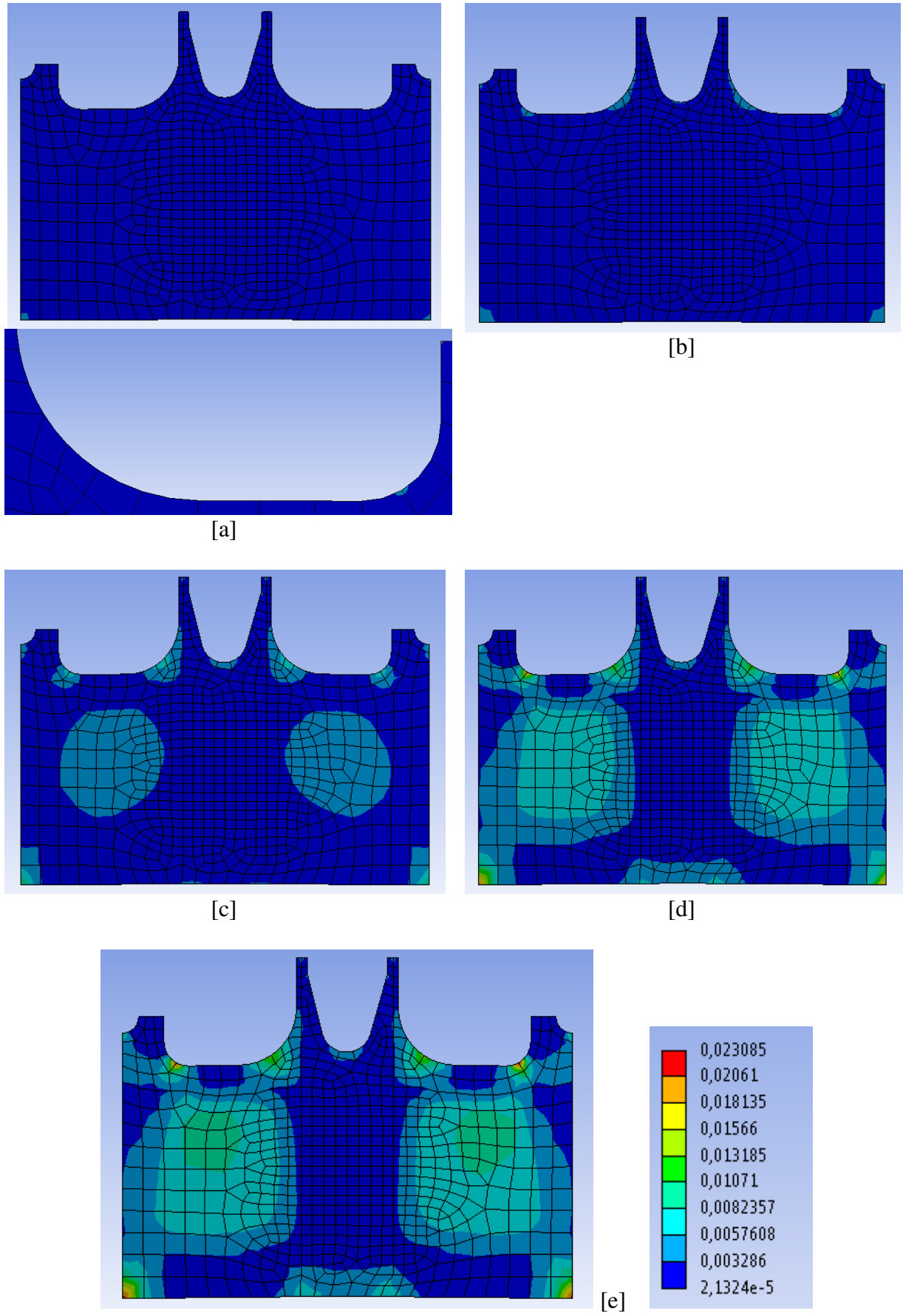


Figure B.35 – Equivalent strain field for  $f_u/f_y=1.10$  (IFEA) at load levels a, b, c, d and e

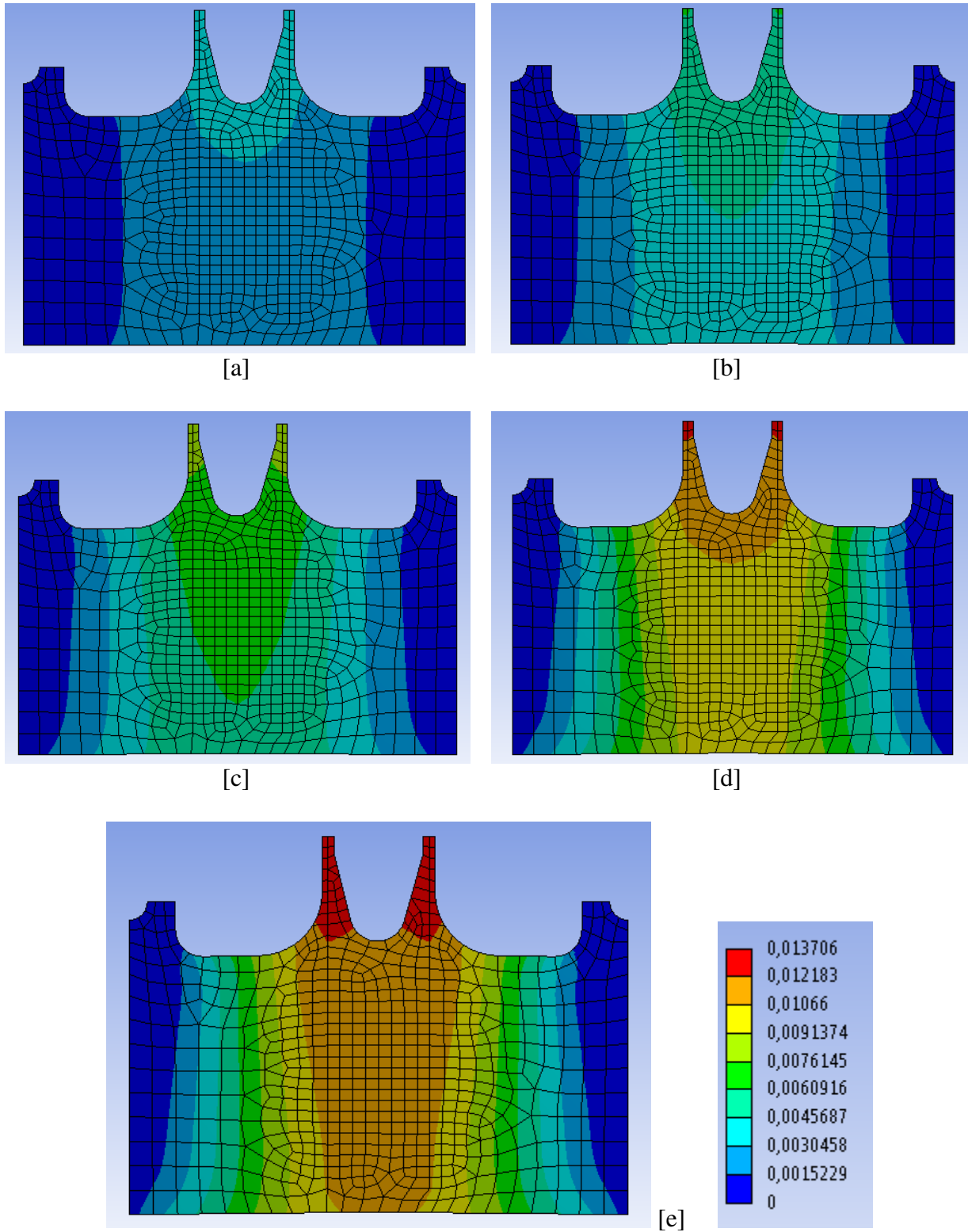


Figure B.36 – Displacement field for  $f_u/f_y=1.10$  (IFEA) at load levels a, b, c, d and e

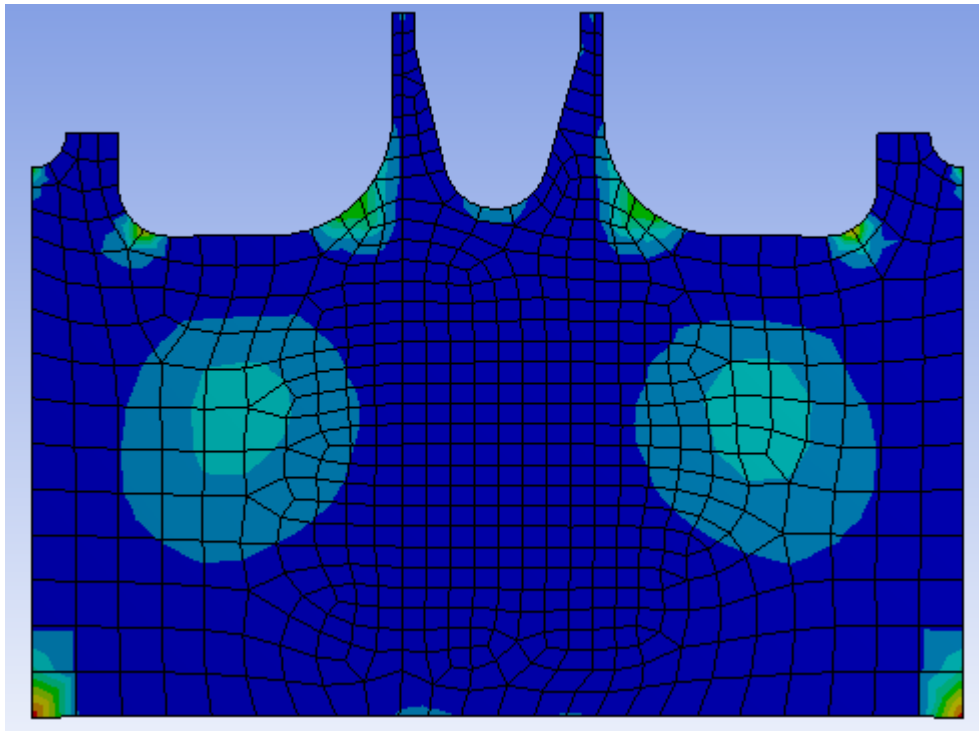


Figure B.37 – Equivalent strain field at  $0.9f_y$  (IFEA) for  $f_u/f_y=1.00$

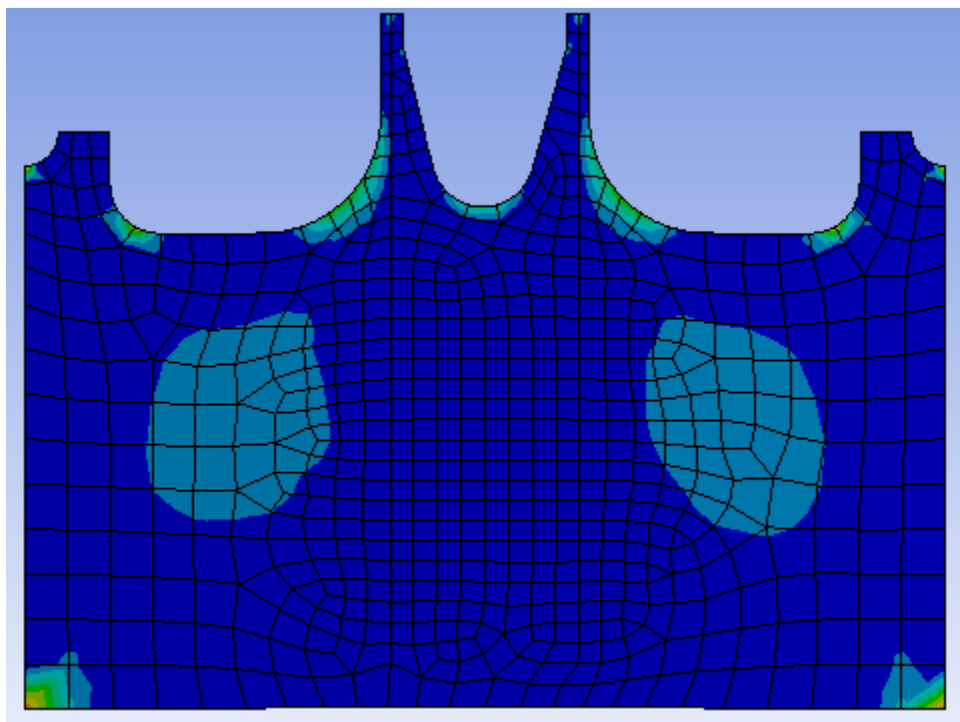


Figure B.38 – Equivalent strain field at  $0.9f_y$  (EFEA)

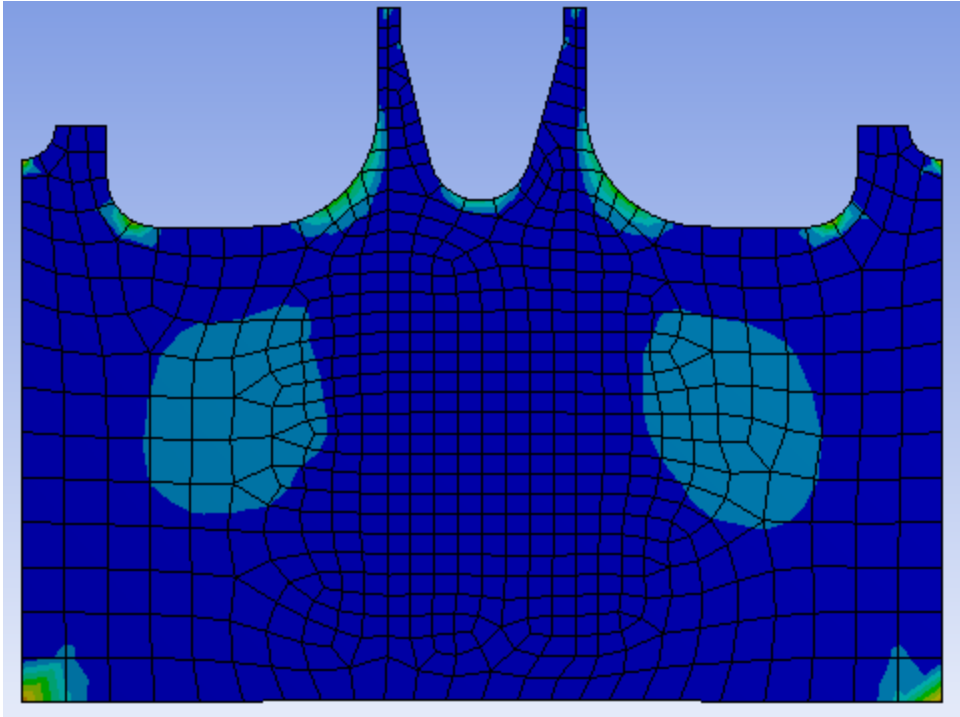


Figure B.39 – Equivalent stress field at  $0.9f_y$  (EFEA)

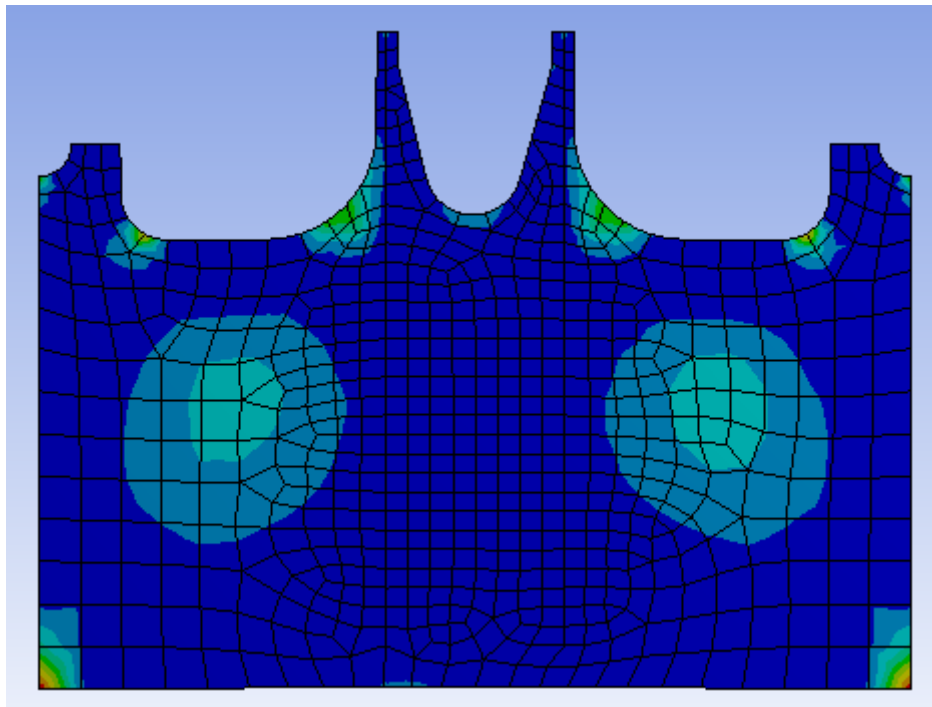


Figure B.40 – Equivalent strain field at  $0.9f_y$  (IFEA) for  $f_u/f_y=1.05$

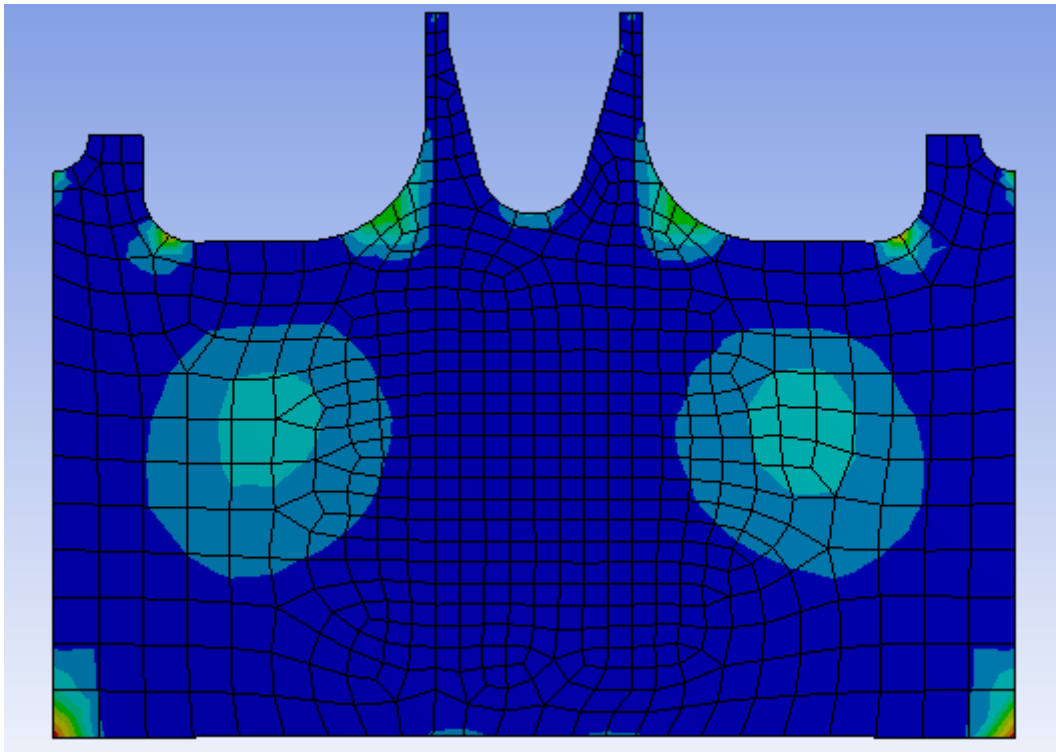


Figure B.41– Equivalent strain field at  $0.9f_y$  (IFEA) for  $f_u/f_y=1.10$

## Nonlinear Analysis – Bridge Joint

For the IFEA of the bridge connections the parameters illustrated in Figure B.42 where used for the analysis.

The screenshot displays the ANSYS Workbench interface. The top part shows a project tree with the following items: Project, Model (A4), Geometry, Coordinate Systems, Connections, Mesh, Static Structural (A5), and Analysis Settings. The 'Analysis Settings' dialog is open, showing the following parameters:

Details of "Analysis Settings"	
<b>Step Controls</b>	
Number Of Steps	15.
Current Step Number	1.
Step End Time	1. s
Auto Time Stepping	On
Define By	Substeps
Initial Substeps	2.
Minimum Substeps	2.
Maximum Substeps	20.
<b>Solver Controls</b>	
Solver Type	Program Controlled
Weak Springs	Off
Large Deflection	On
Inertia Relief	Off
<b>Restart Controls</b>	
<b>Nonlinear Controls</b>	
Force Convergence	On
--Value	Calculated by solver
--Tolerance	0.2%
--Minimum Reference	1.e-002 N
Moment Convergence	Program Controlled
Displacement Convergence	On
--Value	Calculated by solver
--Tolerance	0.2%
--Minimum Reference	0. mm
Rotation Convergence	Program Controlled
Line Search	Program Controlled
Stabilization	Reduce
--Method	Energy
--Energy Dissipation Ratio	1.e-004
--Activation For First Substep	No
--Stabilization Force Limit	0.2
<b>Output Controls</b>	
<b>Analysis Data Management</b>	
<b>Visibility</b>	

Figure B.42 – IFEA of bridge connection: settings

In order to ensure the accuracy of the results, force and displacement convergence are set on. To solve further convergence difficulties due to an unstable problem (the result of a large displacement for smaller load increments) nonlinear stabilization is used. This is understood as adding an artificial damper element at each node of an element that supports this technique. The coefficient used to calculate the damping (stabilization) force is the damping factor. The programme calculates the damping factor based on the energy dissipation ratio specified.

Line search was not used as it can be useful for enhancing convergence, but it can be expensive especially with plasticity.

In the following pictures the strains resulting from the acting stress state on the bridge connection are illustrated. The dark-blue contour represent equivalent strains below the one corresponding to yielding ( $\epsilon_e < \frac{f_y}{E} = 0.0016905$ ) while the other contour plots represent the material that has yielded.

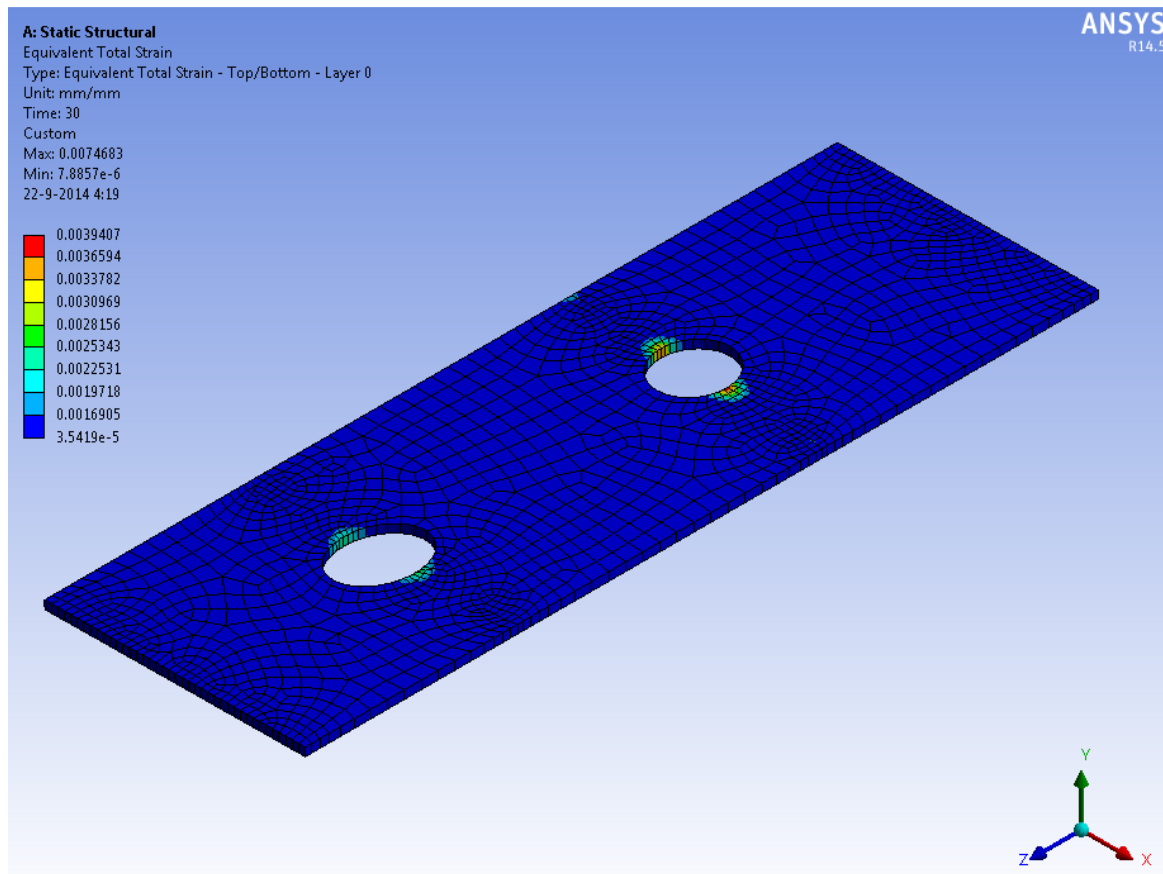


Figure B.43 - Elastic-plastic strains over the top flange (IFEA)

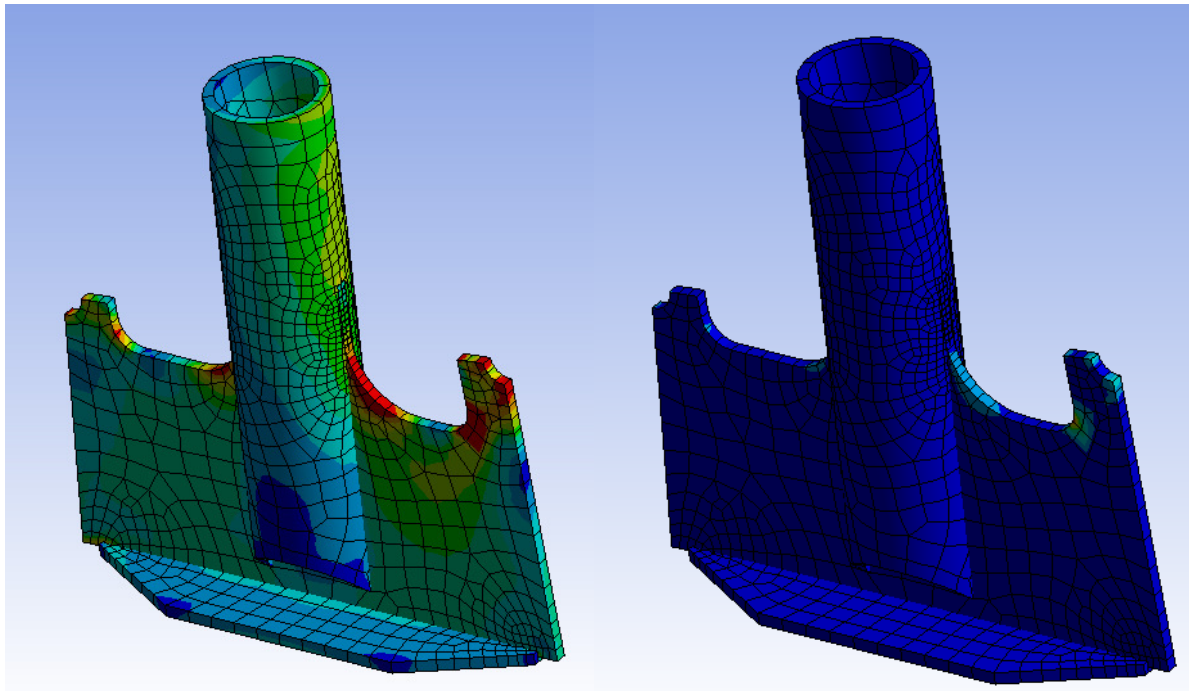


Figure B.44 – Equivalent total strains in the diagonal-gusset plate part

Where: in the left part the red contour represents the material that has yielded and in the right part the dark-blue contour represents the material that has not reached yielding

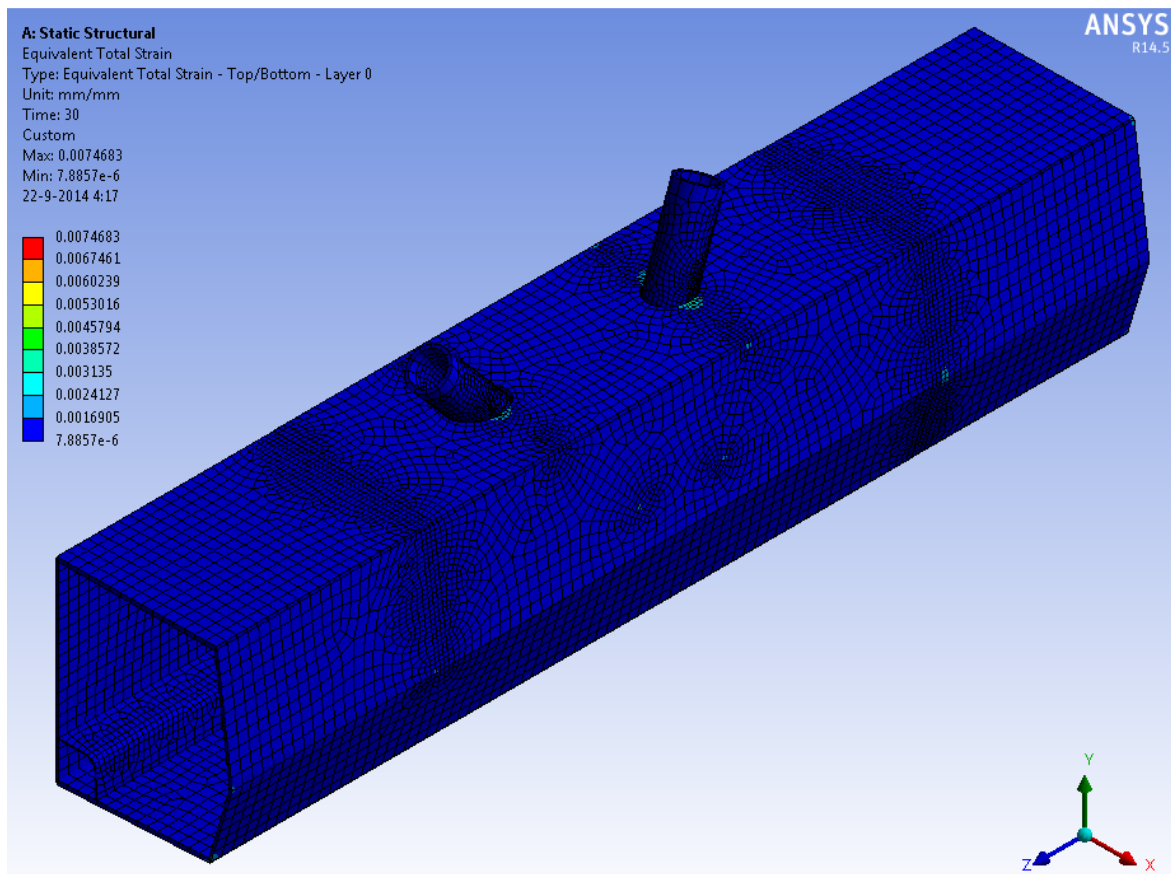


Figure B.45 - Elastic-plastic strains over the joint (IFEA)

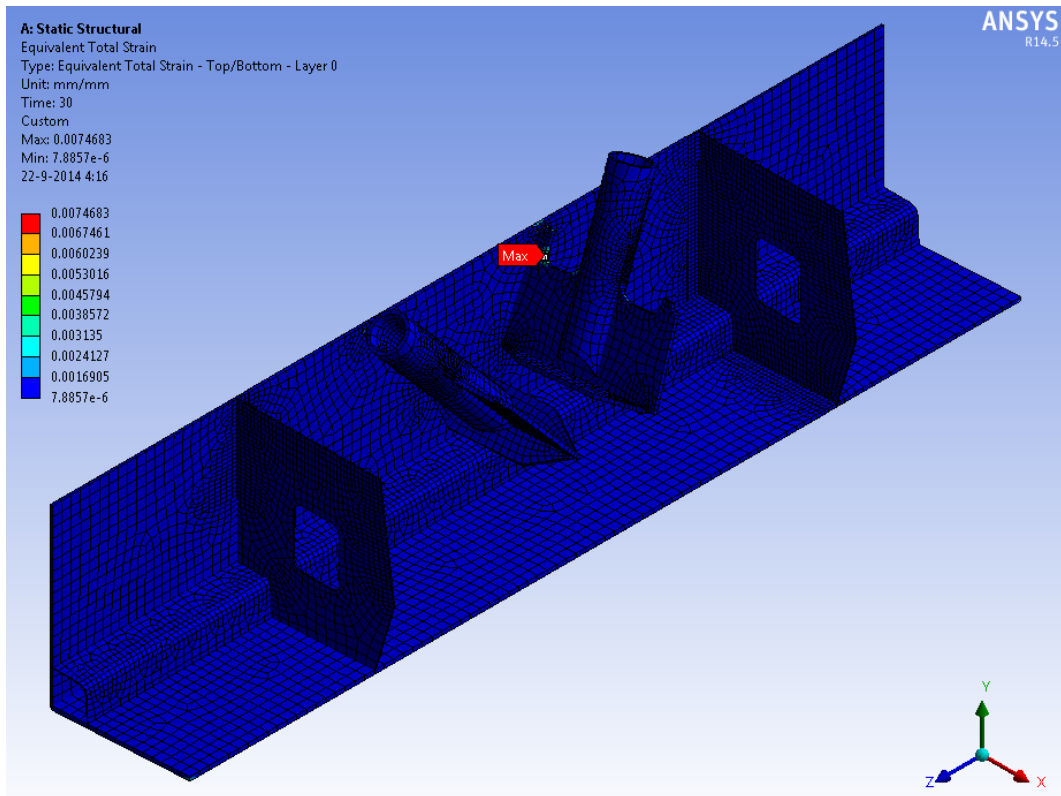


Figure B.46 - Elastic-plastic strains in the joint (IFEA)